Western Australian School of Mines

Use of Low Concentrations of Hydrogen Peroxide in Extracting Gold from Metallurgically Complex Gold Ores

Robert Max Werner Feldmann

This thesis is presented for the Degree of
Doctor of Philosophy
of
Curtin University

March 2016

Declaration

To the best of my knowledge and belief this thesis contains no material previously published by any other person except where due acknowledgment has been made.

This thesis contains no material which has been accepted for the award of any other degree or diploma in any university.

Signature: 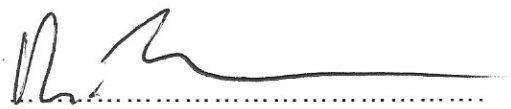

Date: 23/03/2016

Abstract

Gold leaching with cyanide was first industrially practiced in the late 19th century. The process has since been refined to extract more complex bound gold. By the late 20th century hydrogen peroxide additions to the leach were found to be advantageous on ores of refractory nature with high sulphide mineral content. Increased recovery and reduced leach times as well as reduced cyanide consumption were amongst the benefits observed. Whilst the benefits could be empirically proven no exact explanation of the pathways of action of hydrogen peroxide on the gold and mineral surface could be given.

This study found that in cyanide solutions leach rates of electroplated gold/silver alloys in the presence of hydrogen peroxide can increase between 120-185% in aerated solution and up to 200% in oxygenated solution. When the cyanide limiting rate was obtained in the presence of hydrogen peroxide a jump in OCP was observed. This was caused by a silver enrichment on the electrode surface, where hydrogen peroxide has a different oxygen reduction potential than on gold.

Further, it has been shown, that hydrogen peroxide can remove the passivating effect of sulphide ions on gold/silver surfaces. The full oxidation of sulphide ions to sulphate by hydrogen peroxide in solution occurs at a stoichiometric ratio of 4:1. In the presence of cyanide and hydrogen peroxide, the preferential oxidation product of sulphide is thiocyanate. In the absence of cyanide and presence of hydrogen peroxide, sulphide oxidises fast to thiosulphate, which then slowly oxidises further to sulphate. In the presence of cyanide the reaction of thiosulphate to sulphate is preferential over the generation of thiocyanate.

Conductive sulphide minerals can partake in the gold cyanidation redox reaction as additional oxygen reducing sites, when galvanically coupled. The coupling of some minerals will result in an increase in leach rate. This effect can be significantly enhanced in the presence of hydrogen peroxide.

An attempt to develop a simple, cost effective method to determine the benefits of hydrogen peroxide in leaching of industrial gold ores has been made. The outcome shows, that in order to determine possible benefits in a laboratory environment a lot of factors have to be carefully considered. These factors include the taking, transport, and preparation of the sample, the number of repeat tests and testing methodology. The testing methodology is important, and further research should be conducted. In particular, laboratory tests tend to oversupply oxygen and ore reactivity can be lost during transportation, storage, and/or preparation.

Table of Contents

Acknowledgements

Firstly, I would like to thank Dr. Richard Browner and Dr. Paul Breuer for their supervision of this PhD research. Their guidance, advice, encouragement and critical feedback added invaluably to this work. I would also like to thank Alan Hitchiner and Gerhard Arnold for their curious questions and different point of view on this work, which added an out of field perspective on the research.

Secondly, I would like to thank Evonik Industries for their financial support throughout my studies and the sponsoring of this project, which enabled me to conduct this research. To the CSIRO Australian Minerals Research Centre I would like to extend my appreciation for their contribution in time, equipment and laboratory space.

Last, but not least, I would like to thank my partner and family for their understanding and support during my PhD candidature.

Publications and Conferences

Feldmann, R. M. W., & Breuer, P. L. (2015). *An investigation of gold leaching in the presence of hydrogen peroxide using rotating disc electrodes*. Paper presented at the World Gold Conference 2015, Misty Hills, South Africa.

List of Figures

List of Tables

Chapter 1 Introduction

1.1 Importance of gold

Throughout history the metal gold has always been associated with wealth, because of its rarity and appearance. In the past, gold has had limited use, such as a money standard or in jewellery. The use of gold in jewellery is based on its rarity, beauty and properties. Gold has played a major role throughout human history as a currency, which is still valid in the present. It is mainly utilised as a security against inflation during economic uncertainty and in politically unstable environments.

Nonetheless in modern times gold has gained more and more uses due to its physical and chemical properties. Those properties are electrical and thermal conductivity, malleability and infrared (heat) reflectivity. The combination of gold properties makes it a vital metal for electronics, medical and other industrial applications.

Wasserman (2010) notes, that at the dawn of human civilisation and social hierarchy, approximately 5000 B.C., gold had already begun to play a major role in representing the dominant classes, namely royalty, priesthood and nobility. In approximately 2000 BC, gold developed its position even further in Ancient Egypt, where it initially was being monetised. This developed further through the centuries towards the uses of gold known today.

Gold production in 2015 was estimated at 3000 t with the three largest producers being China, followed by Australia, Russia and the United States, producing 490, 300, 242 and 200 t respectively (U.S. Geological Survey, 2016). In 2015, as an integral part of the Australian economy, gold accounted for nearly 5.8% of total exports, making gold the country's third highest export earner (Department of Foreign Affairs and Trade, 2016). Based on that, improving gold extraction technology is important for the survival of the gold mining industry and its value to the Australian economy.

1.2 Occurrence of gold

Gold in the earth's crust is present at an average concentration of 4 ppb. An enrichment of gold in some locations of the earth's crust has occurred naturally and concentrations of greater than 1 ppm are economically extracted (Puddephatt, 1987). According to Fathi Habashi (2009), gold mostly occurs as the native metal. It is, however, frequently alloyed with silver in various concentrations as the mineral electrum. No native alloy with copper is known.

There are some gangue minerals typically associated with gold ore deposits with the most important being: pyrite (FeS_2), galena (PbS), zincblende (ZnS), arsenopyrite (FeAsS), stibnite (Sb_2S_3), pyrrhotite ($Fe_{(1-x)}S$) and chalcopyrite (CuFeS). The presence of various selenium minerals and magnetite (Fe_3O_4) is not uncommon. Some gold ores may also contain carbonaceous matter. Due to its affinity to tellurium gold will also be found as telluride minerals such as: calaverite ($AuTe_2$), and sylvanite ($(Au,Au)Te_2$). Other appearances of gold are with palladium and rhodium as either porpezite (Au containing 5-10% Pd) or rhodite (Au,Rh). Occurrences in so-called locked refractory ores are extremely finely divided gold particles associated with sulphide minerals.

1.3 Chemistry of gold

Gold is the most noble and therefore least reactive metal of all metals (Nicol, Fleming, & Paul, 1987). Its most appealing property is that it does not undergo corrosion reactions in the presence of air, strong acids or bases. Common gold oxidation states in aqueous solutions are +1 (aurus) and +3 (auric), with the respective associated standard reduction potentials of 1710 and 1500 mV (A. J. Bard, 1975). Hence gold cations are thermodynamically unstable in aqueous solutions.

A limited number of ligands, such as cyanide and chloride, are known to form stable complexes with gold cations (Marsden & House, 2006; Nicol et al., 1987). The reaction between an aurous ion (Au^{+}) and a ligand (L^{n}) with either a positive or negative charge can be described by Equation 1-1. The resulting stability constant, ß, can be described by Equation 1-2.

$$Au^{+} + xL^{n} \rightarrow AuL_{x}^{1+nx} \qquad \text{Equation 1-1}$$

$$\beta = \frac{\left[AuL_{x}^{1+nx}\right]}{\left[Au^{+}\right]\left[L^{n}\right]^{x}} \qquad \text{Equation 1-2}$$

The standard reduction potential of the gold complex, $E^{0}_{complex}$, can be related to the standard reduction potential of the aurus ion, $E^{0}_{Au^{+}/au}$, and the stability constant, ß, by Equation 1-3, with R being the universal gas constant (8.314 J $K^{-1}mol^{-1}$), T being the absolute Temperature (K), and F being the Faraday constant (96485 C mol^{-1}).

$$E^{0}_{complex} = E^{0}_{Au^{+}/Au} - \frac{RT}{F}\ln(\beta) \qquad \text{Equation 1-3}$$

It can be deducted that for ligands, which form strong complexes with gold (giving large ß values), the gold complex will be thermodynamically stable in aqueous solutions ($E^{0}_{complex}$ more negative than 1230 mV). This results in the domination of aqueous gold chemistry by the formation of a limited number of stable aurus and auric complexes.

A number of ligands are known to form stable complexes with either auric or aurous cations. A list of metallurgical important gold complexes is given in Table 1-1, including the stability constant and standard reduction potential. This listing is sorted in order of the stability of each complex and shows that the gold cyanide complex is the most stable, as it shows the most negative E^{0}.

Table 1-1: Variety of metallurgical important stability constants and standard reduction potentials of gold complexes (after Zhang, 1997)

Complex	Log ß	Reduction Reaction	E^0/mV
$Au(CN)_2^-$	$2x10^{38}$	$Au(CN)_2^- + e^- = Au + 2CN$	-570
AuS^-	$2x10^{36}$	$AuS^- + e^- = Au + 2S$	-460
$Au(HS)_2^-$	$1.3x10^{30}$	$Au(HS)_2^- + e^- = Au + 2HS$	-90
$Au(S_2O_3)_2^{3+}$	$5x10^{28}$	$Au(S_2O_3)_2^{3+} + e^- = Au + S_2O_3^{2-}$	150
$Au(SC(NH_2)_2)_2^+$	$2x10^{23}$	$Au(SC(NH_2)_2)_2^+ + e^- = Au + 2SC(NH_2)_2^+$	352
$Au(CN)_4^{3-}$	$\sim 10^{56}$	$Au(CN)_4^{3-} + e^- = Au + 4CN$	400
AuI_4^-	$5x10^{47}$	$AuI_4^- + 3e^- = Au + 4I^-$	560
$Au(SCN)_4^{3-}$	10^{42}	$Au(SCN)_4^{3-} + 3e^- = Au + 4SCN$	623
$AuBr_4^-$	10^{32}	$AuBr_4^- + 3e^- = Au + 4Br^-$	870
$AuCl_4^-$	10^{26}	$AuCl_4^- + 3e^- = Au + 4Cl^-$	1002

In recent years ligands, such as chloride and thiourea, have been investigated (La Brooy, Linge, & Walker, 1994) as a replacement for cyanide in the gold industry, but were only successfully utilised in niche applications. A new focus also lies on the commercialisation of an amino acid – glycine process (Eksteen, 2015). To date one commercial application of the thiosulphate process is operational (Gorain, Kondos, & Lakshmanan, 2016), but a complete replacement of cyanide in the near future appears unlikely. Cyanide with its high stability gold complex, $Au(CN)_2^-$, is still the most important reagent industrially used. Based on this the remainder of this thesis will focus on the dissolution of gold by cyanide (cyanidation), and in Section 1.4 a brief review of the basics of the cyanidation process will be provided.

1.4 Processing of gold by cyanidation

McArthur, Forrest and Forrest patented the cyanidation process for gold extraction in 1888. The first industrial application of this process was in 1889 at the Karangahake mine in New Zealand.

The processing of gold by cyanidation is a process consisting of three main steps: liberation, leaching and recovery. Figure 1-1 shows a schematic of a typical carbon in pulp (CIP) leach circuit, showing the three main steps of the process. Most gold plants utilise a CIP or if pregrobbing material is present a carbon in leach (CIL) circuit. Some older and especially South African mining operations utilise thickening and filtration followed by zinc cementation instead of carbon adsorption. The interaction and variation of those steps can significantly influence the recovery and production cost for each ore. The following paragraphs give a brief outline of the basic methods and possible influences of variations to the process.

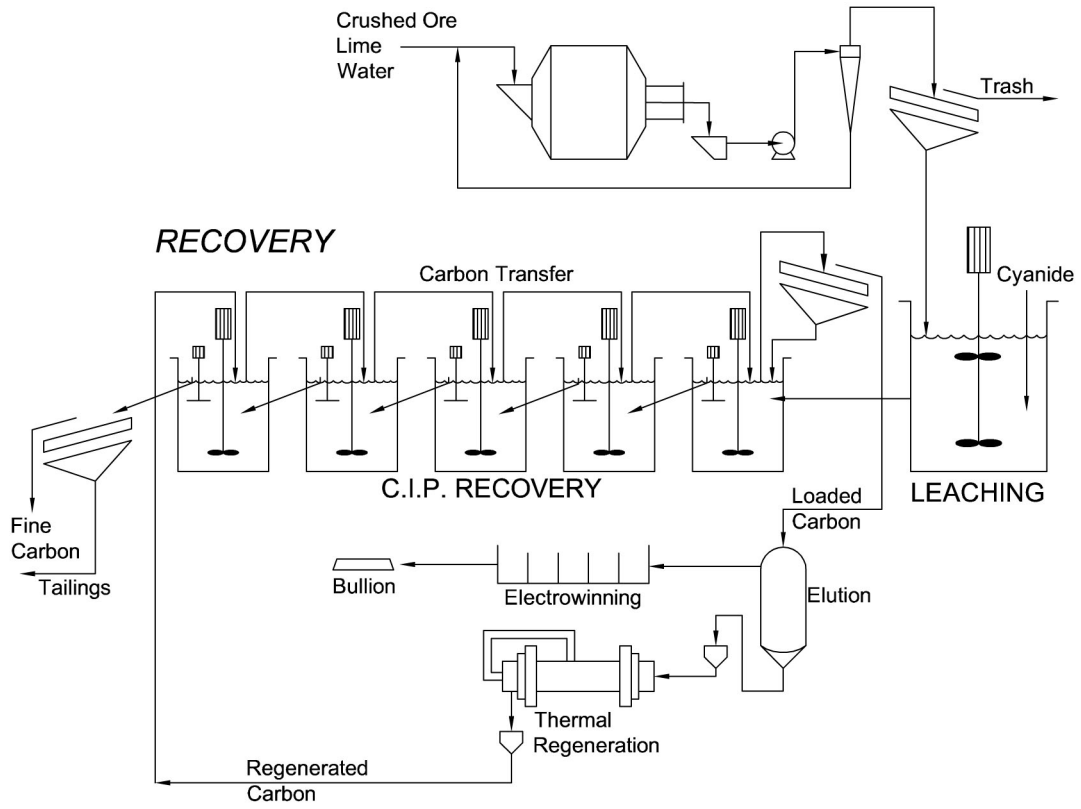

Figure 1-1: Typical cyanidation plant flowsheet consisting of leaching and carbon in pulp adsorption as the recovery process

1.4.1 Liberation

The first step of any hydrometallurgical process is liberation, to expose the valuable component contained in a less valuable gangue mineral. The valuable component in

most ores is present in small particles in surrounding minerals. To make those particles accessible and to expose their surfaces to the leaching reagents (in this case exposing gold to cyanide, water, and oxygen) the ores have to be crushed and ground. Depending on the particle size of the valuable mineral, grind size has to be determined to be as coarse as possible while still liberating the valuable mineral, to keep energy consumption to a minimum. To ensure a consistent particle size as a feed to the leaching step, a classification step takes place before the ground ore is transferred into the leaching section.

1.4.2 Leaching

After the liberation step, the hydrometallurgical process of leaching can take place. Leaching can be described as the dissolution of a high value component out of a low value gangue mineral by a lixiviant. In the case of gold cyanidation the high value component is gold and the lixiviant used is an alkali cyanide solution with oxygen as an oxidant. The Elsner equation (Equation 1-4) can be used to describe the leaching of gold by cyanide, where gold is dissolved and forms the gold cyanide complex, $Au(CN)_2^-$.

$$4Au + 8CN^- + O_2 + 2H_2O \rightarrow 4Au(CN)_2^- + 4OH^- \qquad \text{Equation 1-4}$$

The leaching typically takes place in an agitated tank with oxygen sparging, but heap leaches are used on some occasions. The typical solids to liquid ratio in the slurry is around 50%. Cyanide and lime are the basic reagents, which are added into this tank. The most important factors in a leach system are:

- **Control of cyanide concentration:** In several, especially more complex ores, other reactive minerals, such as copper or sulphur, can consume cyanide. Hence, the available cyanide is monitored and necessary additions are manually or automatically controlled.

- **Control of dissolved oxygen concentration:** Oxygen plays a vital role in gold leaching. Some ores show significant oxygen consuming side reactions and the addition of oxygen as pure oxygen instead of air takes place. The amount of gas sparging and therefore the dissolved oxygen (DO) levels in most modern gold leaching plants are automatically controlled to obtain the most efficient leaching. In some cases, where the oxygen availability is limited, the addition of hydrogen peroxide has been used and still takes place.

- **Control of pH:** Cyanide has a pKa of 9.3 (Fleming, 1992), which indicates pH control in the leach slurry is important to prevent volatilisation of highly toxic HCN gas. It further prevents reagent loss and the resultant increased reagent cost. Most modern gold plants monitor and control the pH by an automated control system.

- **Agitation:** As the solids in the slurry have the tendency to settle, sufficient agitation is necessary. Agitation does improve the mass transfer rate of cyanide and oxygen to the gold particles, and can improve the leaching kinetics.

1.4.3 Recovery

After the gold has been leached out of the ore and is present as the gold cyanide complex, $Au(CN)_2^-$, the next step is the recovery of the gold. There are a few methods available; however two have been mainly used industrially for gold recovery: cementation and carbon adsorption. Both are described in the next sections.

1.4.3.1 Cementation

Zinc cementation in the form of the Merill-Crowe Process was the most common gold recovery process for most of the gold processing plants in the 20^{th} century. The central element in this process is a metal displacement reaction, where zinc displaces the gold according to Equation 1-5.

$$2Au(CN)_2^- + Zn \rightarrow Zn(CN)_4^{2-} + 2Au$$ Equation 1-5

To recover the gold, the leach solution has to be separated from the solids and then the zinc is added for the cementation process. The solid-liquid separation is usually achieved by counter current decantation or vacuum filtration. After separation, the solution is clarified in order to remove any remaining solids and then degassed to remove any remaining oxygen. Finally zinc powder is added which causes gold particles to develop, which can then be filtered out of the solution.

The high cost of the solid-solution separation step, taking place before the cementation, as well as typical gold losses of approximately 1%, have led to intensive research and development of an alternative recovery process (Fleming, 1992). The result of this research and development work over the last 35 years was the carbon in pulp (CIP) process and its variations, which is further described in Section 1.4.3.2.

1.4.3.2 Carbon adsorption

In modern gold extraction technology using carbon adsorption, especially carbon in pulp (CIP) technology is state of the art. The adsorption of gold cyanide on carbon was originally patented in 1894 (Johnston, 1984), but was rarely applied on an industrial scale until the 1970's. From the late 1970's to the early 1980's, the process went through a development of the CIP adsorption technology and rapidly spread from South Africa throughout the world (Fleming, 1992). The major advantage of the CIP process over cementation is that the solution does not need separation from the pulp in order to effectively extract the gold. Coming with comparatively low capital and operational costs, CIP nowadays is the preferred recovery path.

The mechanical side of the CIP process is relatively simple and is an engineering standard, but the actual chemical mechanism behind the adsorption of gold onto activated carbon is rather complex and not fully understood. As shown by Jia, Steele, Hayward, and Thomas (1998), a significant amount of work has been done on trying

to understand the adsorption process in detail. A lot of evidence suggests that gold cyanide is co-adsorbed with cations, mostly calcium. A secondary important mechanism seems to be ion exchange with functional carbon groups. However, it has been shown by Zhang (1997) that gold cyanide is adsorbed without any chemical change.

The CIP process can be broken down into two main steps, adsorption and elution, as shown in Figure 1-1. The adsorption takes place in large, well-agitated tanks, where granular activated carbon is added and then transferred in a counter flow manner to the pulp from the last to the first adsorption tank. During this time the gold cyanide complex adsorbs onto the carbon. In the first adsorption tank the loaded carbon is removed and separated from the pulp by screening. The activated carbon is then usually washed by hot hydrochloric acid, and subsequently the gold cyanide desorbed (eluted) from the carbon with a solution of sodium cyanide and sodium hydroxide (Fleming, 1992). Finally metallic gold is recovered from the eluate solution by electrowinning. After being thermally regenerated, the carbon is added to the CIP circuit in the last tank again.

1.4.4 Peroxide assisted leach (PAL)

In early applications of the CIP process, new ways to provide the oxygen required for the leaching of the gold, as shown in Equation 1-4, were tested. Hydrogen peroxide was only one of the many reagents, which were tested as an oxygen source. This test work resulted in the patenting (Knorre, Loroesch, Gos, Stoll, & Ziegler, 1993) of the peroxide assisted leach (PAL) process. Amongst being an oxygen source there were some other benefits, such as enhanced recoveries and significantly increased leach rates, seen on the leaching of certain ores, which were not understood (Lorösch, 2001). With ores becoming more and more complex these days and conventional cyanidation continuously resulting in lower recoveries, it is necessary to attempt improvements of the process or to develop alternatives. With peroxide assisted leach historically showing significant benefits, understanding this process in more detail could offer a solution for some cases.

1.5 Objectives of this study

The target of this study was to fundamentally understand the phenomena of improved recoveries and leach rates, previously observed in peroxide assisted leaching. It also aimed at being able to produce predictions on which ores or minerals, peroxide assisted leaching will be the most effective treatment and how to apply it. First a literature review on the field of gold cyanidation, hydrogen peroxide in leaching, electrochemistry of gold and selected minerals as well as ore leaching, particularly complex ores took place. A fundamental investigation to elucidate the interaction of hydrogen peroxide on gold surfaces during cyanide leaching was conducted. Then, as historically improved recoveries and leach rates were seen on real ores mainly containing sulphide material, which can result in sulphide passivation of the gold surface or have other effects, the study moves on to investigate the impact of hydrogen peroxide on sulphide ion passivated gold. After thoroughly understanding the effect on the gold surface itself, selected mineral surfaces will be investigated and the interaction between gold and minerals will be targeted. In the final section a simple, standardised, cost and time effective approach on determining the influence of hydrogen peroxide and other pre-treatments on gold leaching will be evaluated.

Chapter 2 Literature Review

This chapter presents a review of the literature. The first part will focus on the cyanidation chemistry of gold and factors influencing cyanidation chemistry, such as oxidant concentration in solution, cyanide concentration and chemical inhibitors. Further, methods to determine leach kinetics are outlined. The second part presents the possible role of minerals when galvanically interacting with gold in a leach environment. The third part shows leaching of industrial gold ores and will outline known benefits that can be achieved with hydrogen peroxide dosing.

2.1 Cyanidation chemistry of gold

2.1.1 The gold cyanide complex

Gold forms a strong complex with cyanide. It is the strongest gold complex known to date and hence cyanide is still the preferred lixiviant in gold hydrometallurgy over lately, more intensively investigated lixiviants, such as thiosulphate (Choi, Baron, Wang, Langhans, & Kondos, 2013; Nicol et al., 1987). Possible gold complexes including their E^0 are listed in Table 1-1, in Section 1.3.

In 1846 Elsner (1846) discovered the requirement of oxygen for the dissolution of gold by cyanide. Based on this discovery the so-called Elsner equation, as shown in Equation 2-1, was derived and is mentioned as the cyanidation equation throughout literature.

$$4Au + 8CN^- + O_2 + 2H_2O \leftrightarrow 4Au(CN)_2^- + 4OH^- \qquad \text{Equation 2-1}$$

Fifty years later, in 1896, Bodlaender (1896) described gold dissolution with Equation 2-2. This equation differs from the Elsner equation as it does not result in a complete reduction of the oxygen to hydroxide but it forms hydrogen peroxide instead. This is the main reaction commonly occurring during the leaching process (Kameda, 1949). If a decomposition of hydrogen peroxide to oxygen is considered as

a subsequent step, the Elsner equation can still stand correctly, at least from a stoichiometric point of view.

$$2Au + 4CN^- + O_2 + 2H_2O \leftrightarrow 2Au(CN)_2^- + H_2O_2 + 2OH^-$$ Equation 2-2

Kameda (1949) and R. W. Zurilla and Yeager (1969) confirmed later, that a direct reduction of the formed hydrogen peroxide, as shown in Equation 2-3, is very limited during gold leaching. Hence, the Bodlaender equation is the most applicable description of the gold leaching reaction.

$$2Au + 4CN^- + H_2O_2 \leftrightarrow 2Au(CN)_2^- + 2OH^-$$ Equation 2-3

2.1.2 Electrochemical interpretation of gold cyanidation reaction

As the leaching of gold is an electrochemical reaction, the reaction, as shown in Equation 2-1, can be broken down into the anodic gold oxidation reaction and the cathodic oxygen reduction reaction (Lorösch, 2001; Nicol et al., 1987).

Anodic gold oxidation

The anodic gold oxidation has been identified as a one-electron reaction on the basis of electrochemical measurements (Cathro & Koch, 1964; Lorösch, 2001). Equation 2-4 shows the anodic gold oxidation reaction.

$$Au + 2CN^- \leftrightarrow Au(CN)_2^- + e^-$$ Equation 2-4

Cathodic oxygen reduction

The cathodic oxygen reduction is a complex multi electron process, as summarised by Lorösch (2001). The overall reaction is represented by Equation 2-5. However, this direct reduction of dissolved oxygen to hydroxyl ions on the gold surface usually does not occur in the potential regions gold leaching takes place (Hoare, 1968). In

the typical potential range of gold leaching, this reaction was found to take place as a two-step reduction with hydrogen peroxide as an interim product (Lorösch, 2001).

$$O_2 + 2H_2O + 4e^- \leftrightarrow 4OH^-$$ Equation 2-5

The two consecutive reduction steps of oxygen as shown in Equation 2-6 and Equation 2-7 were confirmed by F Habashi (1966) and R. Zurilla, Sen, and Yeager (1978). The first step generates hydrogen peroxide as an interim product, which is then further reduced.

$$O_2 + 2H_2O + 2e^- \leftrightarrow H_2O_2 + 2OH^-$$ Equation 2-6

$$H_2O_2 + 2e^- \leftrightarrow 2OH^-$$ Equation 2-7

Lorösch (2001) suggests, that the majority (up to 85%) of the hydrogen peroxide formed diffuses away from the surface. He further mentions, that in solutions aiding the formation of calcium peroxide up to 100% of the formed hydrogen peroxide forms calcium peroxide, being evidence for peroxide being formed. This in turn suggests, hydrogen peroxide added to the solution will not directly contribute to an increase in gold leaching kinetics, but might only cause an increase in dissolved oxygen (DO) levels of the solution.

2.1.3 Kinetics of gold dissolution by cyanide

Reaction kinetics of a solid in a liquid can be controlled by two main factors: reagent diffusion and reaction kinetics (chemical control). Diffusion control takes place, when the reaction of the reactants takes place at a rate, so that fresh reactant cannot reach the surface fast enough and therefore limits the reaction; chemical control occurs, when the reactants contact each other in a sufficient rate, but the reaction itself is slow and therefore represents the limiting step. In order to determine the controlling mechanism, the diffusion conditions must be well controlled and understood.

There are two main approaches for investigating the kinetics of gold dissolution by cyanide. The traditional approach is based on kinetic measurements, such as reactant or product concentration in solution or mass measurement of the leached specimen, as a function of time. A second approach is based around electrochemical measurement and a calculation of the mass leached from the measured current based on the gold leaching half reaction (Equation 2-4). The particular benefits of this second approach are the ability to separate the anodic and cathodic reaction kinetics and detect influences on either half reaction. On the other hand, the calculated mass change might contain some error, as the measured currents might not purely result from the targeted reaction. The theories and known techniques behind both methods are described in this section.

2.1.3.1 Sample geometry and agitation

Due to the nature of most leaching reactions being mass transport controlled, the agitation of the system plays an important role in investigating leaching systems. To choose the best method for investigating leach kinetics, two major factors have to be considered: reproducibility of mass transfer and theoretical mass transfer calculation options. To allow for comparable results with other works, it is important to select an experimental setup, which allows for this to occur. Of further benefit is a system, which allows a comparison between measured and theoretical mass transfer rates, so the nature of the reaction can be determined (diffusion control versus chemical control) (Matthew Ian Jeffrey, 1997).

Typical sample geometries and agitation methods including benefits, disadvantages, and the availability of simple mathematical models are described in the following subsections.

Rotating Disc

Rotating discs are generally specimens with a flat surface, rotating around their central axis. They are usually constructed from a cylinder of the material of interest embedded in an epoxy resin housing. As a result of this geometry, the fluid flow over

the surface is very reproducible and laminar over a wide range of conditions; hence data obtained with rotating disc experiments is very reproducible. An additional benefit is the easy comparability of gathered results to existing data, as well as to a relatively simple model for the diffusion of species to the disc surface (Matthew Ian Jeffrey, 1997). The model is called the Levich equation, which is detailed in Section 3.4.1. The high accuracy of this equation was experimentally confirmed by Gregory and Riddiford (1956). Further Biegler, Rand, and Woods (1975) showed, that the Levich equation can still be assumed valid for non-round material surfaces, as long as they are embedded in a round shape.

Rotating Cylinder

As explained by Gabe and Walsh (1983), similarly repeatable results can be achieved by using a rotating cylinder, instead of a rotating disc. In comparison to the rotating disc, the cylinder is rotated around its central axis and the curved cylinder surface is in contact with the solution, resulting in an equal linear velocity across the whole surface. Only an empirical relationship with limited validity is available for describing the flux of reactant to the surface, as well as higher, turbulent mass transport that is taking place. Due to this fact, comparability between results is reduced.

Agitated Solution

Matthew Ian Jeffrey (1997) describes an agitated solution as the most simple and cost effective form of creating a liquid flux on solid surfaces to promote leaching, but also mentions the disadvantage of complicated reproducibility. Due to the various means of agitating a solution, such as bottle rolls, impellors or gas sparging, re-creating exactly the same experimental conditions as other experimenters and consequently gaining comparable results is very difficult. A single experimenter with the same setup can only obtain reasonable repeatability. Therefore, it is very complicated or not possible to compare results of different authors (Power & Ritchie, 1975). As no modelling of the flux of reactants can be constructed for agitated solutions, a determination between chemical or diffusion control of a reaction proves complicated. Further, depending on the agitation technique, a maximum mass

transfer flux can be reached at a critical stirring rate (Power & Ritchie, 1975). This can give misleading results, when agitating above the critical rate.

As a result from the evaluation of the different agitation methods in Section 2.1.3.1, it can be seen that rotating disc experiments will result in the most comparable data, when investigating leaching kinetics under laboratory conditions. However, the investigation of an impact of an ore cannot be investigated with high accuracy with the rotating disc method.

2.1.3.2 Product/reactant gain/loss measurement methods

The importance of sample geometry and agitation for kinetic experiments has been outlined in Section 2.1.3.1. This section focuses on methods to measure the actual rates in leaching experiments, which are either based on the gain of products or loss of reactants including the precious metal, in this case gold.

Loss of reactants

As presented in Section 2.1.1, four reactants are prerequisite for gold leaching: gold, cyanide, oxygen and water. As a result of this, the reaction rate can be determined (bearing in mind that possible side reactions of cyanide or oxygen cannot be easily accounted for), by measurement of the loss of one or more of the reactants over time (Matthew Ian Jeffrey, 1997). Due to the possible inaccuracy in measuring the loss of oxygen and cyanide contributing to the leach reaction, these methods are typically not utilised as means to determine the leach kinetics for this case. However, historically the measurement of the loss of these reactants was applied to confirm the reaction stoichiometry of gold leaching in cyanide e.g. Kameda (1949), where the gain of the reaction product, gold cyanide was also detected. In other studies the loss of gold was used to measure kinetics, which will be shown in more detail in the following paragraphs of ‘Loss of reactants’.

Matthew Ian Jeffrey (1997) explains, that the most direct approach to determine gold leaching kinetics is by measuring gold mass loss over time with two possible

techniques: measuring the time to completely dissolve a known mass of gold, and measuring the gold mass decrease over time (by using a quartz crystal microbalance). The technique using a known mass and waiting for complete dissolution has the disadvantage of only one data point, and any change over time cannot be observed. Additionally, a large time period is typically required. Zheng, Khan, La Brooy, Ritchie, and Singh (1996) utilised chronopotentiometry as a variation of the simple mass loss measurement, where the time required to dissolve an electroplated film was measured. The benefit of this method is, that only nano-films of metals are leached and rapid results can be obtained. However, chronopotentiometry was not utilised for the investigation of gold cyanidation, as the film thickness after plating gold varied significantly.

As evaluated by Matthew Ian Jeffrey (1997), a further development in mass loss measurement is the quartz crystal microbalance (QCM), which is commercially available. These commercial systems are used for adsorption and deposition measurements and are only available as stationary systems requiring stirred solutions, when analysing gold leaching. Due to the disadvantages of stirred solutions, mentioned in Section 2.1.3.1, QCM's have not been utilised extensively to investigate fundamentals of gold leaching in cyanide. For this reason M. I. Jeffrey, J. Zheng, and I. M. Ritchie (2000) improved the QCM into a rotating QCM and then even further into a rotating electrochemical QCM, which gives the advantages of being able to electroplate and leach gold under controlled, well understood rotating disc conditions (as outlined in Section 2.1.3.1). This REQCM system allows for very high accuracy mass loss measurement in real time (in the order of 1 ng). A further advantage of this system is the ability to conduct electrochemical measurements during the leaching. This system is described in detail in Section 3.3.1.1.

Gain of products

In Section 2.1.1 the reaction products of gold cyanidation are listed as $Au(CN)_2^-$ and OH^-, both soluble in water. A significant number of studies on gold cyanidation (M. M. Aghamirian & Yen, 2005; Guo, Deschênes, Pratt, Fulton, & Lastra, 2005; Guzman, Segarra, Chimenos, Fernandez, & Espiell, 1999) have used the gain (the

increase in concentration) of gold in solution over time as a measure of rate. This is a good method for leach rate determination, as modern solution analysis can detect gold at very low levels with high accuracy. However, if low leach rates occur, the solution volume has to be either very small or a large gold surface needs to be exposed to obtain accurate results in an acceptable timeframe.

2.1.3.3 Electrochemical method

In Section 2.1.2, the electrochemical interpretation of gold cyanidation was presented. In Sections 2.5.1 and 2.5.2, the possibility to measure both of the half reactions separately is shown. As a result, when one of the reagents enabling one of the half reactions is omitted from the test solution in potential scans, both reactions can be investigated individually in detail and potential-current diagrams created. Under the assumption, that the omission of one of the components of the reaction does not change the other half reaction behaviour, absolute values of the anodic and cathodic curves can be overlayed, as shown in Section 2.5.3. The intersection point of the absolute values represents the leach potential and also gives a figure for the current flow, which can be converted into a gold leach rate. This method has been used by some researchers (Cerovic, Hutchison, & Sandenbergh, 2005; Guan & Han, 1994; Li et al., 2010; Nicol et al., 1987; Tshilombo & Sandenbergh, 2001) resulting in fairly accurate predictions of leach rates, especially when investigating influences of additional reagents on one of the gold leaching half reactions.

2.1.4 Factors affecting cyanide leach kinetics of gold

The leach rate measurement of gold in cyanide solution is outlined in Section 2.1.3. It is shown that the gold leach rate mainly relies on the reactant concentration and mass transport to the gold surface, except in the case of chemical control. This section discusses the two limiting reactants (cyanide and oxygen) and their recognised influences on the kinetics of the cyanidation process. Additionally, other chemicals known to impact the leach kinetics are outlined.

Oxygen

When oxygen acts as the electron consumer in the gold leaching redox reaction, the transfer of oxygen to the surface, impacted by agitation and oxygen concentration in solution, usually reflects the limiting factor for leaching kinetics. This particularly applies for gold leaching in ores (La Brooy, Muir, & Komosa, 1991). Senanayake (2008) however shows, when investigating the oxygen reduction on pure gold using the Levich equation, that the current measurement does not calculate into a two or four electron reduction, as shown in Section 2.1.2. This is most likely caused by the slow reaction of cyanide with pure gold and resulting gold surface passivation by cyanide (Matthew Ian Jeffrey, 1997). Matthew I Jeffrey and Ritchie (2000) further show, that on gold/silver surfaces at higher cyanide concentrations the reduction of oxygen occurs in a two step process, with the reduction to hydrogen peroxide being diffusion limited and the subsequent reduction of the peroxide to hydroxide being a chemically controlled reaction. The overall observed reaction rate again does indicate neither two nor four electron reduction.

For gold/silver and silver surfaces the reduction factor mentioned by Senanayake (2008) lies between the two and four electron reduction, the theory of which is presented in Section 2.1.2 suggests. This was explained by the partial removal of the intermediate formed: hydrogen peroxide from the surface before it was able to be further reduced.

Cyanide

Senanayake (2005) states, that in ultrapure solutions at 25°C, the reaction of ultrapure gold with cyanide includes several transition states, which create a chemical reaction limitation and hence result in a limiting rate, not controlled by cyanide or oxygen diffusion. A complex model to prove this was created. Further, Senanayake (2008) postulates for the anodic gold dissolution by CN^-, that interim products of $Au(OH)(CN)^-$ are formed and slow the reaction rate due to the formation of a surface film, which is not highly soluble in aqueous solutions.

Other chemical factors

Some elements or ions of these elements are known to create passivating surfaces on gold during cyanide leaching. The most commonly mentioned and investigated inhibitors are sulphide ions, besides others. This section will provide an overview of the most common inhibitors and possible remedies.

Sulphide ion concentrations as low as 0.1 mM (M. I. Jeffrey & Breuer, 2000) can have a negative influence on pure gold leaching in 5 mM cyanide concentrations. Immediate, significant slowing in leach rate up to a complete halt at the same cyanide concentrations is observable for sulphide additions at concentrations of 1 mM. Mainly the anodic gold oxidation by cyanide (M. I. Jeffrey & Breuer, 2000) and the cathodic oxygen reduction to a lesser extent are affected. It was further established, that high cyanide concentrations of 40 mM resulted in removal of the passivation layer and formation of thiocyanate. The addition (Senanayake, 2008) of lead can improve the gold leaching in cases of sulphide passivation – mainly by aiding as a catalyst in the oxidation of sulphide ions or by forming lead sulphides and therefore leaving the gold surface available for leaching. Contrary to the passivating effect of sulphide ions, Tshilombo and Sandenbergh (2001) demonstrated, that trace amounts of sulphide ions in high NaCN concentrations (2500 mg/L) can result in an activation of the cathodic gold reaction in potential areas where it would usually be passive due to AuCN film formations.

Passivation of gold can also occur during cyanide leaching due to the formation of AuCN or AuOH on the gold surface (Li et al., 2010), as mentioned in the paragraph ‘Cyanide’ in Section 2.1.4. Particularly higher NaCN concentrations (>10 mM) can result in chemical control (Li et al., 2010) instead of mass transport limited gold leaching kinetics. Small quantities of Hg^{2+} ions were found to significantly enhance the anodic current under the usually limited conditions. Hg^{2+} ions impact the oxygen reduction in a positive manner. However, when typical conditions are plotted on a mixed potential diagram even the presence of Hg^{2+} ions only results in minor gains in leach rates. However, the presence of 20 mM hydrogen peroxide in addition to the

Hg^{2+} ions would significantly increase the intersection point and therefore the leach rate.

Native copper from the ore or other metallic copper introduced during cyanide leaching will result in the cementation of already dissolved gold on copper (Nguyen, Tran, & Wong, 1997). After dissolution of the copper, under the presence of oxygen and enough remaining free cyanide, the gold will redissolve. High cyanide consumption is usually the result for copper bearing ores.

The addition of lead in small concentrations (2-10 ppm) can result in enhancement of gold leaching as the lead appears to reduce the adhesion of peroxide species and aids their further reduction to water. In addition lead can increase rate of the oxygen reduction at lower potentials, but no influence at higher potentials is present (Cerovic et al., 2005). Contrary to the beneficial effects of lead on its own or in the presence of sulphide, it requires careful addition as too high lead concentrations in solution can result in surface passivation of gold (Senanayake, 2008).

Senanayake (2008) notes the negative effect of carbonaceous materials like graphite or activated carbon on gold cyanidation due to the formation of coatings, but no remedy is suggested.

2.2 Chemistry of hydrogen peroxide

The primary purpose of this section is to review the chemical and physical properties of hydrogen peroxide. Possible reactions between cyanide and hydrogen peroxide are presented and an overview of applications in laboratory gold leaching experiments and industrial leaching applications are given.

2.2.1 Hydrogen peroxide physical and chemical properties

Hydrogen peroxide has the chemical sum formula H_2O_2, and based on a periodic table (Los Alamos National Laboratory) its molecular weight can be calculated to

34.016 g/M. Pure hydrogen peroxide has a specific gravity of 1.45 g/mL (IFA, 2015), however, industrial strength hydrogen peroxide is usually available in concentrations of 35, 50, and 70% w/w with corresponding specific gravities of 1.13, 1.20, and 1.29 g/mL respectively (US Peroxide, 2015). Industrial strength solutions all indicate an acidic pH, varying depending on strength between pH 0 and 3.7 (US Peroxide, 2015).

Table 2-1 shows a list of common oxidising agents with the corresponding half reactions and the corresponding standard reduction potentials. Some of the reagents listed are commonly used in the gold mining industry (oxygen and hydrogen peroxide). In comparison to oxygen, hydrogen peroxide has a higher oxidising potential for both acidic and basic conditions. It is notable, that the reduction potential of both oxygen and hydrogen peroxide is reduced in an alkaline environment.

Table 2-1: Standard reduction potentials of some selected oxidising agents in acidic and basic solution (pH=0 and pH=14) extracted and/or calculated from Douglas, Alexander, and McDaniel (1997)

Oxidising Agent and Half-Reactions	**$E°_{acid}$**	**$E°_{base}$**
Chlorine		
$Cl_2 + 2e^- = 2Cl^-$	+1.36 V	+1.36 V
Ozone		
$O_3 + 2e^- + 2H^+ = O_2 + H_2O$	+2.08 V	
$O_3 + 2e^- + H_2O = O_2 + 2OH^-$		+1.24 V
Hydrogen peroxide		
$H_2O_2 + 2e^- + 2H^+ = 2H_2O$	+1.78 V	
$HO_2^- + 2e^- + H_2O = 3OH^-$		+ 0.88 V
Oxygen		
$O_2 + 4e^- + 4H^+ = 2H_2O$	+1.23 V	
$O_2 + 4e^- + 2H_2O = 4OH^-$		+0.40 V

Hydrogen peroxide is relatively unstable, especially at elevated temperatures. If no stabilisers are present, it tends to decompose according to Equation 2-8, resulting in molecular oxygen (O_2). Immediately after decomposition an O^- radical (elemental

oxygen) may be present, but the radical typically binds very quickly with either another radical to form aforementioned molecular oxygen or other elements present. This decomposition of hydrogen peroxide can also be caused by the presence of incompatible chemicals, such as alkali or metal ions (Mn, Fe, Pb, Ag, and Pt) (Lee, Park, & Oloman, 2000).

$$H_2O_2 \rightarrow H_2O + 0.5O_2$$ Equation 2-8

2.2.2 Reactivity of hydrogen peroxide and cyanide

As hydrogen peroxide is a known strong oxidising agent, investigations have been carried out to use hydrogen peroxide as a detoxification agent for cyanide containing waste streams (slurries and solutions), showing that usually a suitable catalyst is required for efficient cyanide oxidation. Kitis, Akcil, Karakaya, and Yigit (2005) demonstrated the effectiveness of Cu^{2+} ions as a catalyst for the destruction of weak acid dissociable cyanide in tailings solution by hydrogen peroxide. Copper concentrations of around 30 mg/L significantly enhance the cyanide oxidation. To completely destroy cyanide concentrations of around 60 mg/L, dosages of 300-500 mg/L of hydrogen peroxide were required without a catalyst; with a catalyst present the required hydrogen peroxide dosages were reduced to 150-300 mg/L. Comparing other work, it was highlighted, that cyanide destruction by hydrogen peroxide has to be evaluated on an individual application basis.

Sarla, Pandit, Tyagi, and Kapoor (2004) further revealed, that the oxidation of cyanide by hydrogen peroxide works most efficiently in conjunction with Cu^{2+} ions as a catalyst or in the presence of intense ultra violet (UV) light. Without any additional treatment cyanide destruction by hydrogen peroxide was found to be slow and higher reagent consumption was observed.

A MgO/Ru catalyst also resulted in efficient cyanide oxidation by hydrogen peroxide for an electroplating waste stream with initial cyanide concentrations around 300 ppm (Pak & Chang, 1997). It was further demonstrated, that elevated temperatures of

40-50°C increase destruction speeds and a solution pH range between 6 and 8 leads to a most efficient cyanide oxidation.

Figure 2-1 plots the impact of low hydrogen peroxide concentrations on cyanide concentration as a function of time. It is notable, that this work was conducted in clear solution without the presence of any catalyst. With an initial cyanide concentration of 15 mM, even an addition of hydrogen peroxide to a 100 mM solution concentration only resulted in a reduction of cyanide concentration by around 35% after one hour of reaction time. Lower concentrations show even less impact. Guzman et al. (1999) used silver nitrate titration for the cyanide concentration determination, but the method of end point determination is not mentioned.

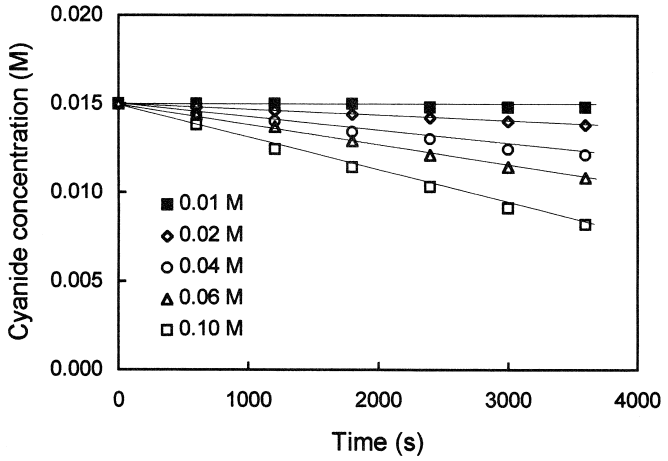

Figure 2-1: Effect of hydrogen peroxide concentration on cyanide ion concentration. Experimental conditions: pH 11.5, 0.015 M initial NaCN, 400 min^{-1} and 25°C (Guzman et al., 1999)

Thus, addition of hydrogen peroxide to gold leaching may result in some oxidation and loss of cyanide, depending on the presence of catalysts.

2.2.3 Hydrogen peroxide in laboratory investigations of gold leaching

Guzman et al. (1999) investigated the effect of oxygen and hydrogen peroxide on pure gold leaching. It was observed, that at pH 10 hydrogen peroxide at solution concentrations approximately above 3 mM is beneficial to the gold leaching rate,

when compared to atmospheric oxygen on its own, however, at an increased pH the leach rate with hydrogen peroxide drops below the rate obtained with conventional cyanidation (oxygen supplied only as the atmospheric oxygen content in air). Below 3 mM a negative impact was noted. At a pH of around 12.5 and above the gold leach rate with oxygen begins to decline. Figure 2-2 presents the impact of different hydrogen peroxide concentrations on leach rate. An ideal addition concentration can be noted around a hydrogen peroxide concentration of 10-15 mM for the selected experimental conditions. Other authors (Marsden & House, 2006) mention a hydrogen peroxide concentration for leaching of 15 mM. Further, as discussed in Section 2.1.4, in pure gold leaching, passive regions caused by AuCN or AuOH films can be present in higher cyanide concentrations (>10 mM). Additions of hydrogen peroxide to form solution concentrations of 20 mM can offer a possible remedy and significant improvement in leach rate (Li et al., 2010). However, it is noted that none of the authors offers a detailed explanation for these phenomena.

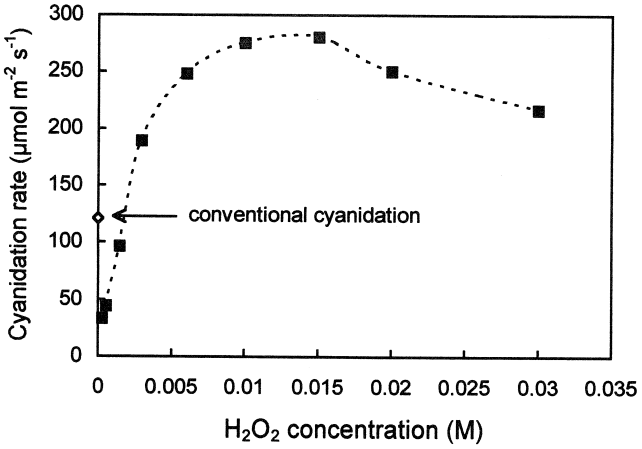

Figure 2-2: Effect of hydrogen peroxide concentration on the cyanidation rate. Experimental conditions: 0.01 M NaCN, pH 10, 400 min^{-1}, 25°C and atmospheric pressure (Guzman et al., 1999)

2.2.4 Peroxide assisted leach (PAL)

Peroxide Assisted Leach (PAL) is a process of hydrogen peroxide addition to cyanide leaching of gold ores patented by Degussa AG in 1993 (Knorre et al., 1993). The process was mentioned by La Brooy et al. (1991) as a means of reducing cyanide consumption and increasing recoveries in ores containing significant

amounts of copper. A maximum dissolved oxygen level achieved of around 40 mg/L is given and hydrogen peroxide consumptions between 0.2 and 0.5 kg/t of ore are estimated. A further variation of PAL is Carbon in Peroxide Assisted Leach (CIPAL), where the activated carbon is already present during the leach (Lorösch, 2001). The following section will review PAL and CIPAL.

Figure 2-3 compares thiocyanate concentrations measured in solution for two comparison tests – one with PAL and one only with aeration. One benefit of PAL is a reduced thiocyanate generation during leaching. A result of this and a second benefit of PAL is reduced cyanide consumption, as presented in Figure 2-4.

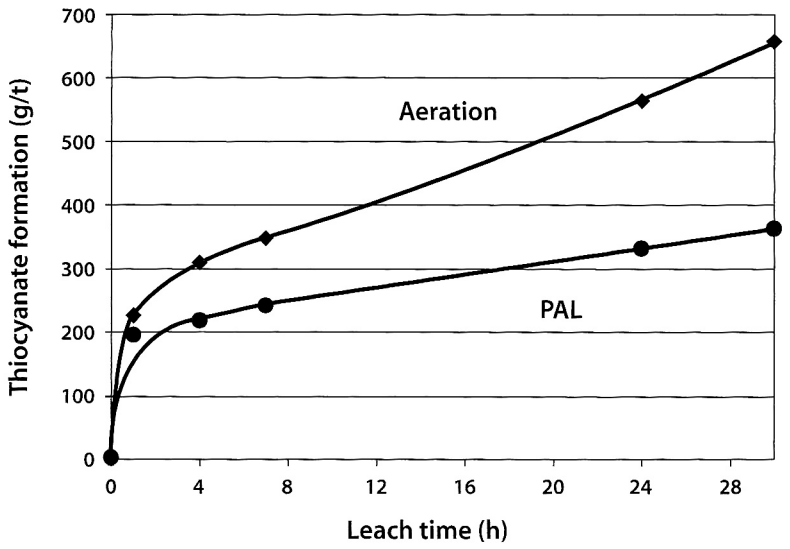

Figure 2-3: Thiocyanate formation during PAL-application in comparison to conventional cyanidation (Lorösch & Kappes, 1991)

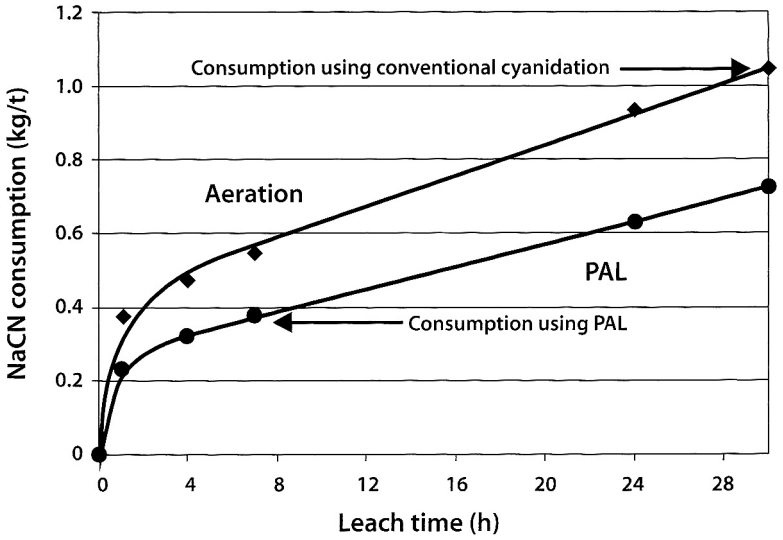

Figure 2-4: Reduced NaCN consumption on a sulphide ore during PAL application as the result of the lower thiocyanate formation. As comparison the NaCN consumption obtained during conventional cyanidation is included (Lorösch & Kappes, 1991)

The requirement of high oxygen levels for fast gold cyanidation was shown in the previous Section 2.1.3. With this requirement in mind, Figure 2-5 presents a third benefit of PAL over regular cyanidation. High dissolved oxygen levels in a pulp for PAL in comparison to aerated cyanidation throughout the whole leach time can be observed (Lorösch, 2001). The immediate result of this is shown in Figure 2-6, where a gold recovery profile comparison of regular cyanidation and PAL is plotted. Leach time reductions to reach the maximum possible recovery without changing any other aspects of the leach (grind, etc.) from 36 to 4 hours is notable (Lorösch, 1990). Figure 2-7 shows another comparison test result, where the leaching of a sulphidic ore is tested under aeration, oxygenation and PAL. In the same leach time, the recoveries observed show a significant advantage of PAL over oxygenation, and aeration (Adam, 1989). However, these cases (sulphidic ores) might reflect extremes of the beneficial effects of PAL.

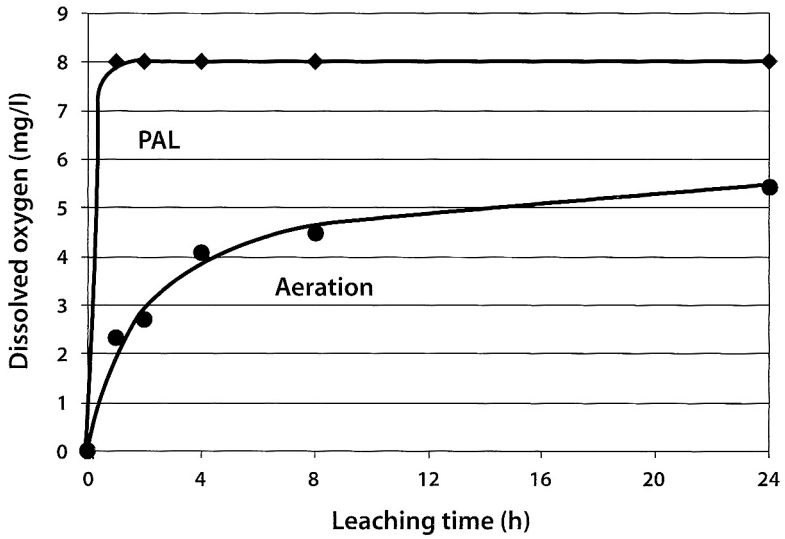

Figure 2-5: Oxygen profile in a laboratory leach test of a sulphidic ore pulp comparing PAL to the application of compressed air (Lorösch, 2001)

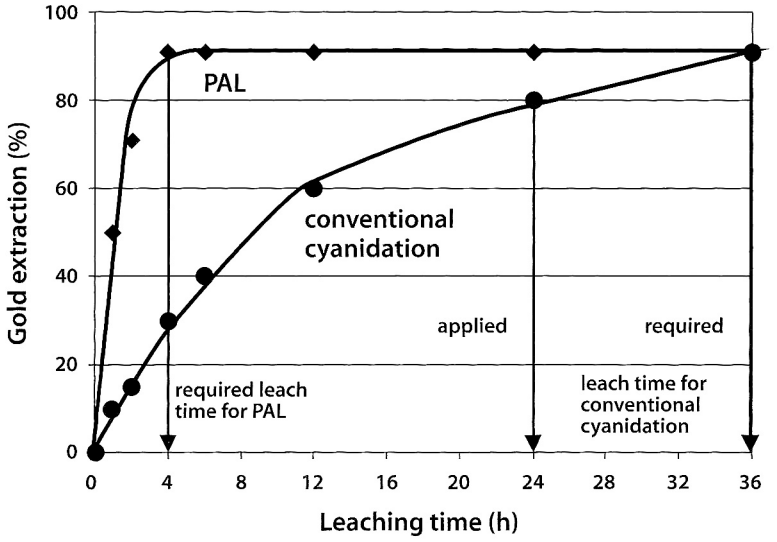

Figure 2-6: Gold extraction kinetics for a sulphidic ore comparing the PAL-application with conventional cyanidation (Lorösch, 1990)

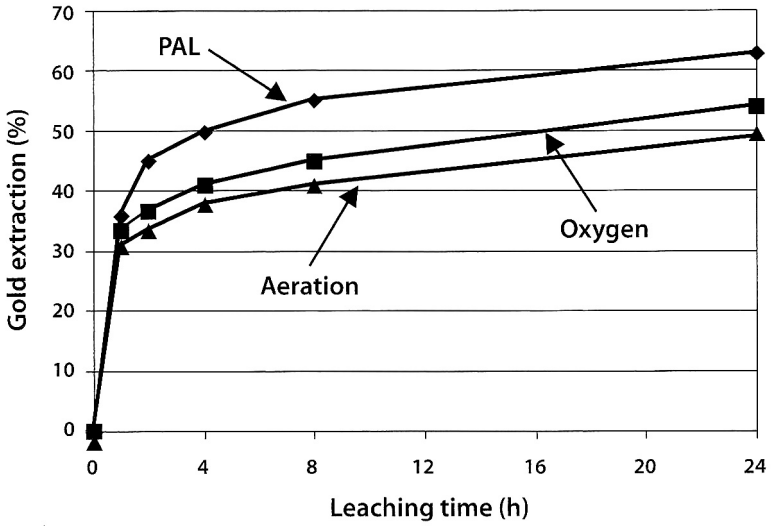

Figure 2-7: Gold extraction profiles obtained on a sulphidic ore comparing the PAL-technology with conventional aeration and the application of pure oxygen. The additional gold recovery in the PAL-application is clearly visible (Adam, 1989)

An additional option in PAL technology is CIPAL, analogue to CIP and CIL technology, as outlined in Section 1.4.3.2. All previous data presented on PAL technology was created with CIP type processes, where the full dissolution is obtained prior to the addition of activated carbon. CIPAL, however, has the carbon already added during the leach stages, where not all gold is dissolved yet. Figure 2-8 (Lorösch, 1989) shows a gold extraction profile for an ore, where regular aeration cyanidation, PAL and CIPAL are compared. In this particular case PAL and aeration produce similar results, but CIPAL results in a significantly higher gold extraction during the 24h leach period observed. This might be due to a preg-robbing ore, but the data presented does not include a CIP result to compare to.

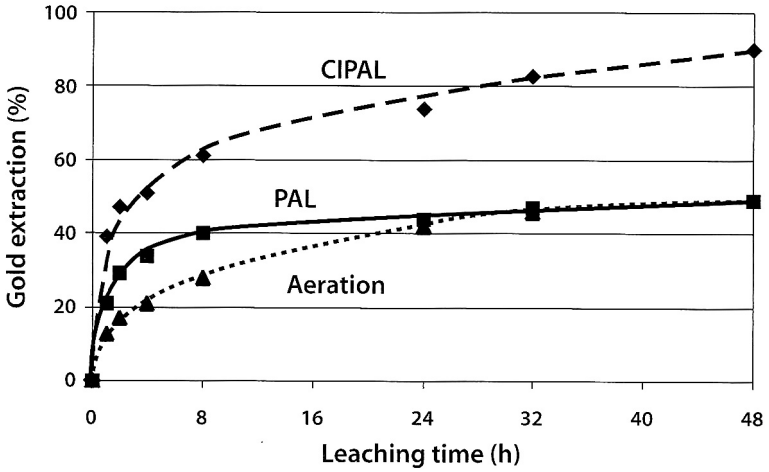

Figure 2-8: Gold extraction profiles obtained on a Greenstone Belt ore comparing CIPAL, PAL and conventional cyanidation (Lorösch, 1989)

In summary, PAL and CIPAL offer three main benefits: reduced side reactions, which reduce cyanide consumption, decreased leach time required and increase in recoveries. These beneficial effects were all observed on sulphidic ores, but no specific mechanism or understanding of these mechanisms resulting in the observed benefits is given in any of the works sighted. It should be noted, that all literature on PAL and CIPAL is originally published by Degussa or associates to the company. No negative effects of hydrogen peroxide were found in the literature, apart from the possible oxidation of cyanide, as mentioned in Section 2.2.2.

2.3 Galvanic interactions of sulphide minerals and gold

Galvanic interactions of sulphide minerals and gold have been investigated because of the common coexistence of sulphide minerals with gold in the ores being processed nowadays. Three main fields of mineral interaction and reactivity have been reported in literature: the fundamental ability of minerals to act as an oxygen reducing surface, the galvanic interaction of gold and minerals in separate solutions and the galvanic interaction observable with gold and minerals in the same solution. These three are summarised in the following subsections. Both work conducted on pure gold and gold/silver are considered, due to the limited availability of material around the galvanic interaction.

2.3.1 Oxygen reduction on mineral surfaces

When conductive sulphide minerals and gold are connected in an ore or contact each other such that an electric current can flow, the oxygen reduction step, as shown in Section 2.1.2, could theoretically take place on the mineral surface instead of or in addition to the gold surface. This would increase the corrosion current flow and therefore allow for faster leach rates of gold. This section summarises the ability of selected, common and conductive sulphide mineral surfaces to act as sites for oxygen reduction.

M. M. Aghamirian and Yen (2005) investigated the minerals: gold, pyrite, pyrrhotite, chalcopyrite and galena. It can be noted, that all tested minerals are capable of oxygen reduction to a certain extent with pyrite and pyrrhotite giving current readings larger than gold, once potentials more negative than around -500 mV vs. standard calomel electrode (SCE) are reached. The mixed potential/open circuit potential of these minerals in aerated 0.01 M cyanide solutions were -420, -264, -108, -224, -85 and -670 mV vs. SCE for gold, chalcopyrite, pyrite, pyrrhotite, galena and chalcocite respectively. When comparing any two of these values to each other, a more negative open circuit potential of one mineral means that in a leaching situation this mineral could act as the oxygen reduction surface/cathode (M. M. Aghamirian & Yen, 2005).

Azizi, Petre, Olsen, and Larachi (2010) conducted potential scans in alkaline (pH 11) solutions on two mineral electrodes prepared from industrial ore (44.2% pyrite, 0.1% chalcopyrite, 0.3% sphalerite, 0.1% galena, 0.1% arsenopyrite, and the remainder gangue) and purified pyrite material (96.6% and gangue). The electrodes contained agar cement and graphite, rather than being solid material electrodes. For both electrodes significant oxygen reduction currents (for some potential regions even greater than could be achieved on a pure gold surface) were reported and oxygen reduction currents were measured at more positive potential regions than on gold

electrodes. These greater currents and more positive potentials, however, might be a result of the electrode composition.

Rand (1977) reports that oxygen reduction is possible on galena, pyrrhotite, arsenopyrite, pyrite and chalcopyrite surfaces. In alkaline solutions the reduction curves measured are similar. Further, for low rotation speeds the maximum diffusion current is closely correlated to the 4-electron limiting current calculated by the Levich equation, however, this is only applicable on new surfaces. When repeated cycling of the minerals took place, especially in alkaline solutions, a reduction in the currents measured was observed. This was explained by possible oxide layer formation or metal dissolution on the mineral surfaces. Similar to Azizi et al. (2010), Rand (1977) observed for pyrite and copper sulphides oxygen reduction properties similar to gold.

Tan, Feng, van Deventer, and Lukey (2006) and Biegler et al. (1975) investigated pyrite and its possible role as an oxygen reduction surface. Potential scans, particularly in alkaline solution show the typical two wave reduction of oxygen with the interim product of hydrogen peroxide. Lower agitation was found to increase the amount of hydrogen peroxide utilised in the secondary reduction step from hydrogen peroxide to hydroxide, as shown in Section 2.1.2. Tan et al. (2006) further determined, that carbon, graphite, activated carbon and clay coatings do not impair the reactivity of pyrite to any significant extent with the antithesis of carbon coatings enhancing the oxygen reduction.

2.3.2 Galvanic interaction – separated solutions

The ability of sulphide minerals for oxygen reduction is presented in Section 2.3.1, which has lead investigators towards testing the effect of galvanic interactions of minerals and gold in separate solutions to isolate the possible detrimental effect, which dissolved ions from minerals may cause, as shown in Section 2.1.4.

The investigations of Lorenzen and van Deventer (1991) and Azizi et al. (2010) were conducted in two electrochemical cells with RDE electrodes, one of gold and one of the mineral, so each cell could be investigated. The cells were connected via a Luggin-capillary and the electrodes were either connected directly or via an ammeter, to detect the possible galvanic current.

When pure gold is galvanically coupled to copper, chalcopyrite, iron, pyrite, pyrrohtite, magnetite, galena, or sphalerite, a decrease in leach rate of up to 79% was observed by Lorenzen and van Deventer (1991). Hematite did not show any impact (full dataset listed below in Section 2.3.3 in Table 2-2). As no dissolved species could have impaired the gold leaching in this test, the formation of a passive surface on the gold as a result of the excess anodic current was assumed to be the cause of the reduced leach rate measured (Lorenzen & van Deventer, 1991). Contrary, when using a gold/silver electrode coupled to mineral electrodes in a similar fashion, Azizi et al. (2010) report an increase in leach rate, over the baseline rate determined. This could be due to using a non-pure gold specimen, which in turn does not exhibit the three passivation regions as can be observed for pure gold (see Section 2.5.4).

2.3.3 Galvanic interaction – same solution

Untangling the impact of galvanic interaction from possible dissolution of detrimental ions, as presented in Section 2.3.2, and their impact on gold leaching kinetics, as shown in Section 2.1.4, aids the fundamental understanding of the complex systems real ores present. However, in the processing of ores the separation of these two phenomena is not feasible. Hence, investigating the galvanic interactions of minerals and gold in the same solution is important. An overview of the effects presented in the literature is discussed here.

Lorenzen and van Deventer (1991), M. M. Aghamirian and Yen (2005) and Azizi et al. (2010) all tested the impact of galvanic coupling on cyanide leaching of gold with RDE experiments, with a gold and mineral electrode in the same solution. Liu and Yen (1995) investigated the galvanic coupling, however, the investigation was less

precise and predictable, as mineral powders were pulped in RDE gold and silver leach test solutions instead of having mineral electrodes besides the gold electrode. It is assumed that the oxygen reduction takes place on the pulped mineral surface and when the mineral randomly touches the gold the contact is sufficient to allow electron transfer to take place.

Table 2-2 shows the effect of galvanic coupling of pure gold with various minerals, as presented by Lorenzen and van Deventer (1991). The column headlined with '1 vessel' outlines the effect of the two electrodes in the same cell, and the column with '2 vessels' shows the effect, where the solutions around the electrodes were isolated from each other but electronically connected, as discussed in Section 2.3.2. For all minerals, except for galena, a larger impairment of the gold leaching was observed, when gold and the mineral electrode were galvanically connected and in the same solution, instead of two solutions. These effects were accounted for by mineral dissolution and subsequent deposition of species on the gold surface. Overall, significant reductions in gold dissolution kinetics were observed with the exception of galena enhancing the gold leaching. This effect is caused by the lead ions in solution aiding oxygen reduction on the gold surface, as shown in Section 2.1.4.

Table 2-2: Relative dissolution rates of a gold electrode in contact with electrodes of metals, minerals and ores in a clear solution of 0.2 g/L KCN (extract from Lorenzen & van Deventer, 1991)

Mineral; metal, ore	**Relative dissolution rate of Au (%)**		**Major metals and impurities**
	1 vessel	**2 vessels**	
Gold (alone)	100	100	Au
Copper	16	21	Cu
Chalcopyrite (2 types)	35-49	50.6-51	Fe, Cu, (Zn)
Iron	59	70	Fe
Pyrite (2 types)	36-40	48-40	Fe, Cu, Co
Pyrrhotite	50	64	Fe, Ni, Cu
Haematite	92	100	-
Magnetite	60	70	-
Galena	153	70	Pb
Sphalerite	52	64	Zn

Contrary to the negative impact of galvanic interaction observed by Lorenzen and van Deventer (1991) on pure gold, investigations on gold/silver electrodes (between 0.3 and 4% silver with gold) did show a positive impact of galvanic coupling with various minerals (M. M. Aghamirian & Yen, 2005; Azizi et al., 2010). Coupling the gold/silver electrode with either pyrite, sphalerite, chalcopyrite or galena in the same solution resulted in a slight increase of the leach rate over the baseline (Azizi et al., 2010). The increase, however, was less than when the electrodes were in separate solutions, as mentioned in Section 2.3.2. The passivation effects seen were thought to be the result of Au_2S coatings on the gold surface, as demonstrated by M. I. Jeffrey and Breuer (2000). Figure 2-9 presents the effect of coupling a gold/silver alloy with various minerals observed by M. M. Aghamirian and Yen (2005) in air saturated (left diagram) and oxygen saturated (right diagram) solution. It should be noted, that the baseline test (gold/silver) shows the same leach rate for aerated and oxygen saturated solution, which theoretically should be different. In both scenarios an increase in leach rate, when galvanically coupled, can be observed for pyrite, pyrrhotite, and galena, whereas chalcopyrite results in a decrease in leach rate. M. M. Aghamirian

and Yen (2005) suggest that an increase in leach rate is likely, even in real world applications, as long as no sulphide coating of the gold surface is taking place.

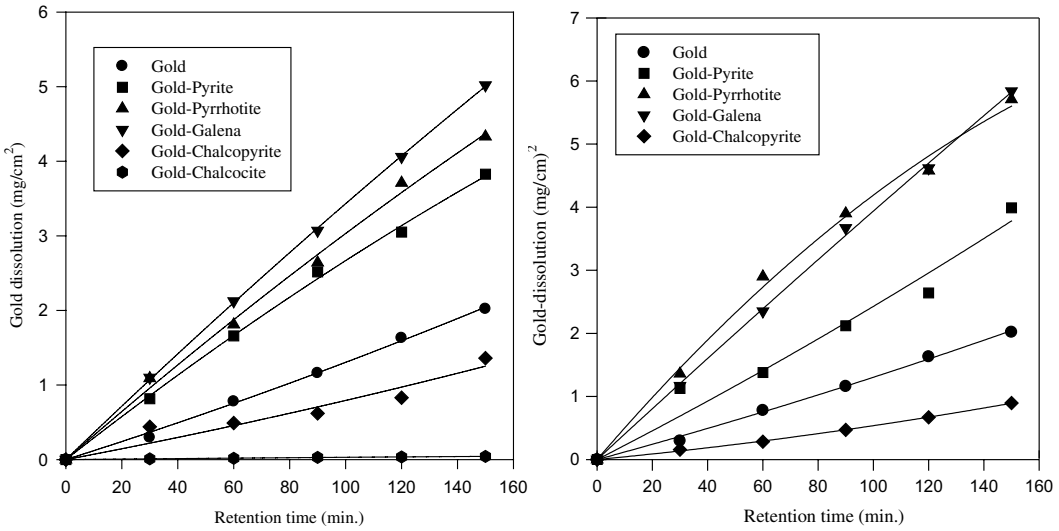

Figure 2-9: Gold dissolution in galvanic coupling experiments at pH 10.5 with 0.01 M NaCN, left in air saturated solution, right in oxygen saturated solution (M. M. Aghamirian & Yen, 2005)

The 'galvanic coupling' effect observed with an RDE in pulped mineral samples by Liu and Yen (1995) suggests that gold and silver leaching will be impaired negatively by pyrite. However, chalcopyrite and pentlandite would increase the leach rate. As this test work might be more representative of real ores, the results are presented in more detail in Section 2.4.1.1.

In summary, various and even contradicting results on the impact of galvanically coupled leaching of gold were presented by several researchers. No definitive answer to the direct benefits can be concluded from the data cited, apart from, that generally an impact can be seen. All research was conducted either in air or oxygen saturated conditions. The possible impact of hydrogen peroxide on the electrochemical interaction between minerals and gold has not been investigated.

2.4 Leaching of gold bearing ores

A vast number of investigations on the leaching of gold bearing ores and gold leaching in the presence of pure mineral blends have been conducted. First, an outline over the conditions chosen for leaching, showing a vast range of conditions, with a particular focus on dissolved oxygen, hydrogen peroxide, cyanide and slurry pH is given. The focus then moves on the research conducted on gold leaching in the presence of sulphur bearing minerals, also showing oxidation pathways of sulphide ions and elemental sulphur.

2.4.1 Cyanidation of gold bearing ores

When using cyanidation for the recovery of gold from ores, the ores can be divided into three main categories: free leaching ores, refractory ores and complex ores (La Brooy et al., 1994). Complex ores can be split into three groups: cyanide consumers containing copper and reactive sulphides, oxygen consumers with reactive sulphides and preg-robbing ores containing carbonaceous matter, sulphides and clays. Various approaches are utilised for these complex ores, instead of straight cyanidation, which would result in limited recoveries or high reagent consumption. These approaches include, but are not limited to: flotation prior to leaching, pre-oxidation, and leaching under the addition of strong oxidants, such as hydrogen peroxide. Other methods are known, including an extensive list of pre-treatments, but most of these have only been developed in the laboratory and many are prohibitively costly (La Brooy et al., 1994). As highlighted in Section 2.1.4 the presence of sufficient oxygen is crucial for efficient cyanidation. La Brooy et al. (1991) summarise the literature in respect of available oxidants and specific beneficial applications, as listed in Table 2-3. In the table, the maximum achievable dissolved oxygen levels for different oxidants are shown.

Table 2-3: Summary of use of different oxygen supplements and plant observations (La Brooy et al., 1991)

Oxidant	**Maximum O_2 achievable/impact**
Air	Max. 9 mg/L, can strip HCN from solution especially at lower pH
Oxygen	Max O_2 of 40 mg/L, increased leach kinetics, CN savings in presence of sulphides
Hydrogen Peroxide	Max O_2 of 40 mg/L, increase kinetics, no HCN stripping, PAL application 0.2-0.5 kg/t, less copper leaching and reduced cyanide consumption
Calcium Peroxide	Max O_2 40 mg/L, increased leach kinetics, no HCN stripping, long activity >20 days in heap leach. Maximum O_2 release at pH 9.

Matthew Ian Jeffrey (1997) lists typical cyanidation plant conditions with cyanide concentrations of 100 ppm CN^- and a pH of 10.0. In different publications, varying values were found, particularly for more complex ores, containing high amounts of copper and sulphides. The range of pH values was between 10.5 and 12 and cyanide concentrations between 250 and 2000 ppm CN^- were mentioned for ore leach test applications (de Andrade Lima & Hodouin, 2006; G. Deschênes & Prud'homme, 1997; Karimi et al., 2010; Yang et al., 2010).

2.4.1.1 Sulphide minerals in ore leaching

Various researchers investigated the impact of sulphide minerals on gold leaching from ores. The main target of these investigations was to find ideal leaching conditions and possible remedies to the detrimental effect caused by the minerals.

The leaching of gold and silver is dependent on cyanide and oxygen concentration, as shown in Section 2.1.4. Liu and Yen (1995) investigated the impact of pure mineral slurries on the leaching of gold (99.39% Au, 0.30% Ag) and silver (99.99% Ag) with rotating discs (400 min^{-1}) in aerated and oxygenated 5 mM NaCN solutions (pH 10.5). Baseline tests with silica slurries indicate only a marginal increase in gold

leach rate compared to silver leach rate, when the oxygen content of the solution is increased from 8 to 32 ppm, which indicates a chemical controlled reaction for the gold, as significant increase in leach rate for the silver is visible. A doubling of the baseline leach rate of gold under oxygenated conditions was observed when slurries of chalcopyrite, or pentlandite were present, indicating a reduction of the chemical control. Contrary to gold under oxygenated conditions, for silver leaching these suspended minerals result in decreased leach rates. Additionally for gold, under all DO conditions, improvements were observed in the presence of pyrrhotite, molybdenite and sphalerite, but silver leaching is impaired, again indicating, that the chemical control of gold dissolution, as mentioned in Section 2.1.4, can be removed by some minerals. In the presence of galena, gold leaching is enhanced under aeration, but is reduced under oxygenation. This contrary effect was explained by accelerated dissolution of galena under oxygenated conditions resulting in increased lead concentrations in solution. These form passive lead compounds on the gold surface. In either aerated or oxygenated conditions, gold leaching was enhanced by arsenopyrite. The complete investigation (Liu & Yen, 1995) can be summarised as follows, always listed from the most positive to the most negative impact with silica as the baseline: gold under aeration: Galena > Arsenopyrite > Pyrrhotite > Sphalerite > Molybdenite > Silica > Chalcopyrite > Pyrite > Pentlandite > Chalcocite > Stibnite; gold under oxygen saturation: Pentlandite > Chalcopyrite > Pyrrhotite > Sphalerite > Molybdenite > Arsenopyrite > Pyrite > Silica > Galena > Stibnite > Chalcocite; silver under aeration: Galena > Arsenopyrite > Sphalerite > Silica > Pyrite > Molybdenite > Pyrrhotite > Pentlandite > Chalcopyrite > Stibnite > Chalcocite; and silver under oxygenation: Silica > Sphalerite > Molybdenite > Arsenopyrite > Pyrrhotite > Pyrite > Pentlandite > Galena > Chalcopyrite > Stibnite > Chalcocite.

Compared to the pure gold and silver electrodes in pure mineral slurries as investigated by Liu and Yen (1995), Azizi et al. (2010) tested the behaviour of gold with 4% silver content in mineral slurries. The mineral powders used contained either pyrite or chalcopyrite as their main constituents. Various scenarios including pre-oxidation without and with the gold electrode in solution were investigated.

None of the tested scenarios resulted in a gold leach rate in excess of gold without mineral influence (conditions 10 mM NaCN, 8.5 ppm O_2, pH 11). However, pre-oxidation did enhance the gold leach rates in the tests with minerals present over tests with no pre-treatment but did not restore it to the leach rates without minerals present. This was accounted for by the consumption of cyanide by the copper and sulphur present in the minerals. Further improvements were seen when the pre-oxidation was conducted without the gold electrode in solution. One of the conclusions assumed was the formation of polysulphides during pre-oxidation with subsequent adsorption on the gold surface (when present) and a reaction of the polysulphides with cyanide to form thiocyanate resulting in reduced leach rates (Azizi et al., 2010). During different testwork Azizi, Petre, Olsen, and Larachi (2011) created a packed bed methodology to further understand the galvanic interaction and detrimental effects of sulphide minerals on gold/silver alloy leaching. Different arrangements of the gold in relation to the mineral allowed for isolation of the detrimental effects from galvanic benefits. It was shown, that most minerals, if not in galvanic interaction, slow gold leaching significantly. However, galvanic connection can override this slowing effect. Pyrite, chalcopyrite and sphalerite were found to enhance gold leaching by galvanic interaction and even overcome the passivation effects observed due to mineral dissolution.

The effect of pre-treatments for leaching of gold ores with sulphide content was also investigated by Guy Deschênes, Rousseau, Tardif, and Prud'homme (1998). Dry ground samples of synthetic ores and minerals were tested for the effect of pre-oxidation and lead-nitrate additions. The minerals tested included pyrite, pyrrhotite and chalcopyrite. In the presence of chalcopyrite any pre-treatment resulted in increased reagent consumption (NaCN), whereas on both other minerals a reduction in reagent consumption was evident. Recoveries observed during the baseline tests without pre-treatment show a significant decrease in recoveries in the presence of chalcopyrite, due to the NaCN consumption by the copper released. Under the same conditions (no pre-treatment) an increase in recovery was detected in the presence of pyrite and pyrrhotite. In a direct comparison on a low-sulphide ore, it was found that changing DO from 7 to 15 ppm did not result in a different recovery within 48 hours,

but the leach kinetics during the first four hours were marginally faster with the higher DO test. For both cases the final recoveries were nearly obtained at the six hour mark. Cyanate formation was assumed as a possible cause for this phenomenon. Testing both low and high sulphide containing ores for the effect of different NaCN concentrations during leaching did show different leach rates and final recoveries, however, there appears to be optimum concentrations for each specific ore. It was concluded, that the mineral composition determines the leaching requirements, be it pre-oxidation, lime, lead nitrate additions and ideal cyanide concentration.

Further works investigating the effect of sulphidic ore constituents have been conducted by Guo et al. (2005), Li et al. (2010), Mahlangu, Sandenbergh, Skudder, and Maree (2007) and Yang et al. (2010), all indicating that the leaching of sulphidic ores can be aided by differing pre-treatments, mainly pre-oxidation by oxygen sparging or hydrogen peroxide addition and additions of heavy metal ions, such as Pb^{2+}, Hg^{2+}, Tl^{+} and Bi^{3+}. Combined treatment or so called co-intensification using a strong oxidising agent and heavy metal ions can enhance the positive effects on leaching rates and recoveries even further. Some ores show significant recovery improvements in excess of 10%. However, all authors mention the presence of optimum additions for all these methods, depending on the ore treated.

In summary, sulphidic ore constituents can negatively impact gold leaching, particularly by the formation of sulphide and polysulphide ions, which can adsorb on the gold surface, form sulphur-cyanide compounds and consume oxygen. The most common result is reduced leach rates and recoveries. Heavy metal ion additions, pre-oxidation and the addition of hydrogen peroxide have been mentioned as remedial to some of these effects, however, applications appear very specific to the particular ore. An assessment of single mineral interactions, as done by some researchers results only in a partial picture and can enhance the understanding of particular processes with one mineral, but industrial applications require the assessment of their ore as a whole to get the best results, when treating complex ores.

2.4.2 Sulphide oxidation pathways and products

As shown in Sections 2.1.4, 2.3 and 2.4.1.1 sulphide minerals and the resulting ions can cause significant disruption of the cyanidation leach kinetics. Complex ores typically contain sulphide minerals and therefore may release sulphide ions into solution. To mitigate this impact, particularly of the sulphide ions, these ions have to be removed or oxidised and therefore rendered harmless for the gold leaching. The reactants for the oxidation, reaction pathways, reaction times, and reaction products are outlined in this section.

Sulphide ion oxidation and sulphur oxidation, both in alkaline solution, by oxygen with and without cyanide takes place as outlined in Figure 2-10. In the absence of cyanide and presence of excess oxygen, sulphide ions will oxidise to thiosulphate and as a final product sulphate. If, however, excess cyanide is present, thiocyanate is formed from thiosulphate, sulphur, and sulphide directly. A final conversion to sulphate from thiocyanate only occurs at very low reaction rates (Lorösch, 2001).

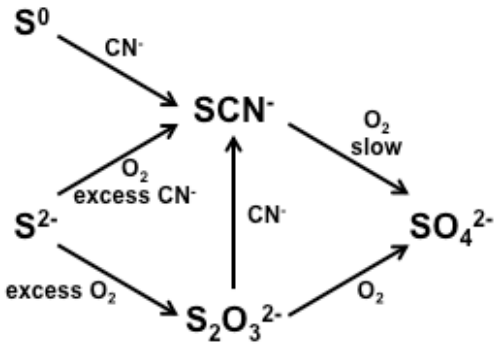

Figure 2-10: Sulphide ion reaction routes in alkaline (cyanide) solutions (Lorösch, 2001)

In any case, with or without cyanide present, sulphide oxidation by dissolved oxygen is a slow process, except in the presence of a catalyst. The presence of lead ions catalyses the oxidation of sulphides by first forming a lead sulphide, which forms a catalytic surface for sulphide ion oxidation prior to being oxidised itself. In the presence of lead, polysulphides form during the oxidation stages and final products and concentrations vary depending on the presence of lead and cyanide and can be sulphite, thiosulphate and thiocyanate (P. L. Breuer, Jeffrey, & Hewitt, 2008). Pyrite

can also act as a catalyst for sulphide oxidation in the absence of cyanide, and whilst catalysing the sulphide oxidation the pyrite itself will also oxidise. In the presence of cyanide, whilst still catalysing the oxidation process, pyrite becomes passive and will not oxidise. In the absence of cyanide the products are mainly thiosulphate whilst in the presence of cyanide a mixture of mainly thiocyanate with traces of sulphite and thiosulphate are present in solution. Again, on either oxidation pathway the presence of polysulphides can be noted (Hewitt, Breuer, Jeffrey, & Naim, 2009).

The most common sulphide mineral oxidation comprehensively investigated is pyrite. In ultra-pure alkaline solutions, pyrite will oxidise, and depending on the alkalinity source the solid oxidation products remaining on the mineral surface vary. In the presence of sodium hydroxide a hematite layer will be formed with small amounts of feroxyhite. Only a thin product layer remains on the surface and most of the oxidation products dissolve into solution. In carbonate solutions the main oxidation product is ferrihydrite and small quantities of iron hydroxide carbonate (Caldeira, Ciminelli, Dias, & Osseo-Asare, 2003). Longer term testing confirms, that the presence of carbonate aids the pyrite oxidation, as it hinders the formation of passive surface films (Descostes et al., 2002). In these solutions a more coarse, granular, growing oxide layer is formed with little material going into the solution (Caldeira et al., 2003).

The oxidation of minerals by hydrogen peroxide has only been investigated in acidic media, as the target elements to extract, which are usually part of the sulphide mineral, are soluble in acid media. In hydrochloric acid media pyrite can be easily and completely oxidised. This oxidation is relating more to processes such as acid copper leaching instead of cyanide leaching of gold. However, it was noted, that the oxidation of pyrite by hydrogen peroxide increases in reagent consumption effectiveness with decreasing agitation. This was accounted for by the fact that stirring will increase the interaction of hydrogen peroxide with the surface in excess of oxidation requirements and therefore aids the decomposition of hydrogen peroxide to oxygen, as shown in Section 2.2.1. This decomposed hydrogen peroxide is

subsequently lost for the oxidation of the mineral (Dimitrijevic, Antonijevic, & Dimitrijevic, 1999).

In summary, the oxidation of sulphide ions by dissolved oxygen has been thoroughly researched, including pathways, interim products and final products. However, the application of different oxidants, such as hydrogen peroxide, on the oxidation of sulphide ions and minerals, has not been extensively investigated. Oxidation of sulphide minerals has particularly been investigated in acidic medium due to the requirement for leaching of other metals than gold, but not to any appreciable extent for alkaline conditions.

2.4.3 Experimental methods applied for kinetic investigations on ores

No systematic studies on laboratory methods and their impact on the results gained (e.g. bottle roll, stirred reactor) and comparability of this work to plant applications are present in literature – the only available knowledge is held carefully by some laboratories and engineering companies (Paul Breuer, 2016). Only few researchers disclose details on how they conducted their studies on ores: Mahlangu et al. (2007) describe the experimental arrangement for investigating leach kinetics in great detail. One kg samples of the crushed and representatively sampled ore were dry ground in a laboratory rod mil. The resulting material was then leached in a baffled glass reactor with overhead stirrer. However, details on stirring speed, stirrer geometry and beaker geometry are not given. Other researchers do not offer as much detail on their testing procedures or use different tests, such as bottle roll tests (Bayat, Vapur, Akyol, & Poole, 2003; G. Deschênes & Ghali, 1988; G. Deschênes & Wallingford, 1995; Karimi et al., 2010).

2.5 Electrochemistry

Electrochemistry plays a major role in understanding the dissolution of gold and silver in cyanide medium. This section outlines the electrochemical principles used for the interpretation of gold dissolution in cyanide medium, as well as any other

reactive materials that can be present during gold leaching and undergo electrochemical reactions.

2.5.1 Anodic reaction

The anodic reaction in any electrochemical system is defined as the reaction releasing electrons (Rieger, 1994). In cyanide leaching of gold, this is the reaction of cyanide with gold, as shown in Section 2.1.2. The oxidation of silver to form silver cyanide is also an anodic reaction in cyanidation.

2.5.2 Cathodic reaction

The cathodic reaction in an electrochemical reaction defined as the electron consuming / receiving reaction (Rieger, 1994). During gold dissolution in cyanide medium with oxygen present the oxygen reduction reaction (as shown in Section 2.1.2) takes the role of the cathodic reaction. Hydrogen peroxide can also undergo reduction and thus be a cathodic reaction in the system.

2.5.3 Mixed potential theory

The occurrence of electrochemical dissolution reactions, such as gold leaching in oxygenated cyanide medium, occurs in local corrosion cells on the materials surface. Such a cell is represented in simplified form, exemplary for gold, in Figure 2-11. In the figure the solid phase (in this case the gold) is represented by the light brown box on the left; the aqueous phase is on the right in the blue box. The white space between the two boxes represents the Nernst boundary layer. The solid phase is split into two distinct areas with their associated reactions: the cathodic (oxygen reduction) and anodic (gold oxidation) area. A flow of electrons from the anodic to the cathodic area takes place. In each specific solution under specific conditions equilibrium of the reactions does occur and results in an apparent electrode potential, the so called mixed potential. Mixed potential theory can be utilised to determine the open circuit potential (OCP) of a system (M. Massoud Aghamirian, 1997). Other terms used in place of OCP are corrosion potential or mixed potential.

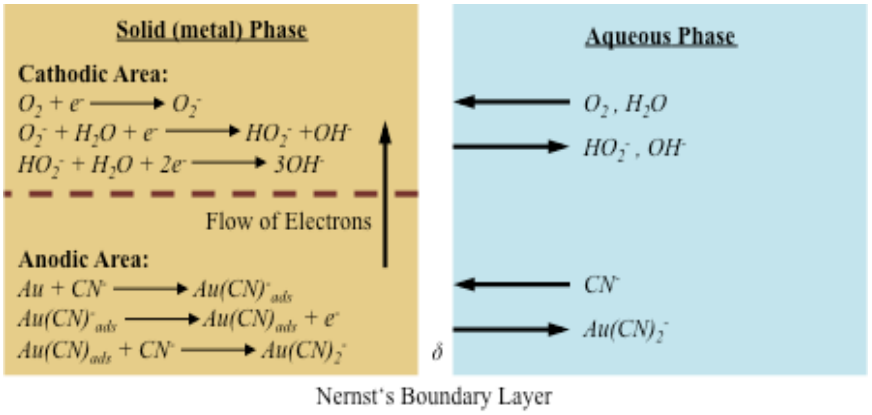

Figure 2-11: Schematic of the solid-liquid reaction of gold-dissolution in cyanide solution, recreated diagram (after Fathi Habashi, 1967)

However, both reactions can be measured separately from each other, as illustrated in Figure 2-12. The figure shows a plot of the resulting anodic (gold oxidation – in absence of oxygen) reaction and the cathodic (oxygen reduction – in absence of cyanide) reaction currents (free corrosion current) versus the applied potential (gold electrode potential). The curves are generated in two measurements, where for one a solution without cyanide present is used and for the other the solution is sparged with an inert gas, such as nitrogen, to remove all dissolved oxygen. The curves are representing several cyanide concentrations and two oxygen concentrations (aerated and oxygenated solution). It is to note, that for the oxygen reduction, the absolute values are plotted instead of the negative currents so that the curves overlay. A plot of this form is also called an Evans-diagram. For each combination of oxygen and cyanide in the system, the current (free corrosion current) and potential ('open circuit potential', depending on the author also called 'free corrosion potential' or 'mixed potential') are represented by the intersection point of the two curves (M. Massoud Aghamirian, 1997). From the current present at the intersecting point for any combination of reagent concentrations (CN^- and O_2), the gold dissolution rate can be estimated, as outlined in detail in Section 2.1.3.3. The gold-cyanide currents shown in Figure 2-12 do not present the passivation regions, as were previously determined by Cathro and Koch (1964), shown in Section 2.5.4.

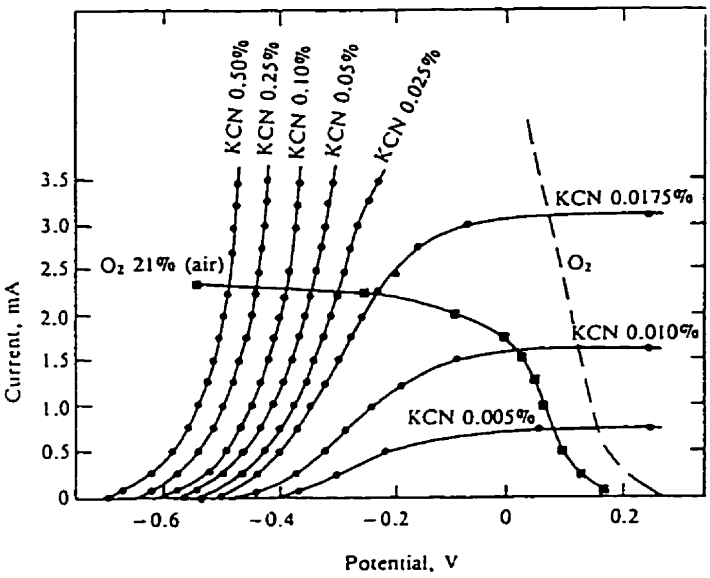

Figure 2-12: Anodic and cathodic current-potential curves for gold (Kudryk & Kellogg, 1954)

2.5.4 Potential scans on gold (and silver)

This section will review the literature of potential scans conducted on gold and gold/silver alloys, separating the anodic and cathodic reaction. The target of this section is to determine the influence of experimental conditions on the results of potential scans due to the behaviour of gold and gold/silver alloys under various cyanidation conditions.

Anodic reaction

The anodic behaviour of pure gold (Lorösch, 2001) in contamination free cyanide solutions is plotted in Figure 2-13. Three current density peaks can be observed, which are inherent with colour/reflectiveness changes of the gold surface. The three peaks correspond to the formation of passive layers. Only the first peak is identified as an $AuCN^-$ compound; the other peaks are not fully identified.

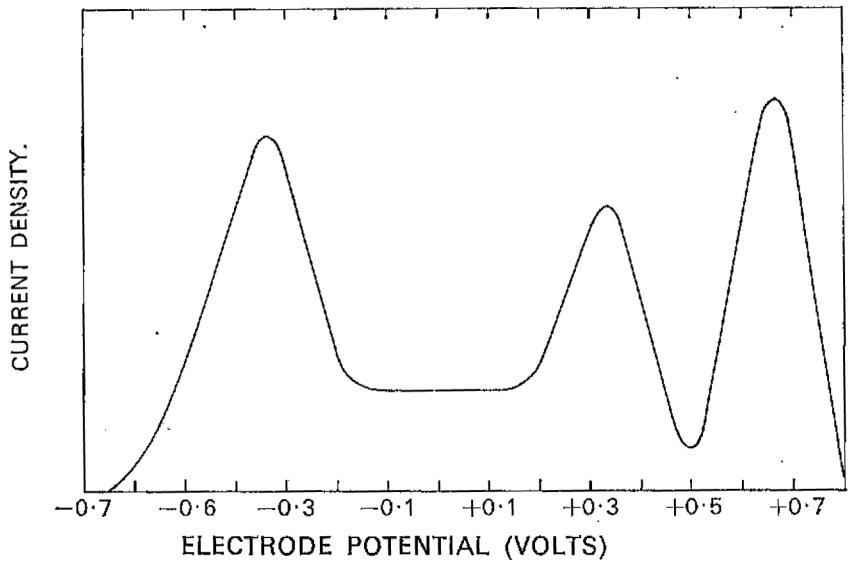

Figure 2-13: Polarization curves for a gold electrode showing passivation in cyanide solutions after Cathro and Koch (1964) (Finkelstein, 1972)

In practised gold leaching situations in the presence of contaminants the anodic gold oxidation by cyanide changes its behaviour, as presented in Figure 2-14. The anodic current of gold and a gold/silver alloy at 0 and 500 min^{-1} are comparatively plotted. The typical passivation of gold, as shown in Figure 2-13, is evident for the pure gold samples, but once silver is present either no passivation or a weaker development of the first passivation peak can be seen (M. Massoud Aghamirian, 1997). Similar results, with a disappearance of passive effects from pure gold to gold/silver alloys can be seen in Figure 2-15.

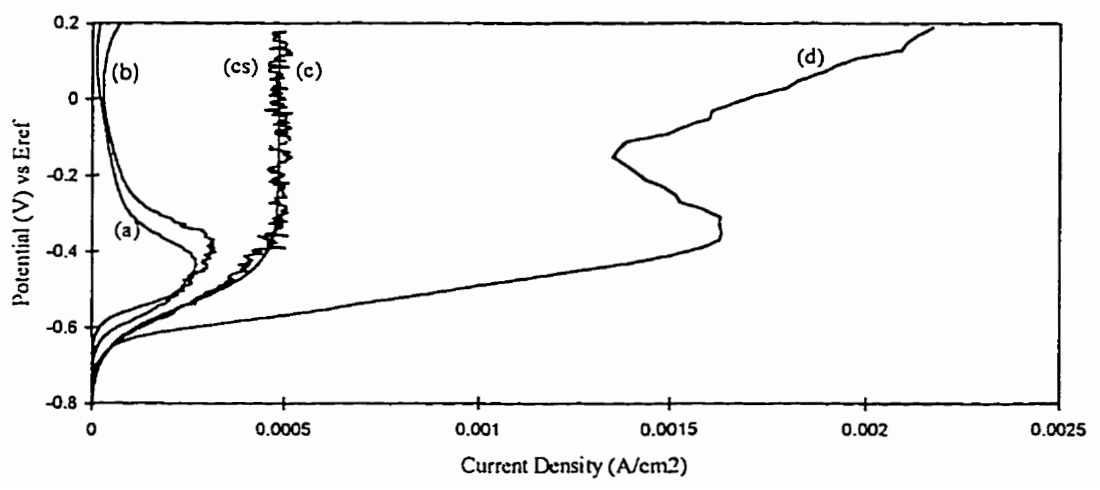

Figure 2-14: Anodic polarization plots of 100% Au at 0 min^{-1} (a) and 500 min^{-1} (b), and 99.7% Au/0.31% Ag at 0 min^{-1} (c) (cs is a simulated estimation of the current development) and 500 min^{-1} (d), pH 10.5, 24°C, initial NaCN conc. 0.01 M, scan rate 0.2 mV/s (M. Massoud Aghamirian, 1997)

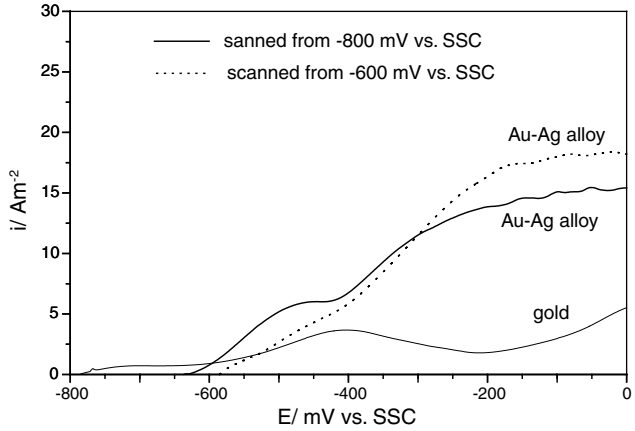

Figure 2-15: Comparative anodic polarization behaviour of gold and a gold–10% silver alloy in a deaerated cyanide solution containing 500 mg/l CN^-, 0.1 M $KClO_4$, with a pH = 11, at a temperature of 298 K. Potential scanning was done from an initial potential of either -800 or -600 mV, as indicated, to 0 mV at a sweep rate of 1 mV/s (Cerovic et al., 2005)

These observations for gold/silver alloys are also similarly applicable for solution based silver, as can be seen in Figure 2-16, where a silver concentration in solution of 1 ppm significantly removes the first passivation peak that can be observed for pure gold (Cerovic et al., 2005). At potentials above -100 mV the gold oxidation curve plateaus due to the reaction becoming cyanide diffusion limited.

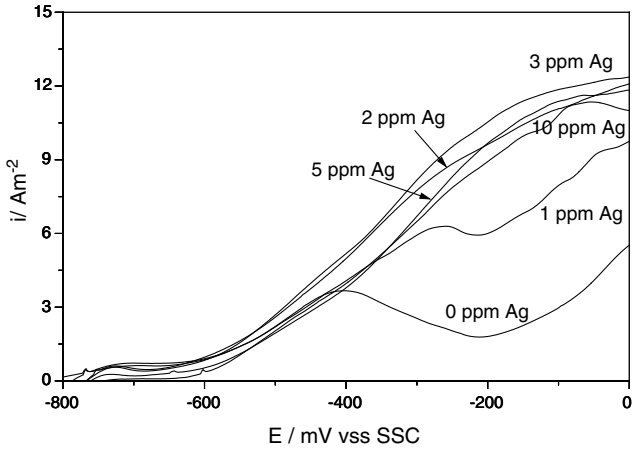

Figure 2-16: Influence of silver nitrate additions on the anodic polarization behaviour of gold in a deaerated cyanide solution containing 500 mg/l CN^-, 0.1 M $KClO_4$, with a pH = 11, at a temperature of 298 K. Potential scanning was done from an initial potential of -800 to 0 mV at a sweep rate of 1 mV/s (Cerovic et al., 2005)

Cathodic reaction

The cathodic reduction of oxygen on the gold surface does not exhibit passive regions, as observed for the gold oxidation in pure solutions. Figure 2-17 shows typical oxygen reduction curves of gold for different rotation rates. It can be seen, that depending on the rotation rate and therefore the diffusion rate the currents reach certain limiting plateaus at potentials below -600 mV vs. SCE (Guan & Han, 1994). Similar shaped curves were obtained by Matthew Ian Jeffrey (1997) as shown in Figure 2-18, however, the maximum currents measured are higher as the solutions used were oxygen instead of air saturated. Matthew Ian Jeffrey (1997) also presents oxygen reduction on silver in this figure, which shows larger currents in more positive potential regions, however, the diffusion limiting values are similar.

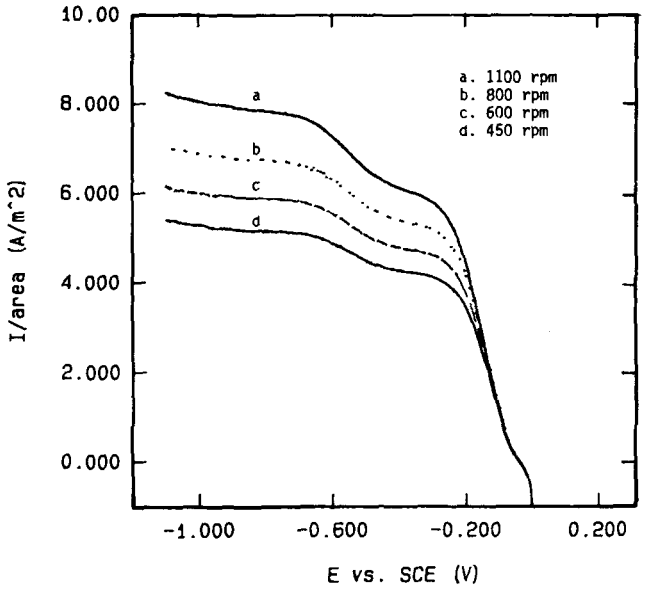

Figure 2-17: Potentiodynamic cathodic polarization plots for the reduction of oxygen on a pure gold electrode at four different disc-rotation speeds. Temperature 25°C, oxygen partial pressure 21.283 kPa, and pH 11.0 (Guan & Han, 1994)

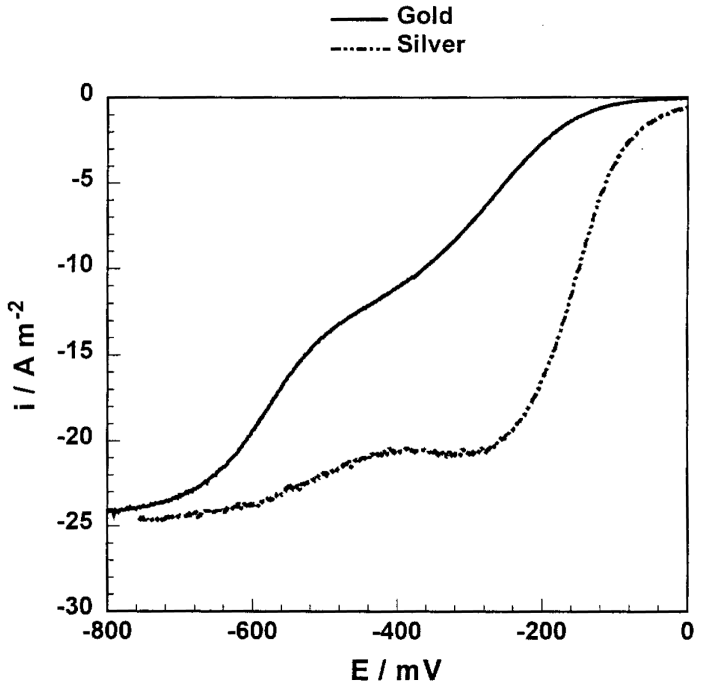

Figure 2-18: Oxygen reduction on gold and silver. Experimental conditions: oxygen saturated solutions, pH 10.0, 1 mV s^{-1}, 25°C, 300 min^{-1} (Matthew Ian Jeffrey, 1997)

Besides the rotation speed and the oxygen saturation in solution, Matthew Ian Jeffrey (1997) found that pH and temperature can have an impact on the oxygen reduction abilities of gold.

The oxygen reduction on gold can also be influenced by the solids in the pulp. The oxygen reduction on gold in a pulp containing some sulphide minerals is shown in Figure 2-19. It is evident, that different minerals can have an enhancing or detrimental effect on the oxygen reduction of gold. For galena the enhancing effect was accounted for by the electrocatalytic influence of deposited or into the double layer adsorbed lead ions on the gold. Similar mechanisms are thought to be the cause behind the negative effect seen by stibnite (Sb deposition) (M. Massoud Aghamirian, 1997).

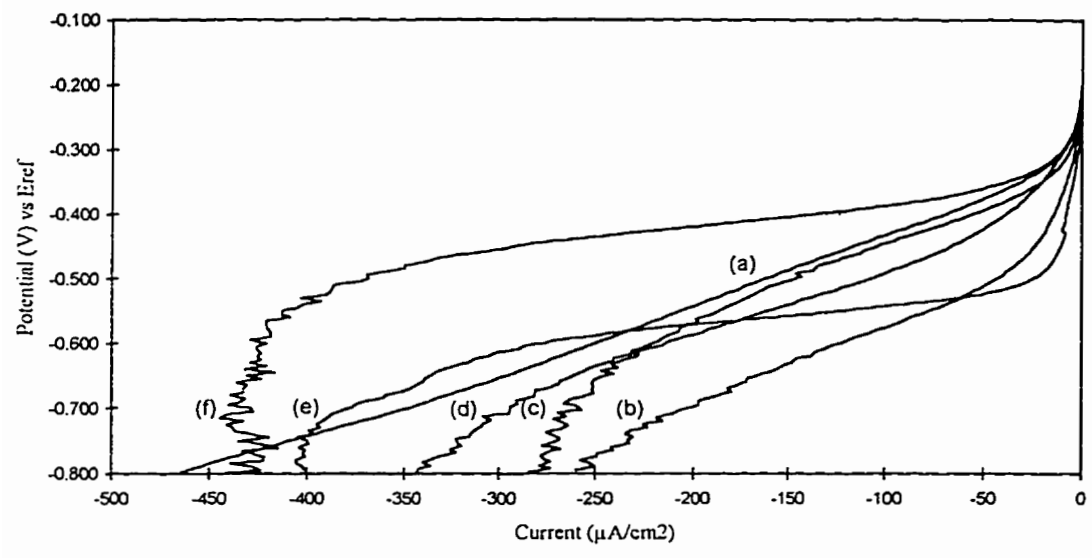

Figure 2-19: Oxygen reduction voltammograms for gold electrode in the absence and presence of different minerals, pH 10.5, scan rate 0.5 mV/s, rotation speed 500 min^{-1}, mineral concentration 8 g/L. Minerals were: a) no mineral, b) with pyrhotite, c) with pyrite, d) with chalcopyrite, e) with stibnite, and f) with galena (M. Massoud Aghamirian, 1997)

Summary

The cathodic and anodic reactions of gold and gold/silver alloys in cyanide and non-cyanide solutions are highly dependent on the purity of the metal and the solutions used. Further, the reactant concentrations play a major role in the magnitude and shape of the voltammograms. The solids composition of the ore can also influence

the reactions. Therefore, only under exactly replicated conditions are results fully comparable.

2.5.5 Potential scans on sulphide-minerals

Various researchers (M. M. Aghamirian & Yen, 2005; Biegler et al., 1975; Rand, 1977) have investigated the oxygen reduction on sulphide minerals with potentiodynamic methods and have shown the ability of conductive sulphide minerals to act as surface sites for oxygen reduction. It was found, that with repeated testing some minerals develop a passive layer which in turn reduces the oxygen reduction ability. As some minerals also react with cyanide the anodic reaction was also investigated.

Cathodic reaction

Figure 2-20 compares the ability of some selected minerals for oxygen reduction currents during potention of the surface with that achieved on gold. It is shown, that some minerals can surpass the oxygen reduction currents achieved on a gold surface for certain potential ranges (M. Massoud Aghamirian, 1997).

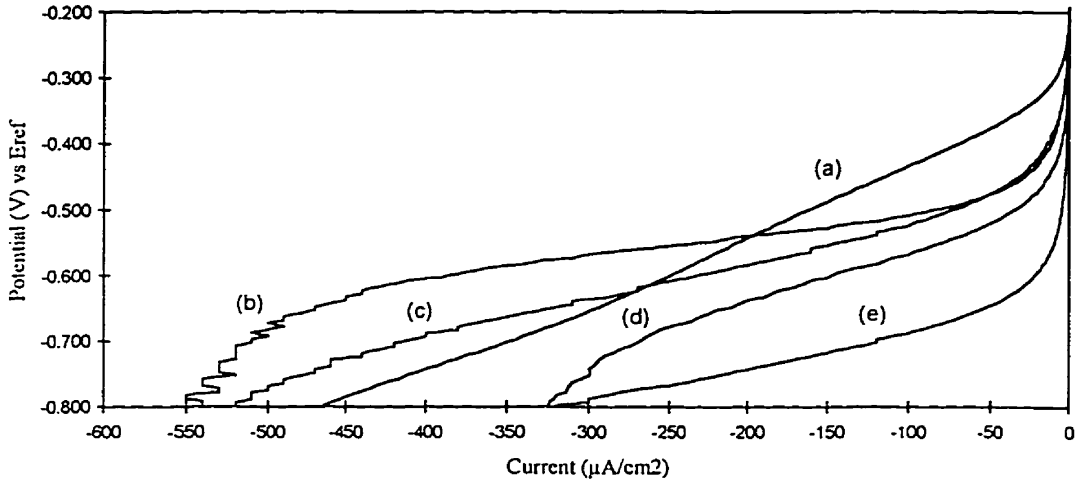

Figure 2-20: Oxygen reduction voltammograms for a) gold in alkaline solutions (no cyanide) and different mineral electrodes in alkaline cyanide solutions, pH 10.5, scan rate 0.5 rnV/s, rotation speed 500 min^{-1}. Electrodes were: b) pyrite, c) pyrrhotite, d) chalcopyrite and e) galena, initial NaCN concentration 0.5 g/L (M. Massoud Aghamirian, 1997)

As demonstrated by M. Massoud Aghamirian (1997) mineral surfaces are capable of oxygen reduction. Figure 2-21 presents the oxygen reduction of an industrial ore (MRI-1) and pyrite (MRI-2) and a gold/silver alloy. It is evident, that the industrial ore and relatively pure pyrite exhibit large oxygen reduction capabilities (Azizi et al., 2010).

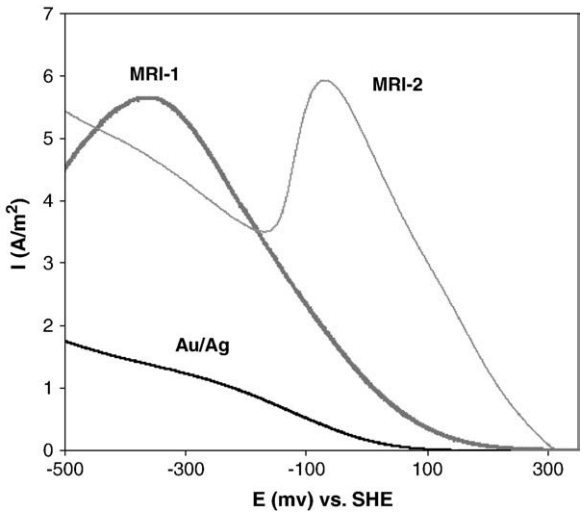

Figure 2-21: Cathodic voltammograms of Au/Ag, MRI-1 and MRI-2 electrodes; CN^- = 0 mmol/L, DO_2 = 0.25 mmol/L, $\Delta E/\Delta t$ = 0.5 mV/s, electrode rotation rate = 500 min^{-1}, pH = 11 (Azizi et al., 2010).

Anodic reaction

Azizi et al. (2010) investigated the oxidation of this same industrial ore and pyrite in cyanide solutions. Figure 2-22 presents the potential scans. It is evident, that the gold/silver cyanide reaction is preferential over the ore reactions for typical cyanidation potential regions.

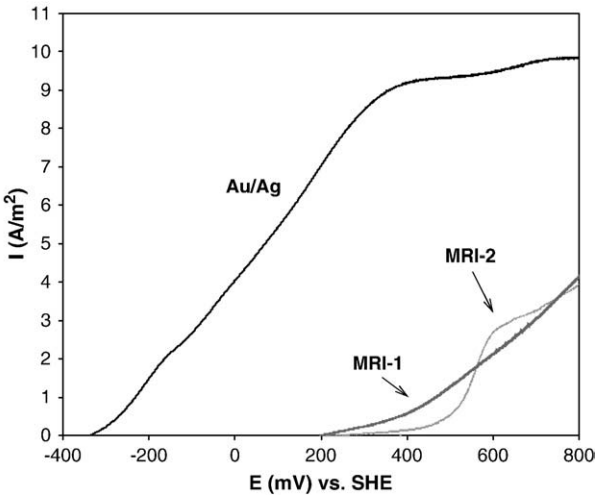

Figure 2-22: Anodic voltammograms of Au/Ag, MRI-1 and MRI-2 electrodes; CN^- = 10 mmol/L, DO_2 = 0 mmol/L, pH = 11, $\Delta E/\Delta t$ = 0.5 mV/s, electrode rotation rate = 600 min^{-1} (Azizi et al., 2010).

Summary

Even though extensive effort was made by researchers investigating mineral behaviour under an oxygen atmosphere, it was usually focused on mineral oxidation, not oxygen reduction on minerals. The most common conductive sulphide minerals readily reduce oxygen under typical cyanidation conditions, which also occurs when the minerals are in ore mixtures. Only very little oxidation of these sulphide minerals takes place under the same conditions.

2.5.6 Open circuit potential in gold leaching

As outlined in Section 2.5.4, the anodic and cathodic reactions of gold are dependent on a range of variables: cyanide concentration, oxygen concentration, pH, and purity of the gold and solution. As a result of this, the OCP under any leaching condition is specific to the particular leaching condition present. In Figure 2-23 a further factor having an impact on the gold oxidation reaction is shown: electroplated gold versus solid gold. A higher reactivity of electroplated gold can be noted. As a result a change in the OCP (marked by the two dots on the intersecting points) can be noted. This change in OCP also coincides with a change in leaching current and therefore leaching speed.

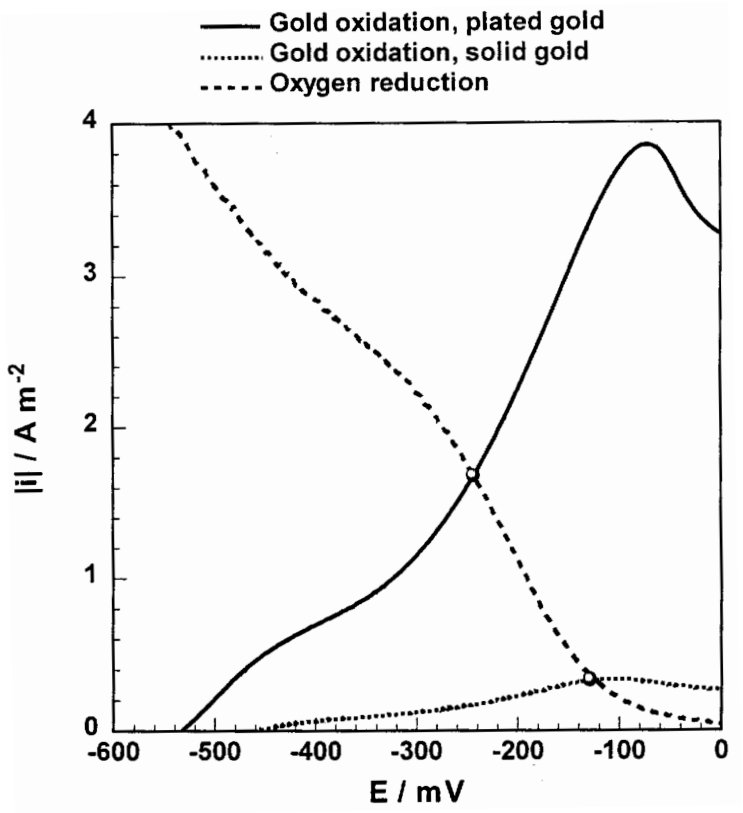

Figure 2-23: Evans-diagram representing the leaching of plated and solid gold in air saturated 20 mM sodium cyanide. Experimental conditions: pH 10.0, 25°C, 300 min^{-1} (Matthew Ian Jeffrey, 1997).

Another impact on the OCP can be oxidants, such as hydrogen peroxide in solution. Typical OCP's observed during aerated or oxygenated cyanide leaching of pure gold are in the range of -400 to -250 mV vs. standard hydrogen electrode (SHE). However, Guzman et al. (1999) observed, that in the presence of hydrogen peroxide the OCP of gold in cyanide solution can change, as shown in Figure 2-24 (results reported vs. Ag/AgCl electrode in the figure). This change in electrode potential to these higher potentials in the presence of hydrogen peroxide was thought to cause a reduction in leach rate, as it takes the surface potential to passive and transpassive regions, as outlined in Section 2.5.4.

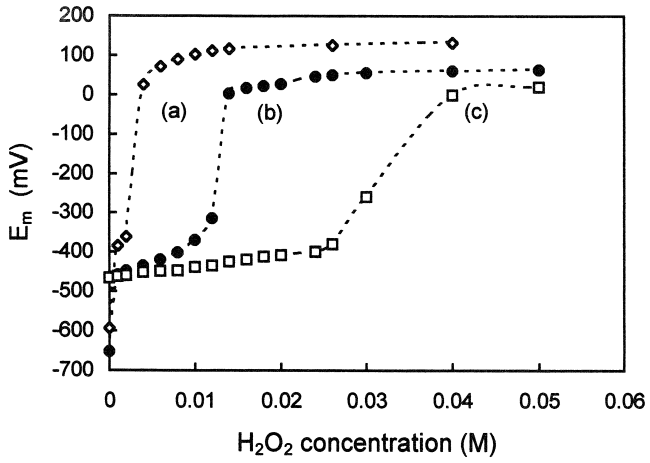

Figure 2-24: Effect of hydrogen peroxide concentration on the rate and mixed potential of cyanidation at different cyanide concentrations. Experimental conditions: 0.21 atm p_{O2}, 400 min^{-1} and 25°C; (a) 0.01 M NaCN, pH 10; (b) 0.02 M NaCN, pH 11.5; (c) 0.02 M NaCN, pH 12.87 (Guzman et al., 1999).

2.6 Conclusions

The fundamentals of gold leaching in cyanide solution were reviewed and a thorough understanding of the process was established from previous researchers. The involvement of peroxide in leaching as a part of the two-step oxygen reduction is clearly proven. No exact quantification of the enhancing effects of peroxide was found.

As peroxide is also an oxidant, the oxidation of cyanide by peroxide was reviewed, with differing results found, depending on the availability of catalysing ions.

Significant effort was made by other researchers to determine the best test method for kinetic experiments, short and long term, with RDE geometry experiments indicated as providing the most repeatable results. However, an advanced RDE method, REQCM, gives the same repeatability with a significantly faster turnaround time and less analytical requirements. A number of factors influencing kinetics in clean solution were determined: oxidant availability (O_2, air, H_2O_2, etc.), cyanide availability, contaminants (S^{2-} ions, Sb, etc.) and catalysts to remedy the influence of these contaminants. Hydrogen peroxide was found to oxidise sulphide ions in solution and typical oxidation pathways are shown.

The usually negative influence of ore material and typical resulting ions in solution, particularly sulphides, were investigated. However, little detail on the possible impact of hydrogen peroxide is available.

Some sulphide minerals are electrically conductive, with previous work showing impact of galvanic coupling, with gold in separated as well as the same solution, varying from strongly enhancing to significantly hindering of gold leaching for various minerals and solutions. This has also been investigated electrochemically, determining the ability of minerals for oxygen reduction and mineral oxidation with cyanide. The influence that hydrogen peroxide could have on such galvanic interaction processes was not available in the literature.

Laboratory investigations offer the ability to produce important insights into fundamental, separate processes taking place but do not offer complete answers to the resulting conditions in ore-leaching, as the systems present are very complex. Hydrogen peroxide was shown to be beneficial in ore leaching in the so called PAL as well as the CIPAL process, but no fundamental explanation of the gains were given in the literature. Further, it appears that no standard procedure to determine the effectiveness of pre-treatments or leaching conditions is currently available. Every laboratory appears to be using variations of two main processes: the more common bottle rolls and stirred tank tests.

Chapter 3 Experimental Methods

The materials and common methods used for this study are described in detail in this chapter. The first subsection lists all materials and reagents used, the second subsection describes the preparation of solutions, and the third subsection gives a description of all apparatus used. In the fourth subsection the experimental methods and methodologies applied during this study are explained and the final subsection details all analytical methods deployed for the experimental data collection.

3.1 Materials and reagents

All reagents, minerals and materials used throughout this study are listed in Table 3-1. All chemicals were used without further purification.

Table 3-1: Reagents, minerals and materials used

Reagent/Material	Purity (%)	Supplier
$(COOH)_2 \bullet 2H_2O$ (oxalic acid)	> 99	Sigma Chemicals
0.45 µm, 47 mm diameter vacuum filter paper – Supor 450		Pall Life Sciences
10 µm alumina polishing powder	> 99.5	Sigma-Aldrich
Acetonitrile HiPerSolv Chromanorm	> 99.9	VWR BDH Prolab
AGAR gel (AGAROSE)		Sigma Aldrich
$AgNO_3$ (silver nitrate)	> 99.9	Rowe Scientific
Air - compressed		Compressed air system on site
Ar gas		BOC gases
Au disc electrode (17.1 mm diameter)	100% Au	Manufactured by CSIRO staff
Au disk electrode (2% Ag) (15.1 mm diameter)	98% Au, 2% Ag	Manufactured by CSIRO staff

Au disk electrode (2% Ag) (6 mm diameter)	98% Au, 2% Ag	Manufactured by CSIRO staff
Conductive epoxy		CW Circuit Works
$CuSO_4$	≥ 99	Sigma-Aldrich
Cr disk for sputtercoating	N/A	BalTec
H_2O_2 (hydrogen peroxide)	50 w/w %	EVONIK Industries
H_2SO_4 (sulphuric acid)	95-98	Sigma-Aldrich
Insulating varnish MR8008		Electrolube
K_2CO_3 (potassium carbonate)	> 99.5	Rowe Scientific
$KAg(CN)_2$ (potassium silver cyanide)	54% Ag	Johnson Matthey
$KAu(CN)_2$ (gold cyanide)	68.3% Au	Johnson Matthey
KCl (potassium chloride)	> 99.8	Ajax Finechem Pty Ltd
KCN (potassium cyanide)	> 97.0	Sigma-Aldrich
KSCN 0.1 M titration standard	0.0999 M, 0.2% accuracy	VWR International
$KMnO_4$ (potassium permanganate)	99-100.5	Ajax Finechem
KSCN (potassium thiocyanate)	> 99	VWR BDH Prolab
Mild Steel Mill Rods 25 x 285 mm	N/A	N/A
Mineral disc electrodes (various surface areas, including pyrite, chalcopyrite, arsenopyrite)	N/A	Manufactured by CSIRO staff from mineral specimens
$MnSO_4 \bullet H_2O$ (manganese sulphate)	98-101	Ajax Finechem Pty Ltd
N_2 gas		BOC gases
$Na_2S \bullet 9H_2O$ (sodium sulphide)	> 98	Sigma-Aldrich
Na_2SO_3 (sodium sulphite)	> 98	Ajax Finechem Pty Ltd
Na_2SO_4 (sodium sulphate)	> 99	Sigma-Aldrich
$NaAsO_2$ (sodium arsenite)	>99	Sigma Chemicals
$NaClO_4$ (sodium perchlorate)	> 98.0	Fluka Analytical
NaCN (sodium cyanide)	> 95.0	Merck

$NaHCO_3$ (sodium bicarbonate)	> 99.7	Ajax Finechem Pty Ltd
NaOH (sodium hydroxide)	> 97	Sigma-Aldrich
NaOH solution HPLC grade	50-52	Fluka Analytical
$NaS_2O_3 \bullet 5H_2O$ (sodium thiosulphate)	99.5-101	Rowe Scientific
$NiSO_4$ (nickel sulphate)	99	Sigma-Aldrich
O_2 gas		BOC gases
pH 10 standard buffer solution	pH 10 ± 0.05	Rowe Scientific
pH 7 standard buffer solution	pH 7 ± 0.02	Rowe Scientific
PTFE (polytetrafluorethylene) thread tape		Kinetic
Pressure filter paper, 330 mm diameter – FP1050		HV
Pt disk for sputtercoating		BalTec
Pt wire	99.95	Johnson Matthey
Silicone – silicone rubber compound – flowable		RS

3.2 Solution preparation

All solutions were prepared from de-ionised (DI) water, except when otherwise indicated, following the procedures described in the following sections.

3.2.1 Hydrogen peroxide (H_2O_2) solutions (low concentration)

Low concentration solutions (1-2 w/w %) of hydrogen peroxide (H_2O_2) were prepared as needed by dilution of industrial grade (50 w/w %) H_2O_2 with water. The dilute solutions were then analysed for their concentration by potassium permanganate ($KMnO_4$) titration, described in Section 3.5.1.2. H_2O_2 dosage volumes

throughout the tests, where used, were adjusted according to the determined concentration.

3.2.2 Sulphuric acid (H_2SO_4) solution (~30%)

Dilute sulphuric acid (H_2SO_4) was made from concentrated (98%) H_2SO_4 by dilution with water. The required amount of water was added into a beaker with a stirrer bar. Under constant stirring, the required amount of concentrated H_2SO_4 was slowly added to ensure no overheating of the solution due to the exothermic heat of dilution.

3.2.3 Manganese sulphate solution ($MnSO_4$) (1 M)

The appropriate amount of manganese sulphate ($MnSO_4$) was weighed into a volumetric flask and dissolved in water. The flask was then filled to the required volume.

3.2.4 Sodium cyanide (NaCN) solution (1 M)

1 M sodium cyanide (NaCN) solutions were prepared by weighing the appropriate mass of NaCN and adding it into a volumetric flask. The flask was then filled to the mark with water. The solution concentration was confirmed by silver nitrate titration, as described in Section 3.5.1.1, and if needed more NaCN was carefully added and a further titration step took place. Upon complete dissolution the solutions were transferred into a storage bottle for subsequent use.

3.2.5 Sodium cyanide (NaCN) solution (various low concentrations)

Several different sodium cyanide (NaCN) solutions were prepared. All solutions were prepared with the addition of 0.01 M sodium bicarbonate ($NaHCO_3$) for pH buffering. Some contained 0.2 M sodium perchlorate ($NaClO_4$), as an electrolyte. The required amounts of $NaHCO_3$ and $NaClO_4$ were weighed out and added into a volumetric flask with water. The required amount of 1 M NaCN solution, as

described in Section 3.2.4 was added with an automatic pipette to the volumetric flask and the flask volume made up close to the mark with water. The pH was measured with a pH-meter, as described in Section 3.3.3, and adjusted to pH 10.5 with the drop wise addition of 1 M NaOH solution, as described in Section 3.2.7. Then the volumetric flask was filled to its mark and mixed appropriately. The resulting solution was put into a storage bottle for subsequent use. The concentration of each solution was confirmed by potentiometric silver nitrate titration, as described in Section 3.5.1.1, and if necessary corrected by a further addition of NaCN solution.

3.2.6 Electrolyte solution

An electrolyte/pH buffer solution was prepared by weighing in the appropriate amounts of the required reagents to obtain the following solution concentrations: 0.2 M $NaClO_4$ and 0.01 M $NaHCO_3$. The reagents were added into a volumetric flask and water was added. Then the pH was adjusted to 10.5 by drop wise addition of 1 M NaOH with continuous measurement with a pH-meter, as described in Section 3.3.3. Once the correct pH was reached, the flask was filled to the mark and the solution then transferred into a storage bottle for subsequent use.

3.2.7 Sodium hydroxide (NaOH) solutions (1 and 0.1 M)

1 M and 0.1 M sodium hydroxide (NaOH) solutions were prepared by weighing the appropriate mass of NaOH and slowly adding it into a half filled volumetric flasks, to let the heat dissipate. Upon complete dissolution, the water was made up to the mark in the volumetric flasks and the solutions were transferred into appropriate bottles for storage and subsequent use.

3.2.8 Potassium cyanide gold/silver electroplating solution

Gold-silver electroplating solutions were prepared to generate a 98 % Au and 2 % Ag alloy, when used for electroplating as detailed in Section 3.4.2. The solutions were made up, using MilliQ (ultrapure) water, in a volumetric flask to 0.02 M

potassium dicyanoaureate ($KAu(CN)_2$), 0.23 M potassium cyanide (KCN), 0.086 M potassium carbonate (K_2CO_3), and 0.0002 M silver nitrate ($AgNO_3$). The $AgNO_3$ was added as 0.001 M solution, as described in Section 3.2.11, for more accurate addition. The concentrations of gold and silver in the solutions were confirmed by atomic absorption spectrophotometry (AAS) analysis, as described in Section 3.5.2, and if necessary corrected by further addition of $KAu(CN)_2$, and $AgNO_3$.

3.2.9 Potassium cyanide gold electroplating solution

Gold electroplating solution was prepared to generate a 100 % Au surface, when used for electroplating. The solution was made up, using MilliQ water, in a volumetric flask to 0.02 M potassium gold cyanide ($KAu(CN)_2$), 0.23 M potassium cyanide (KCN), 0.086 M potassium carbonate (K_2CO_3).

3.2.10 Potassium cyanide silver electroplating solution

Silver electroplating solution was prepared to generate a 100 % Ag surface, when used for electroplating. The solution was made up, using MilliQ water, in a volumetric flask to 0.02 M potassium silver cyanide ($KAg(CN)_2$), 0.23 M potassium cyanide (KCN), 0.086 M potassium carbonate (K_2CO_3).

3.2.11 Silver nitrate ($AgNO_3$) solution (0.01 and 0.001 M)

Silver nitrate ($AgNO_3$) solutions were made by weighing out the required amount of $AgNO_3$ and dissolving it in water. To ensure the correct volume of water was used, the dissolution took place in a volumetric flask. The concentration of the solutions was confirmed by three potentiometric endpoint titrations against 0.1 M KSCN titration standard. If required, the $AgNO_3$ concentration was adjusted by either dilution or a further addition of $AgNO_3$.

3.2.12 Sodium arsenite ($NaAsO_2$) solution (0.03 M)

A 0.03 M sodium arsenite ($NaAsO_2$) solution was made in a 1 L volumetric flask, by weighing in exactly 3.89 g of $NaAsO_2$ powder and adding water. 59.8 mL of 1 M NaOH solution, as described in Section 3.2.7, was added before topping the flask up to the mark with water. This was done to ensure that all cyanide solutions treated with this solution would not release any HCN gas. The solution was used during the day out of the volumetric flask. Once $NaAsO_2$ is dissolved in water, it dissociates to Na^+ and AsO_2^-. This in turn forms $H_2AsO_3^-$, according to Equation 3-1.

$$AsO_2^-(aq.) + H_2O \rightleftarrows H_2AsO_3^-(aq.) \qquad \text{Equation 3-1}$$

3.2.13 Sodium sulphide (Na_2S) solution (~0.5 M)

Sodium sulphide (Na_2S) solutions were made up by weighing out the required amounts of $Na_2S{\bullet}9H_2O$ and dissolving it in water. As $Na_2S{\bullet}9H_2O$ is strongly hydrophilic and oxidises easily, the concentration of the prepared solution was confirmed by silver nitrate titration, as described in Section 3.5.1.1, prior to each use. The volume added to achieve the target concentration in experimental solutions was varied according to the measured concentration.

3.2.14 Potassium permanganate solution (0.02 M)

Potassium permanganate ($KMnO_4$) solution was prepared by adding an exact amount, weighed in to achieve a 0.02 M concentration, of $KMnO_4$ salt into a volumetric flask. Water was added to the flask and the flask was agitated for an extended period of time, to achieve complete dissolution. After the dissolution was completed, the flask was filled to the mark with water.

The potassium permanganate solution was standardised monthly, if used frequently, or prior to use, using the oxalic acid method, as described in the literature (Mar, 1995), using H_2SO_4 solution as described in Section 3.2.2. The concentration result

of the standardisation was noted on the $KMnO_4$ storage bottle and used for subsequent calculations.

3.2.15 High pressure liquid chromatography (HPLC) solutions

All solutions used for HPLC, which are pumped through the separation columns were prepared from MilliQ water and using HPLC grade reagents, where available. All other solutions were prepared with DI water and laboratory grade reagents. For each solution the required amount of reagents was exactly weighed in or metered with an automatic pipette and added into a volumetric flask. The flask was then filled to the mark with water. The solutions were then transferred into the respective reservoir of the HPLC units. The solutions prepared are listed in Section 3.5.4.

3.2.16 Atomic absorption spectroscopy (AAS) standards

Concentrated solutions (1000 ppm) of Au, Cu and Ni were made by dissolving exact amounts of $KAu(CN)_2$, $CuSO_4$, and $NiSO_4$ in water with 0.5 M NaCN and 0.01 M NaOH in a volumetric flask. The flasks were topped up to the mark with water. From these solutions, exactly calculated subsamples were introduced into volumetric flasks to achieve the exact standards concentrations required for calibrating the AAS. NaCN was added to the standards to achieve a 10 mM concentration and prior to topping the flask up to the final volume, the pH was adjusted to pH 10.5 with 0.01 M NaOH solution, as described in Section 3.2.7. The Ag standards were made in a similar manner, but utilising standardised 0.001 M $AgNO_3$ solution, as described in Section 3.2.11, as the Ag source. The concentrations of solutions made are shown in Section 3.5.2.

3.3 Apparatus

3.3.1 Electrochemical apparatus and set-up

The electrochemical equipment used to conduct all electrochemical measurements for this study was a Radiometer Copenhagen PGP201 Potentionstat/Galvanostat. The potentiostat was controlled and the data was collected by a MS-DOS based computer system with a QBasic program. All further equipment used in conjunction with the potentiostat is described in the following subsections of Section 3.3.1.

3.3.1.1 Rotating electrode quartz crystal microbalance (REQCM)

The REQCM is a further development of the electrode quartz crystal microbalance (EQCM), which is commercially available and has been used in many studies for adsorption and decomposition processes (M. I. Jeffrey et al., 2000). The EQCM is a stationary, oscillating quartz crystal. Depending on the piezoelectrically active area, A_p, the shear module, μ_q, of the quartz, its density, ρ_q, and the resonating frequency, f_0, according to the Saurbrei equation (Equation 3-2), there is a good relation between Δf and the mass change, Δm, of the quartz crystal.

$$\Delta m = \frac{-A_p(\mu_q \rho_q)^{0.5} \Delta f}{2 f_0^2} \qquad \text{Equation 3-2}$$

The same principle applies for the REQCM, but the electrode is mounted so that it can be rotated, and as a result it is a combination of an RDE and the EQCM. The main benefit of the rotating electrode is, that due to predictable reactant flow to and across the surface of the electrode, according to the Levich equation (Equation 3-3), it can be easily determined whether a heterogeneous reaction is diffusion or chemically controlled. In Equation 3-3 J_0 is the flux of the species O in solution, D_0 the diffusion coefficient of the species O in the solution, ν the kinematic viscosity of the solution, ω the rotation rate, and $[O]$ the bulk solution concentration of the species O.

$$J_0 = 0.62 D_0^{2/3} \nu^{-1/6} \omega^{1/2} [O]$$ Equation 3-3

In Figure 3-1 a simplified sketch of an REQCM assembly is shown. It shows the main parts of a REQCM. On the rotating shaft the following elements are mounted from top to bottom: drive pulley, electrical sweeping connectors (frequency and working electrode connectors as well as 5 V power supply for the REQCM circuit), the REQCM circuit in steel shielding with lock rings for easy access, if required for trouble shooting or repairs, and the exchangeable electrode assembly at the bottom. The electrode assembly is explained in further detail in the next paragraph.

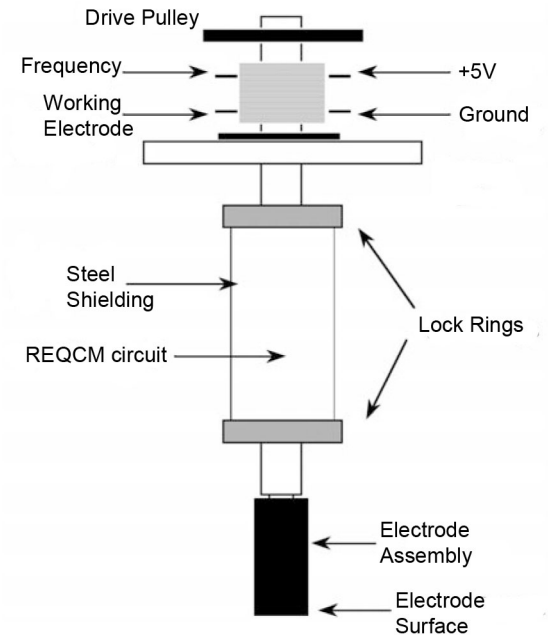

Figure 3-1: REQCM assembly (after M.I. Jeffrey, J. Zheng, & I.M. Ritchie, 2000)

3.3.1.2 The REQCM electrode assembly

The central element of the REQCM electrode is a 10 MHz AT cut quartz crystal, which is mounted in a polyvinyl chloride (PVC) holder. Figure 3-2 shows a schematic of an REQCM electrode assembly.

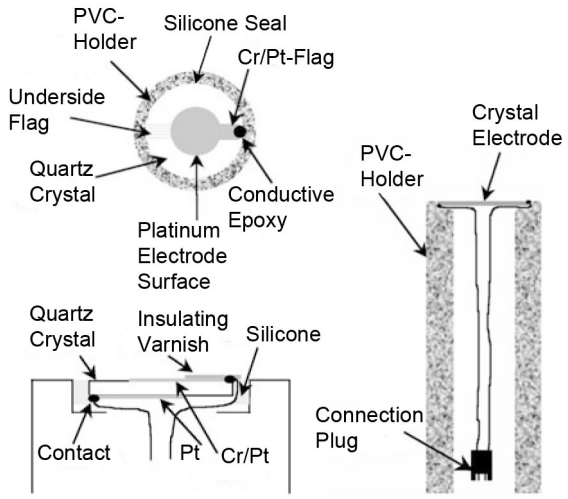

Figure 3-2: REQCM electrode assembly (M.I. Jeffrey et al., 2000)

First, one side of the crystal was sputtered with chrome (the side which will be exposed to solution), and then both sides of the crystal were sputtered with platinum in the shape of a disc with a small flag, using a Baltec SCD050 sputter coating apparatus. Connection wires were glued to the flags each side of the crystal with conductive epoxy resin. Insulating varnish was used to cover the connecting cable ends and flags, so that just a round electrode area stayed exposed. Then the crystals were mounted in the holders and those were sealed with silicone. The exposed platinum area (A) of each crystal was typically 19.6 mm^2. Prior to each leaching experiment, the surface of the electrode was freshly electroplated with either the gold silver plating solution, as described in Section 3.4.2, or silver plating solution made, as outlined in Section 3.2.10. The initial pulse plating current for the gold/silver solution was 250 A/m^2 and the continuous plating current was 25 A/m^2. For the silver plating solution, the initial pulsing current was the same as for gold, however, the continuous plating current used was 50 A/m^2.

3.3.1.3 Rotating disc electrode (RDE)

An RDE arrangement consists of a rotator and an electrode, which is mounted on the rotator. Electrochemical investigations can be conducted if the disk is be made of a conductible material. The main use of RDEs is to conduct voltammetry studies on

different materials in different solutions, as well as leaching kinetic studies. The disadvantage of an RDE over a REQCM for kinetic studies is, that there is no instantaneous measurement of the leached material and therefore leach rate is not available. Only solution sampling and analysis can provide information on leached amounts. This methodology is time consuming and it is difficult to detect rapid initial changes in the leach rate (i.e. formation of a passivation layer), but has the benefit of being able to show long-term effects on leaching kinetics.

The RDE disks used in this study had different surface areas and gold/silver concentrations. Two gold discs with 2% silver content were used with the surface areas of 0.283 cm^2 and 1.791 cm^2, respectively. The pure gold disc used had a surface area of 2.297 cm^2.

3.3.1.4 Auxiliary electrode

The auxiliary electrode was made of a piece of platinum wire 0.5 mm in diameter and 135 mm long. It was coiled and put into the solution.

3.3.1.5 Reference electrode

During this study all potential measurements were carried out using a silver/silver chloride reference electrode (filled with electrode Gel, Model IH-10, IONODE) with a potential of 199 mV (25 °C) against the standard hydrogen electrode (SHE). The electrode usually was in a separate reservoir connected to the electrochemical cell by a Luggin capillary filled with AGAR gel. For the convenience of the reader all potentials reported in this study have been converted to the SHE scale. To obtain the potential in relation to SHE (Eh), from the potential measured with the reference electrode (E), the potential of the reference electrode against SHE($Eh_{Ag/AgCl}$) is added, according to Equation 3-4.

$$Eh = E + Eh_{Ag/AgCl} = E + 199 \quad \text{(mV, at 25°C)} \qquad \text{Equation 3-4}$$

Temperature correction, by the coefficient dE/dT = -1.01 mV K^{-1} for the saturated KCl, Ag/AgCl electrode, was conducted for all other temperatures according to Equation 3-5 (Rieger, 1994).

$$Eh_{Ag/AgCl} = 199 - 1.01(T - 273) \quad (\text{mV}) \qquad \text{Equation 3-5}$$

3.3.1.6 Electrochemical cell

The electrochemical cell is a typical 100 mL water-jacketed glass vessel, which was capable of holding three electrodes, i.e. a working electrode (either RDE or REQCM electrode), a counter electrode and a reference electrode in a separate reservoir connected through a Luggin capillary. The Luggin capillary was fitted through a port in the bottom of the electrochemical cell and ensured separation of the working solution and the reference electrode.

3.3.1.7 Electrochemical system

In Figure 3-3 the electrochemical set-up is shown. When the set-up was used with an RDE solid electrode, a Pine Instruments MSR rotator with speed control rotated the disk. When the REQCM set-up was utilized a rotator with speed control and a matching stand, built in the Monash University Engineering workshop was used. The setup consisted of a glass cell (Section 3.3.1.6) with a Luggin capillary fitted. The Luggin capillary hosted the Ag/AgCl reference electrode (Section 3.3.1.5). The rotator and shaft additionally served as electrical connection for the working electrode. A platinum wire introduced into the solution was used as the auxiliary electrode (Section 3.3.1.4). All electrodes were connected to the potentiostat.

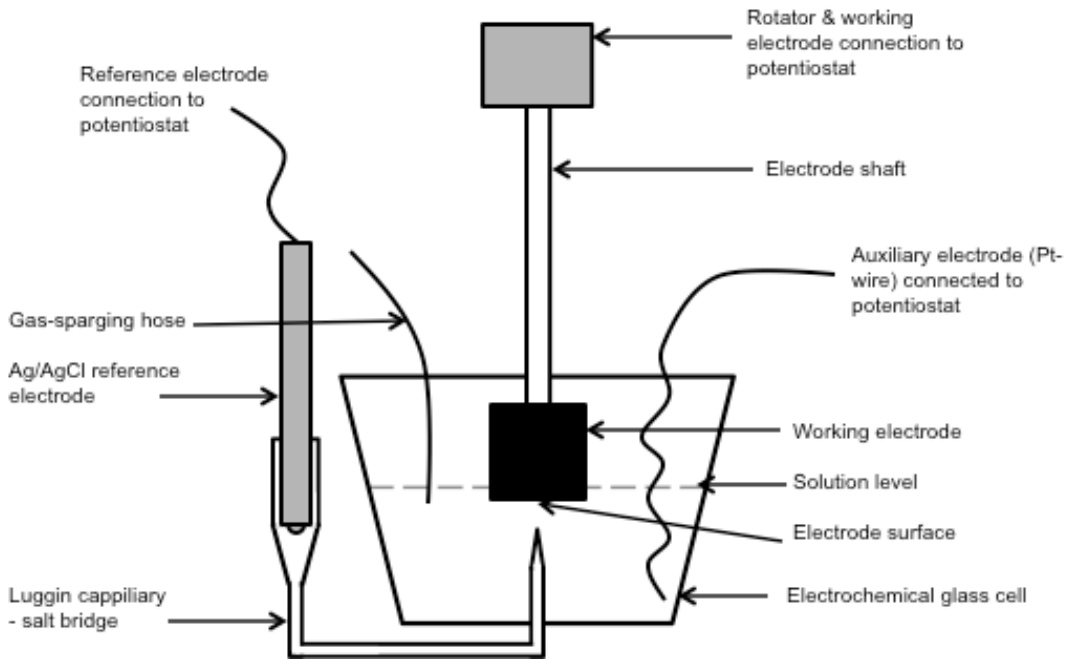

Figure 3-3: Electrochemical cell setup

3.3.2 Dissolved oxygen (DO) meter

The dissolved oxygen meter utilised during the tests was a TPS-W82 with an ED1 probe attached. According to the manual (TPS Pty Ltd, 1998), the unit uses an amperometric type of Clark Electrode and is capable of measuring oxygen pressures in the range of 0 to 100 cm of mercury. The ED1 Clark oxygen electrode consists of a gold cathode and an Ag/AgCl anode, placed in 0.1 M KCl electrolyte. The electrolyte is behind a polyethylene membrane, which allows oxygen diffusion. The electrode system is polarized to about 800 mV. As a result of the polarization, oxygen diffusing through the membrane will be reduced on the gold electrode according to Equation 3-6.

$$O_2 + 2H^+ + 2e^- \rightarrow H_2O_2$$ Equation 3-6

As a result of this reduction, a current is produced through the oxygen electrode. With a thermistor (load resistor) in the electrode this current is converted into a voltage, which is proportional to the oxygen partial pressure. This voltage is

measured by the instrument and converted into a ppm reading and corrected for temperature. The units reading range, if properly calibrated, is 0-20 ppm ± 0.04 ppm.

3.3.3 pH-Meter

A TPS WP-80 pH-meter with a TPS 121207 pH electrode was used for measuring and adjusting the pH of various solutions. The pH-meter was calibrated each day it was used, with buffer solutions of pH 7 and 10, as mentioned in the materials and reagents section, Table 3-1. The units reading range, if properly calibrated, is 0.00-14.00 ± 0.01 pH units.

3.4 Experimental Methods

3.4.1 Theoretical leach rates in rotating disc experiments

Throughout literature, multiple approaches have been taken to calculate theoretical leach rates. The most used calculation for RDE experiments is the Levich equation, shown in Equation 3-7 (Allen J. Bard & Faulkner, 1980; Rand, 1977; Senanayake, 2008). This equation can be used to calculate the flux of reactants to the surface, which then, based on assumed reactions, can be used to derive limiting reaction rates. In the case of cyanide leaching, those reactants are cyanide and oxygen, hence there is a cyanide and an oxygen limiting rate. The factors required to calculate the flux of reactants (J) with the Levich equation are: diffusion coefficient of the reactant (D), rotation rate (ω), bulk liquid viscosity (ν) and bulk reactant concentration ($[O]$).

$$J = 0.62 D^{2/3} \omega^{1/2} \nu^{-1/6} [O] \qquad \text{Equation 3-7}$$

3.4.1.1 Reactant and solution properties for theoretical leach rate calculations

To be able to fully utilise the Levich equation as shown in Section 3.4.1, specific reactant properties, namely the diffusion coefficient, for all involved reactants are

required. Further the bulk liquid viscosity is required, which for this study was assumed as being pure water at 25°C.

Cyanide diffusion coefficient

The cyanide diffusion coefficient of cyanide published by Guan and Han (1994) as $D_{CN} = 2.18 \times 10^{-9}$ m^2 s^{-1} was used by many authors for theoretical calculations of the cyanide limiting rate following the Levich equation. Hence this value is used for all calculations throughout this study.

Oxygen diffusion coefficient

For oxygen in water, the diffusion coefficient published by Guan and Han (1994) as $D_{O2} = 1.94 \times 10^{-9}$ m^2 s^{-1} was used by a range of authors for theoretical calculations of the oxygen limiting rate following the Levich equation. This value is used for all calculations throughout this study.

Hydrogen Peroxide diffusion coefficient

Hydrogen Peroxide diffusion to surfaces has only been investigated on a very limited basis and mainly as a requirement for subsequent experimental steps (Schumb, Satterfield, & Wentworth, 1953; van Stroe-Biezen, Everaerts, Janssen, & Tacken, 1993). Hence, extensive data on hydrogen peroxide diffusion could not be found, except a small array of data points, given on the webpage of a hydrogen peroxide manufacturer (US Peroxide, 2014). This data is presented in Table 3-2 and has been used to extrapolate a diffusion coefficient of hydrogen peroxide at 3 mM. The extrapolated value is 8.72×10^{-10} m^2s^{-1}. Due to this limited amount of information available, the hydrogen peroxide diffusion coefficient used in subsequent calculations has been determined under the existing experimental conditions, as shown in Section 4.2.3.

Table 3-2: Hydrogen peroxide diffusion coefficients after US Peroxide (2014)

H_2O_2 concentration (M)	**Diffusion coefficient (m^2/s) @ 20°C**	**Diffusion coefficient (m^2/s) @ 25°C**
4.78	1.3×10^{-09}	
0.85	1.4×10^{-09}	
0.107	9.7×10^{-10}	
0.011	8.8×10^{-10}	
0.103		1.2×10^{-09}

Kinematic viscosity of water

For the calculations using the Levich equation in this study the kinematic viscosity of water was required. At 25 °C the viscosity of water (μ_{water}) is 0.975 cP and the density of water is (ρ_{water}) is 1 g cm^{-3} (Green & Perry, 2007). The kinematic viscosity of water is calculated according to Equation 3-8 where $\mu = \mu_{water}$ and $\rho = \rho_{water}$ to be $\nu = 9.75 \times 10^{-7}$ m^2 s^{-1} (Green & Perry, 2007). As ν is only used in the Levich equation to the minus one sixth power, this value was considered accurate enough for all calculations.

$$\nu = \frac{\mu}{\rho}$$ Equation 3-8

3.4.2 REQCM − standard electrode preparation for testing

For all REQCM tests the electrodes were freshly plated with the plating solutions, described in Sections 3.2.8, 3.2.9, and 3.2.10. The plating process was conducted at ambient temperature with a rotation speed of 300 min^{-1}. The initial pulse current was set to 250 A/m^2 and applied 2-3 times for approximately 3-5 seconds to create a base layer of the required alloy on the platinum surface of the electrode. Then the remaining alloy to achieve an overall plated mass of 200-300 µg was plated with a

constant current of 25 A/m^2 for all gold containing electroplating solutions and 50 A/m^2 for silver only solution. Upon completion of the plating process the electrodes were removed from the plating solution and rinsed with DI water prior to conducting experiments.

3.4.3 RDE − electrode preparation for testing

Prior to each test the RDE electrodes were first rinsed with demineralised water and then wet sanded on a fresh piece of 1000 grit silicon carbide sandpaper. After sanding the electrodes were rinsed again and then polished with a paste consisting of 10 micron alumina powder and DI water, and then rinsed thoroughly with DI water.

3.4.4 Open circuit potential (OCP) measurement

The open circuit potential, also known as rest potential is the potential of an electrode immersed into a solution without applying any external potential. The mixed potential is determined by all potentials of the anodic and cathodic half reactions occurring on the electrode, with a zero net current flow. As a result of that, the OCP is a so-called mixed potential of all possible reactions on an electrode in a solution. It can be measured under any atmosphere present. In the experiments conducted, the OCP has been measured versus an Ag/AgCl reference electrode. The potentials were measured with a Radiometer Copenhagen PGP201 potentiostat and data was recorded with a QBasic program on a MS-DOS PC.

3.4.5 Voltammetry (Potential scanning)

Voltammetry is a means to investigate electrochemical reactions occurring on conductive surfaces in conductive solutions, including the surface contribution to possible reactions. This is achieved by applying a potential to a working electrode in relation to a reference electrode. The applied potential and resulting current is recorded and plotted, for subsequent analysis. Voltammetry experiments were conducted in an electrochemical cell, as described in Section 3.3.1.6, with a reference

electrode and counter electrode as described in Sections 3.3.1.5 and 3.3.1.4, respectively, connected. All electrodes were connected to a Radiometer Copenhagen PGP201 potentiostat, which was controlled by a MS-DOS computer with a purpose written QBasic program.

3.5 Analytical

All samples taken to obtain data for this thesis were analysed with either standard or standardised methods. All analytical methods applied are detailed in this section.

3.5.1 Titrations

3.5.1.1 Potentiometric endpoint titration for cyanide and sulphide

The potentiometric endpoint titrations to determine CN^- and S^{2-} concentration were conducted using a Metrohm Dosimat TMS 716 Titrando with an Orion 900200 reference electrode and a silver wire as counter electrode. The dosimat was controlled via a MS-Windows based computer, running Metrohm tiamo™ Version 1.1, Build 36. A procedure to control the titration and calculate the NaCN equivalent and S^{2-} concentration in ppm or mM respectively was set up in the tiamo software. The calculations were based on the following inputs: titrant concentration in M, sample volume in mL, the measured titrant dosage in mL associated with the determined endpoint and the molecular weight of NaCN. All data is usually presented as NaCN, as the cyanide was added in the form of NaCN to the tests.

Samples of an accurately measured volume were taken and added into an analysis vial. Then 1-2 drops of 1 M NaOH solution were added to each sample to have all HCN and CN^- available as CN^-, or all Na_2S as S^{2-}. DI water was added to the filling marks on the vials and the vials were mounted in a Radiometer Copenhagen TTA80 Titration Assembly. Then the titration process was initiated on the computer. After completion of the titration the calculated outputs were recorded. Before and after every sample the titration assembly and electrodes were rinsed with DI water.

3.5.1.2 Visual manganometric titration for hydrogen peroxide (H_2O_2)

With a calibrated volumetric pipette a known volume of the H_2O_2 solution was added into an Erlenmeyer flask with approximately 30 mL of water. Then approximately 20 mL of 30% sulphuric acid was added and 5 drops of 1 M $MnSO_4$. This was titrated with a 0.2 M $KMnO_4$ solution until a slight pink colour remained in the solution. The concentration of the H_2O_2 solution can then be calculated according to Equation 3-9, where X is the concentration of the H_2O_2 solution in M, V_S the sample volume and V_T the volume of titrate used, each in mL.

$$X = \frac{V_T * 0.5}{V_S} \quad \text{(M)} \qquad \text{Equation 3-9}$$

3.5.2 Atomic absorption spectroscopy (AAS)

An Agilent Technologies 200 Series AA - 240FS AA atomic absorption unit was utilised to determine concentrations of Au, Ag, Cu, and Ni in cyanide solutions. Atomic absorption spectroscopy works by atomising a sample in an acetylene flame and projecting light through it from a light source with a wavelength specific to the element to be analysed for. The atomised solution and elements absorb this light and based on a calibration curve, the concentration of the element can be determined.
The calibration curve was measured each time prior to running a set of samples (each time the flame had to be restarted) by presenting standards. The standard concentrations used for each element are shown in Table 3-3. If samples were found to be out of the analytical range, they were appropriately diluted and analysed again.

Table 3-3: Detection limits and calibration standards used for AAS

Element	Detection range (mg/L)	Standard 1 (mg/L)	Standard 2 (mg/L)	Standard 3 (mg/L)	Standard 4 (mg/L)	Standard 5 (mg/L)
Gold (Au)	0-50	1	5	10	20	50
Silver (Ag)	0-20	1	2	4	10	20
Copper (Cu)	0-250	10	20	50	100	250
Nickel (Ni)	0-100	5	10	20	50	100

3.5.3 Weak acid dissociable (WAD) cyanide-analyser

An OI Analytical CNSolution FS3100 segmented FIA system cyanide analyser was used for weak acid dissociable (WAD) cyanide concentration analysis. The analyser consists of two analytical segments – one for CN(total) and one for CN(WAD). The segments are usually run simultaneously, so CN(WAD) and CN(total) values are determined at the same time. The unit's operating principle is based on acid addition and UV digestion, which release the cyanide in the sample as hydrogen cyanide. The hydrogen cyanide passes through a membrane into an alkaline solution. The cyanide concentration in this solution is then measured as a current (amperometric detection) and displayed on a computer. The current detected for the samples analysed is related to currents measured for standards, which are taken before any sample analyses. The operating range of the unit is between 50 and 500 ppb of CN(WAD) and CN(total). Because of this samples were diluted to be within this range.

3.5.4 High Pressure Liquid Chromatography (HPLC)

Two HPLC systems were used for the analysis of the following sulphur species: sulphide (S^{2-}), sulphite (SO_3^{2-}), thiocyanate (SCN^-), thiosulphate ($S_2O_3^{2-}$) and

sulphate (SO_4^{2-}). The systems operated with different columns, eluent systems and detectors to determine particular sulphur species in solutions.

All solutions used for HPLC being mentioned in this section were prepared as described in Section 3.2.15. Of all samples presented to either of the HPLC systems, a 1 mL aliquot was added into a sample vial, to which further 0.2 mL of 0.1 M NaOH solution was added. This was done, so all species would be present in detectable form.

System one (HPLC1) consisted of a Waters 2695 Separation Module fitted with a Dionex IonPac AS16 column and matching guard column. The detector used was a Waters 2998 Photodiode Array detector, which is capable of collecting a UV spectrum from 190 to 400 nm. The eluents available for use in the system are listed in Table 3-4.

Table 3-4: Eluents used in HPLC1

Eluent name	Eluent composition
A	MilliQ water (ultrapure water)
B	0.1 M $NaClO_4$, 0.01 M NaCN, 0.001 M NaOH in MilliQ water
C	0.01 M NaOH in MilliQ water
D	0.5 M $NaClO_4$ in MilliQ water

The HPLC1 was operated at an eluent flow rate of 1 mL/min. The eluent composition was controlled by a gradient method with a run time of 25 minutes after each injection of 10 µL. The gradient used a step change in composition at 12 minutes as shown in Table 3-5.

Table 3-5: HPLC1 gradient

Time (min.)	Eluent flow (mL)	Eluent A (%)	Eluent B (%)	Eluent C (%)	Eluent D (%)
0	1	88	2	1	9
12	1	0	2	1	97
19	1	88	2	1	9

Initially standards were run to be able to identify and quantify the expected species. A typical chromatogram obtained with this procedure for a mixed standard containing 1 mM of S^{2-}, SCN^- and $S_2O_3^{2-}$ ions each, is shown in Figure 3-4. The intensity measured is plotted for a 214 nm wavelength, showing the S^{2-}, SCN^- and $S_2O_3^{2-}$ peaks around the 3.5, 6 and 11 minute mark, respectively. Peak area determination for the different species was conducted, at a wavelength for each species, where the peak detected for each species was the most prevalent. This means that S^{2-}, SCN^- and $S_2O_3^{2-}$ peak sizing was conducted at 230, 192 and 214 nm detection wavelength respectively. The obtained peak areas can be directly compared to species concentrations present in the solution.

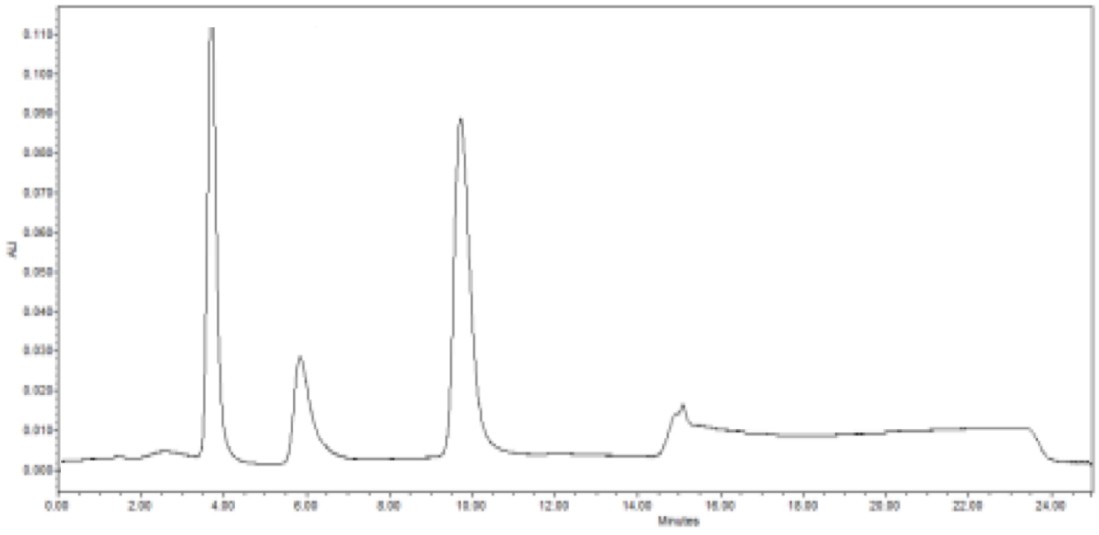

Figure 3-4: Standard mixed UV-chromatogram at 214 nm wavelength for a solution of 1 mM of S^{2-}, SCN^- and $S_2O_3^{2-}$

System two (HPLC2) consisted of a Waters 2695 Separation Module fitted with a Dionex IonPac AS17-C column and two matching guard columns. A Dionex AMMS 300 ion exchange unit was fitted between the separation column and the detector unit array, with the flow directed through the primary side of the ion exchange unit. A constant stream of approximately 10 mL/min of 0.025 M sulphuric acid flowed through the secondary side of the ion exchange column. Two 'Alltech SelectPro™ Fluid Processors' flow switching devices were also fitted into the unit, enabling a flush of the guard columns without interrupting the flow through the separation column. The detectors used were a Waters 2996 Photodiode Array detector, which is capable of collecting a UV spectrum from 190 to 400 nm and a Waters 432 conductivity measurement unit. The eluents used are shown in Table 3-6.

Table 3-6: Eluents used in HPLC2

Eluent name	Eluent composition
A	not used
B	MilliQ water (ultrapure water)
C	0.1 M NaOH in MilliQ water
D	50% acetonitrile in MilliQ water

The gradient method used on HPLC2 was run for 15 minutes after each sample injection. During the method, at the 7.5 minute mark, the two switches are activated, which remove the guard columns from the flow circuit. The guard columns are then rinsed offline with a solution consisting of 0.1 M NaOH and 0.5 mM NaCN until the 15 minute mark. At the 15 minute mark the flow is returned to normal operation, prior to the next injection.

Table 3-7: HPLC2 gradient

Time (min.)	Eluent flow (mL)	Eluent A (%)	Eluent B (%)	Eluent C (%)	Eluent D (%)
0	1	0	89	6	5
2.5	1	0	55	10	35
4.5	1	0	48	17	35
9	1	0	15	50	35
13.5	1	0	89	6	5

Initially standards were run to be able to identify and quantify the expected species. A typical UV-chromatogram obtained with this procedure for a mixed standard containing 1 mM of SO_3^{2-}, SO_4^{2-} and SCN^- ions each, is shown in Figure 3-5. The matching conductivity chromatogram is shown in Figure 3-6. The intensity measured in the UV-chromatogram is plotted at a 192 nm wavelength, showing the SO_3^{2-} and SCN^- peaks around the 8 and 12 minute mark, respectively. In the conductivity chromatogram the SO_4^{2-} peak is visible around the 8 minute mark. Peak area determination for the different species was conducted, at a wavelength for each species, where the peak detected for each species was the most prevalent. This means that SO_3^{2-} and SCN^- peak sizing was conducted at 192 nm detection wavelength, the SO_4^{2-} peak area was determined on the conductivity measurement. The obtained peak areas can be directly compared to species concentrations present in the solution.

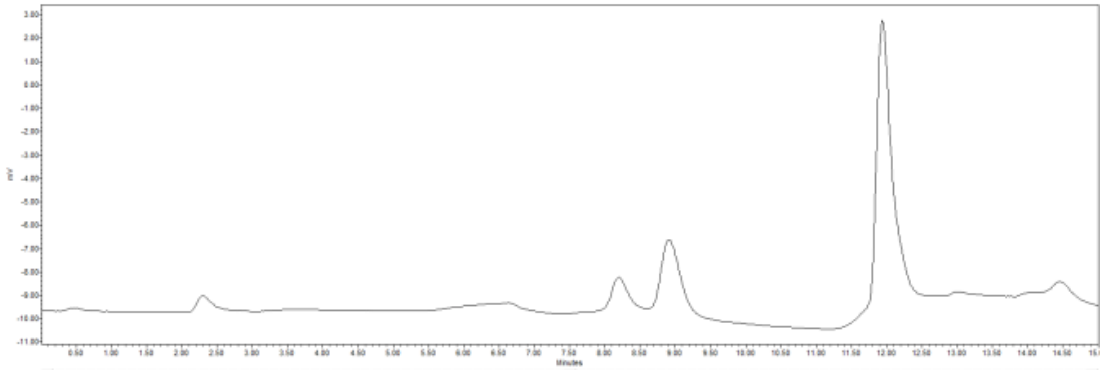

Figure 3-5: Standard mixed UV-chromatogram at 192 nm wavelength for a solution of 1 mM of SO_3^{2-}, SO_4^{2-} and SCN^-

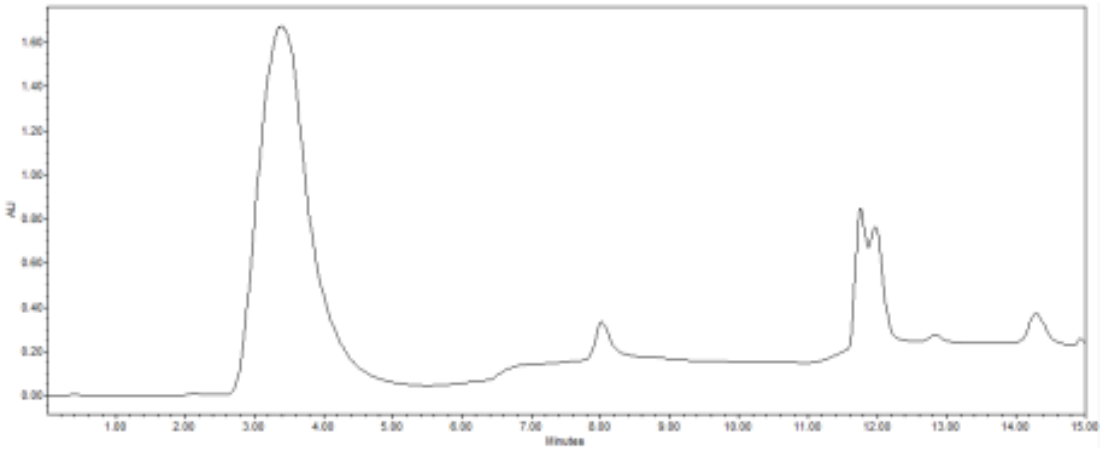

Figure 3-6: Standard mixed conductivity-chromatogram for a solution of 1 mM of SO_3^{2-}, SO_4^{2-} and SCN^-

3.5.5 X-ray photoelectron spectrometry (XPS)

All XPS work, including operating the XPS unit, and peak fitting, was undertaken by Dr. Kane O'Donnell at the Physics Department of Curtin University, Western Australia. The XPS unit is a Kratos Ultra DLD (2013 Model). The radiation source is a monochromatic aluminium source operating at 1486.6 eV and the pass energy for the detector was set at 20 eV. For etching, an argon gas cluster ion gun was used with the following settings: light etch: 5 kV and 23 nA; hard etch: 20 kV and 23 nA. For operation of the unit and peak fitting the Kratos Vision 2 software was used. Peak fitting was done by means of Gauss and Lorentzian methods, with the Lorentzian component being at 30% (GL30). Spin orbit doublets were fixed for height and width ratio. Shirley backgrounds were used wherever possible (Shirley, 1972). In all other cases linear background correction was applied. The machine specific relative sensitivity factors (RSF) were used from the Kratos Elemental Library. Binding energy data for peak identification was also used from the Kratos Elemental Library. Fitment was cross-checked with the data published by Moulder, Stickle, Sobel, and Bomben (1995).

3.5.6 Quantitative X-ray diffraction (QXRD)

The CSIRO AMRC Waterford analytical unit operated the XRD diffractometer. Dr. Robbie McDonald conducted the data analysis and interpretation. The XRD data was collected using a PANalytical Empyrean Series 2 diffractometer and CoKa radiation (40 kV and 40 mA) with scanning from 5–90° 2θ with step size of 0.05° 2θ and a PIXcel3D proton counting X-ray detector used to collect the data. The instrument was fitted with a Panalytical Bragg-Brentano high definition incident monochromator, primary 1/8° divergence and 1/4° anti-scatter slits, and secondary 1/8° anti-scatter slits. Both primary and secondary Soller slits (0.02 radians) were inserted. Mineral phases were identified using a combination of XPlot software utilising an older ICDD data base and PANalytical HighScore Plus software version 3.0d software with both current ICDD and ICSD data bases.

QXRD analyses were performed using the Rietveld method, employing TOPAS version 4.2 software. This method adopts a fundamental parameters approach to line profile fitting, with the combination of known instrumental set-up and published crystal structures used for all crystalline phases. The veracity of the QXRD results were checked by comparing predicted with analysed elemental compositions for the samples.

Chapter 4 Impact of hydrogen peroxide on gold leaching in pure cyanide solutions

4.1 Introduction

This chapter presents an experimental investigation of gold leaching in NaCN solutions under the influence of H_2O_2 addition, utilising REQCM technology. Literature (Section 2.1.3) has shown, that gold leaching rate can be limited by two major factors: reactant transfer (oxygen and cyanide) to the surface (diffusion limited) or reaction rate (chemically limited). The target of this investigation was to determine if gold leaching can be directly influenced by low concentrations of H_2O_2, considering H_2O_2 can act as an oxygen source by either decomposing and being present as elemental oxygen or by directly partaking in the oxygen reduction reaction on the gold surface.

This chapter is split into two major parts. The first part contains preliminary experiments to determine the interaction between the reagents used in the subsequent gold leaching experiments, namely NaCN, H_2O_2, $NaHCO_3$, and $NaClO_4$ in a solution. It also includes the determination of the H_2O_2 diffusion-coefficient, as literature gave only limited information, as illustrated in Section 3.4.1.1. The H_2O_2 diffusion-coefficient is required for subsequent calculations and determinations of the limiting mechanism for reactions involving H_2O_2. The second part utilises a full factorial design (FFD), with the aim to generate a response-surface model (RSM), to determine the possible impacts of H_2O_2 on gold leaching in clear solutions. Based on literature information (see Sections 2.1.4 and 2.2.3), the factors investigated in the FFD are NaCN concentration, H_2O_2 addition and either aeration or oxygenation of the solution. All other factors, such as pH, are set to a fix point based on typical literature values. The experiments were conducted using an REQCM and the observed responses are the gold leach rate and the OCP. This data was also compared to calculated theoretical diffusion limiting rates. All REQCM experiments in this

chapter were conducted with a gold/2%silver alloy, as this is more reflective of real world applications, but will be referred to as gold throughout this chapter.

4.2 Preliminary experiments

In preliminary experiments the oxidation of NaCN by H_2O_2 was investigated. As most experiments with the REQCM were determined to last approximately 10-15 minutes the impact of H_2O_2 on NaCN solutions over similarly short time periods was investigated. As literature has shown that dissolved oxygen levels have significant impact on gold dissolution rates, the release of oxygen as dissolved oxygen into NaCN solutions upon addition of H_2O_2 was also investigated. Further, calculations of theoretical diffusion limiting rates conducted in Section 4.4.2 required the hydrogen peroxide diffusion co-efficient under the experimental conditions. As no value for the exact experimental conditions present was found in the literature, the diffusion co-efficient was also determined.

4.2.1 Cyanide oxidation by hydrogen peroxide

For the tests, each 100 mL of 10 mM solution of NaCN with $NaClO_4$, as described in Section 3.2.5, were placed into a 200 mL beaker on a magnetic stirrer. The stirrer speed was set, so that a slight surface depression from the solution vortex was visible. Three different H_2O_2 additions, as well as one test without H_2O_2 addition were conducted. The NaCN solution used was made up as a single 1 L batch for all tests, from the solutions prepared as described in Sections 3.2.4 and 3.2.6. This solution was analysed by $AgNO_3$ titration, as described in Section 3.5.1.1, for concentration, which was accepted as the initial concentration for each test. During the tests, samples of exactly 5 mL were taken immediately after the addition of the H_2O_2 and after 5, 10, 20, 30, and 60 minutes. These samples were added into a conical flask containing exactly 5 mL of $NaAsO_2$ solution, as described in Section 3.2.12. This was done to neutralise any remaining H_2O_2, as literature has shown interference of oxidising agents, in this case H_2O_2, with cyanide analysers, such as the OI analytical WAD analyser (O.I. Analytical, 2009) used for this study. No

literature was found on possible interference with the $AgNO_3$ titration using a potentiometric endpoint determination. However, some titrations conducted without this pre-treatment (not presented) indicated an interference of the oxidising agent with the titration. After approximately 20 seconds of shaking a 5 mL subsample was taken for potentiometric endpoint titration as described in Section 3.5.1.1. A second subsample of 0.1 mL was taken and diluted with DI water in a 50 mL volumetric flask, prior to analysis with a WAD analyser, as described in Section 3.5.3. This secondary analysis was conducted to increase the confidence in the data gathered with the $AgNO_3$ titration.

4.2.2 Dissolved oxygen increase by hydrogen peroxide

The increase of dissolved oxygen in NaCN solution upon addition of H_2O_2 was measured by a DO-meter, described in Section 3.3.2. A 230 mM H_2O_2 solution was added in incremental 1 mL additions into 100 mL of 10 mM NaCN solution, made from stock electrolyte and concentrated NaCN solution, as described in Sections 3.2.6 and 3.2.4 and the peak DO after each addition noted, before the next addition.

4.2.3 Determination of hydrogen peroxide diffusion-coefficient

To determine the diffusion-coefficient of H_2O_2, two anodic potential scans on a 100% gold electrode with a diameter of 17.1 mm were conducted. The electrode was prepared by sanding with 1000 grit silicon carbide sandpaper, followed by polishing with a paste consisting of 10 µm alumina and demineralised water. The electrode was then thoroughly rinsed with DI water. Both scans were conducted in exactly 100 mL electrolyte solution, as described in Section 3.2.6 at a rotation rate of 500 min^{-1}. For one scan the solution contained 3 mM of H_2O_2, added as 500 mM solution. The electrolyte was sparged with N_2 for 15 minutes, prior to commencing the scans. The scans were conducted with the electrochemical setup described in Section 3.3.1.7, with a scanning speed of 1 mV/s, the current range set to 10 mA from 0 to -1000 mV vs. SHE.

4.3 Statistical experimental design

4.3.1 Leach rates and OCP with hydrogen peroxide

A Full Factorial Design (FFD) was established to determine the impact of H_2O_2 on cyanide leaching of gold in clear solutions, utilising REQCM technology, as described in Section 3.3.1.1. To reduce the margin for error, which may be caused by different electrodes, all tests in the complete sample set were conducted on one electrode. The main factors for the FFD were determined based on typical literature values for pH, pH buffer, cyanide concentration, gas sparging, and H_2O_2 addition (see Sections 2.2.3, 2.2.4, and 2.4.1). In Table 4-1 the factors and their respective levels (for gas sparging only low and high is considered) are shown, where (-) denotes a low level, (o) a medium level and (+) a high level. Based on this a 3x3x2 D-Optimal factorial design was developed, using the software tool Design Expert 8.0.7.1 by Statease. The responses to observe with the REQCM were gold leach rate (calculated from mass change of gold over time), as the main response, as well as the OCP. The software created a design of experiment and determined the testing order, which is shown in Table 4-2, as standard and run order. To determine a basic understanding of experimental error/repeatability one experimental condition was repeated. Hence it is an 18+1 experimental design.

Table 4-1: Factors and selected levels in the 332 full factorial design

Factors	Name	Low level (-)	Medium Level (o)	High Level (+)	Unit
A	Sodium Cyanide Concentration	2.5	5	10	mM
B	Hydrogen Peroxide Concentration	0	3	6	mM
C	Gas Sparging	Aeration	-	Oxygenation	-

Table 4-2: Design matrix for 3 factors and 18+1 experiments

Standard order	Run order	A	B	C
1	2	-	-	-
2	4	o	-	-
3	15	+	-	-
4	3	-	o	-
5	14	o	o	-
6	8	+	o	-
7	13	-	+	-
8	1	o	+	-
9	16	+	+	-
10	12	-	-	+
11	7	o	-	+
12	5	+	-	+
13	9	-	o	+
14	6	o	o	+
15	18	+	o	+
16	10	-	+	+
17	11	o	+	+
18	17	+	+	+
19	19	o	+	+

The results of the tests were entered into the statistical software and analysed for a model match, to be able to analyse the impact of H_2O_2 on gold leaching and predict the gold leach rate and open circuit potentials for any given solution respectively. For better understanding a graphical response surface model was created for the leach rate.

4.4 Results and discussion

All results and data gained throughout this experimental chapter will be outlined, explained and discussed in this section.

4.4.1 Preliminary experiments

4.4.1.1 Cyanide oxidation by hydrogen peroxide

The NaCN concentration data obtained by potentiometric endpoint titration for CN^- during the cyanide oxidation tests is presented in Figure 4-1. The data points at t=0 minutes represents the solution prior to the peroxide additions (hydrogen peroxide was added at time zero with a sample taken immediately thereafter). The initial NaCN concentration measured for the solution used was 9.9 mM of NaCN. At t=0.25, an initial drop in NaCN concentration can be observed for all H_2O_2 additions. Then a linear decline in NaCN concentration appears for all additions, including the baseline with no H_2O_2 addition. The constant decline in NaCN concentration on the baseline can be accounted for by HCN volatilisation, as a constant airflow was present in the fumehood. The measured loss of NaCN concentration over one hour was 0.9, 1.8, 2.7 and 2.7 mM for the 0, 5, 10, and 15 mM H_2O_2 additions respectively. These results were confirmed by the data gathered with the WAD-analyser.

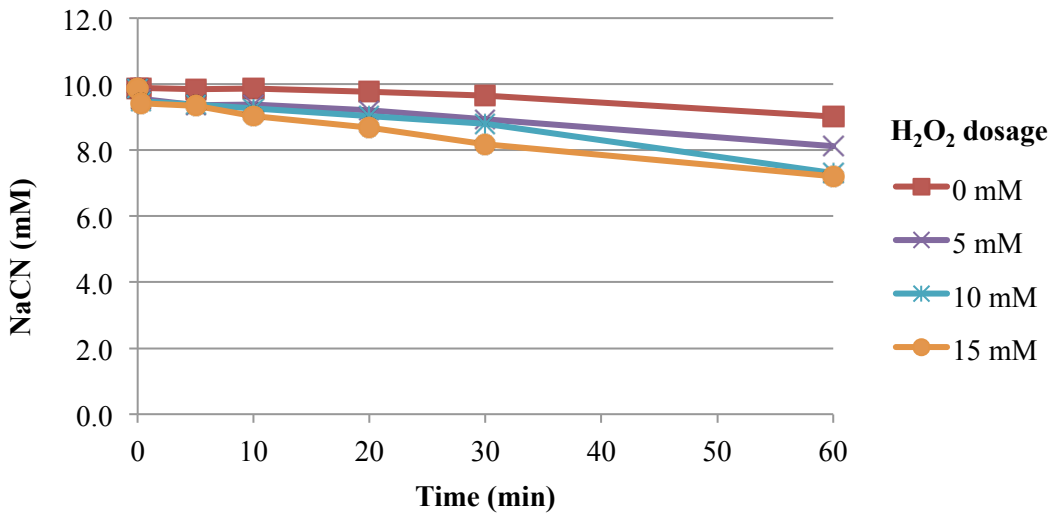

Figure 4-1: 10 mM NaCN with 0.2 M $NaClO_4$ at pH 10.5 – cyanide destruction test with different dosages of H_2O_2 over 60 minutes, analysis by $AgNO_3$

These results suggest only a slow oxidation of cyanide by hydrogen peroxide in the experimental concentrations and solutions selected for the FFD in Section 4.3.1. A further unknown was the oxygen release by H_2O_2 in sodium cyanide solutions used for gold leach testing in this chapter. This was investigated in a further step described in Section 4.4.1.2.

4.4.1.2 Dissolved oxygen increase caused by hydrogen peroxide

Figure 4-2 shows the increase of dissolved oxygen in NaCN solution with the addition of 1.0 mL increments of 230 mM H_2O_2 solution following the procedure described in Section 4.2.2. A low increase of the dissolved oxygen levels can be observed in the solution. The observed increase of dissolved oxygen averages at 0.072 ppm/mL H_2O_2 added. This value is significantly lower than the theoretically calculated maximum increase of dissolved oxygen of 36.8 ppm/mL H_2O_2 added assuming total decomposition of the hydrogen peroxide. It can be concluded, that H_2O_2 does not decompose in the given NaCN-solution, releasing oxygen. The increase of dissolved oxygen above air saturation could be explained by the addition of the H_2O_2 solution which contains a much higher DO than air saturation. In a

decomposition situation the DO increase in solution would be expected as non-linear and increasing with further additions, whereas in the solution tested the DO increase starts to slow with greater additions of H_2O_2. The slowing increase is most likely caused by the solution trying to achieve the DO equilibrium due to the surface being open to air. Due to range limitations in the equipment used for DO analysis, the DO in the H_2O_2 solution could not be determined to verify this increase in DO was caused by the mixing of two solutions. It can be further noted, that the increase in DO was nearly instantaneous (apart from the equalisation time (10-15 sec) required on the DO-meter), offering further support for the mixing theory being the main contribution to the observed increase in DO.

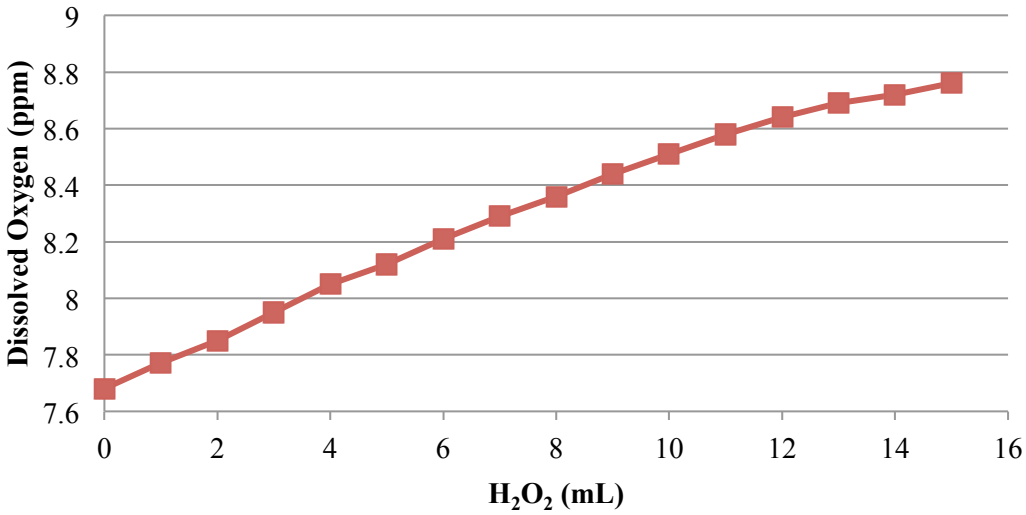

Figure 4-2: Dissolved oxygen increase in 100 mL of 10 mM NaCN solution at pH 10.5 when adding 0.23 M H_2O_2

4.4.1.3 Determination of hydrogen peroxide diffusion-coefficient

Figure 4-3 presents the data gathered during the potential scans on a gold electrode, as described in Section 4.2.3. The measured current in A/m^2 is plotted over the applied potential in mV vs. SHE. The red curve represents the potential scan conducted with N_2 sparged electrolyte. Between the potential of -200 and -800 mV vs. SHE a slow, linear increase in the observed current from 0 to -2.2 A/m^2 can be seen. Between -800 and -1000 mV an inflection in the increase can be observed, and

the final current measured is -5.5 A/m^2. The currents measured are most likely a result of electrolysis of water, and hence hydrogen evolution. The blue curve shows the data measured in N_2 sparged electrolyte solution with 3 mM H_2O_2 present. The measured current starts at -1.9 A/m^2 to then decrease to around -1.1 A/m^2 between -100 and -200 mV vs. SHE. From -200 to -500 mV the measured current increases relatively linear to -7 A/m^2, from -500 to -1000 mV it increases faster to reach a final value of -30 A/m^2. The green curve is a plot of the difference between the scan conducted only on N_2 sparged electrolyte and the scan conducted on the N_2 sparged electrolyte with 3 mM H_2O_2. This has been done to remove any hydrogen evolution and other possible electrolytic effects on determining the final H_2O_2 reduction current. The green curve follows the blue one closely to a potential of -300 mV. Then the green curve begins to show a slightly lower (beginning around 0.3, increasing to 2.1 A/m^2) current until -800 mV. Around -800 mV the green curve starts to level out around a measured current of -24.5 A/m^2. This indicates, that the final H_2O_2 reduction current for this solution, rotation speed and temperature has been reached. Out of this measured current the H_2O_2 diffusion coefficient was calculated to be 8.86 10^{-10} m^{2}s^{-1}. This value was calculated under the assumption of a 2-electron reduction of H_2O_2, utilising the Levich Equation in rearranged form, in combination with Faradays Constant (96485 C mol^{-1}) and Coulombs Law (1 As = 1 C), as shown in Equation 4-1. In this equation D is the diffusion coefficient in m^{2}s^{-1}, j the measured current density in A m^{-2}, ω the rotation speed of the electrode in rad s^{-1}, ν the kinematic viscosity of H_2O at 25 °C (9.75 10^{-7} m^{2}s^{-1}), and $[O]$ the bulk concentration of H_2O_2 in solution in mM or M m^{-3}. The calculated value is in close agreement with the value presented in the literature review for 3 mM H_2O_2, in Section 2.2.1 of 8.72 10^{-10} m^{2}s^{-1}.

$$D = \left(\frac{\frac{-j}{96485*2}}{0.62*\omega^{1/2}*\nu^{-1/6}*[O]} \right)^{3/2} \text{m}^2\text{s}^{-1} \qquad \text{Equation 4-1}$$

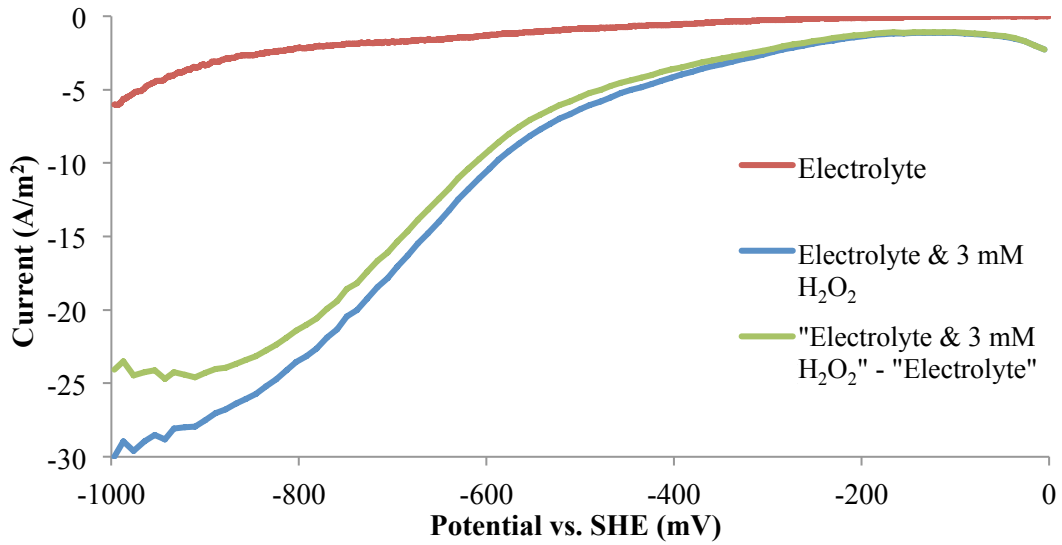

Figure 4-3: RDE cathodic potential scans for pure gold electrode at pH 10.5, N_2 sparged with 3 mM and without H_2O_2, 500 min^{-1}, including calculated curve for H_2 evolution correction

4.4.2 Leach rates of gold and open circuit potential under the addition of hydrogen peroxide

Figure 4-4 and Figure 4-5 each show a typical data set gathered with one run (experiment) of the factorial design as described in Section 4.3. The average leach rate and OCP respectively were calculated from an average of ~100 seconds, once the mass loss and OCP reached a steady state, as marked in the graphs with a shaded area.

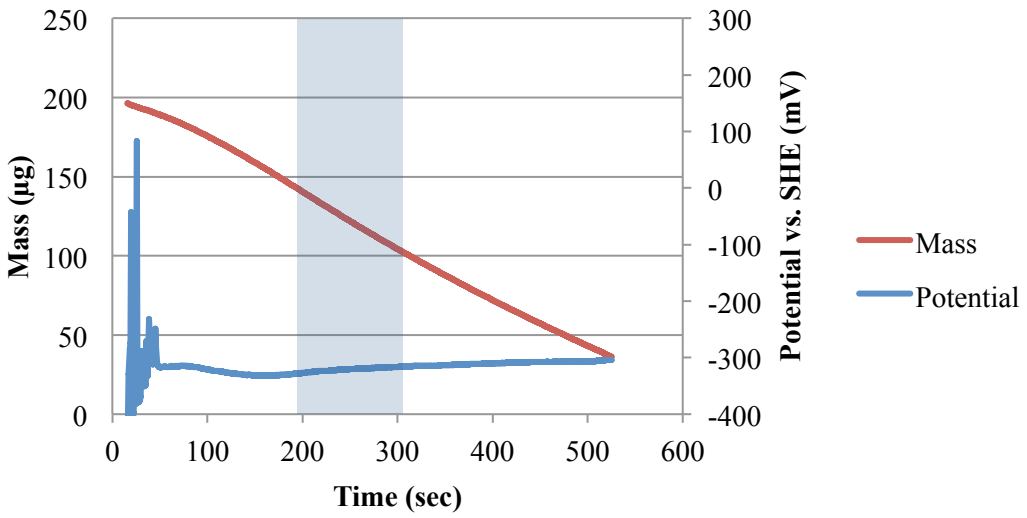

Figure 4-4: Factorial Design Run 7 - REQCM-Experiment Data – Mass and Potential as function of time at 5 mM NaCN, 0 mM H_2O_2, oxygenated, pH 10.5, 300 min^{-1}

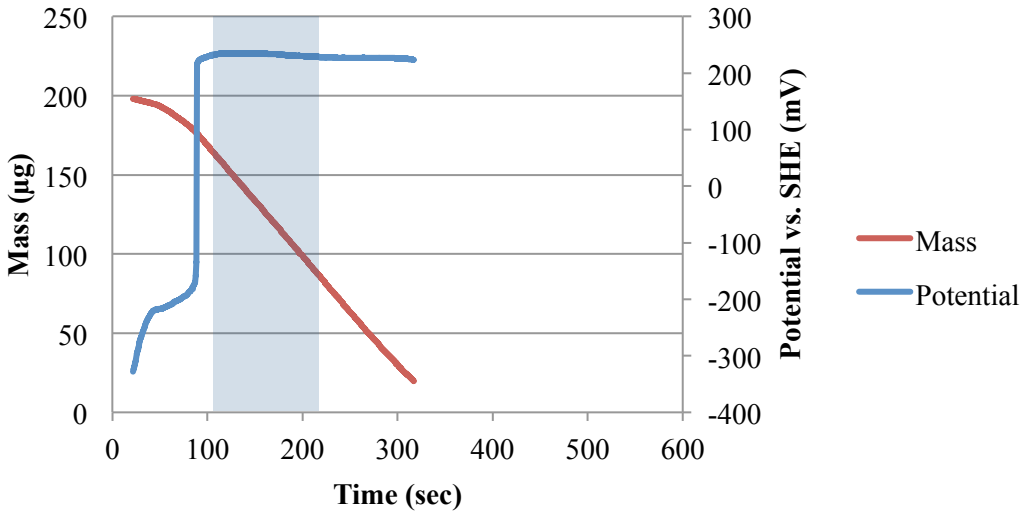

Figure 4-5: Factorial Design Run 11 - REQCM-Experiment Data – Mass and Potential as function of time at 5 mM NaCN, 6 mM H_2O_2, oxygenated, pH 10.5, min^{-1}

Table 4-3 shows the data gathered in the 18 experiment factorial design. From the data plots, as presented in Figure 4-4 and Figure 4-5 and Table 4-3 it is clear, that the OCP response shows a significant step change, which cannot be adequately modelled with RSM models (Anderson & Whitcomb, 2005). The leach rate data was then analysed with Design Expert 8.0.7.1 to create a model.

Table 4-3: Factorial design – measured data

Standard order	NaCN-Concentration (mM)	H_2O_2 concentration (mM)	Gas sparging	Measured Leach rate (10^{-5} mol m^{-2} s^{-1})	Measured OCP (mV)
1	2.5	0	Aerated	3.32	-290.68
2	5	0	Aerated	5.03	-398.95
3	10	0	Aerated	5.32	-432.65
4	2.5	3	Aerated	9.48	253.68
5	5	3	Aerated	12.05	-259.44
6	10	3	Aerated	12.97	-307.00
7	2.5	6	Aerated	8.91	258.13
8	5	6	Aerated	11.15	-271.60
9	10	6	Aerated	14.48	-256.64
10	2.5	0	Oxygenated	8.73	-22.83
11	5	0	Oxygenated	8.84	-316.97
12	10	0	Oxygenated	11.81	-351.99
13	2.5	3	Oxygenated	9.29	249.19
14	5	3	Oxygenated	18.71	218.53
15	10	3	Oxygenated	19.06	-262.69
16	2.5	6	Oxygenated	8.92	256.96
17	5	6	Oxygenated	18.16	230.16
18	10	6	Oxygenated	35.3	211.40
19	5	6	Oxygenated	17.02	236

The data for the leach rate was first transformed with a log function. Consecutively an expected model fit was calculated for all reasonable possible models: i.e. linear, two factor interactions and cubic model. The model fit calculation performed with DesignExpert 8.0.7.1 suggests a quadratic model will give the best results, shown by a low p-value and a good match between the adjusted and predicted R-Squared.

Table 4-4: Model fit calculation performed with DesignExpert 8.0.7.1

Source	Sequential p-value	Lack of Fit p-value	Adjusted R-Squared	Predicted R-Squared
Linear	< 0.0001	0.1228	0.7315	0.6454
2FI	0.2540	0.1275	0.7578	0.5569
Quadratic	*0.0159*	*0.1731*	*0.8730*	*0.672*
Cubic	0.1793	0.2057	0.9253	0.5525

By using the method of partial sum of squares an empiric model was created out of the experimental data, for the gold leach rate in NaCN solution under the influence of H_2O_2. Equation 4-2 shows the formula for the model of the leach rate under aeration, Equation 4-3 for the leach rate under oxygenation respectively, where *AuRA* is the gold leach rate under aerated conditions, *AuRO* the gold leach rate under oxygenated conditions, *H_2O_2Conc.* the hydrogen peroxide concentration and *CNConc.* the cyanide concentration. As the gas-sparging had two fixed settings of oxygen concentration, air and pure oxygen and no mixtures of those were investigated, two equations were necessary to reflect the model. This model can only be assumed valid within the design space and using the same reactive gold surfaces resulting from electroplating.

$$R_{\log\left(AuRA\ (10^{-5} mol\ m^{-2}\ sec^{-1})\right)} = 0.60443 + 0.01788 * CNConc. + 0.11247 * H_2O_2Conc. + 0.00507887 * (CNConc. * H_2O_2Conc.) - 0.014355 * (H_2O_2Conc.)^2 \quad \text{Equation 4-2}$$

$$R_{\log\left(AuRO\ (10^{-5} mol\ m^{-2}\ sec^{-1})\right)} = 0.82309 + 0.017880 * CNConc. + 0.11247 * H_2O_2Conc. + 0.00507887 * (CNConc. * H_2O_2Conce.) - 0.014355 * (H_2O_2Conc.)^2 \quad \text{Equation 4-3}$$

The model was examined for its statistical significance by Fisher's F-test, with the analysis of variance (ANOVA) with the results given in Table 4-5. The p-value reflects the statistical significance, where a p-value less than 0.05 (95% confidence level) indicates statistical relevance. The model itself and factor B are highly significant with a p-value of <0.0001. The factor A with a p-value of 0.0007, C with 0.0004 and B^2 with 0.0206 are also highly significant. Only the factor AB with a p-value of 0.1202 appears to be less significant, but showed significant improvement on the quality of the model. All factors and interactions not displayed in Table 4-5 did not show an improvement on the model or were statistically not significant. Hence these were removed from the model. With a p-value for "Lack of Fit" above 0.05 the model is significant for the data processed. Finally, the fit of quadratic model was assessed by calculating the regression coefficient, R^2. For the gold leach rate model, the calculated R^2 was 0.8724, which is a satisfactory result.

Table 4-5: ANOVA table for fitted quadratic model

Source	Sum of Squares	Degrees of Freedom	Mean Square	F Value	p-value Prob > F
Model	0.87	5	0.17	17.78	< 0.0001
A-NaCN-Concentration	0.19	1	0.19	19.57	0.0007
B-H_2O_2-addition	0.38	1	0.38	38.78	<0.0001
C-DO level	0.23	1	0.23	22.90	0.0004
AB	0.027	1	0.027	2.77	0.1202
B^2	0.068	1	0.068	6.94	0.0206
Residual	0.13	13	0.00984		
Lack of Fit	0.13	12	0.011	26.81	0.1499
Pure Error	0.0003964	1	0.0003964		
Corrected Total	1	18			

Figure 4-6 and Figure 4-7 show the resulting response surface graphs, which can be plotted from the model functions. As the model consists of two equations, two graphs for both options, one under aeration and one under oxygenation are shown. It can be seen, that in comparison with an aerated solution, in an oxygenated solution H_2O_2 has a bigger impact on the leach rate. This indicates, that the effect that H_2O_2 has on an electroplated gold surface, is more than just being an oxygen supplier. To be able to further interpret and relate the presented results, theoretical leach rate calculations were made and are presented in the remainder of this section.

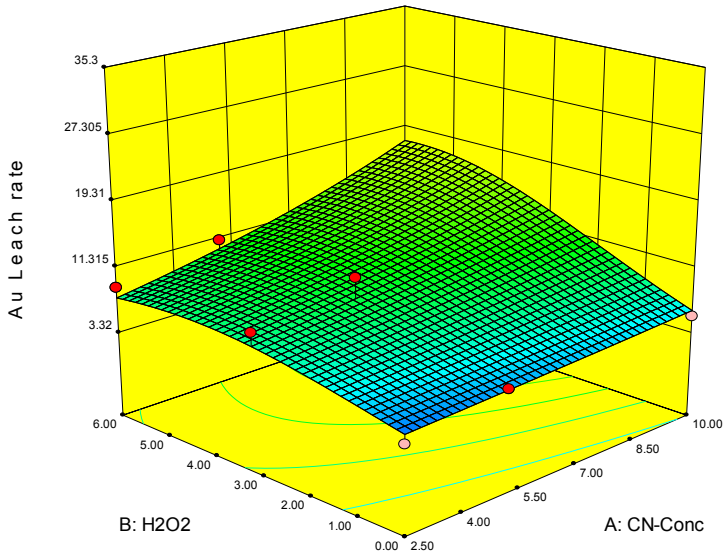

Figure 4-6: Response surface graph showing the relation between NaCN-concentration, H_2O_2 addition and gold leach rate in aerated solution

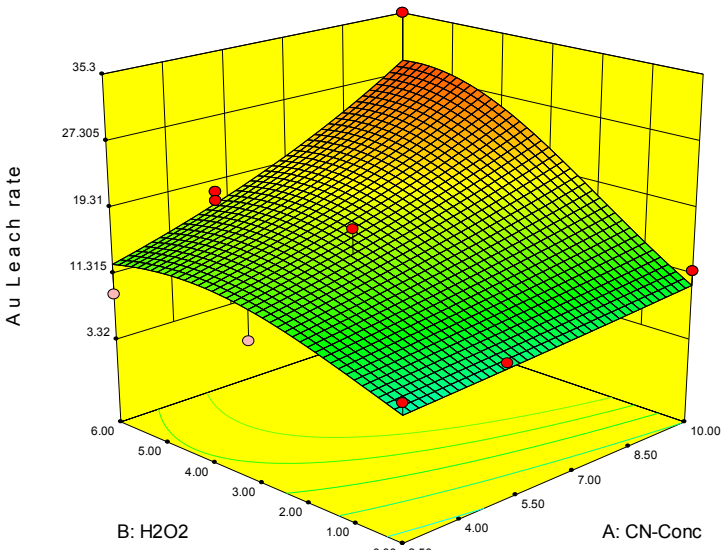

Figure 4-7: Response surface graph showing the relation between NaCN-concentration, H_2O_2 addition and gold leach rate in oxygenated solution

The gained leach rate data was compared with theoretical leach rate calculations. To do so, the maximum theoretical leach rates were computed for the anodic and cathodic reaction steps during gold leaching. In Equation 4-4 the anodic gold oxidation equation is shown. This reaction step will release one electron per atom of gold complexed. The overall reaction of the cathodic oxygen reduction is given in Equation 4-5. Following this equation it can be seen, that two electrons are consumed per molecule of oxygen. The cathodic oxygen reduction can be split up into two steps, as shown in Equation 4-6 and Equation 4-7, resulting in a consumption of four electrons. If instead of oxygen, hydrogen peroxide is the oxygen donor, the oxygen reduction can occur according to Equation 4-7, which reflects the uptake of two electrons per molecule of hydrogen peroxide reduced. If, instead of a direct consumption of the hydrogen peroxide, the hydrogen peroxide decomposes according to Equation 4-8, and then follows the pathways described for oxygen, again two electrons can be consumed by one hydrogen peroxide molecule. This information, combined with the Levich equation and solution/reactant constants as presented in Sections 3.4.1, 3.4.1.1 and 4.4.1.3, were used to calculate the theoretical limiting rates. Table 4-6 presents the cyanide limiting gold leach rates computed for the three cyanide concentrations used throughout the experiments, namely 2.5, 5 and 10 mM, at a disc rotation rate of 31.4 rad s^{-1} (300 min^{-1}). The same calculations were

applied for the oxygen reduction half reaction, considering air and oxygen saturated solution, and hydrogen peroxide concentrations in solution of 0, 3 and 6 mM. The combined possible theoretical limiting gold leach rates (two and four electron for two oxygen concentrations; two electron for three hydrogen peroxide concentrations or no hydrogen peroxide reduction) calculated for the oxygen half reactions are presented in Table 4-7 for the lowest possible and highest possible oxygen and hydrogen peroxide reduction current.

$$Au + 2CN^- \leftrightarrow Au(CN)_2^- + e^-$$ Equation 4-4

Table 4-6: Calculated NaCN diffusion limiting gold leach rates for 25°C, 300 min^{-1}

NaCN concentration (mM)	**Theoretical limiting rate (10^{-5} mol m^{-2} s^{-1})**
2.5	7.33
5	14.67
10	29.34

Table 4-7: Calculated combined oxygen and hydrogen peroxide limiting gold leach rates (10^{-5} mol m^{-2} s^{-1}) for 25°C, 300 min^{-1}

H_2O_2 concentration (mM) / gas composition	**Theoretical limiting rate – lowest possible**	**Theoretical limiting rate – highest possible**
0 / air	2.71	5.43
0 / O_2	13.03	26.06
3 / air	2.71	24.75
3 / O_2	13.03	45.38
6 / air	2.71	44.06
6 / O_2	13.03	64.69

$$O_2 + 2H_2O + 2e^- \leftrightarrow 4OH^-$$ Equation 4-5

$$O_2 + 2H_2O + 2e^- \leftrightarrow H_2O_2 + 2OH^-$$ Equation 4-6

$$H_2O_2 + 2e^- \leftrightarrow 2OH^-$$ Equation 4-7

$$2H_2O_2 \rightarrow O_2 + 2H_2O$$ Equation 4-8

The comparison results of the calculated limiting leach rates and the measured leach rates during the REQCM experiments are outlined in Table 4-8. It can be seen, that depending on the ratio of oxygen and hydrogen peroxide to cyanide available for leaching, the rate will vary between oxygen or cyanide diffusion limitation. Only a few cases show a chemically limited leach rate. It is notable, that the theoretical limiting rates calculated for the cyanide diffusion limiting rate are consistently around 20% lower than the measured leach rates. This may be due to possible inaccuracies in measuring the electrode size, resulting in a larger real surface area than the theoretical one used in the calculations (on the 5.1 mm diameter electrode a diameter increase of only ~0.5 mm could cause an error of this size). Further, for the oxygen limiting diffusion rates it can be observed, that only in significant excess of sodium cyanide, the maximum four electron limiting rate is reached. The theoretical values generated for the oxygen diffusion limiting rate with four electron reduction are all below maximum possible reaction rates. This indicates, that even in presence of excess cyanide, oxygen diffusion limiting rates are rarely reached. This could be due to the diffusion of the interim formed hydrogen peroxide away from the surface, as mentioned in literature, shown in Section 2.1.2.

Table 4-8: Comparison results of theoretical leach rates and measured leach rates for REQCM experiments

NaCN-concentration (mM)	**H_2O_2 concentration (mM) / gas composition**	**Measured Leach rate (10^{-5}mol m^{-2} s^{-1})**	**Limiting step (cyanide diffusion, oxygen diffusion, chemical)**
2.5	0 /air	3.32	chemical
5	0 / air	5.03	oxygen diffusion
10	0 / air	5.32	oxygen diffusion
2.5	3 / air	9.48	cyanide diffusion
5	3 / air	12.05	chemical
10	3 / air	12.97	chemical
2.5	6 / air	8.91	cyanide diffusion
5	6 / air	11.15	chemical
10	6 / air	14.48	chemical
2.5	0 / oxygen	8.73	cyanide diffusion
5	0 / oxygen	8.84	chemical
10	0 / oxygen	11.81	chemical
2.5	3 / oxygen	9.29	cyanide diffusion
5	3 / oxygen	18.71	cyanide diffusion
10	3 / oxygen	19.06	chemical
2.5	6 / oxygen	8.92	cyanide diffusion
5	6 / oxygen	18.16	cyanide diffusion
10	6 / oxygen	35.3	cyanide diffusion

In the literature it has not been observed, that the cyanide limiting rate is consistently achieved for such high cyanide concentrations (see Section 2.1.4). It was considered, that the extreme impact of hydrogen peroxide could be due to the higher reactivity/activity of freshly electroplated gold surfaces, which in literature have shown higher reactivity. Hence further investigations were conducted with electrode

pre-treatment and also the RDE as a comparison method for solid gold. The results are presented in the Section 5.4.1.

4.4.3 Conclusions

The impact of hydrogen peroxide on cyanide leaching of electroplated gold/2%silver has been investigated and a model developed, which will be true for the specific conditions tested. It has been shown, that on electroplated gold/2%silver surfaces hydrogen peroxide can significantly increase the gold leach rates when not cyanide diffusion limited with enhancements of ~120-185% in aerated solutions and up to ~200% in oxygenated solutions observed. When comparing oxygenated and aerated solutions, the impact of the hydrogen peroxide observed was greater in an oxygenated solution. When cyanide diffusion limited conditions occur in the presence of hydrogen peroxide a significant jump in the gold/silver OCP occurred, after an initial leach period. This phenomenon as well as establishing the possible comparability of electroplated gold/silver behaviour versus solid gold/silver behaviour is further investigated in Chapter 5.

Chapter 5 Leaching of plated gold versus solid gold and the mixed potential during gold cyanidation

5.1 Introduction

Chapter 4 has revealed a significant, positive impact of hydrogen peroxide on the leach kinetics of electroplated gold/2%silver. This increase in leach rate was inherent with a sharp jump in the open circuit potential, when cyanide leaching the electroplated gold/silver alloy under certain conditions in the presence of hydrogen peroxide. This potential jump cannot be explained with the typical oxygen reduction, hydrogen peroxide reduction, and gold oxidation curves on gold surfaces as encountered in literature (see Section 2.5.4). Further, literature suggests (see Section 2.5.6), that electroplated gold behaves different to solid gold, when leaching. The target of this chapter was to create an understanding as to whether the findings generated on electroplated gold are transferrable to solid gold and to understand the open circuit potential jump observed.

This chapter consists of three main sections, the first one includes leach experiments with RDE methodology and additionally pre-treated REQCM electrodes, to generate comparative data for the leach kinetics of solid gold to electroplated gold. The second part investigates a passivation phenomenon of solid gold encountered during these leach tests with XPS technology, and the final part utilises potentiodynamic techniques with REQCM and RDE electrodes, to unravel the jump in open circuit potential, when leaching gold with cyanide and hydrogen peroxide.

5.2 Comparison of REQCM results with RDE

Whilst REQCM offers fast results on the impact of different leaching regimens (O_2 concentration, NaCN concentration and H_2O_2 addition), data gained cannot be compared directly with real world applications. This is due to the fact that electroplated gold shows higher reactivity than solid gold, as mentioned in Section 2.5.6. Hence a range of experiments were carried out to verify if data gained with the REQCM could serve as indicative of real world applications. Additionally it was investigated, if certain REQCM electrode pre-treatments can create a material, behaving similarly to solid gold.

5.2.1 REQCM electrode pre-treatment

To understand the impact which different surface preparations of an REQCM electrode can have on leaching, some different electrode pre-treatment between the electroplating and the leaching were investigated. The electrodes were prepared to have an gold/2%silver surface using the method described in Section 3.4.2. This was followed by three different pre-treatments: baking the plated electrode in an oven at 70 °C for four hours; conducting a 3-cycle potential scan from OCP to -500 to 650 mV vs. SHE at a scan rate of 1 mV s^{-1} in electrolyte solution; and allowing the OCP of the electrode in electrolyte solution with 6 mM H_2O_2 present to reach equilibrium prior to the NaCN addition. These pre-treatments were conducted to determine if a pre-treatment will result in an REQCM electroplated surface behaving like a solid gold electrode, when leached. All tests were conducted with cyanide solutions made from stock electrolyte solution and concentrated NaCN solution, as described in Sections 3.2.4 and 3.2.6 at pH 10.5 with oxygen sparging, a NaCN concentration of 5 mM, 6 mM H_2O_2 concentration and at a rotation speed of 300 min^{-1}. The responding OCPs and mass losses over time were recorded.

5.2.2 RDE leach tests

Four leaching conditions from the ones used in the factorial design (see Section 4.3.1) were replicated in RDE leach experiments. A 15.1 mm diameter electrode (98% gold, 2% silver) was used for this test work. The selected conditions were with cyanide solution prepared from the stock solutions described in Sections 3.2.6 and 3.2.4 at a concentration of 5 mM NaCN and electrolyte present. The disk was prepared for each experiment as described in Section 3.4.3 and then mounted in a rotator as described in Section 3.3.1.7. The electrode was rotated at 300 min^{-1} in 500 mL of solution. Four leach tests were conducted, two under aeration and two under oxygenation. One oxygenated and one aerated test each were conducted in the presence of 6 mM H_2O_2 in solution. Samples for analysis were taken every 15 minutes and analysed via AAS, as described in Section 3.5.2 for their respective Au and Ag content. Based on the measured Au and Ag content at the specific times samples were taken, the leach rates for each time segment were calculated. The OCP during those tests was recorded with a potentiostat, as described in Section 3.4.4.

5.2.3 Leached surface analysis with XPS

As the RDE leach tests did show an unusual behaviour, as described in Section 5.4.1.2, which included a visible surface coating, a specimen was prepared for surface composition analysis by XPS (X-ray photon spectrometry). A 15.1 mm diameter, 98% Au / 2% Ag RDE electrode was dismantled, to separate the gold specimen from the rest of the electrode, as the electrode housing cannot be mounted in the XPS unit. A special bracket was constructed to mount the electrode on the Pine MSR rotator used in the RDE setup, as described in Section 3.3.1.3. The surface of the gold specimen was prepared by wet sanding with 1200 grit silicon carbide sand paper, followed by polishing with a paste consisting of 10 µm alumina powder and DI water. Before mounting the specimen in the bracket, it was thoroughly rinsed with DI water. After mounting, the sides of the specimen were covered with PTFE thread tape, to inhibit liquid contact. The specimen was then rotated at 300 min^{-1} in exactly

1 L of 5 mM cyanide solution at pH 10.5, made from the stock solutions as described in Sections 3.2.6 and 3.2.4. Oxygen was bubbled into the solution at a rate of 100 mL min^{-1}. The gold specimen was removed from the solution after 60 minutes of leach time and thoroughly rinsed with DI water and dried with compressed air before introducing it into the XPS-unit for analysis. The XPS unit details, scan settings and interpretation background are described in Section 3.5.5. The sample was scanned four times: first immediately after treatment; second after a light etch of 1 minute; third after a hard etch of 5 minutes; fourth after the sample was polished to create an untreated surface. The etching steps were conducted to determine the strength of the coating.

5.3 Potentiodynamic investigation of gold and silver

On freshly plated REQCM electrodes (gold, silver, and gold / 2% silver) potential scans were conducted. The objective was to understand the behaviour of the OCP observed in Section 4.4.2. For each scan the electrode was freshly plated, as described in Section 3.4.2, to obtain a gold, gold / 2% silver, or a silver surface. All scans were conducted with the electrochemical setup as described in Section 3.4.5. A negative potential scan at a scan rate of 5 mV/s was conducted from +500 to -500 mV vs. SHE with the potential range set to 1 mA. This high scan rate was chosen, as a scan with a lower scan rate resulted in the depletion of the plated surface prior to completion of the scan. The electrode was rotated at 300 min^{-1}. During the scans, the current, potential and electrode mass were recorded. The current density on the electrode surface was automatically calculated, as was the calculated metal oxidation current based on the mass change recorded by the REQCM software. The current calculation from mass change is based on the amount of electrons required for the gold dissolution, as given by the gold dissolution reaction (see Section 2.1.2) and the Faraday constant, following the principle applied by other researches, as summarised in Section 2.1.3.3. With all three plated materials, scans were conducted in the following three solutions: (1) aerated electrolyte, (2) aerated electrolyte with 6 mM H_2O_2 concentration and (3) aerated electrolyte with 6 mM H_2O_2 and 2.5 mM NaCN

concentration. All solutions were mixed fresh, to obtain exactly 100 mL solution in a volumetric flask for each scan from the stock solutions, as described in Sections 3.2.1, 3.2.6, and 3.2.4.

5.4 Results and discussion

The results and discussion section of this chapter is split into two major subsections. The first subsection focuses on the comparison of data acquired with REQCM electrodes to leach rates measured in RDE test work. The second subsection presents the results of the potentiodynamic investigation conducted to understand the phenomenon of the OCP jump observed during the FFD experiment in Section 4.4.2.

5.4.1 Comparison of REQCM results with RDE test work

Due to unexpected results (slowing of oxygenated RDE leaching over time, as shown in Section 5.4.1.2), this section is split into three subsections. The first one will show the information gathered during REQCM electrode pre-treatment and the possible impact on leach rates, the second one includes RDE test work, to determine possible comparability between observations on electroplated gold and solid gold, and the third investigates encountered surface coatings with XPS analysis.

5.4.1.1 REQCM electrode pre-treatment

In this section the results of the REQCM electrode pre-treatment are presented. The purpose of the pre-treatments was to determine if pre-treatments will result in a behaviour of electroplated gold, similar to that of solid gold. In all figures, the horizontal axis represents the time in seconds, the left vertical axis the mass of gold on the electrode in µg, and the right vertical axis the OCP vs. SHE in mV, measured during the tests. The red line always represents the mass and the blue line the OCP.

Figure 5-1 displays the baseline data gathered for non pre-treatment of an electroplated gold/silver REQCM electrode. Observing the potential, it can be seen, that after a short induction period of around 50 seconds, the OCP jumps from around -200 mV to around 230 mV. This indicates a change of either the cathodic (oxygen reduction) reaction or the anodic (cyanide oxidation) reaction, causing the intersecting point to shift, as described in Section 2.5.6. Similarly, the mass decline observed during the test reaches a constant maximum after approximately 50 seconds, and towards the end of the leaching starts slowing down again due to the depletion of gold. The maximum leach rate calculated from the measured data is 17.02 (10^{-5} mol m^{-2} s^{-1}), which is in close agreement with the rate observed during the FFD test work, as presented in Section 4.4.2.

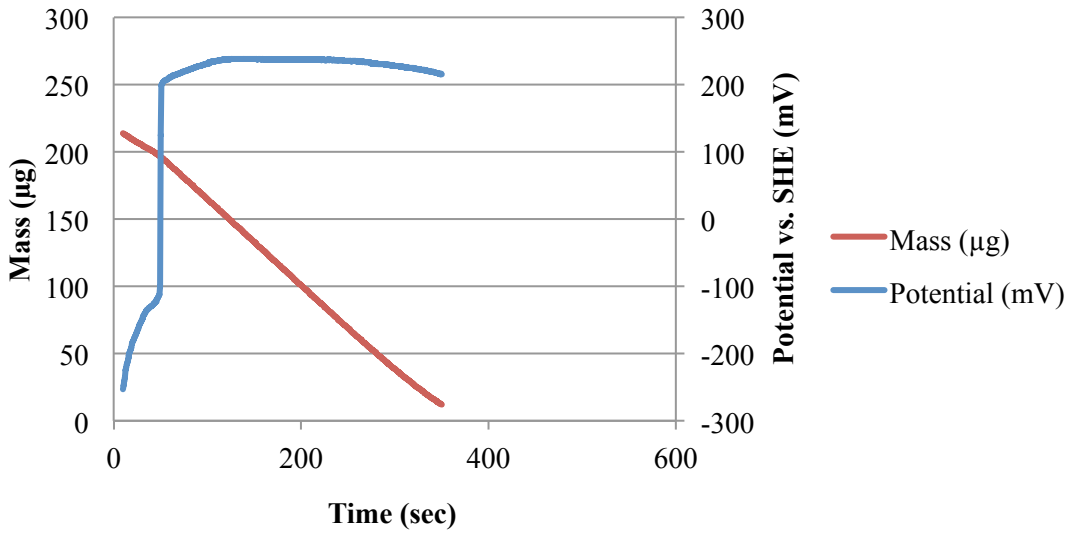

Figure 5-1: REQCM leach data – 5 mM NaCN, 6 mM H_2O_2, oxygen sparging, pH 10.5, 300 min^{-1} – freshly plated electrode

The data gathered for the experiment, where the OCP was allowed to equilibrate prior to cyanide addition is presented in Figure 5-2. At time zero, the cyanide was added and a drop in the OCP of the gold electrode from around 140 mV to around -200 mV can be observed. This is due to the change in reactions occurring on the gold surface. After around 100 seconds the OCP jumps to around 200 mV. This again, represents a change in one of the reactions occurring on the surface. After the initial induction period of around 130 seconds, the mass declines at a constant rate, until the

gold becomes depleted. The maximum leach rate calculated based on the data measured during this test is 15.91 (10^{-5} mol m^{-2} s^{-1}), which can be considered to be the same as baseline leach rate within experimental error.

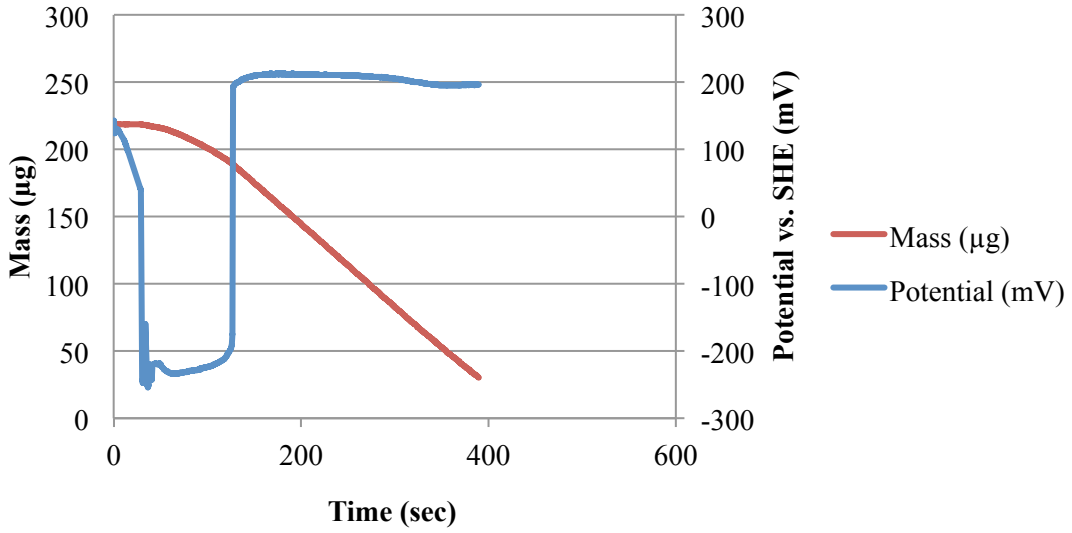

Figure 5-2: REQCM leach data – 5 mM NaCN, 6 mM H_2O_2, oxygen sparging, pH 10.5, 300 min^{-1} – after OCP equilibration in presence of electrolyte and H_2O_2

Figure 5-3 shows the data collected with a gold REQCM electrode after it has been heat-treated. The OCP during the test starts around -240 mV, and then curves down to -270 mV to then slowly increase towards -240 mV; no notable jump in OCP occurs as previously observed (Figure 5-2 and Figure 5-3). The mass decline observed reaches a constant rate after an initial induction period of approximately 60-100 seconds. The leach rate calculated for the linear phase from the measured mass change is 8.88 (10^{-5} mol m^{-2} s^{-1}), which is significantly slower than on the tests conducted on the freshly plated electrode or the test after the OCP equilibration. This indicates, that some of the gold reactivity is lost during the heat treatment. Though not investigated, it cannot be ruled out that there may also be some change in the oxygen reduction reactivity. This indicates also a reduction in the impact of H_2O_2 on the leach kinetics.

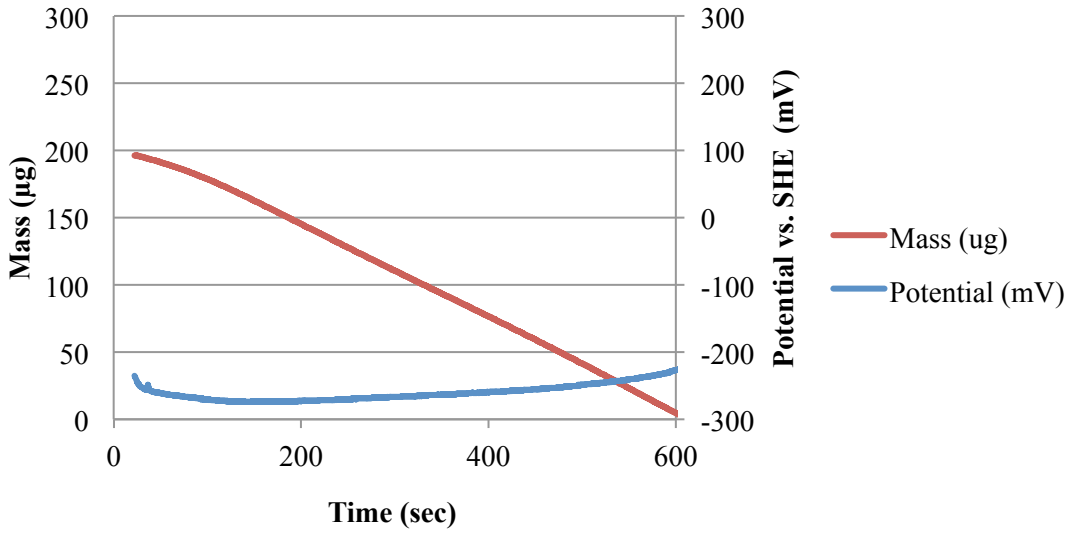

Figure 5-3: REQCM leach data – 5 mM NaCN, 6 mM H_2O_2, oxygen sparging, pH 10.5, 300 min^{-1} – after heat treatment of the electrode

The leach data gathered after conducting a potential scan on a freshly plated gold electrode is plotted in Figure 5-4. The OCP starts at -277 mV and then a constant incline to the final reading of -200 mV can be observed. The mass declines at a constant rate, after an induction period of approximately 120 seconds. This constant rate changes again for the last 50-60 seconds of the leach, indicating the depletion of gold. The leach rate determined for the period of constant mass loss is 10.68 (10^{-5} mol m^{-2} s^{-1}), which is marginally faster than on the heat-treated electrode, but still significantly slower than on the freshly plated gold surface. This indicates, that conducting a potential scan on a freshly electroplated gold surface also causes some of the gold reactivity to be lost, similar to a heat treatment process.

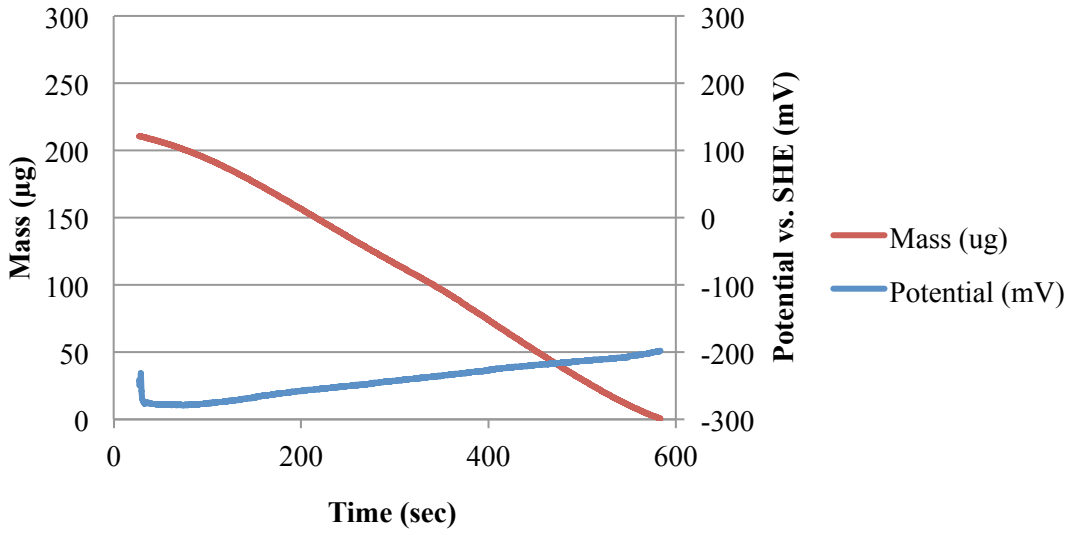

Figure 5-4: REQCM leach data – 5 mM NaCN, 6 mM H_2O_2, oxygen sparging, pH 10.5, 300 min^{-1} – after potential scan

It can be summarised that a freshly plated electrode gold does show a higher reactivity than treated electroplated gold. This was similarly observed in the literature (see Section 2.5.6) in the comparison of the reactivity of electroplated gold to solid gold. However, this test work did not involve the addition of hydrogen peroxide. Some pre-treatments have stronger impacts on the gold reactivity than others. This would be in the order of: no pre-treatment < OCP equilibration < potential scanning < heat treatment. However, hydrogen peroxide might be able to reactivate those surfaces, if it is given longer periods of time, as both leaches with slower leach rates observed show a constant increase of the OCP during the short period available for testing with the REQCM. To be able to draw further conclusions on this impact on 'passive' gold surfaces, which are similar to solid gold, RDE experiments were conducted, as illustrated in Section 5.4.1.2.

5.4.1.2 RDE leach tests

Figure 5-5 presents the increase of gold in solution measured during the RDE leach tests with a gold / 2% silver electrode over time. The first leach test was conducted with air and no hydrogen peroxide addition and its according leach rate is shown

with the red line. A relatively constant increase in Au in solution was measured. An average leach rate of 2.52 (10^{-5} mol m^{-2} s^{-1}) was calculated from this data. The second leach test conducted was with oxygen sparging and no hydrogen peroxide, and is represented by the purple line. After the first 30 minutes a slowing increase of the gold content in solution is observable. The initial leach rate was calculated to be 3.88 (10^{-5} mol m^{-2} s^{-1}), which then declines to a final leach rate of 1.08 (10^{-5} mol m^{-2} s^{-1}). The turquoise line represents the data gathered for the third test under air and with 6 mM hydrogen peroxide in solution. For the first two data points a leach rate of 3.45 (10^{-5} mol m^{-2} s^{-1}) can be calculated, for the points at the 45 and 60 minute mark a slightly increased rate of around 4.25 (10^{-5} mol m^{-2} s^{-1}). The last test, conducted under oxygen sparging with 6 mM hydrogen peroxide present, is plotted in orange. An initial leach rate of 4.23 (10^{-5} mol m^{-2} s^{-1}) can be calculated from the data. A near linear increase in leach rate is observable from there to a final calculated leach rate of 5.70 (10^{-5} mol m^{-2} s^{-1}). It can be seen, that the initial leach rates observed for air sparging are slower than for oxygen sparging. The addition of hydrogen peroxide enhances the leach rates observed for air or oxygen respectively. It is also notable, that hydrogen peroxide in low concentrations in clear solutions appears to have an additional slow effect on the leach rates, as they increase over time. The decrease in leach rate with oxygen sparging to nearly a complete stop could not be explained at this point, but a grey coloured surface coating on the gold was observed. It is to note, that this passivation did not occur once hydrogen peroxide was present in solution. Several repeat tests did show this behaviour reoccurring, even when using fresh reagents. Hence, further investigation on this film and possible causes were conducted, as described in Section 5.4.1.3. This data indicates, that the oxygen reduction limitation on solid gold appears to be more prevalent, than on freshly electroplated gold, as illustrated in Section 4.4.2. Data gathered by REQCM cannot be compared directly to solid gold leaching, as the leach rates observed for the investigated cases may vary by as much as 260% (oxygen and 6 mM hydrogen peroxide RDE maximum rate: 5.7 (10^{-5} mol m^{-2} s^{-1}) versus REQCM maximum rate: 18.2 (10^{-5} mol m^{-2} s^{-1})). Even using a heat treated REQCM electrode, as presented in Section 5.4.1.1, will still generate a difference of around 50%. This means, that

REQCM test work might give an indication on how hydrogen peroxide impacts cyanide leaching of gold. However, the technology is not capable of making accurate forecasts for the behaviour of solid gold.

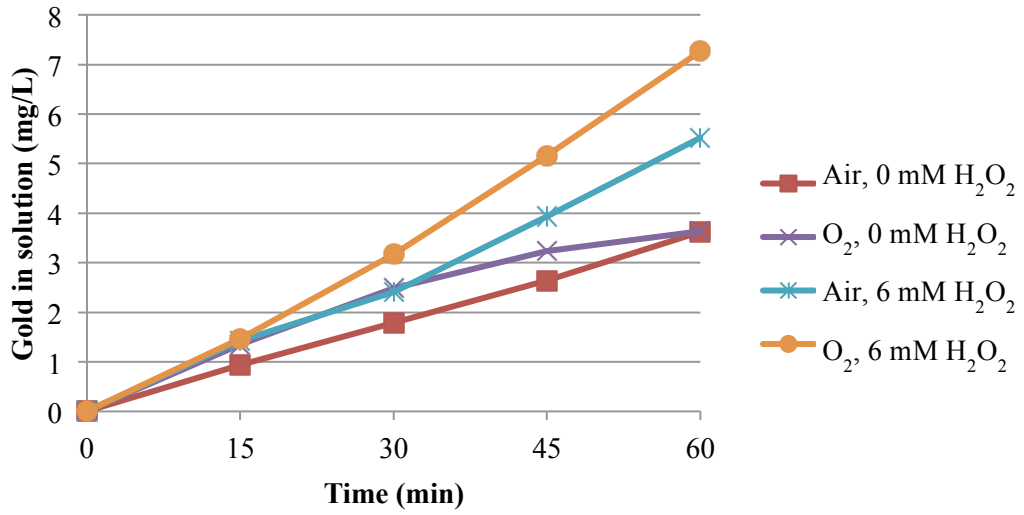

Figure 5-5: Gold concentrations measured in solution during RDE-experiments with 5 mM NaCN, pH 10.5, 300 min^{-1} - varying H_2O_2 concentrations and gas sparging

The measured OCP during the RDE leach tests is plotted against time in Figure 5-6. It can be noted that both curves for aerated solution follow a similar trend, with OCP values after around 30 minutes of leaching reaching similar values around -265 mV vs. SHE. The difference is in the initial 30 minutes of leaching, where the aerated test with H_2O_2 present starts already around the final OCP, but the test without H_2O_2 present starts around -300 mV vs. SHE and slowly increases to the final value. A similar behaviour of the OCP for the oxygenated tests can be seen, where the test without H_2O_2 present starts at around -290 mV vs. SHE and the test with H_2O_2 present round -255 mV vs. SHE. After an induction period of around 15 minutes the OCP for both the oxygenated tests runs in near parallel and reach final values of around -210 mV vs. SHE. The test without H_2O_2 shows a dip of around 20 mV in the OCP between 25 and 42 minutes of leaching, which might be caused by the passivation phenomenon observed for the leach test. The test with H_2O_2 present shows an increase in OCP over the last 8-10 minutes of leaching to around -185 mV

vs. SHE. This could be indicative of the onset of the potential jump, as observed for the REQCM tests in Section 5.4.1.1. This could also explain the constant increase in leach rate over time observed for the test with oxygenation and H_2O_2 present. However, the jump itself could not be observed, most likely due to depletion of H_2O_2 in solution.

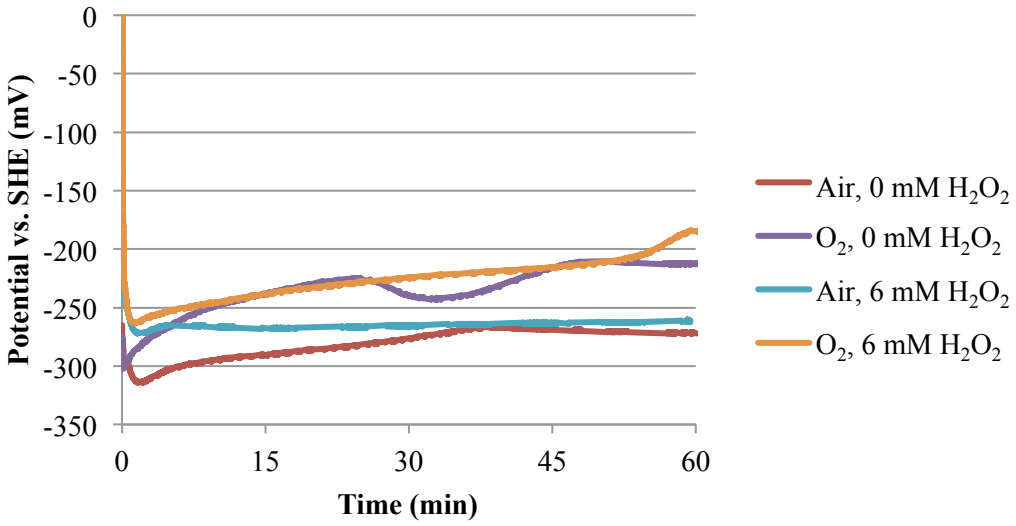

Figure 5-6: OCP measured during RDE-experiments with 5 mM NaCN, pH 10.5, 300 min^{-1} - varying H_2O_2 concentrations and gas sparging

The cyanide concentration in solution during these tests was not measured, as the possible loss during the time of the experiments was considered negligible, taking the cyanide oxidation data presented in Section 4.2.1 into consideration.

5.4.1.3 XPS analysis

The pictures presented in Figure 5-7 show the gold specimen, which was used for the XPS analysis. The left picture shows the highly reflective and polished gold surface (camera visible in the reflection) prior to being introduced into the leach solution. The right picture shows the gold surface after being exposed to the leach solution for 60 minutes. The grey/dark yellow tarnishing of the surface is clearly notable. It can

also be noted, that the crystalline structure of the gold is not showing, as it did in all leach tests with a constant or increased leach rate, as described in Section 5.4.1.2.

Figure 5-7: Gold specimen for XPS – left, as polished before leach – right, as removed from leach

Due to the complexity of interpreting XPS raw data, the data is interpreted in Appendix A, and only the summaries and interpretation of the obtained information are presented at this point.

The raw data gathered on the specimen after leaching is interpreted in Section A.1. The two subsequent sections, A.2 and A.3, show the specimen after light and hard etching and therefore will give indication on the thickness and strength of the surface coating. Section A.4 presents the data gathered on the sample without any coating on the surface, so the coating can be differentiated from baseline data.

In Table 5-1 all identified peaks for all four scans are presented. For each peak the position in eV and the corresponding atomic concentration are shown. Peaks, which are thought to be caused by the same element in the same chemical state in the different scans are listed in the same row. Hence, if a peak does not occur for a scan the corresponding place in the table is blank.

Polished electrode

The polished electrode does show one gold peak (Au 1s @ 84.1 eV), which represents the gold in its natural state. The atomic concentration shown correlates with a 98% Au, 2% Ag electrode. There are two silver peaks present, one of which (Ag 3d I @ 368.1 eV) can be assumed as silver in metallic state. The second identified peak (Ag 3d II @ 368.8 eV) could be silver in its charge transfer state (Eremenko et al., 2011). The overall atomic percentage is in range for a material of gold/2%silver.

The oxygen peaks observed are most likely due to adventitious oxygen, settled in the crystalline structure of the specimen. The amount of oxygen detected as O 1s II at 532.9 eV could be bound with the Ag 3d II peak as a silver oxide, bearing in mind that XPS readings can be within +-1% of the actual value, especially at such low concentrations.

Adventitious carbon might be the reason for the detection of the carbon peak. However, the amount of carbon observed also correlates with the O 1s I peak, if CO_2 could be present in the surface layer (9.3% O, 5.6% C).

Electrode after leaching

For the electrode after leaching, compared to the polished electrode, a significant decrease in the atomic gold concentration can be seen (80.7% -> 18.5%). With this significantly reduced availability of gold to the surface, the decrease in leach rate observed in Section 5.2.2 can be explained. A minimal shift in the peak position from 84.1 to 84.0 eV is observable. This might be due to the impact of the high concentrations of other materials on the surface on the peak position.

Four different silver peaks are observed, which indicates that the silver is present in four different chemical species. The first two peaks (Ag 3d I and Ag 3d II) are showing at the same binding energy positions (-0.1 eV), as observed in the polished scan. It can be concluded, that these two species are the same as on the polished

electrode, elemental silver in its metallic state and in its charge transfer state (Eremenko et al., 2011). The observed relative quantities between these two species are the same, as for the polished electrode. However, the overall concentration observed is increased 2.5 fold. Two further silver peaks are observed, and matching with the other elements observed is suggested below.

Two oxygen peaks are detected, however with significantly different binding energies, than on a polished surface. The first oxygen peak is at 532.4 eV, the second at 533.9 eV (compared to 531.6 and 532.9 eV). The corresponding atomic concentrations determined are 28.3% and 5.8%. It can be assumed, that the oxygen observed is chemically bound differently when compared to the oxygen seen on the polished electrode. Further, as hydrogen cannot be detected with XPS, one of the oxygen peaks could represent water (H_2O) on the surface, possibly bound to a carbonate.

Significant amounts of carbon were observed on the surface in four different peaks. The C 1s I peak could represent carbon in its natural state and therefore be adventitious carbon, the C 1s III peak correlates with metal carbonate species, as shown in Section A.1. Within the error of XPS analysis and considering the penetration depth and layering of products, the C 1s III and O 1s II peak, in combination with one of the Ag 3d I, Ag 3d II or Ag 3d IV peaks, could be silver carbonate on the surface. However, the chemical binding of the C 1s II and C 1s IV peak would require further detailed investigation for a complete understanding, which was not in the main focus of this study.

The sulphur observed on the surface was in the binding energy range for metal sulphides, as shown in Section A.1. It is also known, that silver tarnishes under atmospheric conditions (McMahon, Lopez, Meyer, Feldman, & Haglund, 2005) and forms Ag_2S from atmospheric H_2S and carbonyl sulphide, OCS. Considering the atomic concentrations of both the sulphur peaks and the Ag 3d II peak, part of the surface coating could be Ag_2S. It is assumed, that the solution composition during

these specific RDE tests does enhance the reaction between the atmospheric sulphur compounds and the silver present on the surface of the electrode.

Light etched electrode

After a light etch the gold available on the surface has increased from 18.5 to 28.5%, which indicates a reduction of the other species at the specimen surface. This can be interpreted in a way, showing that some of the species on the surface hindering the leach are easily removed and it is only a very thin layer.

Two silver peaks are observed (reduced from four on the leached specimen), as seen in the scan on the polished specimen, including matching binding energies. However, the concentrations observed are slightly increased compared to the freshly leached specimen. This could be accounted for by the removal of other species on the surface, so the silver is more predominant in the surface composition. Another explanation could be, comparing the overall concentration of silver (leached specimen: 6.6%, etched scan: 6.7%), by a peak fitting resulting in the detection of fewer peaks, than on the initial scan (shown in sections A.1 and A.2). There is still a silver enrichment of elemental silver in the surface composition present (Ag 3d I). Furthermore, the quantity of silver detected as the Ag 3d II can be well matched with the S 2p I peak, and therefore could represent an Ag_2S coating.

The oxygen concentration observed on the surface is significantly increased over the initial scan on the specimen (from 28.3+5.8% to 39.4+7.4% - for O 1s I + O 1s II). This can only be explained by the reduction of other surface components. The relation of the O 1s I to O 1s II peak is only marginally changed between the initial scan and the scan after the light etch. The peak position of the O 1s I peak only shifted marginally from 532.4 to 532.6 eV. The chemical binding of the oxygen can be assumed to be similar to the scan conducted on the leached surface. Due to the method XPS uses for elemental detection hydrogen cannot be detected. A possible explanation of the high O 1s I peak could be the presence of water (H_2O) on the surface, possibly bound to a carbonate or adsorbed into the crystalline structure.

The amount of carbon detected on the surface is reduced significantly compared to the specimen as received. Also, one less peak has been detected. The C 1s I peak could be interpreted as adventitious carbon, and the other two species might be some chemically bound carbon, particularly carbonate species are possible. However, it is unclear how the carbonate species would bind to the surface.

The sulphur amount detected on the surface is slightly reduced over the amount detected in the initial scan. Within the analytical error of XPS quantification, the S 2p I peak could be matched with the Ag 3d II peak to result in a 1:2 ratio, as would be encountered for Ag_2S. This was already similarly observed in the initial scan. However, the peak positions are shifted compared to the initial scan. The second sulphur peak might be due to sulphide ion adsorption on the gold surface.

After hard etching

The additional hard etching did not produce a significant change to the surface composition observed after the light etch. The atomic fractions of gold, silver, oxygen, carbon and sulphur stayed nearly the same as prior to hard etching. Only the spread over the different peaks detected for carbon is changed within +-2% for each peak and the sulphide peak detected could not be split into two peaks. This indicates, that the species bound to the surface or adsorbed within shallow areas of the surface lattice of the specimen are relatively strong.

Summary

The analysis of the surface coatings via XPS could not reveal a perfect answer to the constitution of the surface layer. But it was evident, that the solution and experimental conditions used during the test aided the adsorption of atmospheric sulphur onto the surface and a reaction with the silver. Further the adsorption of carbonate species is indicated, but cannot be confirmed. This phenomena has not been observed by other experimenters and as such appears to be very rare. Even though carbonaceous (including carbonates) hindrance of gold leaching has been

shown before (Tan, Feng, Lukey, & van Deventer, 2005), it appears usually to be ore grinding related. The reaction of atmospheric sulphur species with silver, mainly H_2S and OCS were also previously investigated (McMahon et al., 2005), however, have not been observed in solutions.

Table 5-1: Summary of XPS analysis results for variously treated gold/silver surfaces

	after leaching		after light etch		after hard etch		after polish	
Peak name	**Peak Position (eV)**	**Atomic Concentration (%)**	**Peak Position (eV)**	**Atomic Concentration (%)**	**Peak Position (eV)**	**Atomic Concentration (%)**	**Peak Position (eV)**	**Atomic Concentration (%)**
Au 4f	84.0	18.5	84.1	28.5	84.1	30.1	84.1	80.7
Ag 3d I	368.0	4.9	368.1	5.1	368.1	4.8	368.1	1.8
Ag 3d II	368.7	1.1	368.8	1.6	368.8	1.4	368.8	0.3
Ag 3d III	366.8	0.3						
Ag 3d IV	370.6	0.3						
O 1s I	532.4	28.3	532.6	39.4	532.4	39.7	531.6	9.3
O 1s II	533.9	5.8	533.9	7.4	533.9	7.5	532.9	2.4
C 1s I	284.6	15.9	284.8	7.6	284.9	6.2	~280-290	5.6
C 1s II	286.4	18.2	286.5	8.0	286.4	6.4		
C 1s III	288.0	3.7	288.1	1.2	288.7	3.0		
C 1s IV	290.1	1.2						
S 2p I	160.9	1.2	161.5	1.0				
S 2p II	162.1	0.6	163.7	0.3	162.1	1.1		

5.4.2 Potentiodynamic investigation of gold and silver

The unexpected jump in the OCP observed for some tests in Section 4.4.2 with a gold REQCM electrode has given rise to the suggestion of some unusual behaviour of either the gold oxidation or the oxygen reduction occurring on the gold surface during leaching. To investigate this behaviour several potential scans were conducted, as presented in this Section.

Gold/silver electroplated

In Figure 5-8**,** a potential scan conducted with a freshly plated REQCM electrode, of gold oxidation with cyanide present under oxygen depleted conditions is presented. The measured current density, along with the calculated anodic (gold oxidation from mass change) and the calculated cathodic (oxygen reduction) current densities are plotted against the potential. The calculated cathodic current is a result of the subtraction of the calculated anodic current from the measured current. The measured and the calculated anodic current density from mass loss both show a linear rise up to a potential of -100 mV and then near flatline at their maximum current until the endpoint of the scan at 500 mV. The calculated cathodic current density is nearly a flat line around 0 A/m^2, with a small spike to -0.8 A/m^2 at a potential of -130 mV. This spike in the cathodic current was possibly caused by side reactions on the surface with components of the solution. The scan was repeated 3 times, always giving consistent results (the currents observed were within 1% of the other scans). As the change in current is not reflected in the current calculated from mass change, no change in gold dissolution took place. After the initial test showing this spike (2h), nitrogen purging of the solution took place but did not result in a change of the obtained data. The maximum measured and calculated (from mass loss) anodic current density, is in close agreement with the theoretically diffusion limiting calculated current for this NaCN concentration, as shown in Section 3.4.1, with 6.9 versus 7.1 A/m^2 for the measured and theoretical currents respectively. The gold oxidation current density curve observed on this surface aligns with previously

gathered data by other experimenters (see Section 2.5.4) and therefore no significantly unexpected results are obtained.

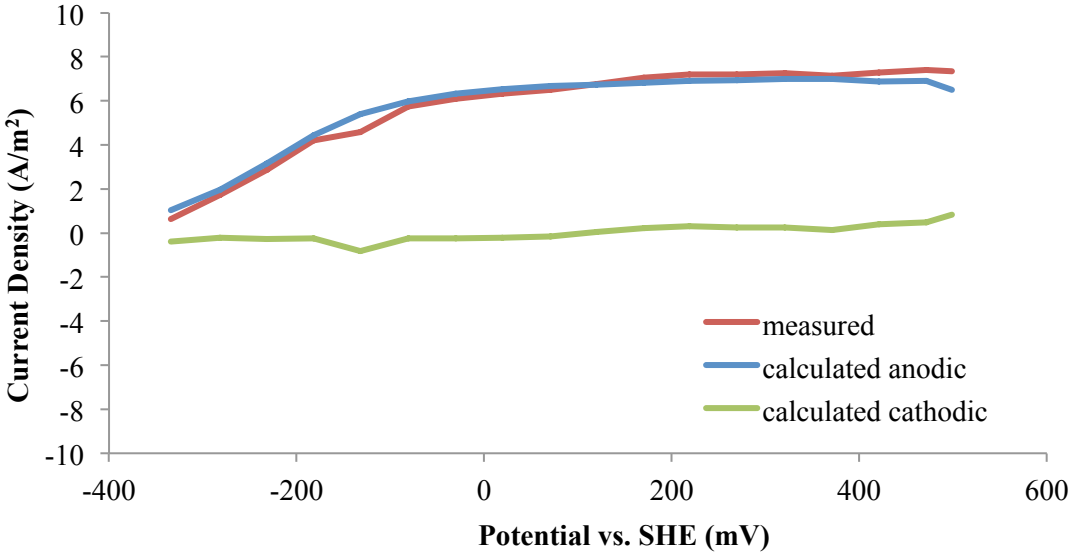

Figure 5-8: Potential scan on Au/2%Ag fresh plated surface, 2.5 mM NaCN, N_2 sparged, pH 10.5, 300 min^{-1}, positive direction, scan rate 5 mV/s

The cathodic curve and the anodic current density calculated from observed mass loss for cyanide free solution with air and H_2O_2 are presented in Figure 5-9. It can be seen, that the current density resulting from mass change is 0 A/m^2 throughout this scan, indicating no measurable mass loss or gain is occurring on the surface. The measured current density in the negative potential area matches a typical oxygen reduction on gold for solutions with H_2O_2 present, as presented in Section 4.4.1.3, however, a greater current is measured due to the higher H_2O_2 concentration used in this test. In the positive potential region, a positive current can be noted. This is most likely caused by the oxidation of peroxide and a resulting early onset of oxygen evolution, aided by the presence of H_2O_2, as previously shown by Gerlache, Senturk, Quarin, and Kauffmann (1997). No behaviour of this system, explaining the jumps in the OCP, as observed in Section 4.4.2, can be identified.

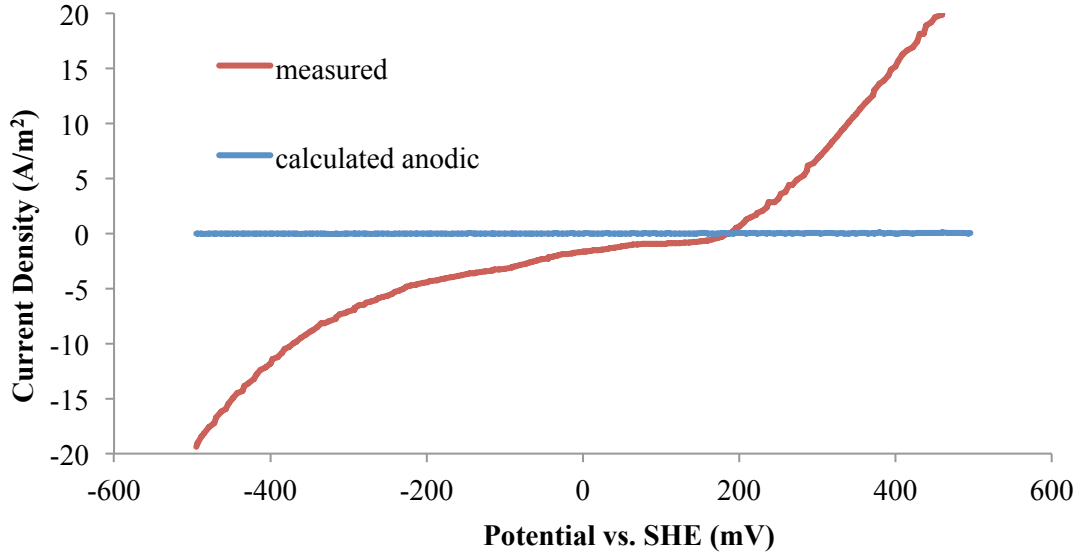

Figure 5-9: Potential scan on Au/2%Ag fresh plated surface, 6 mM H_2O_2, aerated, pH 10.5, 300 min^{-1}, negative direction, scan rate 5 mV/s,

The complete leach system, with NaCN and H_2O_2 present was scanned and the resulting current densities are plotted in Figure 5-10. The blue line represents the calculated anodic (from mass change) current density assuming gold oxidation is the only anodic reaction occurring. The red line shows the measured current density. The green line is the cathodic current density, calculated from the mass change and measured current density. The purple line is an inverted plot of the calculated cathodic current density, to enable easy observation of the intersecting points of the anodic and cathodic current densities. The anodic current density closely matches the data obtained during the nitrogen sparged anodic scan, as shown in Figure 5-8. However, the cathodic current density curve shows two highly active regions, one below the potential of around -250 mV, as expected for oxygen reduction, and one between 0 and 300 mV, which is attributed to peroxide reduction. Between these two active regions a more passive region can be observed.

The inverted cathodic and the anodic current densities intersect at three potentials in this figure: -226, -28 and 272 mV. The first potential is in close agreement with typical gold leaching OCPs observed (see Section 2.5.6), however, the second and the third are unusual. The third potential of 272 mV agrees with the OCPs observed

during the factorial design test work, as presented in Section 4.4.2, when a potential jump was observed. This shows, that in the presence of NaCN, H_2O_2 displays a different reduction behaviour than with no NaCN present.

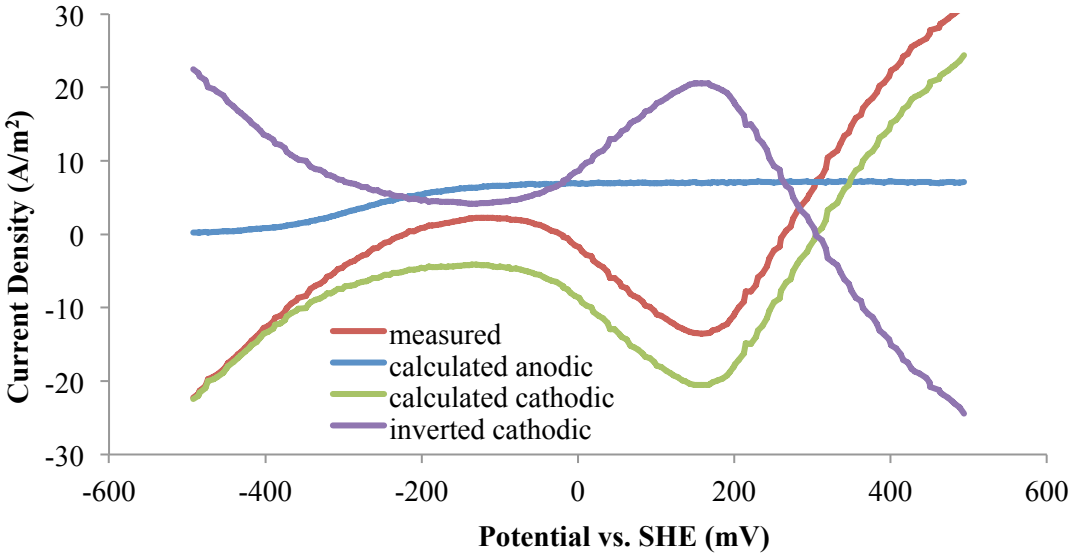

Figure 5-10: Potential scan on Au/2%Ag fresh plated surface, 2.5 mM NaCN, 6 mM H_2O_2, aerated, pH 10.5, 300 min^{-1}, negative direction, scan rate 5 mV/s

Silver electroplated

All previous leach test work and potential scans were conducted on gold/silver electrodes, and a similar behaviour was not found in the literature review for gold/silver alloys (see Sections 2.5.4 and 2.5.6). To further understand the role silver might have on this phenomenon tests were also conducted on pure electroplated silver.

Figure 5-11 presents the measured and calculated (from mass change) current densities versus potential observed during a scan on a pure silver electrode in an aerated electrolyte solution. The calculated current density stays around 0 for the whole scan, within a range of 0.5 to -0.45 A/m^2. This is assumed to be experimental error, possibly caused by some noise in the frequency and therefore mass reading. Cleaning of the electronics and checking of wires did not result in complete

eradication of the issue. The measured current follows a typical oxygen reduction curve as it could also be observed on gold (see Section 2.5.4).

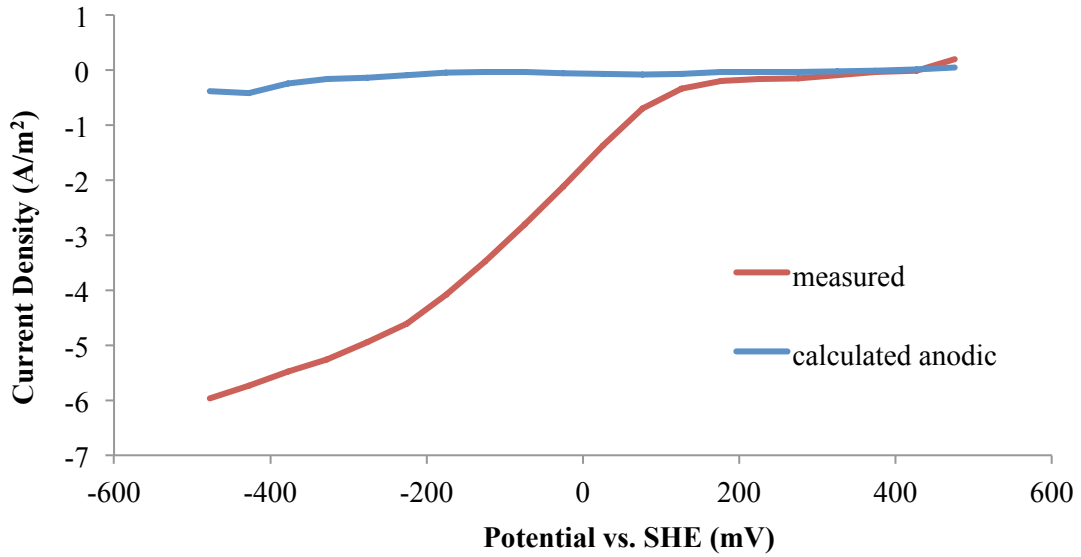

Figure 5-11: Potential scan on Ag freshly plated surface, aerated, pH 10.5, 300 min^{-1}, negative direction, scan rate 5 mV/s

The scanning of the potential and measuring the resulting current density for a plated silver surface in an aerated H_2O_2 electrolyte solution resulted in the data shown in Figure 5-12. The calculated current density from mass change stays nearly constant at 0 A/m^2. This indicates no mass change, hence no deposit or removal of mass on the surface occurs. The measured current density shows two strongly developed cathodic (oxygen reduction) areas, one below -250 mV and the second one around 150 mV, with a relatively passive area between them. It can be concluded, that H_2O_2 reduction on silver occurs in both areas and is significantly different to the oxygen reduction (aerated) on silver. It can also be noted, that this curve displays similar passive and active regions to the ones observed for the gold/silver oxygen reduction curve with H_2O_2 and NaCN present, as shown in Figure 5-10.

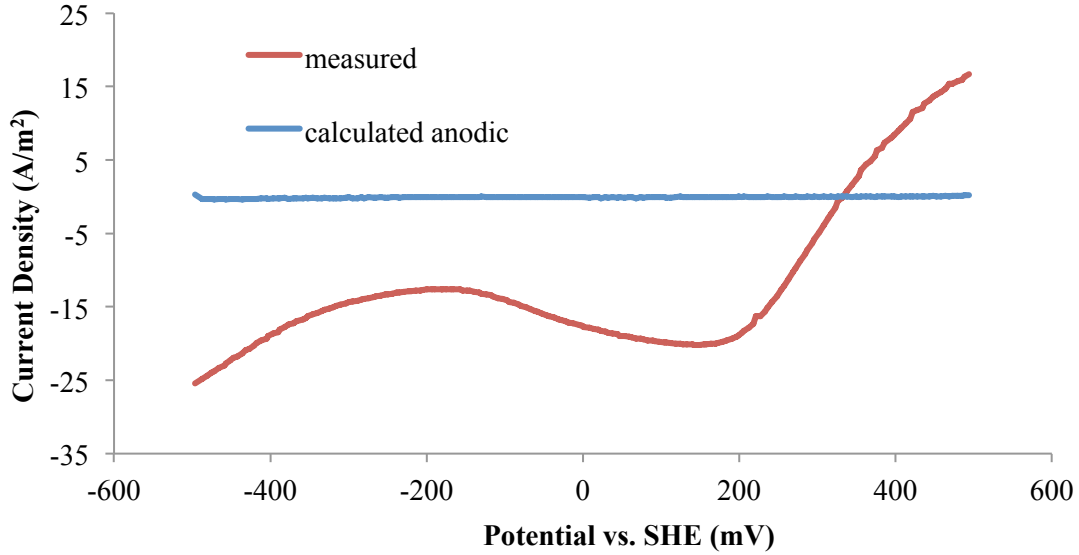

Figure 5-12: Potential scan on Ag freshly plated surface, 6 mM H_2O_2, aerated, pH 10.5, 300 min^{-1}, negative direction, scan rate 5 mV/s,

Figure 5-13 plots the current density, measured and calculated, against potential for a pure silver electrode leach with NaCN and H_2O_2 present. The calculated (from mass loss) anodic current starts at a current density of 0 and then shows a linear increase in the potential region from -350 to -100 mV to a maximum current density of around 7.0 A/m^2. This value is in close agreement with the current density obtained for gold in Figure 5-8 (gold and silver have the same limiting rates, as the oxidation reaction is the same), showing that the silver oxidation by cyanide is not influenced by the presence of oxygen or hydrogen peroxide. The calculated cathodic curve starts around -21 A/m^2 and then a decrease in current can be observed with a low plateau between the potential of -290 and -70 mV. The low plateau shows a current density of around -8.5 A/m^2. Then a second peak in current density of around -27.7 A/m^2 is visible between 100 and 200 mV, followed by a linear decline and transfer into the positive current region. This shows, that H_2O_2 reduces in two potential regions on silver, with a passive area present between them. This shape of two distinct oxygen reduction regions was already observed on silver without NaCN, as shown in Figure 5-12, but it indicates, that the presence of NaCN enhances H_2O_2 reduction on the silver surface, as the second region appears more prominent. The inverted oxygen reduction and calculated current density only shows one point of intersection at a

potential of 313 mV and a disconnection of the possible other points. This potential is close to some OCPs observed during the gold leach tests, as shown in Section 4.4.2.

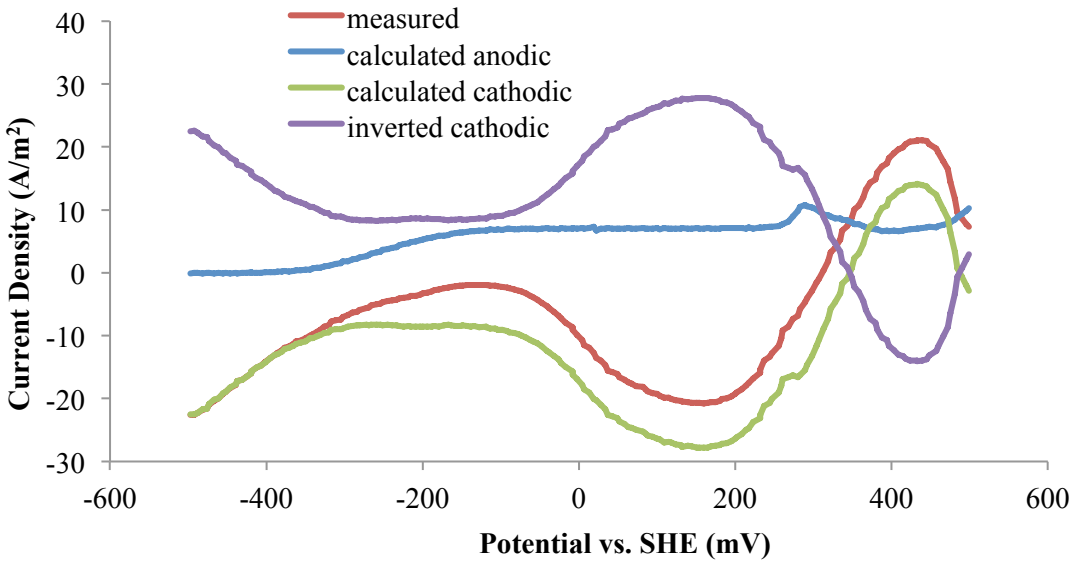

Figure 5-13: Potential scan on Ag freshly plated surface, 2.5 mM NaCN, 6 mM H_2O_2, aerated, pH 10.5, 300 min^{-1}, negative direction, scan rate 5 mV/s

Gold electroplated

The behaviour of gold and gold/silver is shown in the previous part of Section 5.4.2. To further understand the role that pure gold might have on the phenomenon of the sudden potential jump noted in Section 4.4.2, tests were also conducted on pure, electroplated gold.

Figure 5-14 presents the measured and calculated (from mass change) current densities versus potential observed during a scan on a pure gold electrode in an aerated electrolyte solution. The calculated current density stays around zero for the whole scan. The measured current follows a typical oxygen reduction curve on gold as described in literature (see Section 2.5.4).

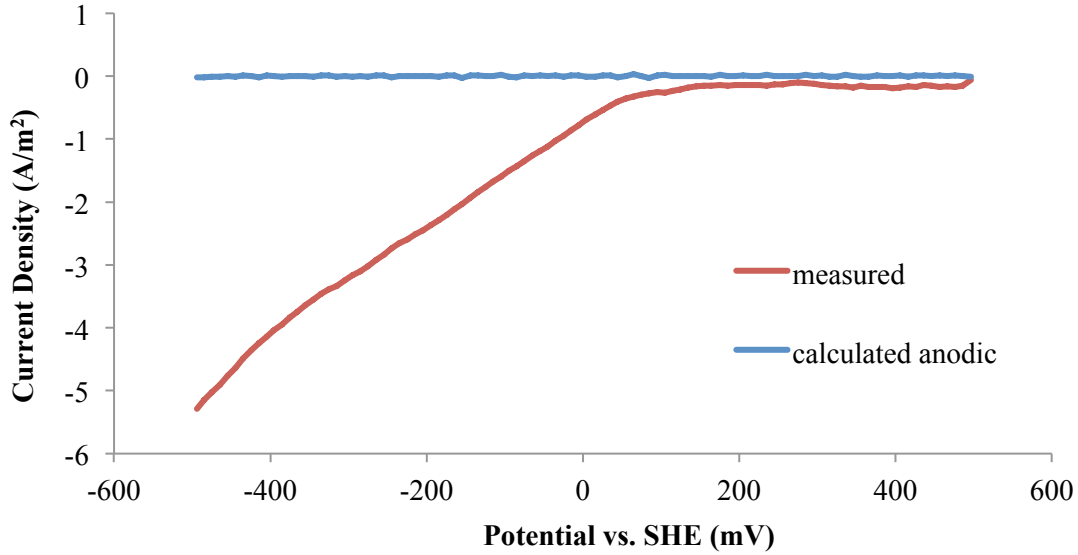

Figure 5-14: Potential scan on Au freshly plated surface, aerated, pH 10.5, 300 min^{-1}, negative direction, scan rate 5 mV/s

The data shown in Figure 5-15 is based on scanning the potential and measuring the resulting current density for a plated pure gold surface in an aerated H_2O_2 electrolyte solution. The calculated (from mass change) anodic current density stays near constant at 0 A/m^2. It can be concluded, that no notable mass change takes place during this scan. The measured current density shows an oxygen reduction curve, as expected for gold with very high dissolved oxygen levels in solution (beyond the normally achievable 32 ppm under oxygen sparging). It can be concluded, that H_2O_2 reduction on gold functions similar to the oxygen reduction of aerated solutions.

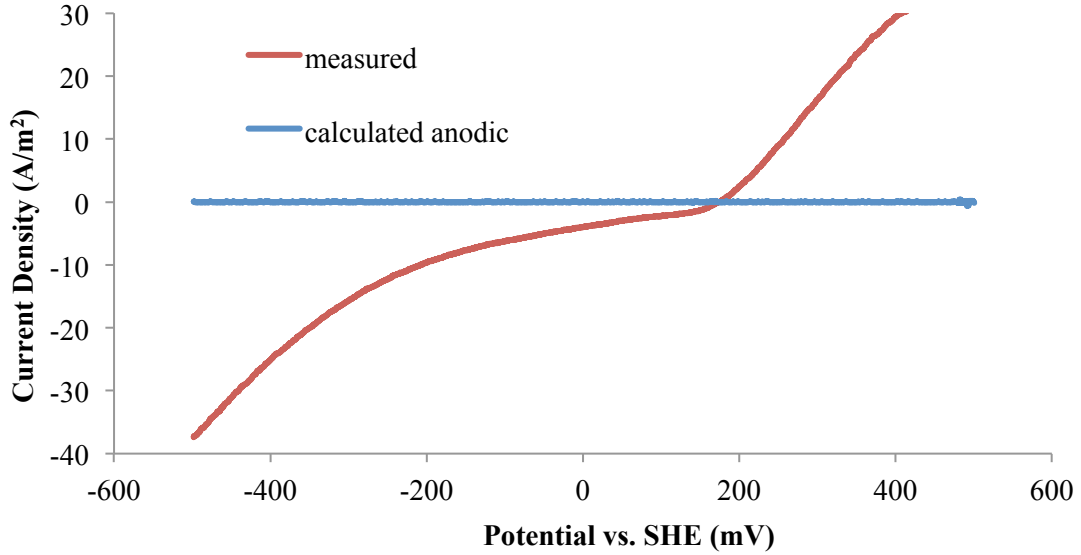

Figure 5-15: Potential scan on Au freshly plated surface, 6 mM H_2O_2, aerated, pH 10.5, 300 min^{-1}, negative direction, scan rate 5 mV/s

Figure 5-16 plots the current density measured and calculated against the potential for a pure gold electrode with NaCN and H_2O_2 present. The calculated (from mass loss) anodic current density starts at a current density of zero and then shows a linear increase in the potential region from around -350 to -100 mV to a maximum current density of 7.1 A/m^2. This value is in close agreement with the gold oxidation current obtained in Figure 5-8. The calculated cathodic curve starts around -26 A/m^2 and then a decrease in current can be observed with a low current density between the potential of -290 and -70 mV. This low current density is around -2 A/m^2. Then a second peak in current density of around -27.8 A/m^2 is visible between 100 and 150 mV, followed by a linear decline and transfer into the positive current region. This shows, that H_2O_2 reduces in two potential regions on pure gold, with a passive area present between them. The second region was not observed on pure gold without NaCN, as shown in Figure 5-15, but it appears that the presence of NaCN changes the H_2O_2 reduction on the gold surface. The inverted oxygen reduction and calculated current density curves show three points of intersection at the potentials of -159, 35, and 230 mV.

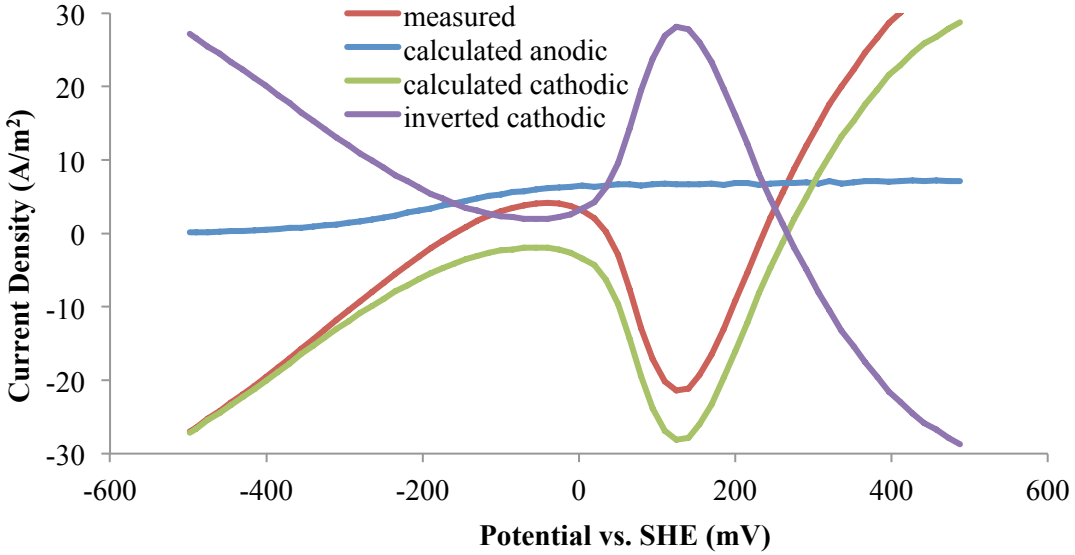

Figure 5-16: Potential scan on Au freshly plated surface, 2.5 mM NaCN, 6 mM H_2O_2, aerated, pH 10.5, 300 min^{-1}, negative direction, scan rate 5 mV/s

Summary

It appears that the potential jumps observed during some tests presented in Section 4.4.2 are caused by the reduction of H_2O_2 on a silver surface. This assumption is based on the disconnection of the two lower intersecting points of cathodic and anodic reaction, which were only observed for the pure silver scan with NaCN present, shown in Figure 5-13. All other tests retain two additional possible leach points at lower potentials. As all tests in Section 4.4.2 utilised a gold/silver surface, and the tests presenting the jump in OCP did have a low cyanide:oxidant ratio, a highly silver enriched surface can be concluded as the cause for the potential jump observed, considering literature postulates a preferred leaching of gold under these cyanide limiting conditions (Dai & Breuer, 2013). This would also explain the induction period required, before the maximum leach rate and the potential jumps were noted, as shown in Section 4.4.2.

5.4.3 Conclusions

The behaviour of pre-treated electroplated gold and solid gold in synthetic solutions without known contaminants has been investigated. It has been shown, that the

highly reactive nature of electroplated gold can be reduced similar to that of solid gold by heat treatment or potential scanning of the plated gold. It was further shown that leach rates measured for electroplated gold cannot be compared with leach rates obtained by solid gold leaching experiments, due to the different reactivity of the two materials. Unexpected passivation of the solid gold during leach tests was observed. The cause was identified as a combination of the solution composition aiding the formation of a carbonate coating as well as a silver sulphide on the surface from atmospheric sulphur, possibly attained during sample transfer to the XPS facility. This coating only occurs, when the oxygen reduction reaction as well as the gold oxidation reaction are occurring at similar rates caused by corresponding diffusion limiting rates. It has further been shown that hydrogen peroxide at low concentrations is capable of stopping the occurrence of this coating.

Further, it was demonstrated that the potential jump observed during the leaching of electroplated gold/silver alloy in the presence of hydrogen peroxide, as observed in Chapter 4, is caused by an enrichment of silver on the leach surface. This enrichment leads to a different reduction of hydrogen peroxide on the surface causing the OCP potential of the electrode to jump.

The next chapter investigates the impact of sulphide ions on gold leaching and the possible remedial effect of hydrogen peroxide, as some results of this chapter indicate a possible beneficial effect.

Chapter 6 Impact of sulphide ions and hydrogen peroxide on gold leaching in clear solutions

6.1 Introduction

This chapter presents an experimental investigation of the impact of sulphide ions on gold leaching in NaCN solutions, with a focus on possible remedial effects of H_2O_2 addition, utilising RDE technology. As outlined in Section 2.1.4, the gold leaching rate in a clear system can be significantly hindered by sulphide ion adsorption to the gold surface; the presence of sulphide ions in solution coming from the dissolution of sulphide minerals during processing. This hindrance can be remedied by the lead assisted oxidation of the adsorbed sulphide ions. Typical oxidation pathways of sulphide ions, particularly of the lead catalysed oxidation, and the resulting products in alkaline solutions (with and without oxygen) are described in Section 2.4.2. The target of this investigation is to determine the species produced when cyanide, sulphide, and H_2O_2 are added in various orders into solutions without lead nitrate present and the effects on the dissolution of gold from a 2% Ag, 98% Au alloy. The main objective is to determine if the retarding effects of adsorbed sulphide ions on the gold surface during leaching can be removed or mitigated by the addition of H_2O_2 in various scenarios. As a secondary objective, these scenarios are to be evaluated in terms of possible reagent consumption.

This chapter is divided into two major parts. The initial part contains preliminary experiments to determine, whether pH control during the leaching experiments with sulphide addition would be necessary. The second part investigates the addition of sulphide ions after or prior to NaCN addition in the form of Na_2S on RDE leach tests. The sulphide concentration chosen for these tests was based on literature sources (M. Massoud Aghamirian, 1997; M. I. Jeffrey & Breuer, 2000), investigating the effect of lead nitrate and other remedial reagents on sulphide-hindered leaches. H_2O_2 addition

was chosen, based on possible stoichiometric reactions with S^{2-} ions and NaCN in alkaline solutions.

6.2 Preliminary experiments

6.2.1 pH-stability and sulphide ion oxidation in homogeneous solution

As sulphide addition and oxidation may have an impact on the solution pH, preliminary scoping experiments on just solutions were undertaken to ensure the solution pH was stable within a typical safe operating range between pH 10 and 11. A pH was targeted to avoid pH control during the planned leach tests, as described in Section 6.3. Two tests with 100 mL electrolyte solution, as described in Section 3.2.6 were conducted in a 150 mL glass beaker with a magnetic stirrer set at a low speed and with constant oxygen sparging. The experiments were conducted according to Table 6-1, and Table 6-2, using Na_2S solution, H_2O_2 solution, and concentrated NaCN solution as described in sections 3.2.13, 3.2.1, and 3.2.4 respectively. The pH was monitored as indicated in Tables 6-1 and 6-2, and a final solution composition of sulphide species was measured using the HPLC, according to Sections 3.3.3, and 3.5.4, respectively.

Table 6-1: pH and sulphide species scoping experiment 1 schedule

Time (min)	Solution changes	Sampling/Measurement
0	Electrolyte + 10 mM NaCN	pH
0	+ 1 mM Na_2S	pH
30	-	pH
30	+ 8 mM H_2O_2	pH
120	-	pH HPLC samples

Table 6-2: pH and sulphide species scoping experiment 2 schedule

Time (min)	Solution changes	Sampling/Measurement
0	Electrolyte	pH
0	+ 1 mM Na_2S	pH
30	-	pH
30	+ 8 mM H_2O_2	pH
90	-	pH
90	+ 10 mM NaCN	pH
180	-	pH HPLC Samples

6.3 RDE-Leach tests

6.3.1 Hydrogen peroxide addition after exposure to sodium cyanide and sulphide

RDE leach tests with exactly 1 L of 10 mM NaCN solution, made from electrolyte solution and concentrated NaCN solution, as described in Sections 3.2.6, and 3.2.4, were conducted. All tests were conducted with oxygen sparging at a gas flow rate of 50 mL/min, resulting in oxygen saturation of the solution. Initially the polished gold RDE electrode, containing 2% Ag, as described in Section 3.4.3, was exposed to the leach solution. The rotation speed was set to 300 min^{-1} throughout all experiments. After leaching for 60 minutes, S^{2-} ions in the form of 500 mM Na_2S solution were added, targeting a concentration of 1 mM Na_2S in the solution. Thirty minutes after the Na_2S addition, 500 mM H_2O_2 was added to give the following stoichiometric ratios of H_2O_2 : sulphide: 2:1, 4:1, 6:1 and 8:1. The leach was then conducted for a further 90 minutes. During the whole experiment run time, the OCP of the gold electrode against a Ag/AgCl reference electrode was measured with a potentiostat and stored via a computer, as described in Section 3.4.4.

Samples were taken as shown in Table 6-3, and analysed with an AAS for their respective Au and Ag content, as described in Section 3.5.2. Samples were also analysed for S^{2-}, SCN^{-}, SO_3^{2-}, $S_2O_3^{2-}$, and SO_4^{2-} with HPLC analysis, as described in Section 3.5.4. Further samples were titrated with silver nitrate for their respective NaCN concentration with the method described in Section 3.5.1.1.

Table 6-3: Sample table for sulphide hindered leach tests – NaCN before H_2O_2 addition

Time (min)	AAS samples	HPLC samples	NaCN titration samples
0	AA 1	--	CN 1
30	AA 2	--	--
60	AA 3	HPLC 1	CN 2
90	AA 4	HPLC 2	--
120	AA 5	HPLC 3	CN 3
150	AA 6	HPLC 4	--
180	AA 7	HPLC 5	CN 4

6.3.2 Hydrogen peroxide addition after sulphide addition, prior to sodium cyanide addition

Additional RDE tests were conducted, where the order of reagent addition was altered. The RDE electrode was prepared as described in Section 6.3.1 and then introduced into exactly 1 L of electrolyte solution, as described in Section 3.2.6, with addition of 500 mM Na_2S to target a 1 mM concentration in the solution. The electrode was rotated at a speed of 300 min^{-1} for all experiments. After 30 minutes, H_2O_2 was added in the stoichiometric ratios H_2O_2:sulphide of 2:1, 4:1, 6:1 and 8:1. After a further 60 minutes, concentrated (1 M) NaCN solution, as described in Section 3.2.4, was added into the solution, targeting a 10 mM NaCN concentration in the solution. The leach was conducted for a further 90 minutes. Samples were taken as shown in Table 6-4 and analysed as described in Section 6.3.1.

Table 6-4: Sample table for sulphide hindered leach tests – NaCN after H_2O_2 addition

Time (min)	AAS samples	HPLC samples	NaCN titration samples
0	--	HPLC 1	--
30	--	HPLC 2	--
60		HPLC 3	--
90	AA 1	HPLC 4	CN 1
120	AA 2	HPLC 5	CN 2
150	AA 3	HPLC 6	CN 3
180	AA 4	HPLC 7	CN 4

6.4 Results and discussion

The interaction between the three reagents, namely H_2O_2, NaCN and Na_2S, was observed. It was found, that depending on the order of mixing, the resulting reactants and reagent consumption varied significantly. The results are presented in Sections 6.4.1 to 6.4.3.

6.4.1 Preliminary tests

6.4.1.1 pH-stability

The development of the pH over time in the first test scenario, as described in Section 6.2.1, is presented in Figure 6-1. It can be seen, that once the Na_2S is added the pH immediately rises from 10.66 to 10.90, reflecting the protonation of the S^{2-} ions forming an equilibrium with HS^- (Awe & Sandström, 2010). The protonation equilibrium equation is given in Equation 6-1. Over the first 30 minutes, the pH decreases to 10.77 and then rapidly drops to pH 10.62, with the addition of H_2O_2. This may be explained by the oxidation of the S^{2-} ions with NaCN to SCN^- ions, by

the oxygen from the DO in the solution, as indicated in the literature in Section 2.4.2. Then the rapid step change in pH is caused by H_2O_2 addition at the 30 minute mark.

$$S^{2-} + H_2O \leftrightarrow HS^- + OH^-$$ Equation 6-1

In the remainder of the experiment the pH decreases to 10.52, which reflects a possible further oxidation of S^{2-} to SCN^-. This pH range was accepted to be sufficient for the subsequent leach tests and no additional pH adjustment was considered. The HPLC results showed a final distribution of the initially added S^{2-} ions as follows: 0%, 1.8%, 92.7%, and 5.5% for S^{2-}, $S_2O_3^{2-}$, SCN^- and SO_4^{2-} respectively. This indicates a complete conversion of S^{2-} ions during the test period, which will be further investigated in Section 6.4.2.2.

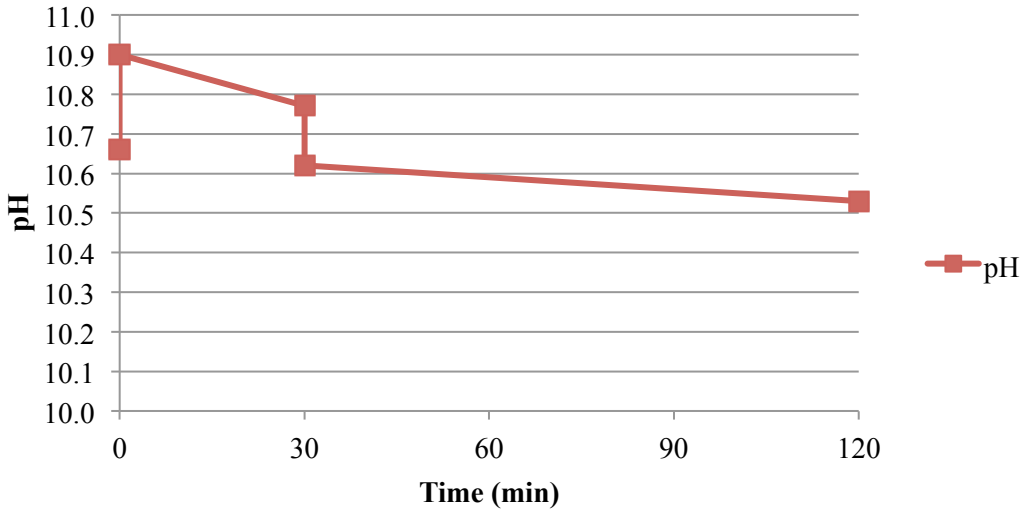

Figure 6-1: pH change in NaCN solution with addition of Na_2S and H_2O_2

Figure 6-2 shows the pH over time in the second experiment, as described in Section 6.2.1. It can be seen, that with the addition of Na_2S the pH rises significantly from 10.66 to 10.96, which may be explained by the protonation of the S^{2-} ions. Then the pH decreases to 10.90, prior to the H_2O_2 addition. Immediately after the H_2O_2 addition the pH drops to 10.63. The initial slow decrease of pH during the first 30

minutes could be explained by the oxidation of S^{2-} ions with the DO present in solution from oxygen sparging. The rapid decrease in pH after the H_2O_2 addition can be explained by rapid oxidation of the S^{2-}. In both cases the oxidation of S^{2-} can be associated with the release of H^+ ions. The pH then keeps decreasing to pH 10.42, before NaCN addition. It is assumed, that this may be due to further oxidation of S^{2-} ions and other interim species in solution and the formation of SO_4^{2-}. With the addition of NaCN the pH rises to 10.50 and then slowly decreases to 10.38 over the remainder of the experiment. This may be accounted for by the formation of SCN^- from $S_2O_3^{2-}$ (see Section 2.4.2). The pH range during this experiment was considered sufficient for the following leaching experiments to be conducted without additional pH control. The HPLC results showed a final distribution of the initially added S^{2-} ions as follows: 0%, 26.7%, 18.6%, and 54.7% for S^{2-}, $S_2O_3^{2-}$, SCN^- and SO_4^{2-} respectively. This indicates a complete conversion of S^{2-} ions during the test period, which will be further investigated in Section 6.4.3.2.

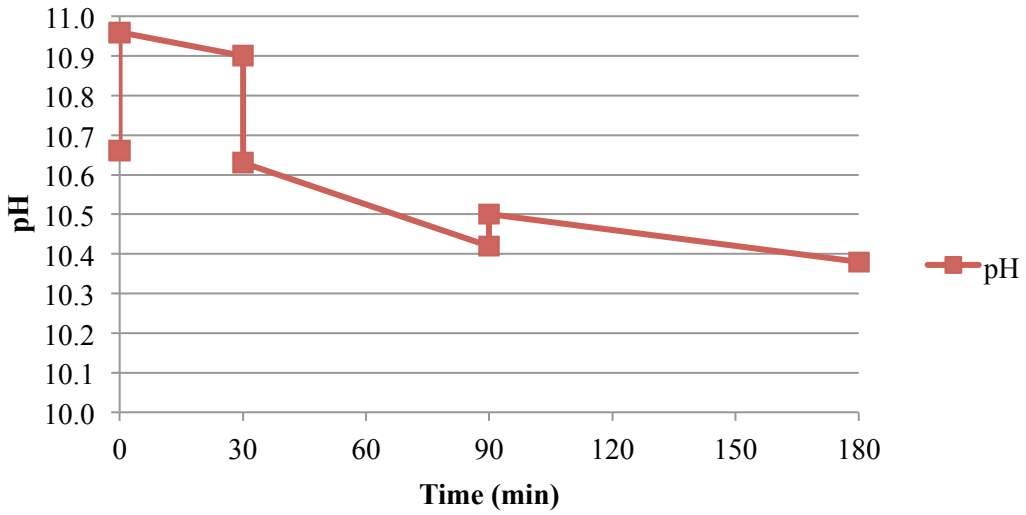

Figure 6-2: pH change in electrolyte solution with addition of Na_2S, H_2O_2, and NaCN

Both preliminary tests indicated that the variations in pH during these experiments were acceptable for the leaching experiments to be conducted without additional pH control. The pH varied within the chosen limits of pH 10 to pH 11. It can also be

observed, that the resulting oxidation species of S^{2-} ions and NaCN with H_2O_2 vary significantly in their composition with the different addition orders. If H_2O_2 is added prior to NaCN the main products are SO_4^{2-} and $S_2O_3^{2-}$ ions, whereas when the H_2O_2 is added after the NaCN the major product of the reaction is SCN^- ions. This may have an impact on cyanide consumption during gold leaching as well as waste water treatment and recycling.

6.4.2 RDE leach tests: Sulphide and hydrogen peroxide addition after sodium cyanide addition

6.4.2.1 Gold and silver in solution

Figure 6-3 shows the gold in solution for the four experiments conducted according to the description in Section 6.3.1. For all four H_2O_2 additions a similar initial leach rate can be observed, with variations caused by possible analytical error or slight differences in the electrode surface preparation. A possible cause for the leach inhibition during the initial stage of some experimental runs might be due to a passivation phenomenon, as already encountered and explained in Chapter 5. After the addition of the S^{2-} ions all leaches become significantly hindered, indicating passivation of the gold surface by S^{2-} adsorption. A resumption of the leaching could only be observed for the 6 and 8 mM H_2O_2 additions within the experimental run time. For the continuation of the leach to become apparent, a period of approximately 30 minutes after H_2O_2 addition was required to completely remove the adsorbed sulphide and reactivate the gold surface. These two tests indicate a higher final leach rate than the initial leach rate before the addition of S^{2-} ions. This may be explained by the enhancement of the leaching with H_2O_2, as shown in Section 4.4.2. The additions of 2 and 4 mM H_2O_2 respectively are not sufficient for the removal of S^{2-} off the gold surface and therefore, reactivation of the leach, within the experiment run time. Due to analytical error resulting from the very low Ag concentration, the measured Ag content is not shown. On average, the measured silver content correlated to the 2% Ag content of the RDE electrode used.

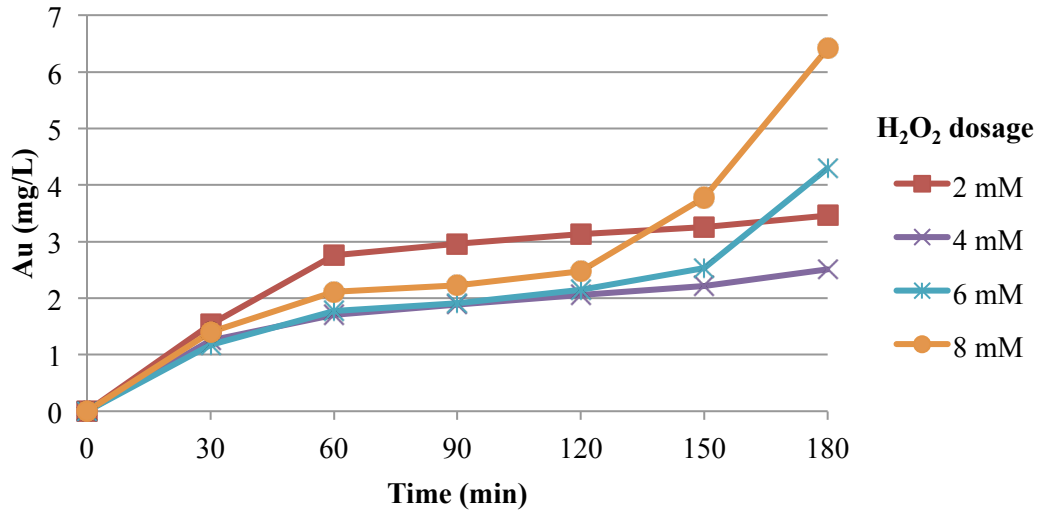

Figure 6-3: Au in solution for four different H_2O_2 additions. NaCN added at 0 min, S^{2-} at 60 min and H_2O_2 at 90 min

6.4.2.2 Sulphide and other sulphur species in solution

In Figure 6-4 the S^{2-} ion concentration in mM in solution over time is shown. Even though accurate dosing and analysis was ensured by titrating the Na_2S solution prior to use for each test and running calibration standards in the HPLC prior to experimental samples, some variability in the results can be seen. This is due to the low concentrations of S^{2-} ions in the analysed solution and also the high content of other ions present, including ClO_4^-, and CN^-. However the trends can be considered accurate, only the absolute numbers may vary slightly. It can be seen, that for all four experiments the S^{2-} ion concentration stayed constant prior to H_2O_2 addition. After the H_2O_2 addition the S^{2-} concentration decreased at different rates. The 6 and 8 mM H_2O_2 additions result in a total consumption of the S^{2-} ions within 30 minutes. This possibly could occur faster, but due to analytical limitations cannot be checked. In the same time the 2 mM H_2O_2 addition only reduces the S^{2-} ion concentration by ~67%, and the 4 mM addition by ~84% respectively. A further decrease of the S^{2-} concentration was then observed at a constant rate for both, the 2 and 4 mM H_2O_2

additions. The 2 mM addition did not result in a zero S^{2-} concentration measurement within the experimental run time.

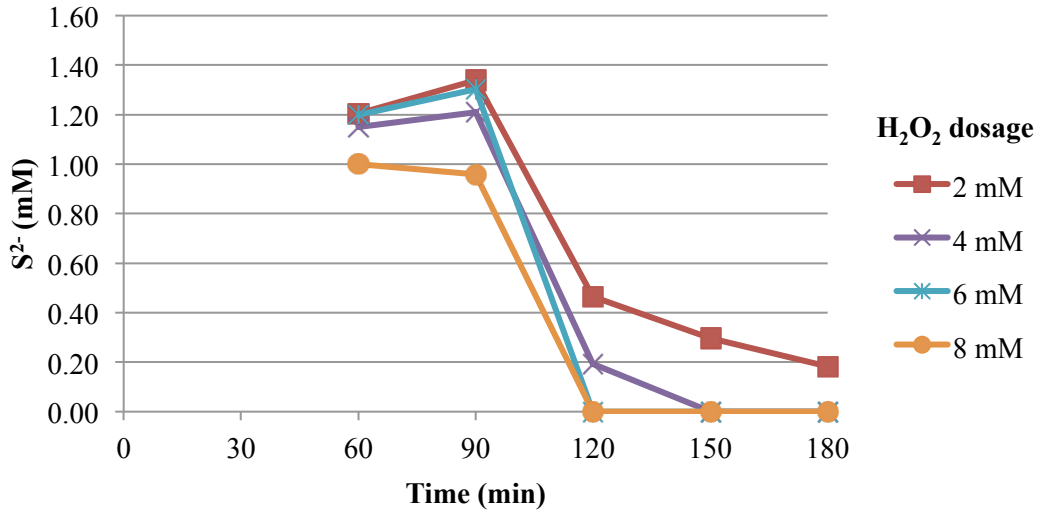

Figure 6-4: S^{2-} in solution for four different H_2O_2 additions. NaCN added at 0 min, S^{2-} at 60 min and H_2O_2 at 90 min

Figure 6-5 shows the measured SCN^- ions in solution for the experiments. It can be seen, that with only oxygen sparging, resulting in a theoretical dissolved oxygen content of ~38 ppm, the oxidation of the S^{2-} to SCN^- ions is very slow. Once H_2O_2 was added to the system a rapid increase in SCN^- ion concentration can be observed over the first 30 minutes for all H_2O_2 additions. For the two lower H_2O_2 additions of 2 and 4 mM the SCN^- ion content continues to increase slowly after the initial rise. For the two higher additions of 6 and 8 mM the concentration of SCN^- ions in solution stays constant. This indicates a complete conversion of available S^{2-} to SCN^- ions within the first 30 minutes for the two higher H_2O_2 additions.

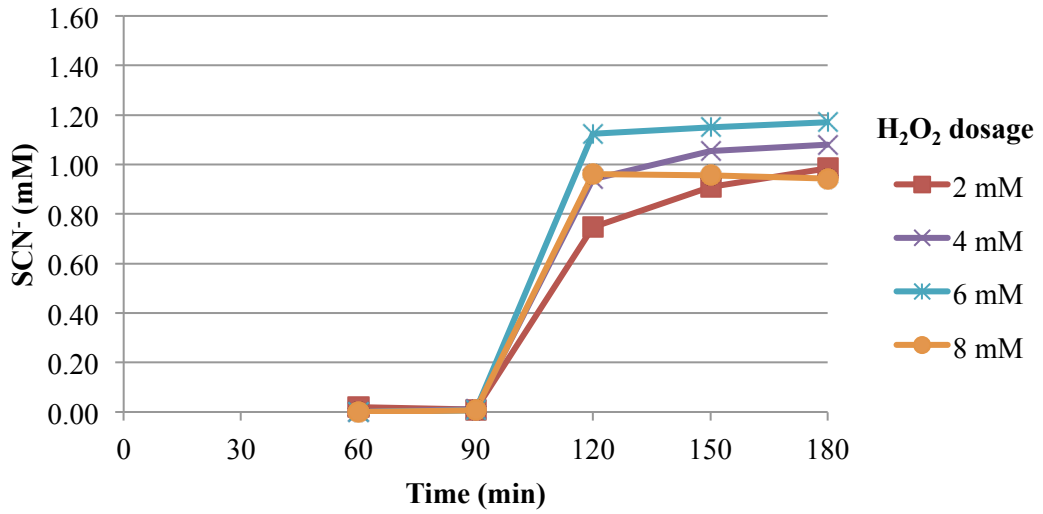

Figure 6-5: SCN^- in solution for four different H_2O_2 additions. NaCN added at 0 min, S^{2-} at 60 min and H_2O_2 at 90 min

Figure 6-6 shows the measured $S_2O_3^{2-}$ ion concentration in solution. The concentrations for all tests range between 0.026 and 0.065 mM, which is very close to the accurate detection limits of the analytical method used. It can be concluded, that in these experiments $S_2O_3^{2-}$ ions were, if at all, only present as a minor species or only an intermediate product in the generation of SCN^-, and SO_4^{2-} ions, as previously suggested by Lorösch (2001).

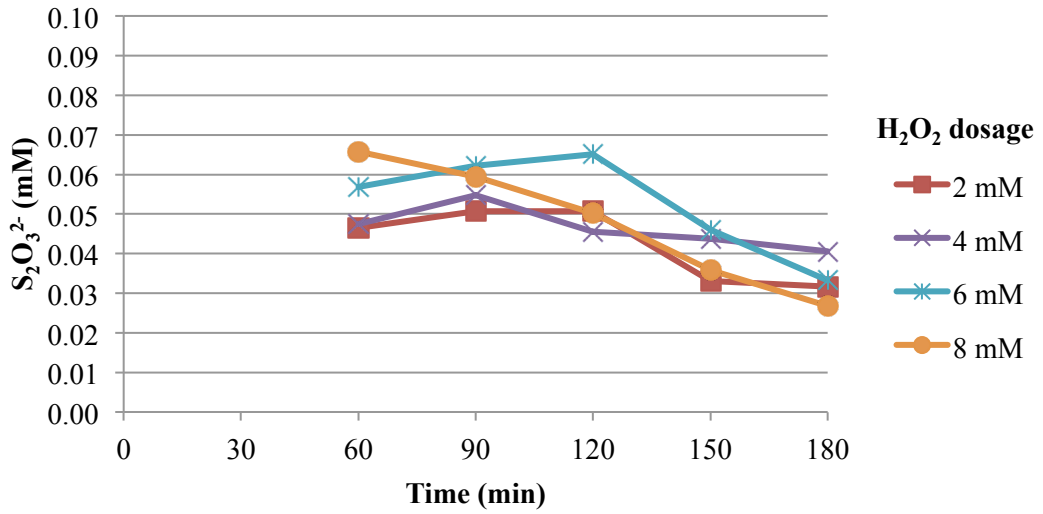

Figure 6-6: $S_2O_3^{2-}$ in solution for four different H_2O_2 additions. NaCN added at 0 min, S^{2-} at 60 min and H_2O_2 at 90 min

All other observed sulphur species were below accurate detection (<0.01 mM) limits throughout this set of experiments or could not be clearly identified in the HPLC spectra due to interference and are therefore not presented.

The sulphur sum calculated for the experimental run time is plotted against time in Figure 6-7. It is calculated as the sum of measured S^{2-}, SCN^- and 2 x $S_2O_3^{2-}$ in mM for any given sample time. It can be seen, that for each H_2O_2 addition the sulphur balances are fairly even and nearly match the initial S^{2-} measured in solution for each sample time. It can also be noted, that an overall small loss (~0.05-0.1 mM) of the observed sulphur balance is shown, which may be due to the generation of small, undetected quantities of SO_4^{2-} from S^{2-}, $S_2O_3^{2-}$ or SCN^-.

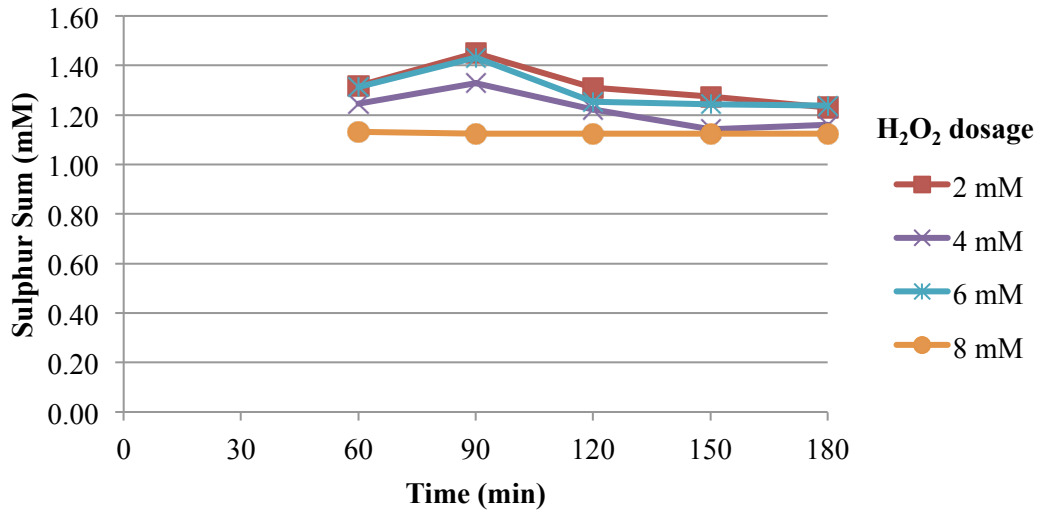

Figure 6-7: Sulphur Sum in solution for four different H_2O_2 additions. NaCN added at 0 min, S^{2-} at 60 min and H_2O_2 at 90 min

6.4.2.3 Sodium cyanide in solution

The NaCN concentration measured during the four experiments is shown in Figure 6-8. It is notable, that not all of the trends are following a straight line. This is most likely due to interference of S^{2-} ions and H_2O_2 with the silver nitrate titration technique, even though diligent care has been taken when interpreting the recorded titration curves of ORP versus volume of $AgNO_3$ to determine the equivalence point. Overall a loss of NaCN can be observed in all experiments, from 11.0 to 10.0 mM, 9.1 to 7.9 mM, 10.5 to 8.4 mM, and 10.4 to 7.9 mM for the 2, 4, 6, and 8 mM H_2O_2 additions respectively. In conjunction with Section 6.4.2.2, approximately 1 mM NaCN loss in each experiment can be accounted for by the generation of SCN^- ions. The remainder of the NaCN loss could be explained by the oxidation of NaCN by H_2O_2, as shown in Section 4.2.1. The H_2O_2 added into the system appears to be utilised to oxidise S^{2-} and reacts with NaCN to form SCN^-, according to the overall Equation 6-2 (Lorösch, 2001), and Equation 6-3, which shows the evolution of O_2 from H_2O_2. Following these equations, the reaction of S^{2-} with NaCN and H_2O_2 only requires a stoichiometric ratio of H_2O_2:S^{2-} of 1:1, leaving excess H_2O_2 available in solution for the oxidation of NaCN.

$$S^{2-} + CN^{-} + {}^{1}/_{2}\,O_2 + H_2O \leftrightarrow SCN^{-} + 2OH^{-}$$ Equation 6-2

$$2H_2O_2 \rightarrow O_2 + 2H_2O$$ Equation 6-3

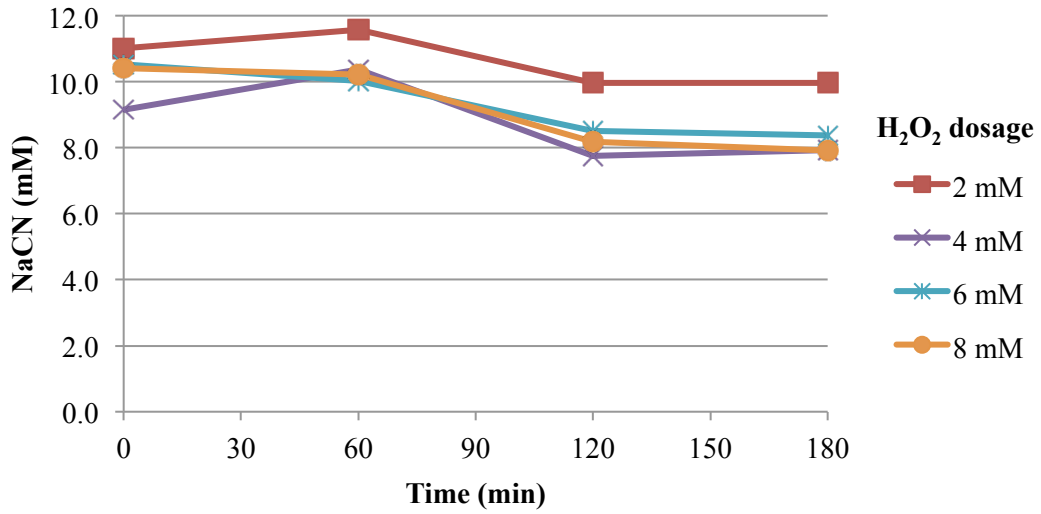

Figure 6-8: NaCN in solution for four different H_2O_2 additions. NaCN added at 0 min, S^{2-} at 60 min and H_2O_2 at 90 min

6.4.2.4 Open circuit potential

Figure 6-9 shows the OCP observed during the leach test with 8 mM H_2O_2 addition after the addition of NaCN and S^{2-} ions. Only this result is presented, as all other OCP curves measured show minimal variations to Figure 6-9 and would render them hard to differentiate. It can be seen, that the initial OCP starts at -320 mV and then slowly rises to -264 mV prior to the addition of the S^{2-} ions. With the addition of the S^{2-} ions into solution the OCP decreases immediately to around -290 mV. With the addition of H_2O_2 the potential recovers to ~ -280 mV and keeps rising to a maximum of ~ -170 mV, where it fluctuates, before dropping back to ~ -230 mV. For lower H_2O_2 additions the rise and fluctuation is less prominent.

The additional rise of potential compared to the initial leaching potential, after recovery from S^{2-} surface inhibition by H_2O_2, indicates an excess availability of oxygen to the gold surface. This shifts the oxygen reduction curve on the gold oxidation curve and results in the elevated OCP, as outlined in Section 2.5.6.

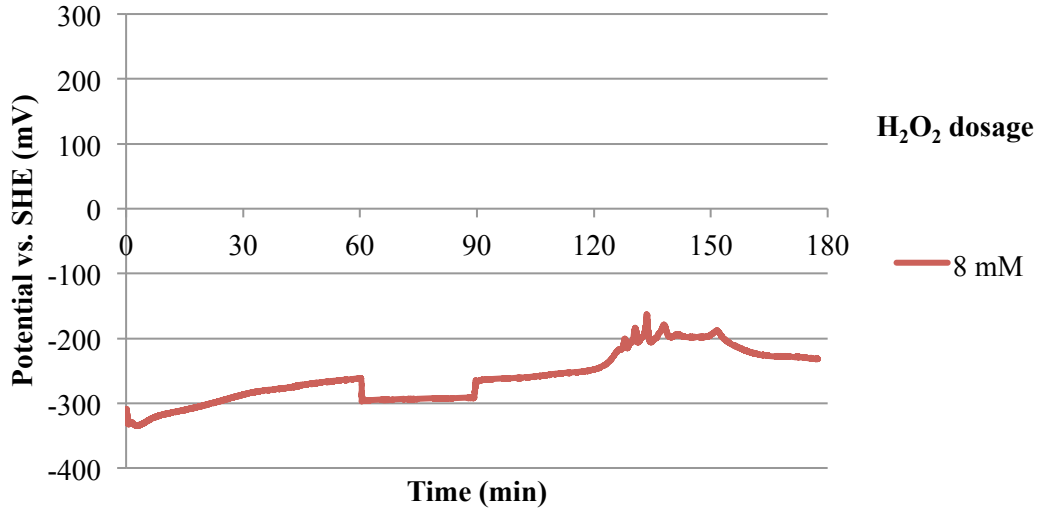

Figure 6-9: OCP example for NaCN addition.
NaCN added at 0 min, S^{2-} at 60 min and H_2O_2 at 90 min

6.4.3 RDE leach tests: Sulphide addition prior to hydrogen peroxide and sodium cyanide addition

6.4.3.1 Gold and silver in solution

Figure 6-10 shows the gold in the solution for the four experiments conducted according to the description in Section 6.3.2. It can be seen, that the leaching of the gold commences, once the NaCN was added into solution at the 90 minute point of the experiments. For the tests with 2 and 4 mM H_2O_2 addition, the resulting gold in solution (0.56 and 0.83 mg/L after 90 minutes leaching) indicates a highly passive gold surface. The passive behaviour of the gold can be explained by small quantities of S^{2-} ions remaining on the surface (M. I. Jeffrey & Breuer, 2000), as the data in Section 6.4.3.2 suggests. The tests with 6 and 8 mM H_2O_2 addition show good

leachability (3.03 mg/L and 5.40 mg/L after 90 minutes leaching respectively) after an initial induction period (from NaCN addition) of about 30 min. The higher amount of leached gold for the higher H_2O_2 addition of 8 mM could be explained by excess H_2O_2 remaining in solution, which has already been shown to have a beneficial effect on leaching in Section 4.4.2. Due to analytical error resulting from the very low silver concentration, the measured silver content is not shown. On average the measured silver concentration correlated to the 2% silver content of the RDE electrode used.

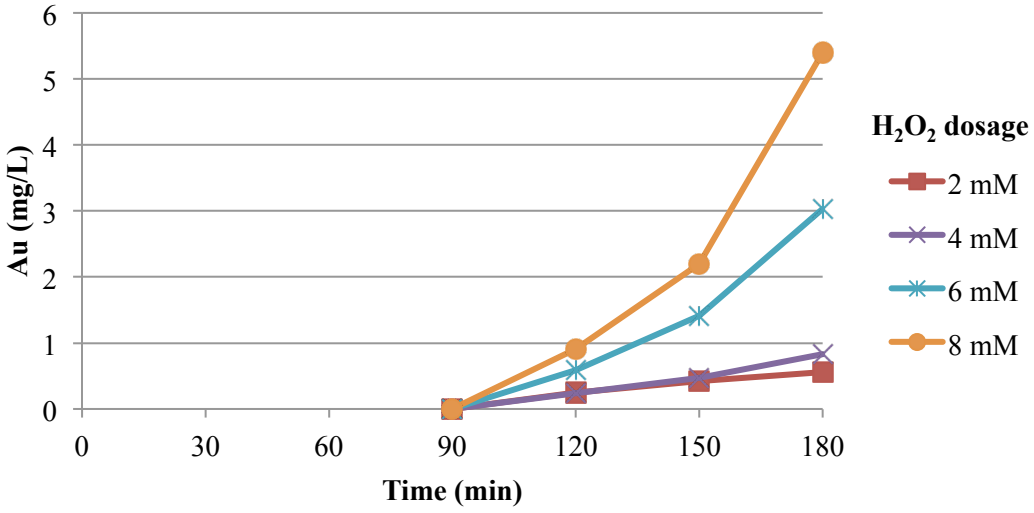

Figure 6-10: Au in solution for four different H_2O_2 additions prior to NaCN addition

6.4.3.2 Sulphide and other sulphur species in solution

The S^{2-} concentration measured in the test solutions (in mM) is plotted against time in Figure 6-11. Even though accurate dosing and analysis was ensured by titrating the Na_2S solution prior to each test and the running of calibration standards in the HPLC prior to experimental samples, some variability in the results can be seen. This is due to the low concentration of sulphide ions in the analysed solution and also the high content of other ionic species ($NaClO_4$, NaOH, $NaHCO_3$, and NaCN). However, the trends can be considered accurate and only the absolute numbers may vary

slightly. It can be seen, that within the first 30 minutes after the addition of H_2O_2 at the 30 minute mark, the concentration of S^{2-} ions drops rapidly. Only the additions of 6 and 8 mM H_2O_2 reduce the S^{2-} ion concentration in solution from ~1 to 0 mM within the first 30 minutes after addition. The addition of 2 mM H_2O_2 only reduces the concentration by ~80% within the first 30 minutes followed by a slow decline. The addition of 4 mM H_2O_2 reduces the S^{2-} concentration by ~95% within the first 30 minutes and then continues to decline slowly towards 0 mM S^{2-} ions in solution (similar to the trend observed for the 2 mM H_2O_2 addition curve). The concentration of the main reaction products are presented in Figure 6-12, Figure 6-13 and Figure 6-14.

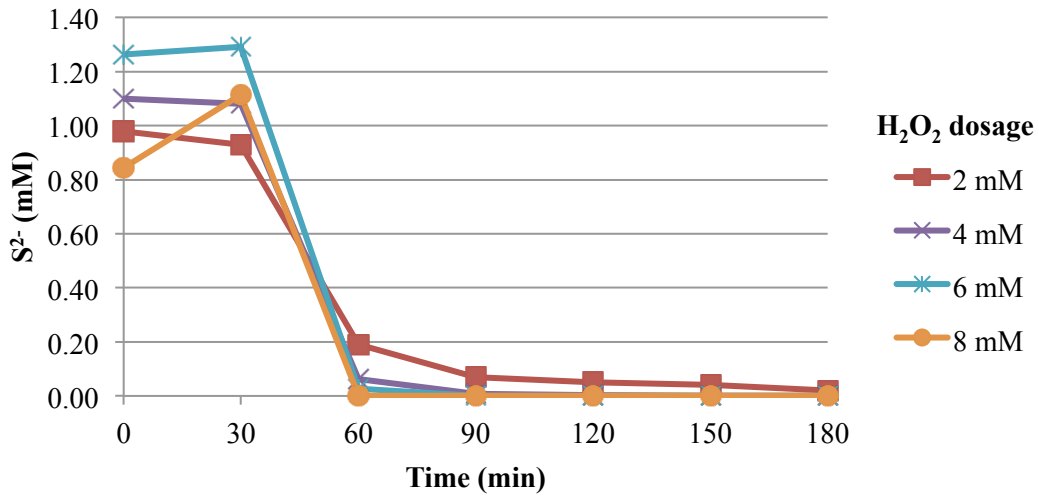

Figure 6-11: S^{2-} in solution for four different H_2O_2 additions prior to NaCN addition

Figure 6-12 shows the measured SCN^- ion concentration in the leach solutions during the experiments with H_2O_2 addition prior to NaCN (90 min) addition. During the test run time SCN^- is first measurable after the addition of NaCN and then increases relatively linearly for the remainder of the experiment. The highest SCN^- ion concentration of 0.17 mM can be observed for the highest H_2O_2 addition; the lowest SCN^- ion concentration of 0.12 mM for the lowest H_2O_2 addition. During the experimental run time a maximum of ~20% S^{2-} ions initially present in the solutions

are converted (possibly via interim S^{2-} oxidation products, such as $S_2O_3^{2-}$) by reaction with NaCN to form SCN^- ions.

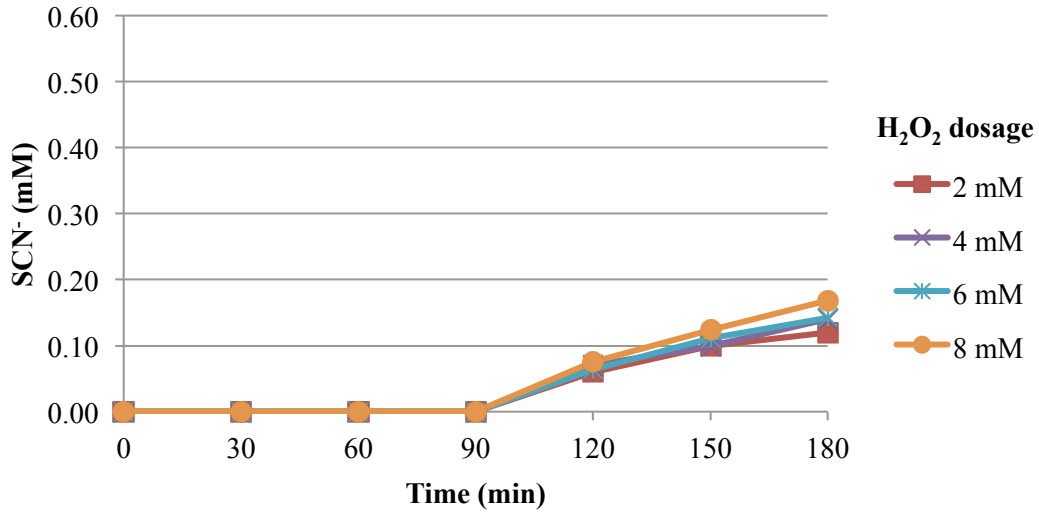

Figure 6-12: SCN^- in solution for four different H_2O_2 additions prior to NaCN addition

Figure 6-13 plots the concentration of $S_2O_3^{2-}$ ions in the solution during the experiments. A sharp increase of $S_2O_3^{2-}$ ions can be observed within the first 30 minutes after H_2O_2 addition at 30 min. The measured concentration of $S_2O_3^{2-}$ ions at 60 minutes experimental run time accounts for nearly all the sulphur available in solution being consumed. The two lower H_2O_2 additions of 2 and 4 mM resulted in a lower conversion of S^{2-} to $S_2O_3^{2-}$ ions. The difference notable at the first data point is reflecting the analytical limits and a possible deterioration of the Na_2S stock solution, even though it was prepared fresh and titrated for its concentration prior to each test. After the initial rise, the $S_2O_3^{2-}$ ion concentration stays roughly constant for the lowest H_2O_2 addition of 2 mM. For all other H_2O_2 additions a constant decrease from the peak $S_2O_3^{2-}$ ion concentration can be observed. The fastest rate can be observed for the highest H_2O_2 addition of 8 mM.

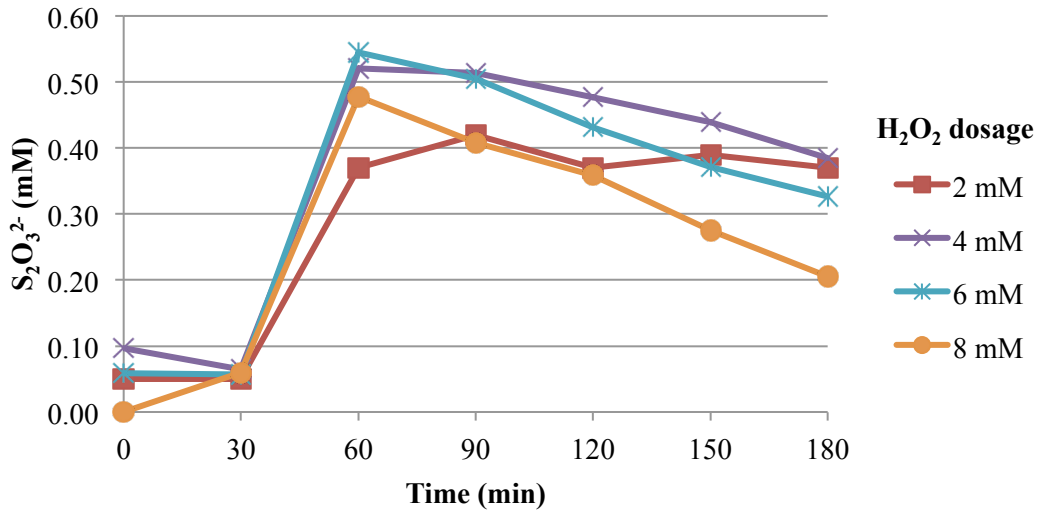

Figure 6-13: $S_2O_3^{2-}$ in solution for four different H_2O_2 additions prior to NaCN addition

Figure 6-14 shows the measured SO_4^{2-} ion concentration in solution throughout the experiments. It can be seen, that within the first 30 minutes after the H_2O_2 (30 min) addition the SO_4^{2-} ion concentration in solution increases sharply (it may react faster, but due to analytical limitations samples could only be taken every 30 minutes). With increased H_2O_2 addition higher resulting initial SO_4^{2-} rises can be observed. Then the SO_4^{2-} ion concentration continuously increases at a nearly constant rate for the remainder of the experiment for all tests. This rate varies for the different H_2O_2 additions, resulting in a final SO_4^{2-} ion concentration of 0.23, 0.39, 0.49 and 0.66 mM at the end of the experiments for the respective H_2O_2 additions of 2, 4, 6 and 8 mM. The oxidation of S^{2-} by H_2O_2 to SO_4^{2-}can follow multiple pathways. The most direct oxidation path is shown in Equation 6-4, where a 4:1 H_2O_2:S^{2-} stoichiometric ratio is required. The initial jump in SO_4^{2-} concentration on all tests after the H_2O_2 addition most likely follows this pathway. However, at the same time the oxidation to of S^{2-} to $S_2O_3^{2-}$ according to Equation 6-5 most likely takes place, which then further is further oxidised to SO_4^{2-}, as shown in Equation 6-6. This oxidation via the interim of $S_2O_3^{2-}$ appears to be slower than the direct oxidation to SO_4^{2-}, as notable on the graph after the initial jump in SO_4^{2-} concentration.

$$S^{2-} + 4H_2O_2 \rightarrow SO_4^{2-} + 4H_2O$$ Equation 6-4

$$2S^{2-} + 4H_2O_2 \rightarrow S_2O_3^{2-} + 3H_2O + 2OH^-$$ Equation 6-5

$$S_2O_3^{2-} + 2OH^- + 4H_2O_2 \rightarrow 2SO_4^{2-} + 5H_2O$$ Equation 6-6

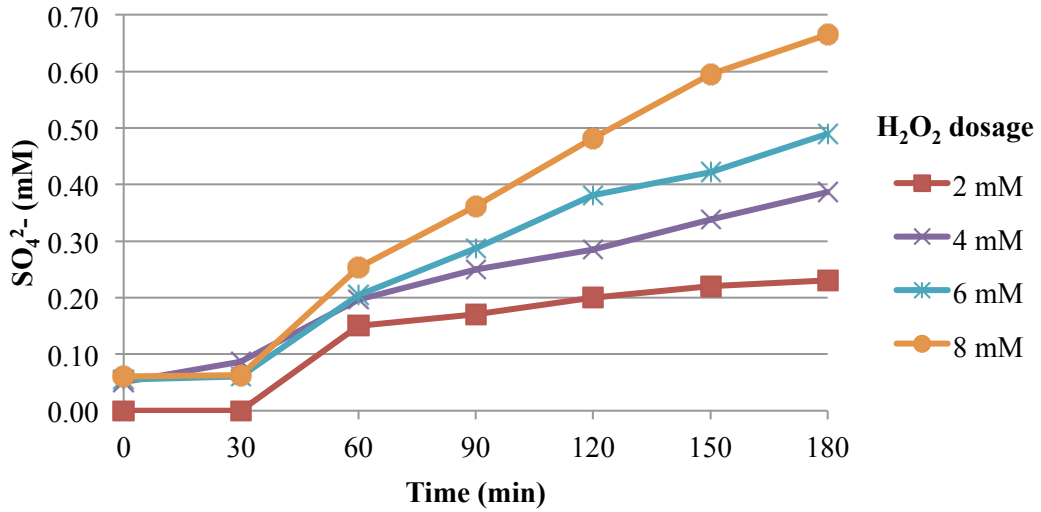

Figure 6-14: $SO4^{2-}$ in solution for four different H_2O_2 additions prior to NaCN addition

The SO_3^{2-} concentration was below the detectable limits throughout all experiments described in this section and is therefore not shown.

The sulphur sum calculated for each sample time is presented in Figure 6-15. It is calculated as the sum of measured S^{2-}, SCN^-, 2 $S_2O_3^{2-}$, and SO_4^{2-} in mM for any given sample time. It can be seen, that for each H_2O_2 addition the sulphur balances are fairly even and nearly match the initial S^{2-} measured in solution for each sample point. Only the 8 mM addition line shows a rather large deviation at t=0 indicating a measurement error of one of the sulphur species. It can be concluded, that no other major sulphur species were present throughout these experiments.

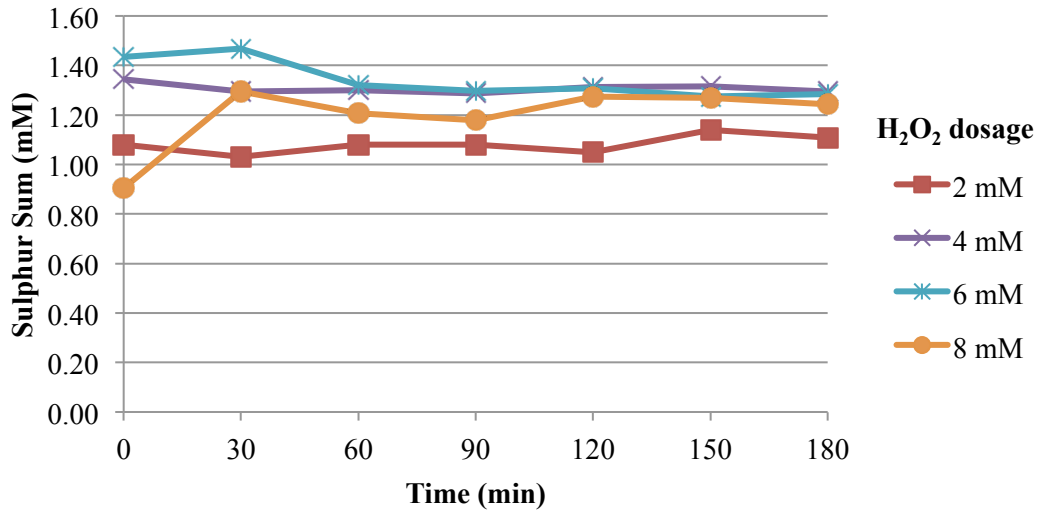

Figure 6-15: Sulphur sum in solution for four different H_2O_2 additions prior to NaCN addition

6.4.3.3 Sodium cyanide in solution

Figure 6-16 shows the NaCN concentrations in the leach solutions. The data gained for the test with a 2 mM H_2O_2 addition shows a constant (within analytical error) NaCN concentration in the solution with no losses during the time of the experiment. The curves for the 4, 6 and 8 mM H_2O_2 additions show a drop for the second titration, which then recover back to their original values (within analytical error). This phenomenon may be accounted for by the interference of H_2O_2 with the silver nitrate titration, as it may interfere with the potential between the reference electrode and the silver wire electrode. It can be concluded, that the loss of NaCN during these sets of experiments was close to zero. This correlates well with the SCN^- formation, which has been found to be very small in these experiments (below 0.2 mM for the experimental run time).

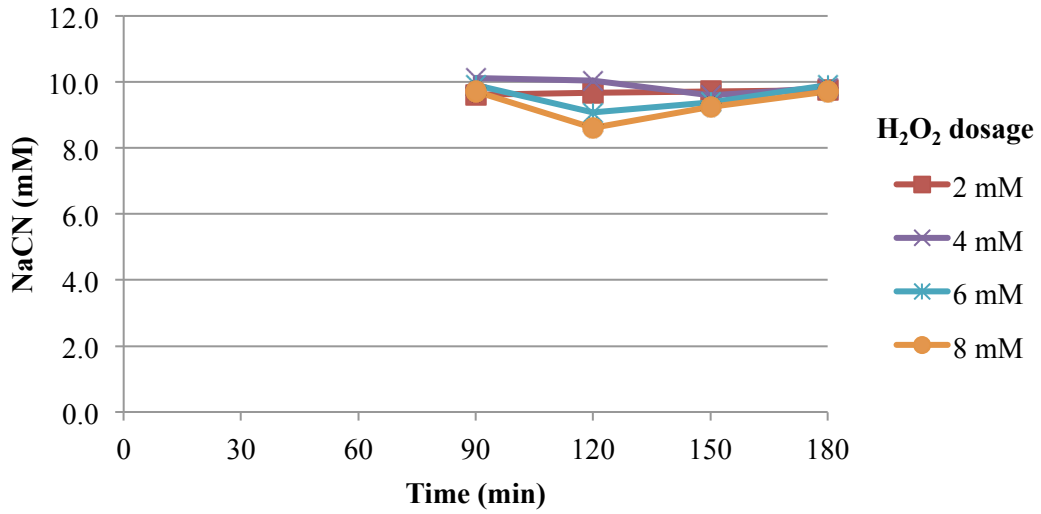

Figure 6-16: NaCN in solution for four different H_2O_2 additions prior to NaCN addition

6.4.3.4 Open circuit potential

Figure 6-17 shows the OCP measured during the experiment with 8 mM H_2O_2 addition prior to the addition of NaCN. Only this result is shown, as all other OCP curves measured show only minor variations to this curve. Initially, with only S^{2-} present, the OCP is stable at ~ -100 mV. It then increases rapidly with the addition of H_2O_2 and keeps rising continuously to ~230 mV, prior to the addition of NaCN. This rise is less prominent with lower H_2O_2 additions. With the addition of NaCN the potential drops to ~ -280 mV and then slowly recovers to ~ -210 mV during the rest of the experimental run time. This final potential observed is higher than the usual gold leaching potential, which again indicates a significant change in the oxygen reduction curve, as mentioned in Section 6.4.2.4, caused by the hydrogen peroxide.

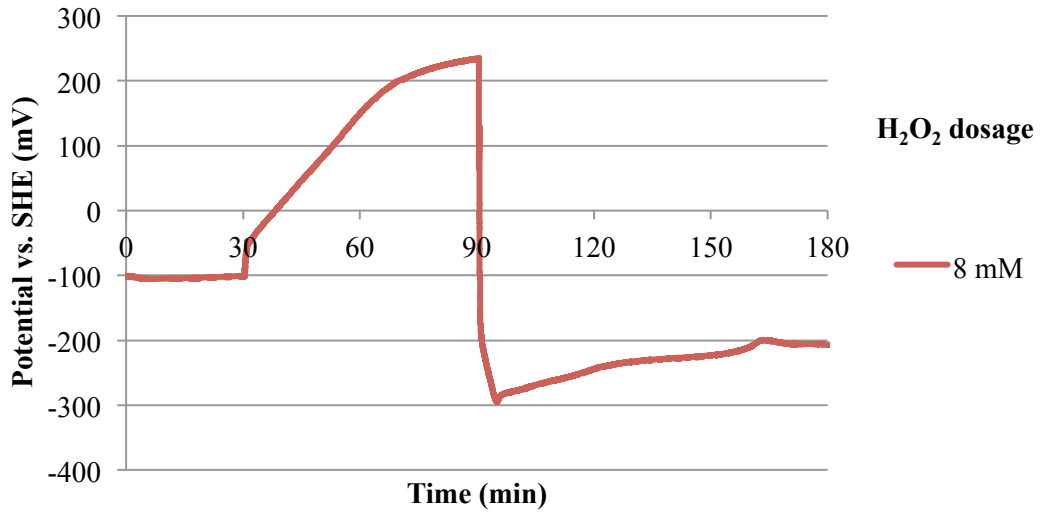

Figure 6-17: OCP example for NaCN addition after Na_2S, and H_2O_2 addition

6.4.4 Conclusions

It has been shown, that H_2O_2 is a strong oxidant, capable of fully oxidising sulphide ions at stoichiometric ratios of as low as 4:1 for H_2O_2 : S^{2-}. This can be utilised, at the right addition, to significantly improve the leachability of gold in solutions containing S^{2-} ions, or even when gold surfaces show passivation caused by sulphide adsorption. The most likely oxidation product of S^{2-} and $S_2O_3^{2-}$ ions in the presence of NaCN appears to be SCN^-, as shown in Section 6.1. This outcome can be shifted by changing the addition order of reagents, adding the H_2O_2 prior to the NaCN, resulting in lower NaCN consumption for SCN^- generation, but instead generating more $S_2O_3^-$ and SO_4^{2-}, as shown in Sections 6.4.2 and 6.4.3, which agrees with the oxidation of sulphide as previously demonstrated by other authors (see Section 2.4.2). However, this might only have limited benefits in industrial leach processes as sulphide ions are usually released into solution after NaCN addition. From the observations made in the experiments, Figure 6-18 can be drawn for the preferential oxidation of sulphide ions with reduced thiocyanate generation. It can be seen, that upon H_2O_2 addition, only 20% of the sulphide present gets oxidised to its most stable form, SO_4^{2-}, and 80% get oxidised to $S_2O_3^{2-}$. Once NaCN is added 40% of the $S_2O_3^{2-}$

present gets converted to SCN^- and 60% to SO_4^{2-}. The generation of SO_4^{2-} appeared to be occurring at the same rate with or without NaCN present, and hence must be chemically limited. In an ideal case, one would target for complete oxidation of all sulphide ion species to SO_4^{2-}, as this will not be able to consume any cyanide or hinder a leaching process.

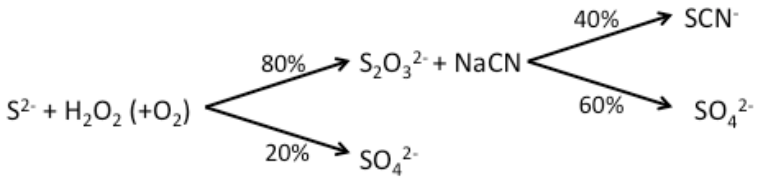

Figure 6-18: Sulphide ion reaction route observed during H_2O_2 addition (8:1 ratio of H_2O_2:S^{2-}), prior to NaCN addition

If in a gold leach a slow leach rate is observed, caused by sulphide adsorption to the surface, H_2O_2 addition can be used as a remedial measure. It is important to consider the order of reagent addition: when H_2O_2 is added prior to NaCN, more S^{2-} in solution will be converted to $S_2O_3^{2-}$ and SO_4^{2-} instead of forming SCN^-. There may also be the opportunity to reduce the time between the H_2O_2 addition and the NaCN addition, as the initial S^{2-} conversion to $S_2O_3^{2-}$ appears to be very fast and the reaction to SO_4^{2-} at a constant rate. This will require further investigation to determine the ideal timing for the addition of reagents.

Chapter 7 Mineral electrodes and their galvanic interaction with gold under the influence of hydrogen peroxide

7.1 Introduction

Some minerals, especially sulphides and tellurides, are known to be electrically conductive, as shown in Section 2.3. Those include, but are not limited to: pyrite, chalcopyrite, and arsenopyrite. Cyanide leaching of gold is an electrochemical process, as detailed in Section 2.1.2. The oxygen reduction step, which is the diffusion limiting step in most cases, could also take place on conductive mineral surfaces that are galvanically connected with gold (see Section 2.3) and therefore enhance the gold leaching kinetics. This chapter investigates the ability of certain minerals to perform as the oxygen reduction surface for the cathodic (oxygen reduction) half reaction first by means of potentials scans. Then leaching tests are conducted to verify the possibility of leach rate enhancement by galvanic interaction. These tests were all conducted with and without hydrogen peroxide present, to investigate the possible impact of hydrogen peroxide on the cathodic reaction occurring on the mineral surfaces.

7.2 Cathodic potential scans

Exactly 100 mL of electrolyte solution, as described in Section 3.2.6, was introduced into an electrochemical cell and aerated for 10 minutes prior to each test. The reference electrode used, as described in Section 3.3.1.5, was bottom mounted to the cell using a luggin capillary. A platinum wire, as described in Section 3.3.1.4 was used as the counter electrode. The gold/2%silver (referred to as gold throughout Chapter 7) and mineral electrodes were rotated at 500 min^{-1} using a Pine MSR rotator. The potential was scanned from the initially measured OCP to -1000 mV at a

scan rate of 1 mV/s with the current range of the potentiostat, as described in Section 3.3.1.7, set to 10 mA. This scan rate was selected, as previous research (see Section 2.5.4) under similar conditions for pure gold and gold silver used the same scan rate and therefore to aid comparability of the results. The electrode surface areas were 10.2, 41.2, 35.5, and 43.1 mm^2 for gold, pyrite, chalcopyrite and arsenopyrite, respectively. The gold electrode was prepared by polishing it with a paste consisting of 10 µm alumina powder and demineralised water. After polishing, the electrode was thoroughly rinsed with demineralised water. All mineral electrode surfaces were refreshed by sanding on 1200 grit silicon carbide sandpaper with demineralised water and then rinsed thoroughly with demineralised water. All gold and mineral electrodes were used immediately after the rinsing step. All tests were conducted under aeration, to represent typical industrial plant conditions, of a DO concentration of approximately 8 ppm (see Section 2.4.1). Hydrogen peroxide additions were made to a concentration of 3 mM from a solution, as described in Section 3.2.1, when applicable.

7.3 Galvanic interactions of gold and mineral electrodes during leaching

The galvanic impact on the leach rate of gold when connected to a mineral electrode was measured with RDEs. The minerals tested in conjunction with the gold electrode were pyrite, chalcopyrite and arsenopyrite. The electrodes were the same as the ones used in Section 7.2. All tests were conducted in 100 mL of 10 mM air saturated NaCN solution, made from the stock solutions described in Sections 3.2.6 and 3.2.4 at a pH of 10.5. All electrodes were rotated by Pine MSR rotators at 500 min^{-1}. In each test, the solution was added into a petri dish and the polished gold electrode was introduced into the solution to commence the test. The gold electrode was connected to the potentiostat to monitor the OCP before commencement of each test. After 60 minutes, the electrode of the mineral to be tested was introduced into the solution and electrically connected to the gold electrode and potentiostat to measure the mixed

OCP. The test then continued for a further 60 minutes. Each test was repeated with the addition of hydrogen peroxide as a 500 mM solution, to generate a 3 mM solution prior to test commencement. Samples of 5 mL were taken at times 0, 30, 60, 90 and 120 minutes and analysed by AAS for their respective gold and silver content.

7.4 Results and discussion

The results section contains two main subsections. The first one investigates and compares the ability of selected minerals to partake in the cathodic part of the gold leaching redox reaction and the influence hydrogen peroxide can have on this reaction. The second part presents the leach data for galvanically coupled gold and mineral electrodes and conducts a comparison of these.

7.4.1 Cathodic (oxygen reduction) potential scans

The current-potential diagrams for gold, pyrite, arsenopyrite and chalcopyrite under aeration, measured as described in Section 7.2, are presented in Figure 7-1. All four curves show two waves of oxygen reduction. For the gold, pyrite, arsenopyrite and chalcopyrite the first wave can be seen at a potential between approximately 0 and -400, 200 and -350, 200 and -300, and 200 and -300 mV, respectively. The second wave can be seen between approximately -400 and -800, -350 and -800, -300 and -650, -300 and -800 mV for gold, pyrite, arsenopyrite and chalcopyrite, respectively. In the literature the first wave of oxygen reduction has been interpreted as the reduction of O_2 to H_2O_2, the second wave as the reduction of H_2O_2 to OH^- (see Sections 2.1.2 and 2.5.4). It is noteworthy, that at more positive potentials all minerals show a greater cathodic current than gold. However, at more negative potentials only pyrite and arsenopyrite show a greater cathodic current and therefore indicate a better reduction of H_2O_2 to OH^- than gold. For gold, pyrite and chalcopyrite, the onset of hydrogen evolution becomes very visible from around -850 mV.

The calculated limiting current for a 4-electron O_2 reduction, following the Levich Equation and Faradays Law with the material constants shown in Sections 3.4.1, 3.4.1.1, and 4.2.3 for air sparging is -6.76 A/m^2. The measured currents are -8.7, -7.8, -9.6, and -6.8 A/m^2 at -800, -500, -600 and -600 mV for gold, pyrite, arsenopyrite and chalcopyrite, respectively. This is in close agreement to the measured data and therefore indicates the full 4-electron reduction of O_2. The higher measured rate at less than -900 mV compared to the theoretical value is most likely caused by the onset of hydrogen evolution, as shown in Section 4.4.1.3. The observed 4-electron reduction aligns with observations of other researchers on the reduction of O_2 on minerals in alkaline solution, as shown in the Section 2.3.1.

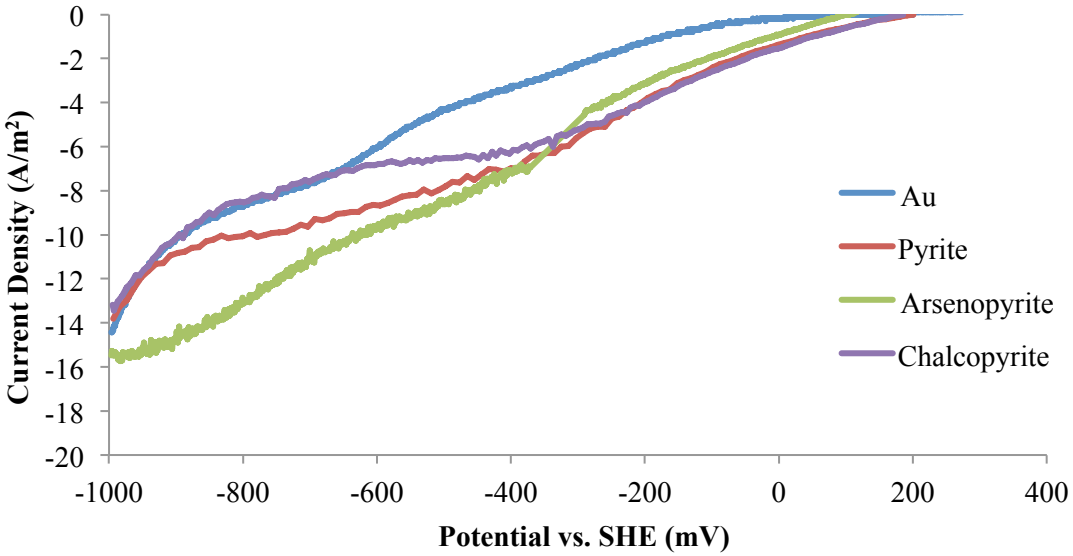

Figure 7-1: RDE cathodic potential scans for gold, pyrite, arsenopyrite and chalcopyrite at pH 10.5, aerated, 500 min^{-1}

Figure 7-2 shows the cathodic oxygen reduction curves for gold, pyrite, arsenopyrite and chalcopyrite under aeration and 3 mM H_2O_2 addition, measured as described in Section 7.2. All four curves exhibit two waves of oxygen reduction. The waves are located in approximately the same potential ranges, as explained for Figure 7-1, for the respective electrodes. The first wave of reduction from O_2 to H_2O_2 is least developed for gold, followed by arsenopyrite. Pyrite and chalcopyrite show the largest currents at more positive potentials. The currents observed in the first

reduction wave are all exceeding the currents, which can be seen in Figure 7-1 by a factor of approximately 2.5, indicating an increase in dissolved oxygen for the tests with H_2O_2 present. The second reduction wave from H_2O_2 to OH^- is a lot stronger developed for all electrodes. All minerals show greater reduction currents than gold at more positive potentials, with chalcopyrite and pyrite nearing their maximum reduction current already around a potential of -400 mV, followed by arsenopyrite around -500 mV and gold at -700 mV. Again, the corresponding currents are greater (by a factor of around 4.5) than the ones observed in Figure 7-1. This confirms the two step reduction of O_2 on gold and mineral surfaces, as the H_2O_2 content in the solution is increased and not just generated by the first reduction step of oxygen.

For the solution with air and H_2O_2 present, the resulting maximum current can be calculated to be -30.82 A/m^2, for 2 electron reduction of H_2O_2, when assuming the O_2 in solution takes part in a 4 electron reduction, and contributes -6.76A/m^2 to the total reduction current, as indicated by the data acquired during the scans without H_2O_2 present (see Figure 7-1). These values were computed, as outlined in Section 3.4.1. Comparing the theoretical to the measured values of -36.6, -39.1, -33.5 and -36.2 A/m^2, at -800, -500, -600 and -600 mV for gold, pyrite, arsenopyrite and chalcopyrite, respectively, it appears that the H_2O_2 is utilised in a 2 electron reduction step on all electrodes (taking the surface roughness and onset of hydrogen evolution into account). This 2 electron reduction could either be interpreted as the reduction step of H_2O_2 to OH^- or a decomposition of two H_2O_2 molecules to one O_2 molecule on the surface, immediately prior to the 4 electron reduction seen by the O_2 in solution as a result of the aeration, as indicated in Sections 2.1.2 and 2.2.1. Further, the increase in current at higher (more positive) potentials indicates, that a decomposition of H_2O_2 and subsequent use as O_2 in the oxygen reduction reaction occurs over the whole potential range.

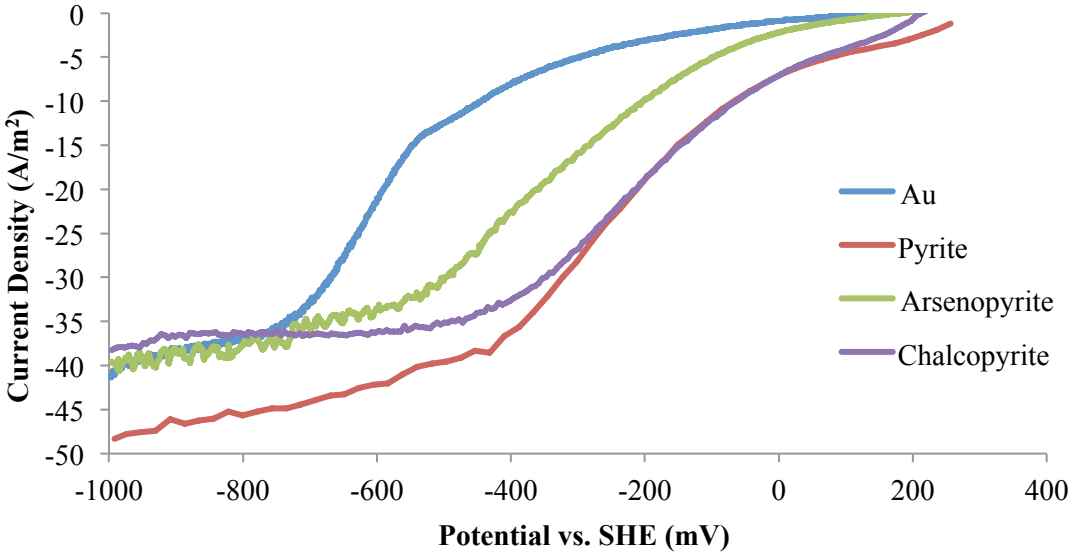

Figure 7-2: RDE cathodic potential scans for gold, pyrite, arsenopyrite and chalcopyrite at pH 10.5, aerated with 3 mM H_2O_2, 500 min^{-1}

In summary, the minerals tested are all capable of partaking in the cathodic part of the gold leaching redox reaction by reducing either oxygen or hydrogen peroxide. However, the possible contribution in a galvanic coupled environment will vary, as they are showing different potential regions for the reduction.

7.4.2 Galvanic interactions of gold and mineral electrodes during leaching

In the following section, the results for galvanic coupled leaching of a gold electrode with, a pyrite, an arsenopyrite and a chalcopyrite electrode respectively are presented. The coupled leaches were conducted with and without hydrogen peroxide present. The results focus on the amount of gold leached and the OCP to interpret the results. The measured silver dissolution is not shown, as the values detected were too small to interpret with any accuracy. In this section, the aerated and aerated with peroxide addition results are not overlayed, as the surface area of the mineral electrodes were different and hence a direct comparison would be inaccurate. An attempt at correcting the leach rates for the differing surface areas has been made in Section 7.4.3. All figures shown in this section will contain two lines: a blue and a red line, which represent the results for paired experiments, one conducted with, and

one without H_2O_2. The blue line will always represent the results obtained during the experiment without H_2O_2 present and the red line always the experiment with 3 mM H_2O_2 in the solution.

Gold-Pyrite coupling

Figure 7-3 shows the leach rate of gold measured over time. Each data point represents the average leach rate for the previous 30 minute bracket. The initial leach rates observed at the 30 minute mark are 1.18 and 1.73 (10^{-5} mol m^{-2} s^{-1}) for the test without and with H_2O_2 respectively. At the 60 minute mark, the observed leach rates in the tests are 0.52 without H_2O_2 and 1.94 (10^{-5} mol m^{-2} s^{-1}) with H_2O_2 present. A slight increase for the leach rate with H_2O_2 present is observed, but a decrease by around 50% for the leach rate in the experiment without H_2O_2. This could be due to a passivation phenomenon, similar to that observed in Section 5.4.1.2. After the connection and introduction of the pyrite electrode at the 60 minute mark the leach rate increased in both cases. The leach without H_2O_2 present reached a value of 2.61 at the 90 minute mark and 1.98 (10^{-5} mol m^{-2} s^{-1}) at the 120 minute mark. The leach with the presence of H_2O_2 resulted in a leach rate of 7.82 at the 90 minute mark and 6.21 (10^{-5} mol m^{-2} s^{-1}) at the 120 minute mark. In all tests, the observed leach rate was well below the theoretical cyanide limiting rate of 37.9 (10^{-5} mol m^{-2} s^{-1}), as calculated following the procedure and reagent constants in Sections 3.4.1 and 3.4.1.1. Both tests show an improvement in leach rate, once the mineral electrode was connected. However, a decrease of the leach rate after the initial improvement is also observed. In the test with H_2O_2 present, this might be due to the consumption of H_2O_2 and therefore a reduction in H_2O_2 levels. The decrease in the test without H_2O_2 cannot be explained, but may be due to the continued passivation phenomenon of the gold surface. In the absence of H_2O_2, the average gold leach rate increased by 170% on connection of the pyrite electrode due to the additional surface area and preferential reduction of oxygen on the pyrite electrode. With H_2O_2 in solution the gold leach rate increased 282% on connection of the pyrite electrode. The greater increase in gold leach rate in the presence of H_2O_2 on connection of the pyrite

electrode is due to the greater reduction current achieved on pyrite in the presence of H_2O_2 at more positive potentials than on gold, as can be seen in Section 7.4.1.

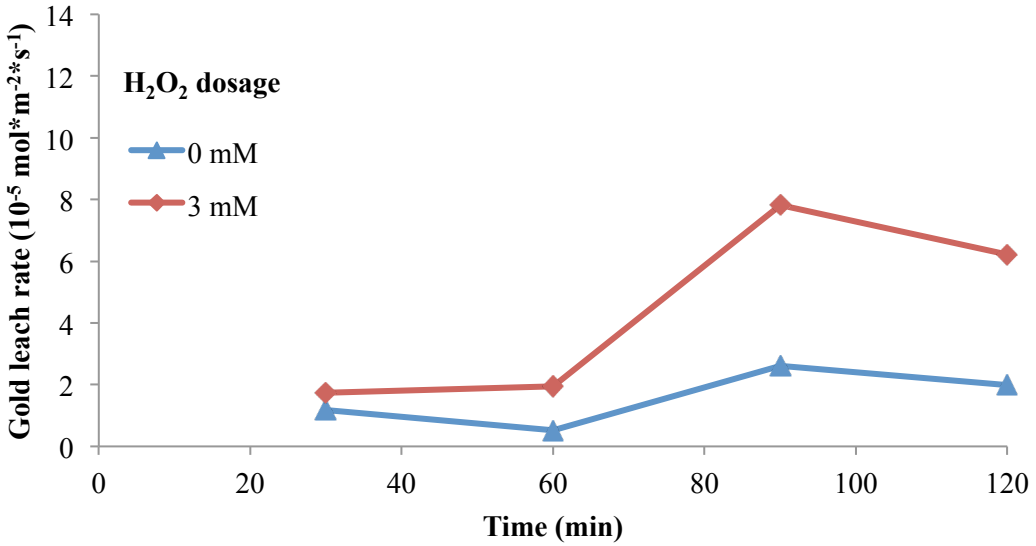

Figure 7-3: Gold leach rate in galvanic interaction with pyrite – pyrite electrode introduced at t=60 min.

In Figure 7-4, the OCP measured during the galvanic leach experiment with gold and pyrite is shown. Up to the 60 minute mark, the potentials for both curves are stabilising around -250 mV. The test without H_2O_2, after initial equalising, started at a potential of -300 mV, the test with H_2O_2 present at -280mV. Upon connection and introduction of the pyrite into the solution at the 60 minute mark, the potential rapidly increases for both tests. In the aerated test the mixed OCP then settles around -200 mV. In the H_2O_2 added test, the potential settles around -40 mV. This is an indication for the strong influence of the oxygen and hydrogen peroxide reduction half reactions on the OCP. The positive shift in OCP can be explained by the additional surface area available for oxygen and hydrogen peroxide reduction but not for gold oxidation, as can be deducted from the literature in Section 2.5.6 in conjunction with the anodic scans for pyrite plotted in Section 7.4.1.

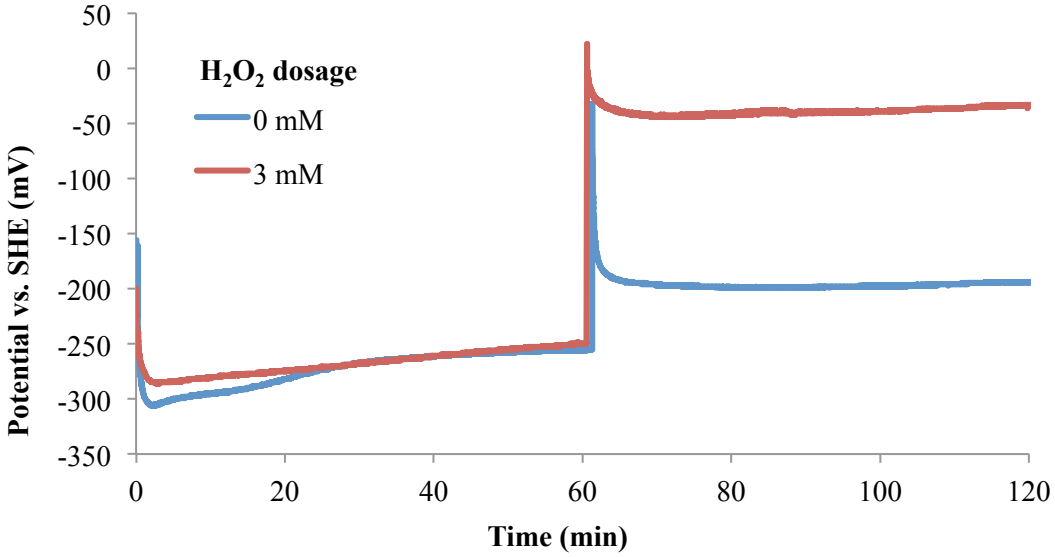

Figure 7-4: OCP measured for gold leaching in galvanic interaction with pyrite – pyrite electrode introduced at t=60 min.

Gold-Arsenopyrite

The data of the gold leach rate in galvanic coupling with arsenopyrite observed over time is presented in Figure 7-5. Two experiments are shown: one with and one without H_2O_2. Any data point represents the average leach rate observed during the previous 30 minute period. The gold leach rate for the first 30 minutes is 1.13 and 1.81 (10^{-5} mol m^{-2} s^{-1}) for the aerated solution and the solution with H_2O_2 present, respectively. The values at the 60 minute mark are 0.67 and 1.69 (10^{-5} mol m^{-2} s^{-1}) for the test without and with H_2O_2 respectively. The decrease in leach rate for the test without H_2O_2 could be caused by a passivation phenomenon, as described in Section 5.4.1.2. These values are within experimental error of the ones shown in the gold-pyrite experiments, confirming experimental consistency. After the connection and introduction of the arsenopyrite electrode into solution at the 60 minute mark, the gold leach rate determined at the 90 minute mark was 3.03 and 6.13 (10^{-5} mol m^{-2} s^{-1}) for the aerated and the solution with H_2O_2 respectively. The leach rates determined at the 120 minute mark are 2.25 and 4.95 (10^{-5} mol m^{-2} s^{-1}). This indicates an increase in the average gold leach rate, when galvanic coupled with arsenopyrite, of 194% and 216% in aerated and solution with H_2O_2 present respectively. This indicates, that arsenopyrite acts as an additional oxygen reduction surface, however, the cathodic

reduction of O_2 or H_2O_2 is not as favoured as on pyrite in a solution with H_2O_2 present.

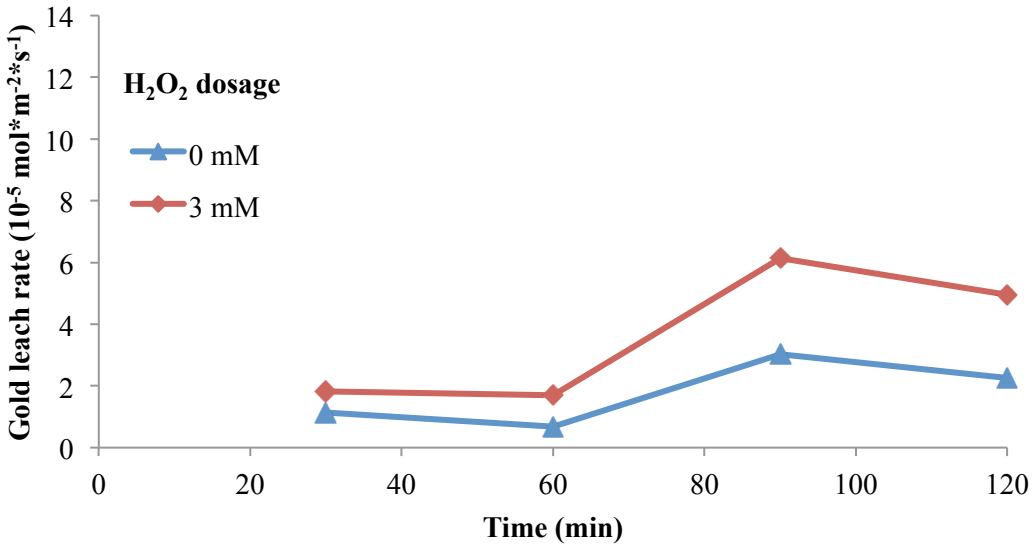

Figure 7-5: Gold leach rate in galvanic interaction with arsenopyrite – arsenopyrite introduced at t=60 min.

The OCP data measured over time during the galvanic coupled leach for gold-arsenopyrite is presented in Figure 7-6. For the first 60 minutes of the experiment, the data closely matches the data measured during the gold-pyrite galvanic coupled leach and is therefore not explained again here. This further confirms that identical and consistent experimental conditions for these experiments were achieved. At the 60 minute mark, coinciding with the connection and introduction of the arsenopyrite electrode, a spike in the measured OCP can be observed. After this spike, the now mixed OCP for the experiment without H_2O_2 present stabilises around -185mV, the mixed OCP in the experiment with H_2O_2 present stabilises around -80mV.

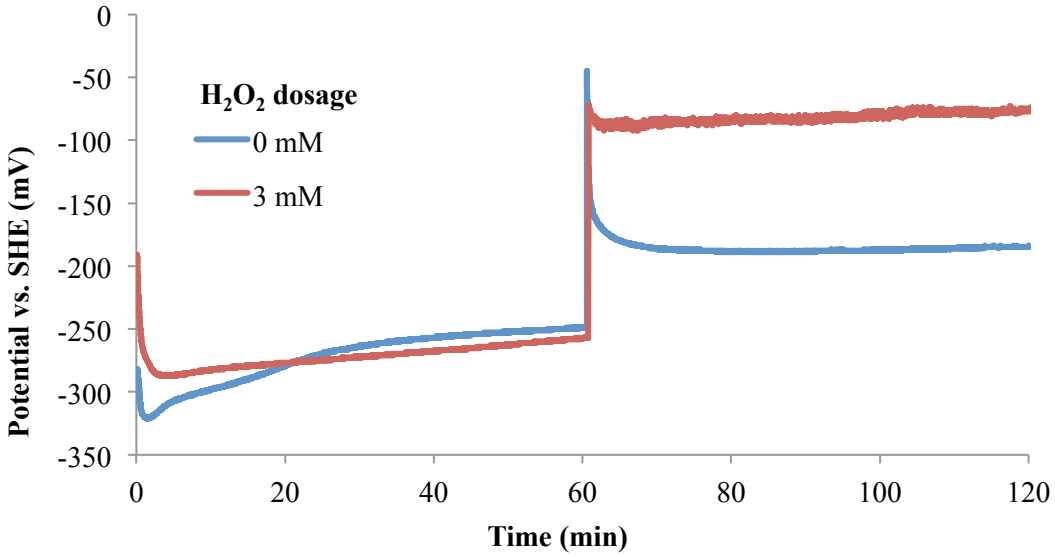

Figure 7-6: OCP measured for gold leached in galvanic interaction with arsenopyrite – arsenopyrite introduced at t=60 min.

Gold-Chalcopyrite

Figure 7-7 shows the gold leach rate over time in the galvanic coupled leach experiments with chalcopyrite. Each data point represents the average leach rate for the previous 30 minutes for the corresponding experiment. At the 30 minute mark the gold leach rate is 1.18 and 1.86 (10^{-5} mol m^{-2} s^{-1}) for the experiment without and with H_2O_2 in solution, respectively. During the next 30-minute bracket (shown at the 60 minute mark) the leach rates are 0.47 and 1.57 (10^{-5} mol m^{-2} s^{-1}) for the test without and with H_2O_2 in solution respectively. These values are within an acceptable error margin, compared to the results measured during the pyrite and arsenopyrite experiments. The changes in leach rate can be explained, as shown in the Section 'Gold-Pyrite' above. This indicates consistent experimental conditions. At the 90 minute mark, after connection and introduction of the chalcopyrite electrode, the leach rates measured are 2.44 and 12.37 (10^{-5} mol m^{-2} s^{-1}) for the experiment with aeration and the one with H_2O_2 added, respectively. The final values at the 120 minute mark are 1.88 and 11.82 (10^{-5} mol m^{-2} s^{-1}) for the test without and with H_2O_2 present, respectively (the cyanide limiting rate would be 37.9 (10^{-5} mol m^{-2} s^{-1}), calculated as described in Section 3.4.1). The increase in average leach rate from

before to after chalcopyrite connection can be computed to 161% and 606% respectively for the experiment without and with H_2O_2. This is consistent with chalcopyrite readily acting as an oxygen reducing surface for H_2O_2 as seen in the potential scan data, in Section 7.4.1, where chalcopyrite had a stronger ability to reduce H_2O_2 to OH^- at higher potentials compared to the other minerals tested.

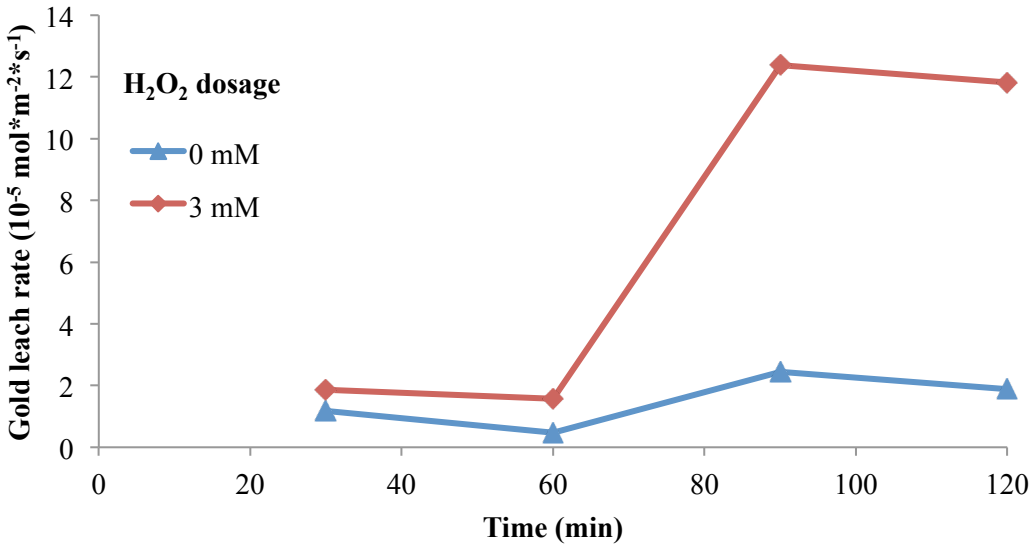

Figure 7-7: Gold leach rate in galvanic interaction with chalcopyrite – chalcopyrite introduced at t=60 min.

The OCP data measured during the galvanic coupled leach experiment is shown in Figure 7-8. The data for the first 60 minutes very closely agrees with the data obtained during the first 60 minutes of the galvanic leaches with pyrite and arsenopyrite, confirming experimental repeatability. At the 60 minute mark, with connection and introduction of the chalcopyrite electrode, a sharp increase in the measured mixed OCP can be seen. The mixed OCP then settles for the remainder of the experiments around -190 mV and 20 mV for the leach without and with H_2O_2 present, respectively. The larger (compared to the pyrite and arsenopyrite galvanic leaches) difference in the observed mixed OCP after the 60 minute mark, represents

a bigger impact of the oxygen reduction half reaction on the mixed OCP and gold leach rate than seen with the other minerals.

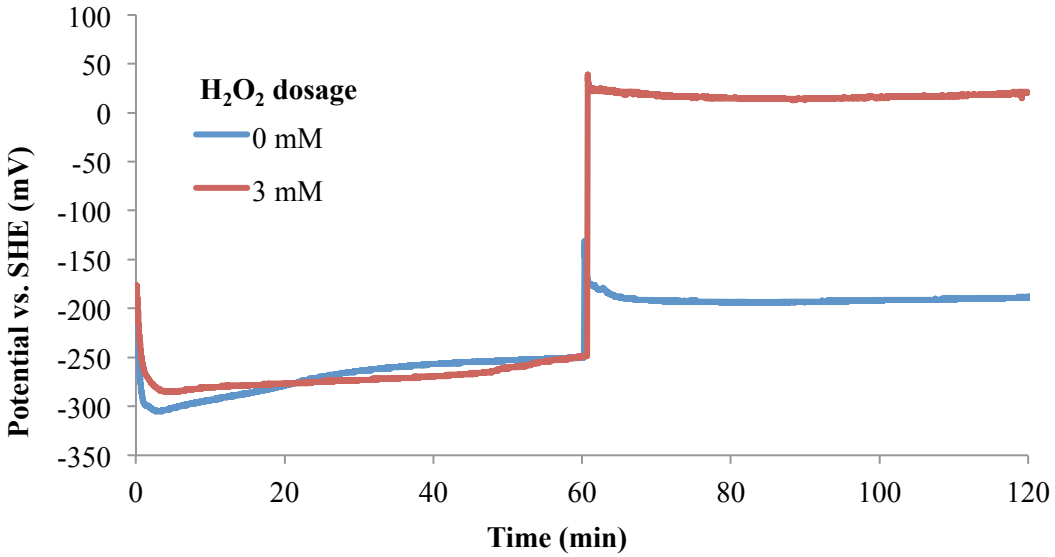

Figure 7-8: OCP measured for gold leached in galvanic interaction with chalcopyrite – chalcopyrite introduced at t=60 min.

7.4.3 Summary

It has been shown, that various minerals can enhance the oxygen reduction reaction during the leaching of gold with sodium cyanide. In Table 7-1 a summary of the gathered data is presented. It should be noted, that the obtained leach rates are not corrected for the surface area of the mineral electrode, however, this was attempted in Table 7-2 and will be discussed in the following paragraph. Table 7-1 demonstrates that the beneficial effects of the minerals in aerated solution, in order of strength can be deducted to be: arsenopyrite > pyrite > chalcopyrite. Once hydrogen peroxide is present at 3 mM in solution, the beneficial effects, in order magnitude are: chalcopyrite > pyrite > arsenopyrite. The beneficial effects seen were always further enhanced in the presence of hydrogen peroxide. It is also notable, that particularly for the tests with hydrogen peroxide in solution, that the OCP appears to be correlating with the observed leach rate in the following manner: the higher the observed leach rate, the more positive the OCP measured.

Table 7-1: Observed leach rates and average OCP during galvanic coupling experiments

Mineral Electrode	**Without H_2O_2**		**With H_2O_2**	
Mineral	Gold leach rate (10^{-5} mol m^{-2} s^{-1})	OCP vs. SHE (mV)	Gold Leach rate (10^{-5} mol m^{-2} s^{-1})	OCP vs. SHE (mV)
None	0.86	-260	1.77	-260
Pyrite	2.30	-200	7.01	-40
Arsenopyrite	2.64	-190	5.54	-80
Chalcopyrite	2.16	-190	12.10	15

The leach rate values listed in Table 7-2 represent an attempt to correct the measured leach rates for the different sizes of mineral electrodes used. As the cathodic reaction was identified to be the limiting factor in all tests, a linear standardisation of the obtained leach rates to an equivalent mineral surface area of 400% of the size of the gold electrode was made. It can be noted, that the order of enhancement, as deducted from Table 7-1 does not change for the tested mineral specimens, even when the surface area corrections are made.

Table 7-2: Observed galvanic leach rates and mineral size corrections during galvanic coupled leaches

Mineral	**Mineral surface area**	**Leach rate (calculated @ 400%) (10^{-5} mol m^{-2} s^{-1})**	
Mineral	(in % of gold surface)	Area-corrected aerated	Area-corrected with H_2O_2
Pyrite	404%	2.28	6.94
Arsenopyrite	348%	3.03	6.37
Chalcopyrite	423%	2.04	11.44

7.4.4 Conclusions

It has been shown, that galvanic interaction of gold and the conductive sulphide mineral surfaces investigated, during leaching of gold in the same solution, can all increase the leach rate by a factor of around 3. When low concentrations of hydrogen peroxide (3 mM) are added, this factor can increase up to around 6 for the minerals

investigated; chalcopyrite almost doubles the gold leach rate achieved by the other minerals. These benefits may not be seen in real world applications, as sulphide-ions released into solution from sulphide minerals may passivate the gold surface or hydrogen peroxide may be rapidly decomposed in the leach slurry. The passivation of gold by sulphide ions and hydrogen peroxide as a possible remedy has been investigated in Chapter 5.

Further, the increase of the OCP during galvanic coupling appears to be linked with increased leach rates. However, no exact relation could be determined during this study.

Chapter 8 Leaching of gold bearing sulphidic ores

8.1 Introduction

Three industrial ores from different sites were used to investigate if a simple, standardised test can be utilised to indicate the effectiveness of hydrogen peroxide treatment on complex ores. This was done, as literature (see Section 2.4.3) presents various methods for ore-leach tests but no industry standard (standard volume, standard agitation, etc.) appears to be available. These ores shall be called Ore A, B and C throughout this section, as the donors would like to remain anonymous. The ores were selected, as they were known to contain sulphidic minerals. All ores were characterised by elemental analysis and QXRD. The ores were prepared for bottle roll leach tests and the required conditions (pH, NaCN addition and gas sparging) for each ore were determined by scoping tests and test work previously completed by the corresponding donors, if available. Only the optimised conditions (baseline) from the scoping tests are presented along with evaluation of peroxide use to enhance gold recovery. With the treatment baseline determined, the impact of a range of pre-treatments on the leachability and reagent requirement as well as leach discharges were tested by a 'standardised' bottle roll method (constant gas sparging, rotation speed, sample volume, cyanide addition, etc.). The experimental setup, analytics and results are presented throughout the subsequent sections. A conclusion on the ability to use a simple test standard method to establish the beneficiary effects of hydrogen peroxide is drawn.

8.2 Ore characterisation

To characterise the ores treated, as much information as was viable during the course of this investigation was collected. The information collected included particle size

distribution, elemental analysis for selected elements and QXRD analysis for phase identification, as described in Section 3.5.6.

The particle size distribution for each ore was determined by wet screening through a 25 μm screen and subsequent filtering of the two fractions with an Amdel PF1000 filter press and drying of the two fractions in an oven at 70°C. Dry screening with a Retsch AS200 control 'g' Rotap unit and the following screens: 38, 53, 75, 106, 150, 212, and 300 μm, was conducted. All size fractions were weighed on an analytical scale and a size distribution and an estimated P80 were calculated.

The elemental analysis was conducted via ICP-OES, operated and reported by the CSIRO AMRC Waterford analytical unit. The results provided included the following elements: Ag, Al, As, Bi, Ca, Cd, Co, Cr, Cu, Fe, K, Mg, Mn, Mo, Na, Ni, P, Pb, Sb, Si, Zn, Ti and V.

Separate sulphur analysis and carbon analysis was conducted with a carbon-sulphur analyser by the CSIRO AMRC Waterford analytical unit.

The gold content was determined by a 25 g sample fire assay, which was executed by ALS minerals, Perth, WA, and only the assay values were reported. However, every sample was assayed in duplicate. In case of discrepancies between the duplicate analysis a repeat with 50 g sample was conducted.

8.3 Ore A

8.3.1 Sample preparation

Ore A was received as a dry sample with a particle size of -850 μm. The sample was split into four subsamples of 8 kg weight with an ESSA 8-bucket rotary splitter. In this process some leftover sample was generated and set aside. These subsamples were fed through the splitter four more times to create representative samples and then split into 32 subsamples. The sub-samples obtained in this way had a weight of

1000±50 g. The samples were bagged and their weight was adjusted to 1000±1 g by either adding or removing some sample with a scoop from part of the left over sample set aside.

Three test grinds of different duration were conducted on a purpose build (by CSIRO) laboratory rod mill with 16 mild steel rods of the dimensions of 25 mm diameter and 285 mm length. Two of these grinds were conducted at 15 and 30 minutes, resulting in two different P80 values. A simple curve was drawn and the target time to give a P80 of 80 µm estimated and confirmed by a third grind. The resulting samples were split with a riffle type sample splitter and an ~100g subsample was produced. This subsample was sized, as described in Section 8.2.

8.3.2 Leach experiments

Based on the results gathered during preliminary scoping work, a test matrix as shown in Table 8-1 was created. This included pre-oxidation, as the donor site uses pre-oxidation to increase recoveries. The quantity of NaOH solution was determined to obtain a slurry pH of around pH 11 at the time of cyanide addition and a final pH above pH 10. The DI water quantities were calculated to obtain 50% solids to liquid ratio in the slurry, when all other reagent additions are completed.

Table 8-1: Tests conducted on Ore A and solution quantities added

Pretreatment	**DI-water (mL)**	**1M NaOH (mL)**	**~500 (mL)**	**mM H_2O_2**
none	953	22	0	
1 h Pre-Oxidation	953	22	0	
3 mM H_2O_2	946	22	6.7	
1 h Pre-Oxidation and 3 mM H_2O_2	946	22	6.7	

Prior to each test, a baffled (4 baffles) 3 L bottle roll bottle and a matching lid were weighed to determine the bottle tare weight. The lids had an ~8 mm diameter hole in the centre, to allow for gas injection and sampling, whilst the bottle was rotated on the bottle roller. One bag of sample (1000 g) was introduced into the laboratory rod mill with 16 mild steel rods of the dimensions of 25 mm diameter and 285 mm length and dry ground for exactly 20 minutes. Due to the target of creating an easy test for the impact of hydrogen peroxide, the decision for dry grinding was made. No information on further downstream implications of wet versus dry grinding was found in the literature or in discussions with experts from the WASM gold group (Wardell-Johnson, 2014b). Immediately after grinding, the resulting product was introduced into the bottle. Exact amounts of 1 M NaOH solution, made as explained in Section 3.2.7 and DI water, as given in Table 8-1, were added. Then the lids were put on the bottles and the bottles put on the bottle roller, which agitated the slurry at a constant speed fixed for all tests. Metered compressed air was introduced into the bottle and where applicable, the pre-oxidation period started. Air injection took place at a rate of 100 mL min^{-1}. After the pre-treatment, 1 M NaCN solution, as described in Section 3.2.7, was added targeting a NaCN concentration of 25 mM in the solution. The exact amount of NaCN solution required was calculated based on the weight of the bottles and hence the amount of slurry in the bottles. The leach time for each test was 48 hours. Samples were taken at the following times: immediately prior to the NaCN addition, immediately after the NaCN addition (t=0 h), 0.5, 1, 2, 4, 6, 24 and 48 hours. The samples were drawn with a syringe and hose attachment through the hole in the lid of the rotating bottles. The bottle weights were recorded before and after sampling. The samples were put into vacuum filter towers with 0.45 µm filter paper. Prior to engaging the vacuum, the pH and DO of the slurries were measured in the top of the filter towers with a DO- and a pH-meter as described in Sections 3.3.2 and 3.3.3, respectively. The solutions collected were analysed for their CN^- content by $AgNO_3$ titration, as described in Section 3.5.1.1. The following sulphur species in solution were determined by HPLC methodology, as described in Section 3.5.4: S^{2-}, SCN^-, $S_2O_3^{2-}$ and SO_4^{2-}. The solutions were also analysed for their respective content of Au, Ag, Cu and Ni by means of AAS as described in Section 3.5.2. The solids remaining after the filtration were not returned to the leach to retain consistent solids

to liquid ratio during leaching and not to alter the solution chemistry. At the end of each test, the remaining slurry was filtered with an Amdel PF1000 pressure filter. The filter cake was washed twice with tap water prior to drying it in an oven for 24 hours at 70 °C. The dry weight was measured and the filter cake was pulverised by manual means and then split by a riffle type sample splitter for fire assay in order to determine the remaining Au content of the solids. The fire assay was conducted in duplicate by ALS minerals from 25 g samples. Some repeat analysis was done on 50 g samples, again in duplicate.

8.4 Ore B

8.4.1 Sample preparation

Ore B was received as a collection of three wet filter cakes with filter paper still attached. The sample was dried for 48 hours at 70 °C in an oven. Once dried, the remaining filter paper was removed. Big agglomerates were separated with a Sala International laboratory cone crusher. The sample was split with an ESSA 8-bucket rotary splitter and distributed into 4 subsamples of 8 kg weight, which then were fed three times through a splitter in order to obtain representative samples. In this process some left over material was generated. The final split was distributed in 4 subsamples of 8 kg weight, which then were split again to achieve 1 kg subsamples. The subsamples were bagged and the weight was adjusted to 1000±1 g, as described for Ore A in Section 8.3.1. The bags were purged with nitrogen before sealing. These samples were stored in a freezer ready for use in the leach experiments. Sizing of the sample was conducted as described in Section 8.2.

8.4.2 Leach experiments

A test matrix was created, as shown in Table 8-2. This was based on results gathered during preliminary tests as well as some site data. The NaOH amount was determined targeting a slurry pH of at least pH 11 and remain above pH ~9.5 during

the leach time without further adjustments. All other liquid volumes were calculated to obtain a 50% solids to liquid ratio of the slurry.

Table 8-2: Tests conducted on Ore B and solution quantities added

Pretreatment	**DI-water (mL)**	**1 M NaOH (mL)**	**~500 mM H_2O_2 (mL)**
none	895	80	0
1 h Pre-Oxidation	895	80	0
3 mM H_2O_2	888	80	6.7
6 mM H_2O_2	881	80	13.4
1 h Pre-Oxidation and 3 mM H_2O_2	888	80	6.7
1 h Pre-Oxidation and 6 mM H_2O_2	881	80	13.4

Prior to each test, a baffled (4 baffles) 3 L bottle roll bottle and a matching lid were weighed to determine the bottle tare weight. The lids featured an ~8 mm diameter hole in the centre, to allow for gas injection and sampling, whilst the bottle was rotated on the bottle roller. One bag of ore was added into each bottle used for the experiments. Calculated amounts of DI water and 1 M NaOH solution, as described in Section 3.2.7, were added to obtain an initial pH of ~11.5. The lids were put on the bottles and the bottles placed on the bottle roller, which agitated the slurry at a fixed speed for all tests. Compressed air was metered into each bottle at a rate of 100 mL min^{-1} and the pre-oxidation time started where applicable. On completion of the pre-oxidation time H_2O_2 was added as ~500 mM solution, as described in Section 3.2.1. After the pre-treatments a calculated amount (based on the bottle weight) of 1 M NaCN solution, as described in Section 3.2.4, was added targeting a NaCN concentration of 25 mM in the solution. The leach time for each test was 48 hours. Samples were taken immediately prior and after (t=0) the NaCN addition, as well as after 0.5, 1, 2, 4, 6, 24, and 48 hours with a syringe and hose attachment through the opening in the bottle lid. The bottles were weighed before and after sampling. The samples were put into a vacuum filter tower with 0.45 µm filter paper. The pH and

DO values were measured in the top of the filter towers, prior to filtration. The utilised DO- and pH-meters are described in Sections 3.3.2 and 3.3.3. The solution was analysed for its NaCN content by $AgNO_3$ titration, as described in Section 3.5.1.1. HPLC methodology, as described in Section 3.5.4 was used to detect the following sulphur species in the filtrates: S^{2-}, SCN^-, $S_2O_4^{2-}$ and SO_4^{2-}. The solutions content of Au, Ag, Cu and Ni was determined by means of AAS, as described in Section 3.5.2. The remaining solids were not returned to the leach, to retain a constant solids to liquid ratio of the leach. At the end of each test, the bottle was weighed prior to the remaining slurry being filtered with an AMDEL PF1000 pressure filter and paper. The filter cake was washed twice with tap water prior to drying it in an oven for 24 hours at 70 °C. The dry weights of the filter cakes were determined prior to pulverising it. The resulting broken up material was split with a riffle type sample splitter to obtain a representative fraction for submission for fire assay, to determine the remaining Au content. The fire assay was conducted in duplicate by ALS minerals from 25 g samples. Some repeat analysis was done on 50 g samples, again in duplicate.

One repeat test was conducted, for the pre-oxidation test, with all test parameters being the same, apart from the addition of 1.08 mL of concentrated H_2SO_4 with the DI water, prior to starting the pre-oxidation time. This slurry was agitated for 5 minutes and then a calculated amount of NaOH was added to neutralise the acid added, before commencing the pre-oxidation step as described for the other tests on Ore B. The target was to investigate if the sulphide surface had become passivated during sample preparation and to potentially reactivate the mineral surface, as Ore B in scouting tests did show significantly lower reactivity than observed by the ore donor. As a mistake was made in the quantity of NaOH added initially and when noticed the remainder required to equal the amount of alkalinity available in solution to the other tests was added at the six hour mark.

8.5 Ore C

8.5.1 Sample preparation

The sample received was float tail regrind cyclone overflow and arrived as a wet filter cake. The sample was repulped in DI water and split into three equal size filter cakes with an Amdel PF1000 pressure filter. The filter cakes were bagged, remaining on the filter paper in cake form, so representative slices could be cut from them. The filter cakes were stored in a fridge to decrease possible sulphide oxidation. The moisture content of each filter cake was determined by means of drying a slice of each of the filter cakes and measuring the wet and dry weight. A fraction was taken and sized, as described in Section 8.2. As in the industrial process, where this ore stems from, no further grinding took place. Slices of the filter cakes were used for the subsequent leach experiments.

8.5.2 Leach experiments

Four leach experiments were conducted, based on data provided and the insights gained with the scoping tests, as shown in Table 8-3. The amount of DI water added to the tests is not shown, as this was calculated accordingly based on the moisture content of the filter cake used (variance in moisture content of the filter cakes was around 2%), targeting a solids to liquid ratio of 40% in the slurry.

Table 8-3: Tests conducted on Ore C and solution quantities added

Pretreatment	**1 M NaOH (mL)**	**~500 mM H_2O_2 (mL)**
none	10	0
1 h Pre-Oxidation	10	0
3 mM H_2O_2	10	4.8
1 h Pre-Oxidation and 3 mM H_2O_2	10	4.8

Due to the limited amount of material available, for each test a 500 g dry solids equivalent slice of filter cake was added into the bottle roll vessel. The bottle tare was recorded prior to adding the material. 1 M NaOH and a calculated quantity of DI water was added to each test. The lid was tightened on the bottle and the bottle placed onto the bottle roller. The gas injection hose was inserted into the opening of the bottle roll lid and oxygen sparging commenced at a rate of 100 mL min^{-1}. The H_2O_2 was always added after the pre-oxidation time, immediately prior to the NaCN addition. After differing pre-treatments, as shown in Table 8-3, calculated quantities of 1 M NaCN solution, as described in Section 3.2.4, were added to the tests, targeting 20 mM NaCN concentration in solution. Samples were taken immediately prior to the NaCN addition, and at (t=0), and at 0.5, 1, 2, 4, 6 and 24 hours. The samples of approximately 80 g were drawn with a syringe with a hose attached through the opening of the bottle lid and then put into a vacuum filter tower with 0.45 µm filter paper. The bottles were weighed before and after taking each sample. Prior to engaging the vacuum, the pH and DO of the slurries were measured in the top of the filter towers, with the instruments described in Section 3.3.2, and 3.3.3. Upon completion of the filtration the solids were discarded in order to retain a constant solids to liquid ratio in the leach. The filtrates were analysed for their NaCN content by $AgNO_3$ titration, as described in Section 3.5.1.1. Further the Au, Ag, Cu and Ni content were determined by AAS, as outlined in Section 3.5.2. The following sulphur species were measured in the solutions by HPLC, as described in Section 3.5.4: S^{2-}, SCN^-, $S_2O_3^{2-}$ and SO_4^{2-}. The bottles were weighed at the end of each test, prior to the remaining slurry being filtered with an AMDEL PF1000 pressure filter. The filter cake was washed twice with tap water prior to drying it in an oven for 24 hours at 70 °C. Following dry weight measurement the filter cake was pulverised manually in a plastic bag by crushing it with a wooden bar in a rolling motion against a table surface. The resulting powder was split with a riffle type sample splitter to obtain a representative fraction for Au fire assay. The fire assay was conducted in duplicate by ALS minerals from 25 g samples. Some repeat analysis was done on 50 g samples, again in duplicate.

8.6 Results and discussion

8.6.1 Ore characterisation

Sizing

The three ore samples were supplied as: ready for leaching being concentrate regrinds or overflow regrinds, or as mill feed. The mill feed sample was prepared by the donating party to be an -850 µm size fraction.

Figure 8-1 plots the size distribution curve measured for Ore A with the final grind time of 20 minutes, which was applied to all tests. The measured P80 is 77.5 µm. A P80 of around 80 µm was targeted, as it matches the donor sites grind size.

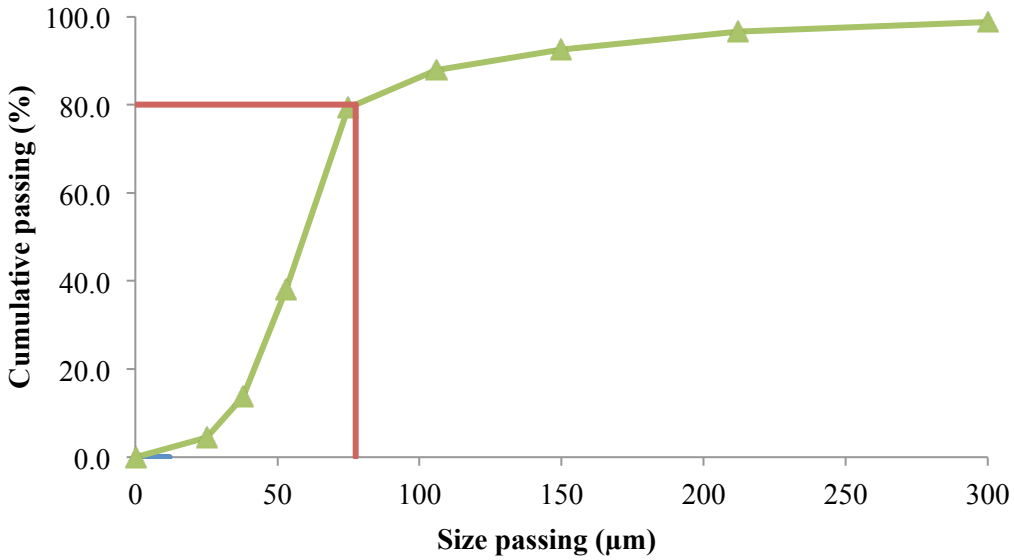

Figure 8-1: Size distribution measured for Ore A after 20 minute grind, marking P80

The size distribution curve obtained for Ore B is shown in Figure 8-2. It can be seen, that the majority of material (94.8%) is passing 25 µm, hence, with the measurement methods available an exact number for the P80 cannot be determined. The estimated P80 for Ore B is 21.1 µm.

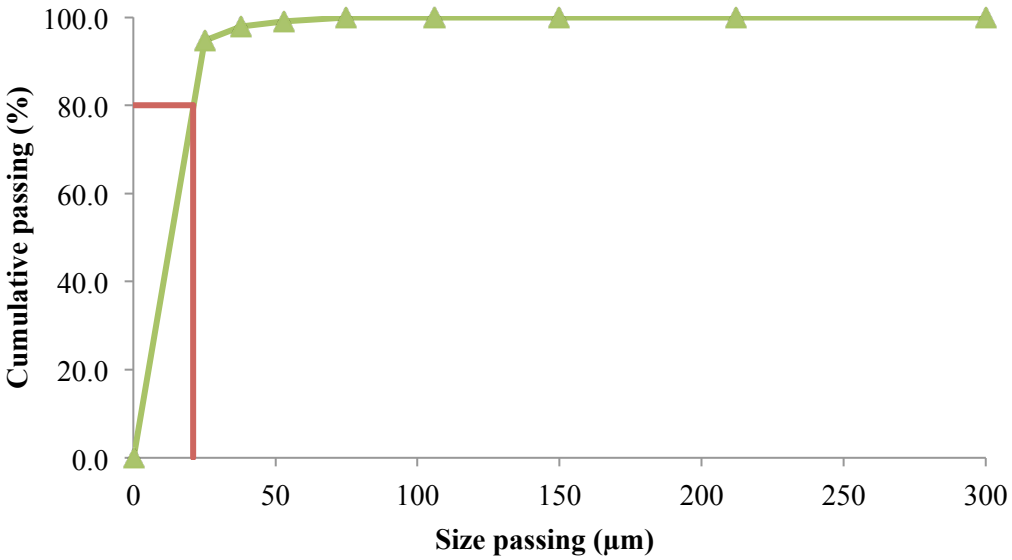

Figure 8-2: Size distribution measured for Ore B, marking the estimated P80

In Figure 8-3 the obtained size distribution curve for Ore C is shown. As 84.6 % are passing the 25 µm screen, only an estimation can be made for the P80. The estimated P80 is 23.6 µm.

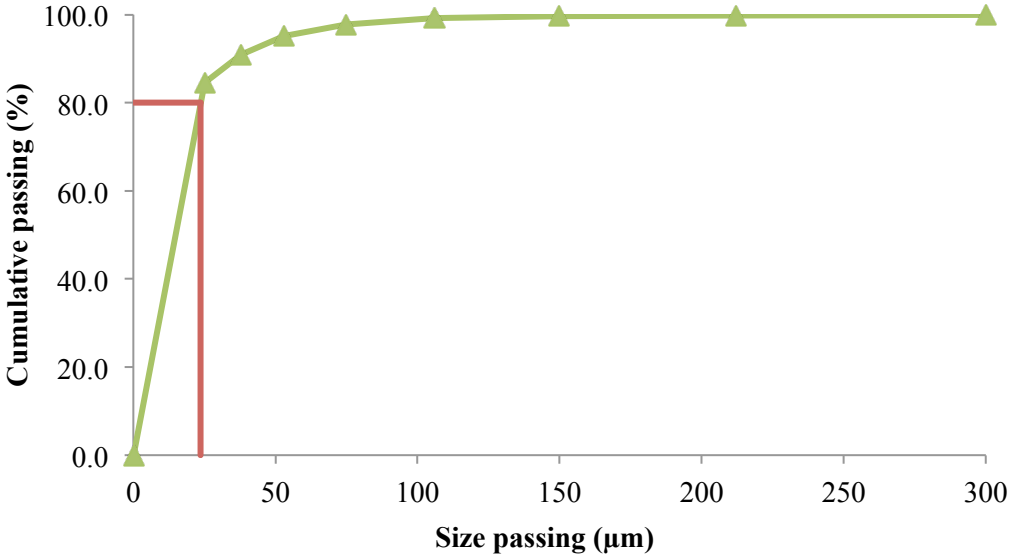

Figure 8-3: Size distribution measured for Ore C, estimated P80 marked

With their size distributions Ore B and Ore C are clearly fine grinds, indicating very fine gold particles. Ore A however, is indicated (Wardell-Johnson, 2014a) to show

coarser gold mineralisation and little encapsulation of gold in sulphide minerals, hence the decision for the coarser grind.

Elemental analysis

The elemental analysis of the selected elements for the ores is reported in Table 8-4. The average errors reported are based on triplicate analysis conducted on Ore A. Exempt from this are the average errors reported for Au, C and S. For Au, the errors were calculated for each ore separately and then averaged, as each ore was assayed twice. For the C, and S values, the error is based on a single repeat analysis of Ore A. Absolute errors are not reported, but it is evident, that on elements with low reported concentrations, the error percentage is increased. All samples did contain detectable amounts of sulphur, with Ore B reporting the highest amount with 11.8 %, a value in the typical range for a floatation concentrate.

Table 8-4: Elemental analysis as reported for the three Ores

	Ore A (%)	Ore B (%)	Ore C (%)	Average error (± %)
Au	1.25E-04	19.8E-04	1.86E-04	8.9
Ag	0.020	0.049	0.013	14.4
Al	6.54	6.91	8.69	1.8
As	0.060	0.097	0.006	21.0
Bi	<0.002	<0.002	<0.002	N/A
C (TC)	2.52	1.06	0.1	0.9
C (TOC)	0.14	0.04	0.04	1.0
C (TIC)	2.38	1.03	0.06	1.0
Ca	3.85	2.98	2.89	1.3
Cd	<0.002	0.005	<0.002	N/A
Co	0.006	0.014	0.005	19.3
Cr	0.068	0.013	0.012	1.4
Cu	0.013	0.178	0.147	28.2
Fe	6.93	14.8	5.49	3.7
K	1.54	2.35	2.19	5.0
Mg	2.90	1.54	1.77	1.2
Mn	0.132	0.152	0.045	2.0
Mo	<0.002	<0.002	0.004	N/A
Na	1.20	0.944	1.89	2.2
Ni	0.033	0.062	0.016	8.2
P	0.062	0.128	0.068	5.8
Pb	0.009	0.046	0.008	18.3
S	1.380	11.800	1.080	2.2
Sb	0.004	0.008	<0.002	13.2
Si	24.0	18.3	28.4	1.6
Zn	0.013	0.695	0.015	2.8
Ti	0.316	0.336	0.353	2.3
V	0.011	0.017	0.008	5.6

Quantitative X-ray Diffraction (QXRD)

The results of the QXRD analysis of the materials used for leach testing are presented in this section.

Figure 8-4 shows the XRD data gathered as well as the peak fitting result for Ore A. It can be seen that there is a good agreement between the data gathered and the model fitted.

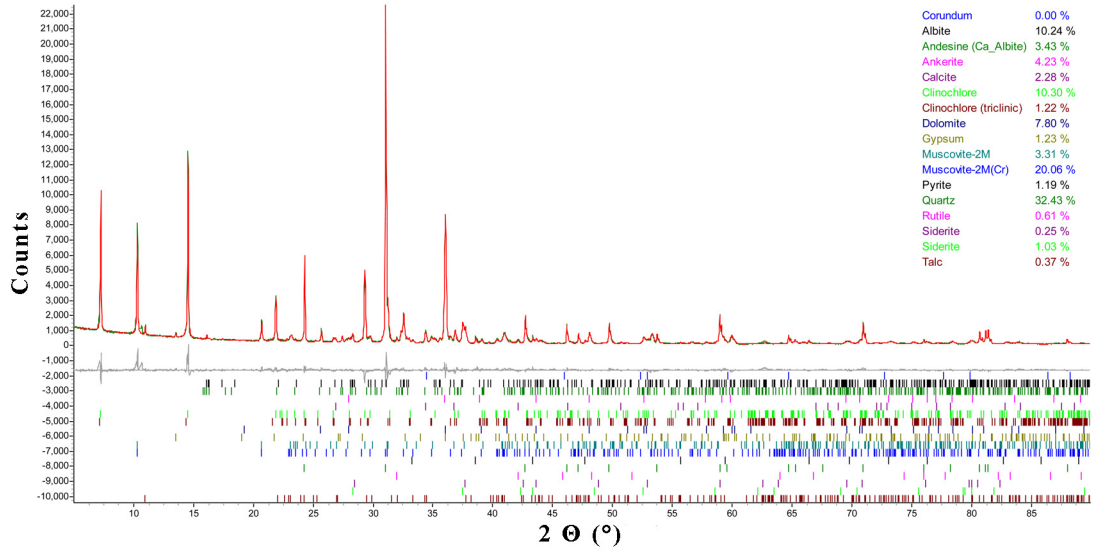

Figure 8-4:QXRD peak data and peak matching for Ore A

The XRD data gathered and the model fitted to the data for Ore B are plotted in Figure 8-5. Strong agreement between the recorded data and the model can be observed.

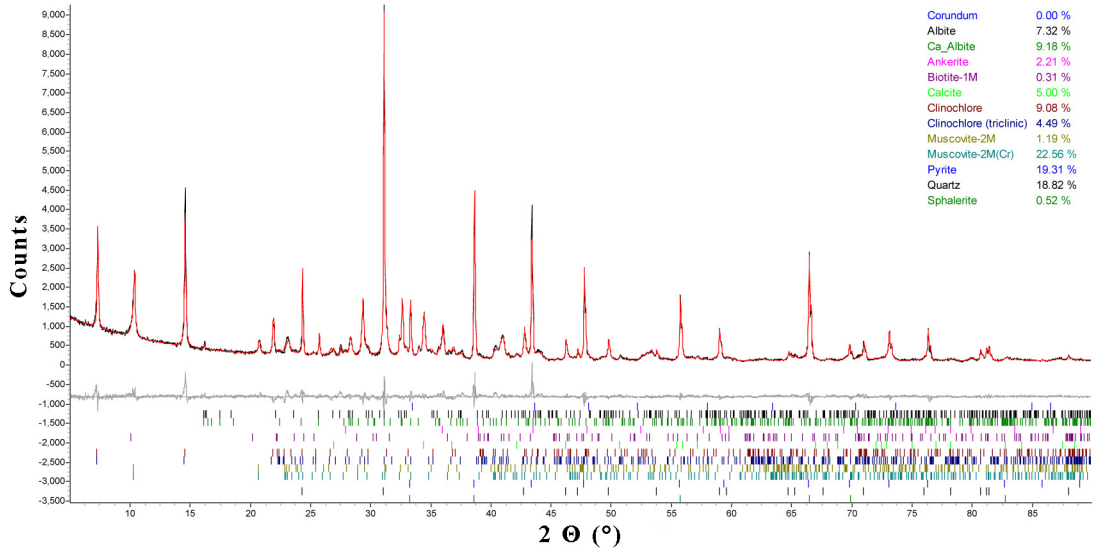

Figure 8-5: QXRD peak data and peak matching for Ore B

For Ore C the recorded XRD data is plotted in Figure 8-6. This plot also includes the model created for quantification. A good match of the two curves can be seen.

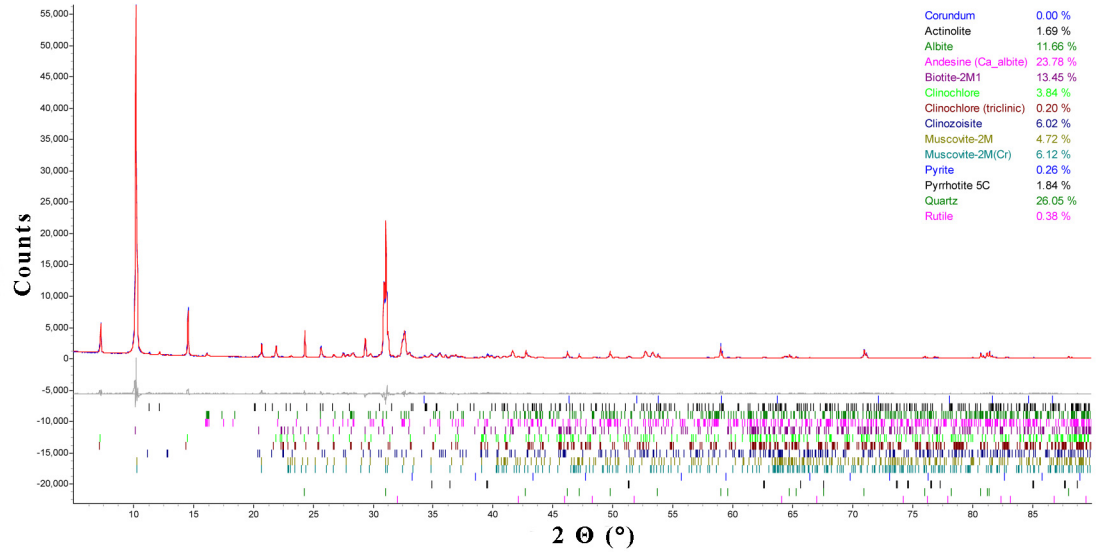

Figure 8-6: QXRD peak data and peak matching for Ore C

The minerals identified and quantified by QXRD for the three ores, as received, are listed in Table 8-5. A firm agreement between the elemental compositions of the

ores, as presented in the paragraph 'Elemental analysis' above, and a chemical composition calculated from the mineral data was found.

The following sulphur containing minerals could be identified: pyrite (FeS_2), pyrrhotite ($Fe_{(1-x)}S$ with (x=0-0.2)), sphalerite ((Zn,Fe)S) and gypsum ($CaSO_4$). Ore A only contained a small amount of pyrite (1.2%), and some gypsum (1.3%), but gypsum can be considered relatively inert, as it is a calcium sulphate (sulphate is the most oxidised state of sulphur). Ore B shows a large amount of pyrite (19.3%) and some sphalerite (0.5%), and Ore C contains some pyrite (0.3%), and some pyrrohotite (1.8%). As a result Ore B was assumed to be most reactive and most likely to respond well to pre-oxidation or H_2O_2 pre-treatment, as benefits of H_2O_2 treatment in leaching with gold galvanically coupled to pyrite were observed in Section 7.4.2. Further benefits were seen in Section 6.4.3, with the removal of sulphide passivation by H_2O_2 pre-treatment.

Table 8-5: Minerals identified and quantified by QXRD

Mineral	Ore A (%)	Ore B (%)	Ore C (%)
Albite/Andesine	13.9	16.5	35.4
Ankerite	-	2.2	-
Calcite	2.3	5.0	-
Ankerite/Dolomite	11.8	-	-
Siderite	1.5	-	-
Clinochlore	11.4	13.6	4.0
Biotite	-	-	13.5
Muscovite	23.4	23.8	10.8
Pyrite	1.2	19.3	0.3
Pyrrhotite	-	-	1.8
Sphalerite	-	0.5	-
Actinolite	-	-	1.7
Clinozoisite	-	-	6.0
Gypsum	1.3	-	-
Rutile	0.6	-	0.3
Quartz	32.4	18.8	26.0
Talc	0.4	-	-

8.6.2 Ore A

8.6.2.1 Leach experiments

The results of the leach experiments are split into five sections. These sections present the following in subsequent order: metals measured in solution, NaCN in solution, slurry dissolved oxygen, slurry pH and sulphur species observed in solution.

Metals in solution

Gold recovery curves were calculated from the amount of gold measured in solution as well as from the tails assays, creating 'calculated head grades' for each test. The calculated head grade as well as the head grade determined by fire assay is shown in Table 8-6. It should be noted, that the calculated head grades determined were all between 0.91 and 1.03 g/t Au. The determined head grade by fire assay was 1.25±0.14 g/t, which could indicate a high variability in gold content throughout the ore producing a significant sampling analytical error (greatest absolute deviation equals 27.2%, which will mean the error in recovery calculation might be the same). A possible analytical error might be caused by preg-borrowing material in the ore, which might have caused some gold to be washed of the solids during the filter cake wash and therefore unaccounted for in the analyses. The tail grade for the test with pre-oxidation and H_2O_2 added was 0.30 and 0.53 g/t, again confirming the variability in the ore or analytical methods. The 0.30 g/t value was used for calculation of the calculated head grade, as this value was closer to all other tail grades of around 0.30±0.01 g/t.

Table 8-6: Measured and calculated head grades of Ore A

Test	Au in solution (mg/L)	Au in solids (g/t)	Head grade (g/t)
Fire assay	-	-	1.25±0.14
No pre-treatment	0.73	0.30	1.03
Pre-oxidation	0.63	0.29	0.92
3 mM H_2O_2	0.69	0.31	1.00
Pre-oxidation and 3 mM H_2O_2	0.61	0.30	0.91

The calculated recovery curves are plotted in Figure 8-7. No significant difference in the final recoveries at the 48 hour mark can be observed for all tests. It appears, that the initial gold recovery, up to the six hour mark shows some variability, indicating, that on this particular ore sample under the leaching regime chosen, no pre-treatment or only pre-oxidation results in a better initial recovery. However, observing the

variability of the data, especially in the calculated head grades, the test data obtained cannot be used as statistically sound to determine the benefit of any given treatment.

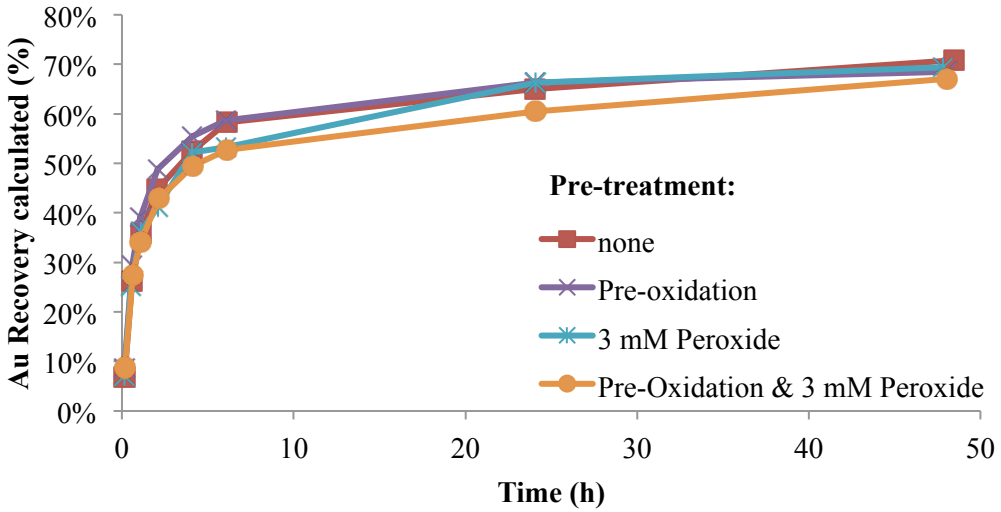

Figure 8-7: Au recoveries over time for tests conducted on Ore A

The Ag head grade measured for this ore sample is 170±30 g/t. The Ag leach curves for the tests are presented in Figure 8-8. It can be seen, that only a very small fraction (~0.1 %) of the Ag was leached under the conditions prevailing during the tests. No statement about a clear benefit or disadvantage of any pre-treatment can be made for the Ag leaching kinetics and amount leached.

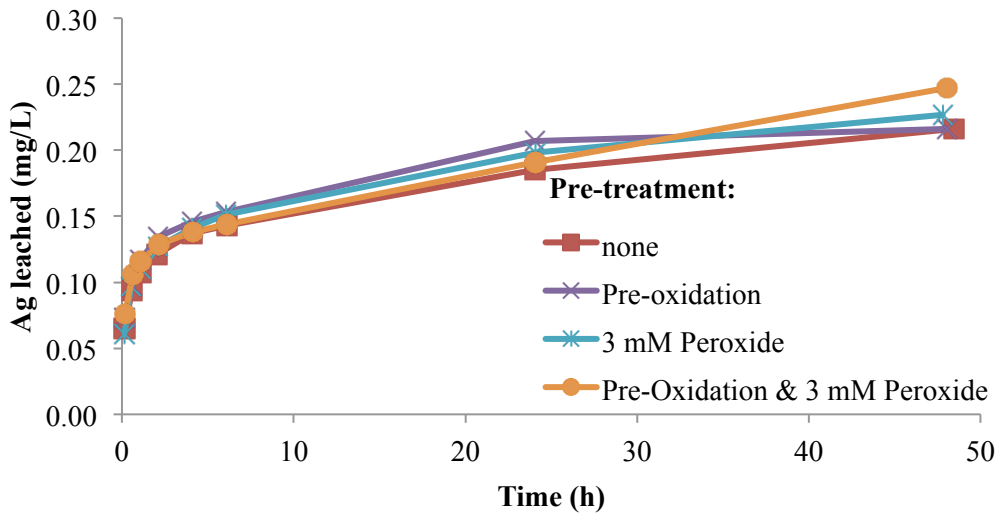

Figure 8-8: Ag leached over time for tests conducted on Ore A

The Cu leached during the leach tests on Ore A sample is presented in Figure 8-9. The final amount of Cu leached equates to approximately 20% of the copper determined as head grade (170±40 g/t). No significant difference in the final copper content in solution can be observed. Two of the data points gathered appear to be outliners, namely: no pre-treatment, and pre-oxidation with H_2O_2 at the 24 hour mark. A repeat analysis of these two samples by AAS was conducted and gave the same results (±0.2 mg/L) and therefore must be considered real. No explanation for this effect could be found, apart from possible Cu precipitation due to variability in the slurry pH. The behaviour also does not coincide with a lack of free cyanide and precipitation of copper as a result.

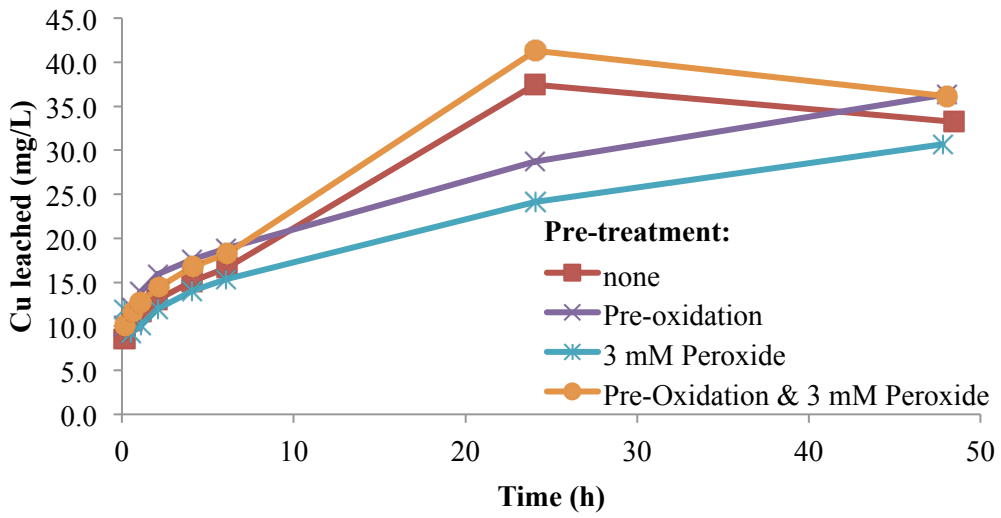

Figure 8-9: Cu leached over time for tests conducted on Ore A

The Ni head grade determined on Ore A is 340±10 g/t. Only around 3% of the Ni present in the ore was leached, as shown in the recovery curves in Figure 8-10. No significant benefit of any pre-treatment can be seen at this point.

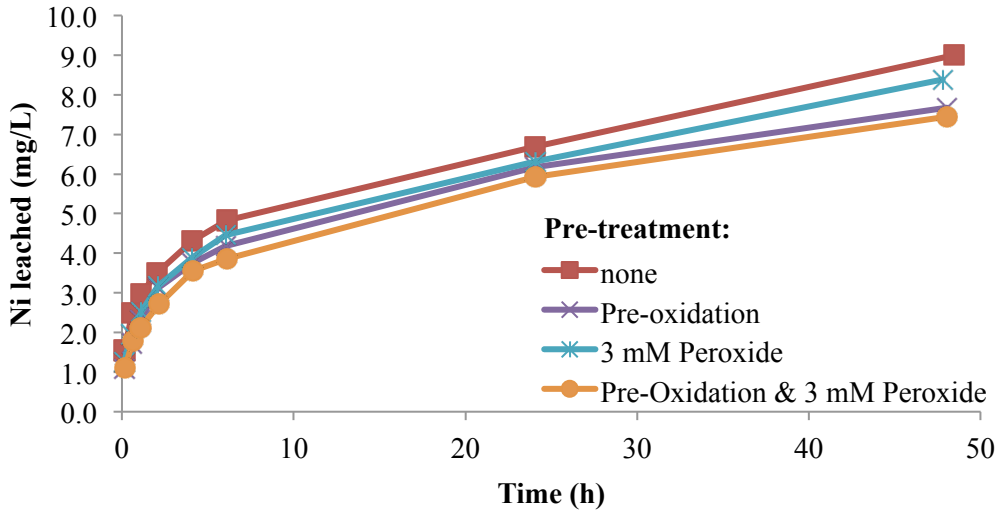

Figure 8-10: Ni leached over time for tests conducted on Ore A

Differing pre-treatments of the Ore A sample only appear to marginally affect the recovery of Au and other minerals during these tests. This indicates, that either the

test methodology used is not sufficient to indicate possible benefits of H_2O_2 on real ores, or that no benefit was achieved.

NaCN

The free cyanide concentrations, shown in NaCN equivalent, observed during the tests were all very linear for the duration of the tests, not showing the typical big initial drop during the first hour of leaching. The total NaCN consumption determined for the four leach tests were 13.4, 14.4, 11.7 and 15.5 mM (or between 0.57 and 0.76 kg/t) for no pre-treatment, pre-oxidation, 3 mM H_2O_2, and pre-oxidation with 3 mM H_2O_2, respectively. An increase in the cyanide consumption of this ore can be observed when pre-oxidation is applied. It could be further concluded, that without pre-oxidation, H_2O_2 has the ability to reduce cyanide consumption.

DO

Only the first four hours of the DO measurements during the leach tests are plotted in Figure 8-11, as no further changes were observed after the four hour mark. It can be seen, that immediately prior to NaCN addition, the tests without pre-treatment and with pre-oxidation show DO levels around 2 ppm below air saturation at sea level at 25°C (Lorösch, 2001). The two tests with H_2O_2 addition show a DO of 17.0 and 22.0 ppm for no pre-oxidation and pre-oxidation, respectively. Immediately after the NaCN addition, the test with pre-oxidation and H_2O_2 addition drops to air saturation levels, whereas the other tests drop slightly more to ~6.6 ppm. By the one hour mark, all tests show DO levels close to oxygen saturation for air sparged solutions, indicating very low reactivity of Ore A sample.

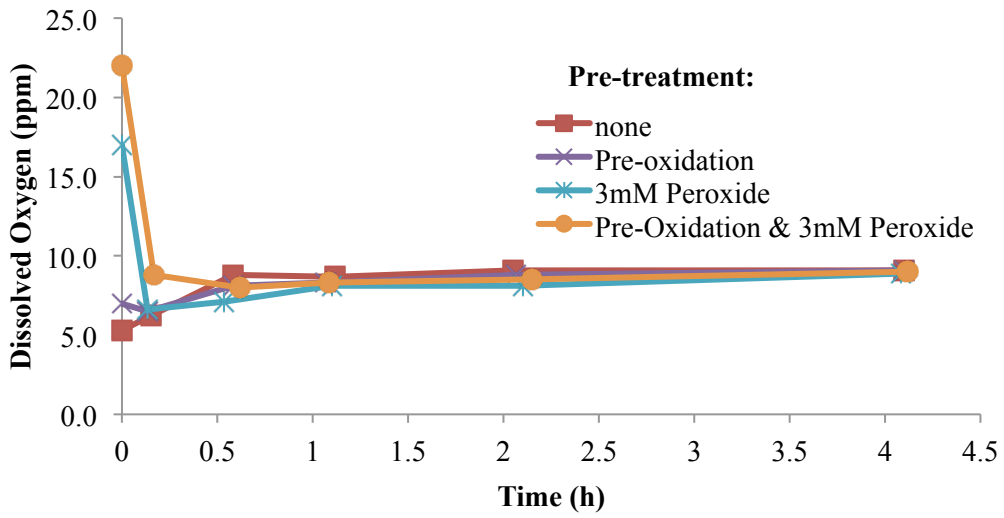

Figure 8-11: Dissolved oxygen in the slurries during the first four hours of the leaches of Ore A

pH

The pH development during the leach tests conducted on the Ore A sample is shown in Figure 8-12. It can be seen, that immediately prior to the NaCN addition the initial pH values varied between pH 10.6 and 11.1. Immediately after the NaCN addition the pH in each test increased slightly due to the alkalinity of NaCN. After this initial increase, during the first four hours of the leach, the pH in all slurries decreased on average by 0.4 pH points, with no significant deviation. After this rapid initial decrease the pH appeared to decrease at a linear rate on all tests with the final values recorded being between pH 9.6 and 9.7. It can be concluded, that the overall alkalinity consumption of Ore A sample under the treatment regimens tests is low, only requiring 22 mM of alkalinity to sustain the pH in an acceptable range for cyanidation.

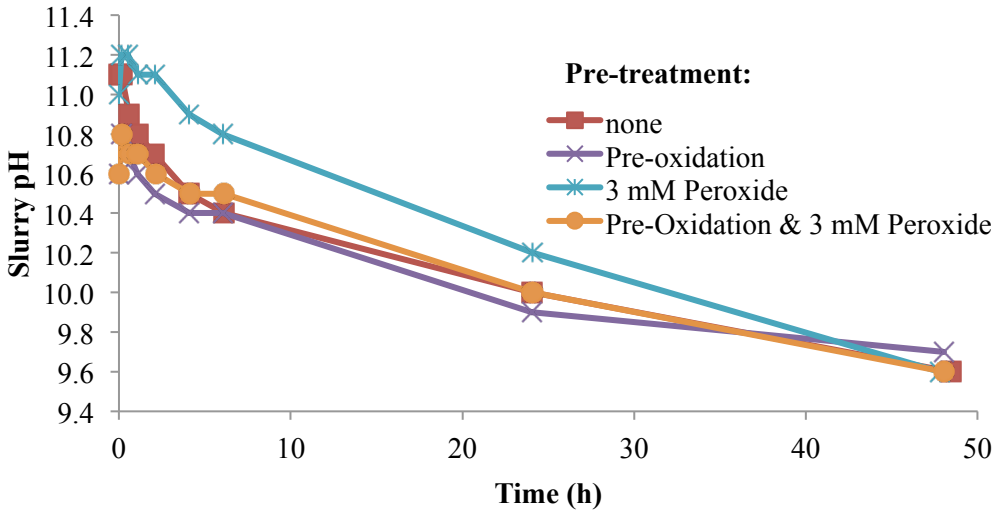

Figure 8-12: pH in the slurries during the leaches of Ore A

Sulphur species

For all tests conducted on the Ore A sample, no S^{2-} ions were detected at any sampling point during the experiments. The SCN^- ion content of the solutions during the leach experiments is plotted in Figure 8-13. The initial SCN^- ion concentration for all tests, prior to NaCN addition, is 0 mM. Within the first two hours after NaCN addition, an increase in SCN^- ion concentration to between 0.10 and 0.14 mM can be seen. After this, a near linear increase to the final SCN^- concentration between 0.45 and 0.62 mM is visible. This variability is very marginal and can be explained by ore variability and analytical error.

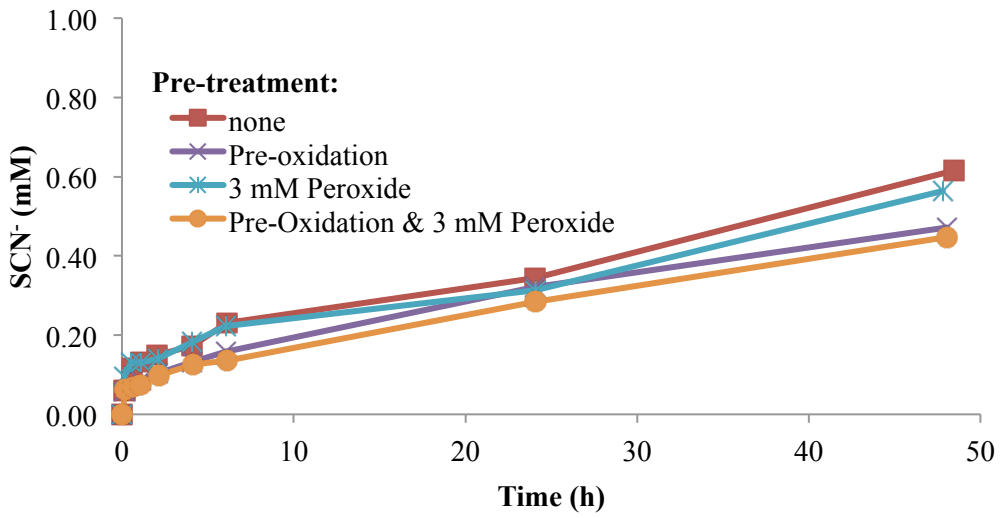

Figure 8-13: SCN^- measured in solution for the tests with Ore A

Figure 8-14 presents the $S_2O_3^{2-}$ ion concentration measured in solution during the leaching on Ore A. The initial values measured, prior to NaCN addition were between 0.01 and 0.06 mM $S_2O_3^{2-}$ ions. Only a small linear increase to final values between 0.02 and 0.13 mM $S_2O_3^{2-}$ ions in solution was observed for all tests. The tests with pre-oxidation trend along the higher values given, whereas the tests without pre-oxidation trend along the lower values measured. This indicates, that pre-oxidation oxidises some minerals in the ore and releases their sulphur content into solution as $S_2O_3^{2-}$. H_2O_2 additions of 3 mM appear to have no notable influence on this. Further, this data should only be used as an indication of $S_2O_3^{2-}$ present, as some other, unidentified species did show in the HPLC spectrum with a slight overlap. Therefore the accuracy on these readings is relatively low, especially being at the lower detection limits.

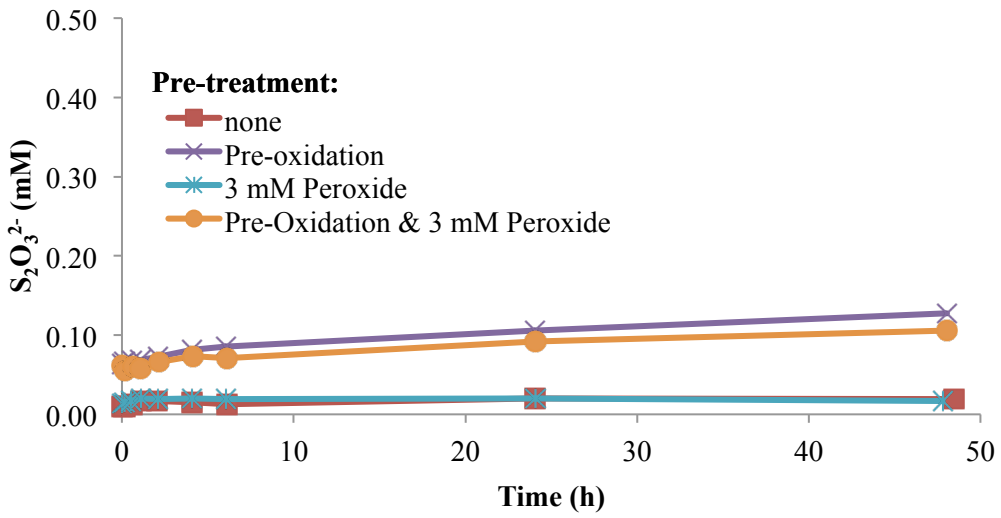

Figure 8-14: $S_2O_3^{2-}$ measured in solution for the tests with Ore A

The SO_4^{2-} ion concentration measured during the leach tests on Ore A sample are plotted in Figure 8-15. The initial values, measured immediately prior to the NaCN addition range between 7.98 and 10.30 mM SO_4^{2-} ions. No clear trend, in that stronger pre-oxidation by either just air or air and H_2O_2 will increase the initial present SO_4^{2-} content, can be derived. After the initial variance in SO_4^{2-} ion concentration, up to the six hour mark, with a general increasing trend for all curves, the SO_4^{2-} ion concentration stabilises and reaches final values between 10.11 and 10.64 mM. No significant change in concentration can be observed and linked to any pre-treatment. Again, the variance in values observed might be due to analytical inaccuracies, as a lot of noise was present on the spectra due to ionic species that were not identified.

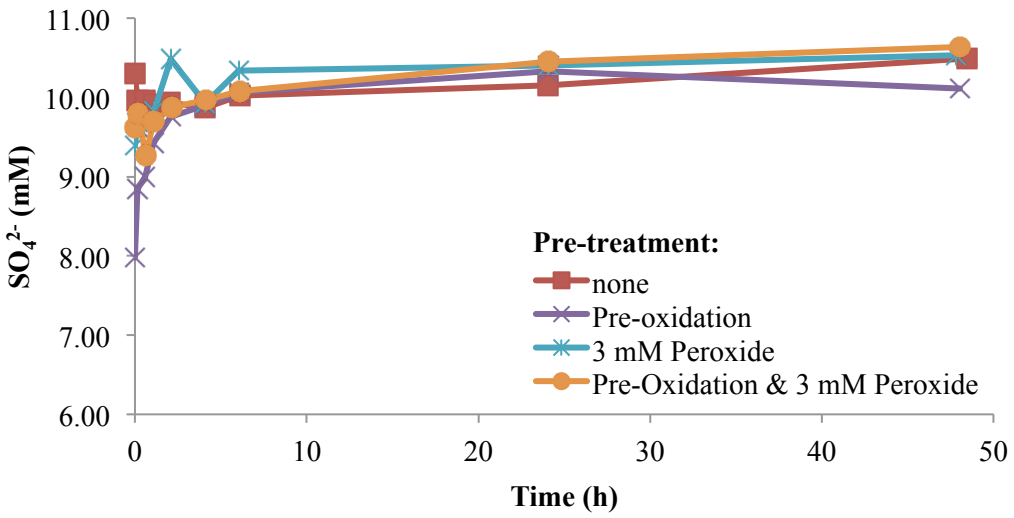

Figure 8-15: SO_4^{2-} measured in solution for the tests with Ore A

Relatively low sulphide species concentrations for all leach tests were observed. No significant differences in the sulphide ion concentrations, which could be linked to the pre-treatments, could be found in this set of tests. This indicates, that either the test methodology does not provide the environment showing possible benefits of H_2O_2 or the ore was not susceptible to H_2O_2 pre-treatment.

Summary

The scoping tests (not presented in this thesis) conducted on Ore A indicated susceptibility of the ore to pre-treatment with pre-oxidation, shown by differing amounts of Au leached and differences in the NaCN consumption. However, after adjusting the NaOH dosage and NaCN dosage according to the requirements determined in the scoping tests, none of this susceptibility could be replicated. It should, however, be noted that the scoping tests were conducted with wet grinding, whereas the final tests were conducted on dry ground material, as the target was to develop a simple test methodology and wet grinding added significant amounts of additional complexity. This indicates, that wet or dry grinding might affect the ore slurry and leach chemistry to an extent, that possible differences noted on the scoping tests cannot be noted any further. As the scope of this study was to

investigate the impact of H_2O_2 treatment, this was not investigated any further, but it is a potential area for future work.

8.6.3 Ore B

8.6.3.1 Leach experiments

The leaching experiments designed and conducted, based on plant information as well as some scoping tests (not presented in this thesis) are presented throughout the following sections. Six different pre-treatment regimens, assumed to possibly show significant differences in the solution chemistry and gold recoveries were investigated.

Metals in solution

Based on the experimental results, calculated Au head grades were determined for each test. The calculated head grades as well as the measured fire assay result are listed in Table 8-7. It is notable that the head grades vary between 19.5 and 21.0 g/t. This translates into a total maximum deviation of approximately 7.1% on the final recovery – meaning any change on the final recovery less than 7.1% can only be interpreted as random error. Cause for this variability may be sample variability as well as analytical error.

Table 8-7: Measured and calculated head grades of Ore B

Test	Au in liquid (mg/L)	Au in tails (g/t)	Head grade (g/t)
Fire assay of supplied ore	-	-	19.78±0.18
No pre-treatment	15.5	4.7	20.1
Pre-oxidation	17.4	3.6	21.0
Pre-oxidation repeat	16.0	3.9	19.9
3 mM H_2O_2	15.4	4.4	19.7
Pre-oxidation and 3 mM H_2O_2	15.9	3.6	19.5
6 mM H_2O_2	15.7	4.5	20.3
Pre-Oxidation and 6 mM H_2O_2	16.1	4.8	20.9

The Au recovery curves during the leach tests on Ore B are plotted in Figure 8-16. It can be seen, that the majority of the Au is recovered during the first six hours of the leaches. Slight differences in the initial leach rates are observable, with no pre-treatment appearing to have the lowest initial leach rate. The final recoveries calculated in ascending order are: 76.9% (no pre-treatment), 77.2% (pre-oxidation & 6 mM H_2O_2), 77.6% (6 mM H_2O_2), 77.9% (3 mM H_2O_2), 81.7% (pre-oxidation and 3 mM H_2O_2) and 82.9% (pre-oxidation). This would mean an improvement in Au recovery, depending on the pre-treatment, of up to 6 % from no pre-treatment. This is still below the possible error determined, based on the calculated tails. As the test with pre-oxidation appeared to be a significant outliner in the dataset, prior to receiving the tailings fire assays, a repeat test was conducted, as described in Section 8.6.3.1. The final Au recovery observed during the repeat test is 80.6 %, which again indicates enhancement in the recovery, even though not as much as in the test without the H_2SO_4 addition. It has to be noted, that the repeat test also received an additional H_2SO_4 treatment, prior to commencing the test. This was done, as the

solution analysis indicated a significant loss in reactivity of this ore compared to the site data provided (sample donor, 2015), and reactivation of the surfaces by acid etching was envisaged. However, no significant effect was noted, apart from the recovery being slightly lower than on the original pre-oxidation test. Overall, it appears that pre-treatment is beneficial to the Au recovery on this ore. No clear statement can be made on which pre-treatment, apart from pre-oxidation, possibly in combination with a low H_2O_2 addition, showed the best results. The tails Au fire assays did show a relatively high variability between the duplicate tests of up to 10 %, indicating, that a large variability in the ore could be the cause for this result. A single test matrix with the standard methodology used appears to be not suitable to determine possible benefits of H_2O_2 pre-treatment or pre-oxidation on the gold leaching of Ore B.

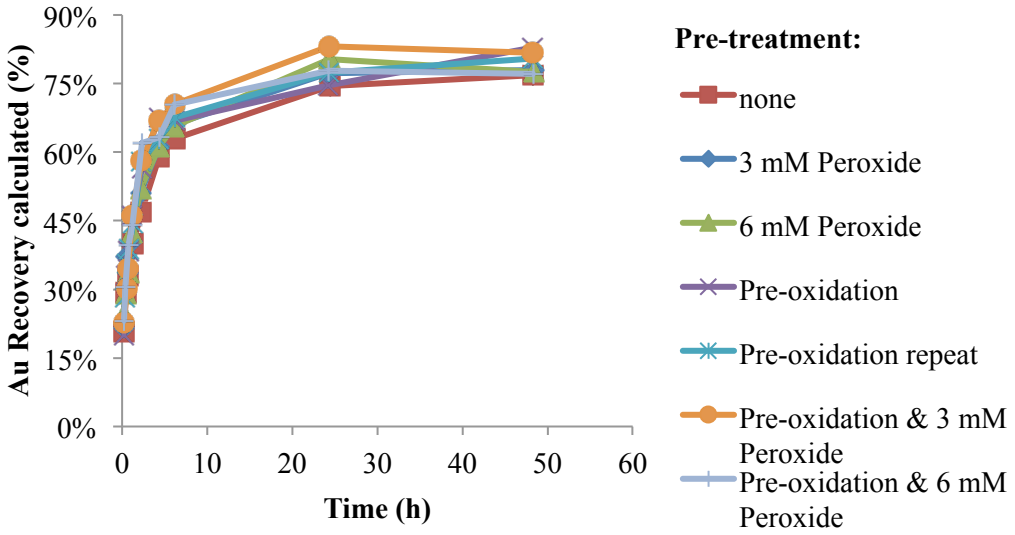

Figure 8-16: Au recoveries during leach tests on Ore B

Figure 8-17 presents the amount of Ag leached over the test duration for all tests on Ore B. Within the first six hours of each test the bulk of the Ag is leached, and a slower leach rate can be observed from there until the final sample. Three distinctive final recovery regions can be observed: one high, including the test with pre-oxidation, and pre-oxidation and 6 mM H_2O_2 at values around 16.3 mg/L Ag, one low for the pre-oxidation repeat test at 12.4 mg/L Ag and a middle region where all

other tests are located around 15.2 mg/L Ag. Apart from the pre-oxidation test this data appears disconnected from the gold recoveries observed.

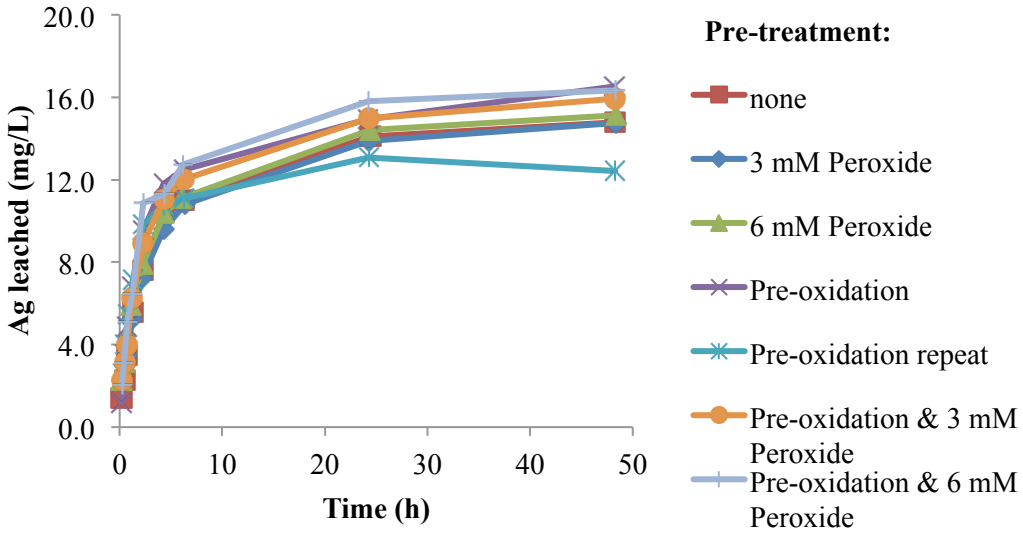

Figure 8-17: Ag leached during leach tests on Ore B

The Cu leached during the leach tests on Ore B is plotted in Figure 8-18. Similar to the Au and Ag curves, approximately two thirds of the final Cu amount leached, is leached during the first six hours of each test. Then a slowing in the leach speed occurs. The final Cu amounts leached range between 250 and 273 mg/L. No clear benefit of any pre-treatment can be determined.

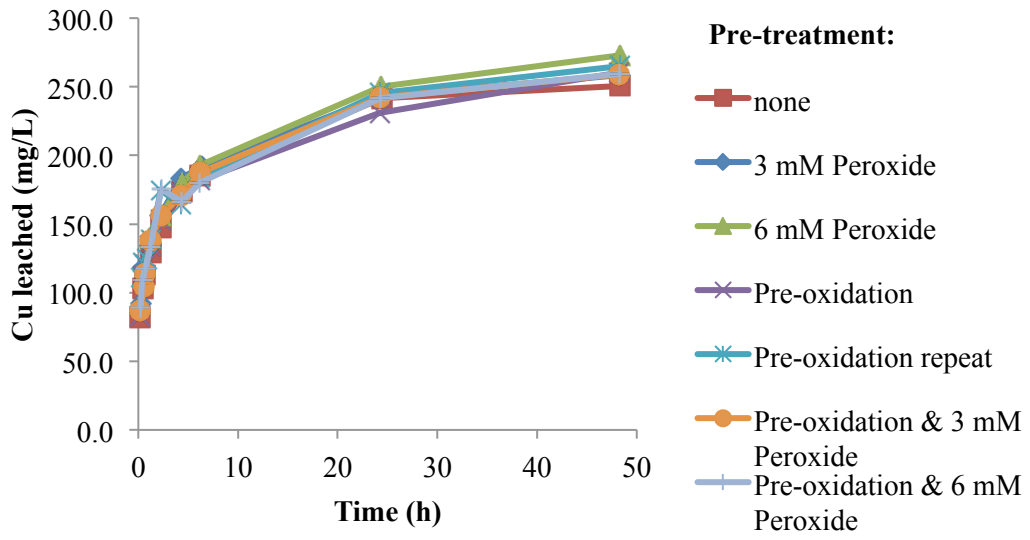

Figure 8-18: Cu leached during leach tests on Ore B

Figure 8-19 gives the amount of Ni extracted in the leach tests on Ore B over time. Throughout the run time of the experiments no significant slowing in the Ni leaching can be observed for any of the tests, except for the pre-oxidation repeat test. The pre-oxidation repeat test leaching of Ni comes to a near standstill from the 24 hour mark onwards. Three different final Ni leached regions can be observed: the first is at 35.7 mg/L Ni for the test with no pre-treatment, the second at 20.2 mg/L for the pre-oxidation repeat test and the third for all other tests is around 33 mg/L. It can be noted, that any pre-treatment of the ore appears to marginally reduce the amount of Ni leached. However, the pre-oxidation repeat test result could only be explained by the reaction of the H_2SO_4 added prior to the leach with some Ni bearing mineral and resulting in the formation of a compound not soluble at high pH values and with cyanide.

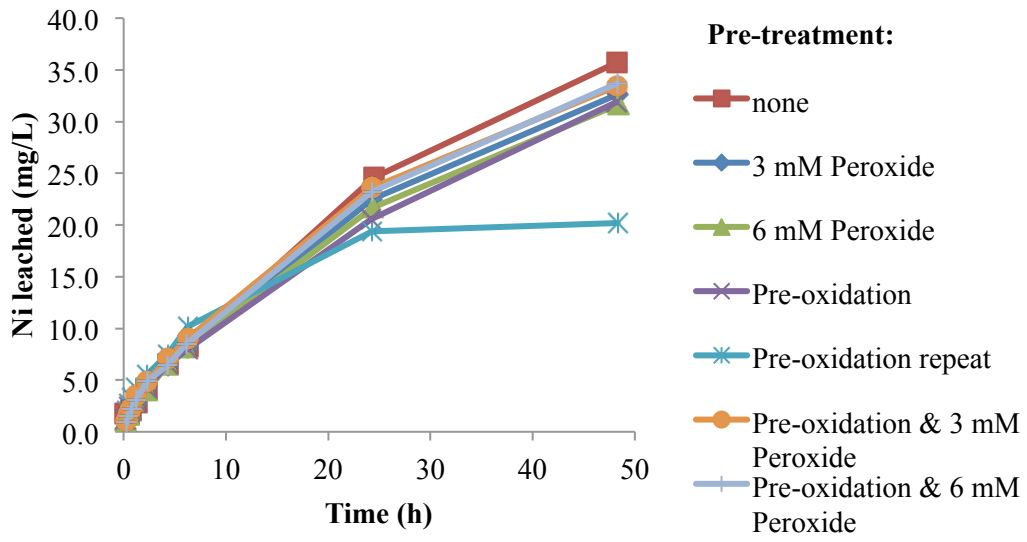

Figure 8-19: Ni leached during leach tests on Ore B

NaCN

The measured free cyanide concentrations, shown in NaCN equivalent, in solution during the leach tests on Ore B are shown in Figure 8-20. The majority of NaCN consumption from the initial calculated concentration of 25 mM occurs during the first six hours of the leach and then slows significantly on all tests. At the six and 24 hour mark, a separation between the NaCN levels in solution can be made. At the 24 hour mark the tests with pre-oxidation and 3 or 6 mM H_2O_2 addition, as well as the test with the 6 mM H_2O_2 addition appear to have a lower cyanide requirement compared to the other tests with a concentration difference around 2.5 mM noticeable. The final NaCN concentrations of all tests range between 2.3 and 3.4 mM, and no clear benefits of any given pre-treatment can be distinguished.

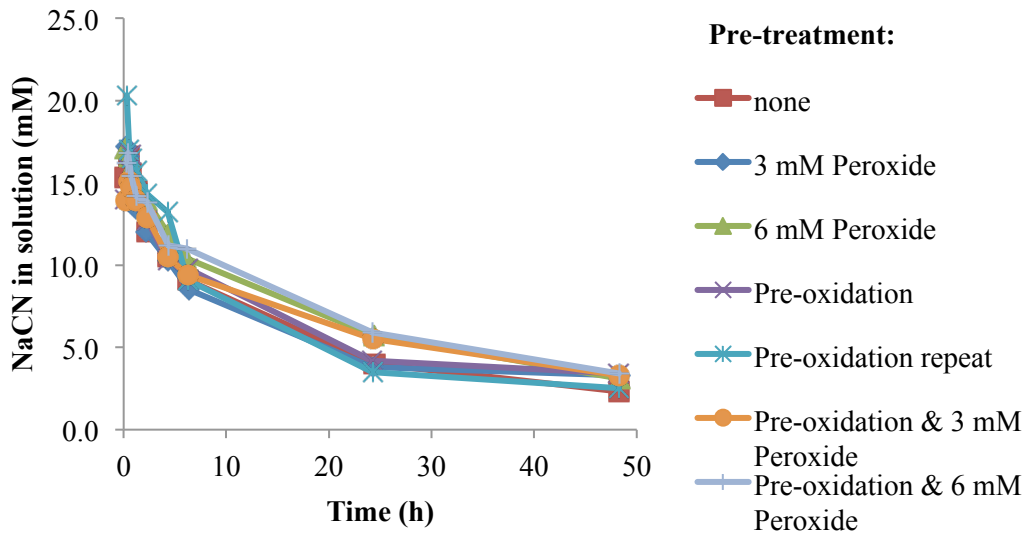

Figure 8-20: NaCN in solution during the leach tests on Ore B

DO

The dissolved oxygen levels in the slurries during the leach tests on Ore B are displayed in Figure 8-21. It can be seen, that the measured DO values vary even within the regions assumed to be more stable (24 hours onwards). This might be due to measurement error, as DO readings were not measured with ideal agitation (see Section 8.4.2). The DO values measured prior to NaCN addition ranged between 0 (no pre-oxidation) and 12 ppm (pre-oxidation and 6 mM H_2O_2), with only pre-oxidation giving a DO of around 3 ppm. This indicates, that Ore B has significant amounts of oxygen consuming species, however, H_2O_2 is able to raise the DO levels past air saturation levels, possibly aided by catalysed H_2O_2 decomposition, as indicated in Section 2.2.1.

The initial DO readings, immediately after NaCN addition, vary between 0 ppm (no pre-treatment) and 3.4 ppm for both tests with 6 mM H_2O_2 additions. The tests with only pre-oxidation show values around 0.5-1 ppm DO and both tests with 3 mM H_2O_2 additions had DO values around 1.5-2 ppm. This indicates, that no pre-treatment or only pre-oxidation are not sufficient to supply enough oxygen into the slurry for adequate gold leaching kinetics. By the six hour mark all tests have reached DO levels between 6.3 and 7.4 ppm, which is close to oxygen saturation for air sparged solutions near sea level (Lorösch, 2001). Over the residual time of the

tests, a slight increase in DO levels to final values between 7.4 and 8.3 ppm can be observed. The lowest final value can be observed for the test with no pre-treatment. This suggests, that the pre-treatments tested help to reduce the oxygen uptake of Ore B to a small degree, and that with ongoing oxygenation more oxygen consumers become passive.

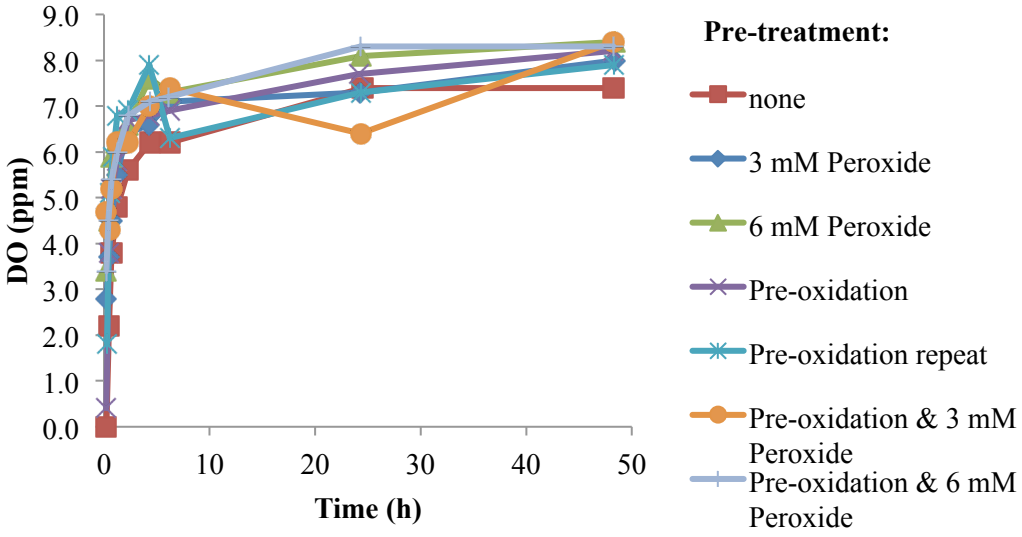

Figure 8-21: Slurry DO measured during the leach tests on Ore B

pH

The slurry pH measured over time for the tests conducted on Ore B is plotted in Figure 8-22. All tests with pre-oxidation show a pH of 11.2, immediately after the NaCN addition, except for the pre-oxidation repeat, which did show a pH of 10.5, due to the addition of the wrong volume of 1 M NaOH solution. The tests without pre-oxidation have a pH of 11.6, immediately after the NaCN addition. This difference in pH could be due to the oxidation of sulphide minerals, namely pyrite, which makes up ~20% of Ore B, as shown in Section 8.6.1. Pyrite is known to release H^+ ions, when oxidised (Blodau, 2006). It is further known, that pyrite oxidation will come to a near standstill, once cyanide is present in solution (PL Breuer, Hewitt, & Meakin, 2008). This would explain, why the tests without pre-oxidation present a higher pH immediately after NaCN addition. In all tests the pH slowly decreases during the test duration time, with final pH values for all tests of

9.5±0.1. The only exception is the pre-oxidation repeat test, which shows a step increase in pH at the six hour mark, when the missing NaOH was added. The final pH of the pre-oxidation repeat test is pH 10.

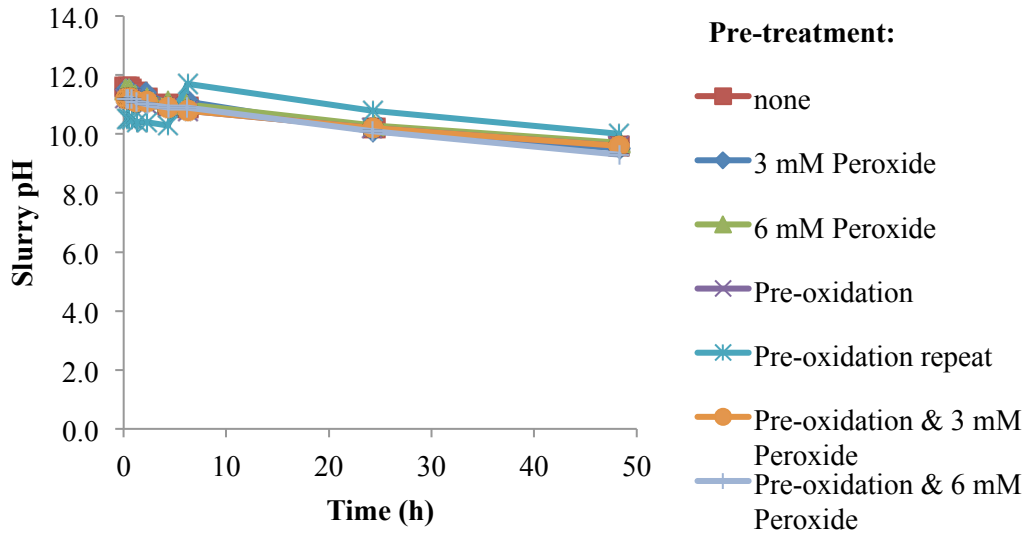

Figure 8-22: Slurry pH during leach tests on Ore B

Sulphur species

No S^{2-} ions were detected in any of the solutions analysed during the test work on Ore B, indicating a slow release and immediate oxidation of these ions.

Figure 8-23 shows the SCN^- ion concentration in solution over time for all leach tests conducted on Ore B. The first data point after NaCN addition is equal to the SCN^- ion concentration in solution immediately prior to the NaCN addition. The initial SCN^- ion concentration is due to the ore supplied being a flotation concentrate, which was dried without prior washing. As process water is reused in the plant, SCN^- ions were present in the water at this stage of the process. This value was in the range of 0.80±0.07 mM for all tests. Up to the six hour mark the majority of SCN^- ions were formed in solution, with the values observed ranging around 3.6±0.15 mM for all tests. The only exemption is the test with a 3 mM H_2O_2 addition showing a SCN^- ion concentration of 4.36 mM at the six hour mark, which could be an outliner. After the six hour mark, a further, slower incline in SCN^- ion concentrations in solution

can be observed for most tests, with final values ranging between 3.72 and 4.96 mM. The highest final SCN^- concentration was observed for the test with 6 mM H_2O_2 addition upfront, and the lowest for the 3 mM addition. Further, the tests with pre-oxidation show lower SCN^- ion concentrations compared to the tests without pre-oxidation, be it with or without H_2O_2 addition.

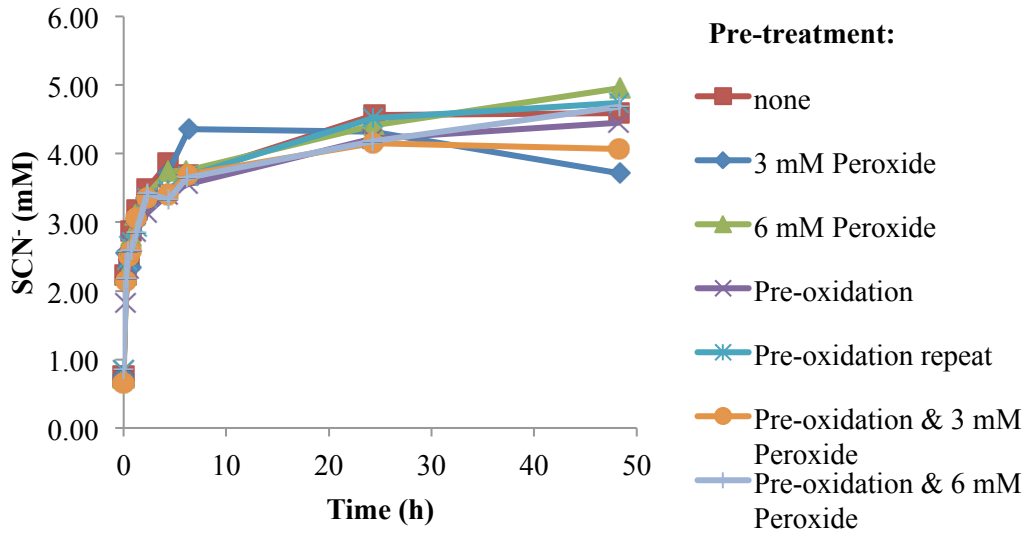

Figure 8-23: SCN^- ions measured in solution during the leach tests on Ore B

In Figure 8-24, the $S_2O_3^{2-}$ ion concentrations determined during the leach tests on Ore B are plotted against time. The concentrations observed immediately prior to the NaCN addition can be split into two groups with different concentrations: the first group without pre-oxidation at a measured concentration of 1.15±0.01 mM; the second group including all pre-oxidation tests with a concentration of 1.69±0.12 mM. This indicates that pre-oxidation causes the release and oxidation of sulphur ions from the ore. Immediately after the NaCN addition (the first values shown in the graph) the $S_2O_3^{2-}$ concentration in solution decreased by ~0.3 mM for each test. This can be explained by the formation of SCN^- ions, as supported by literature and also findings in a previous chapter (see Sections 2.4.2 and 6.4.4). After this initial drop, the $S_2O_3^{2-}$ ion concentration starts increasing again at a fast rate up to the six hour mark. Then the concentration increase starts to slow, and two tests even show a decrease between the 24 and 48 hour marks (both tests with 3 mM H_2O_2

addition, regardless of pre-oxidation). The final concentrations of $S_2O_3^{2-}$ ions in solution vary greatly, but indicate a trend of tests with pre-oxidation ending at higher values, when compared to the tests without pre-oxidation treatment. It appears, that the formation of $S_2O_3^{2-}$ and its subsequent reactions is a very complex process for this ore, which can be greatly influenced by pre-treatment with means of pre-oxidation and H_2O_2. However, there appears to be a requirement for a certain H_2O_2 concentration that is neither too high nor too low to achieve the best results (lowest $S_2O_3^{2-}$ concentration), when using H_2O_2.

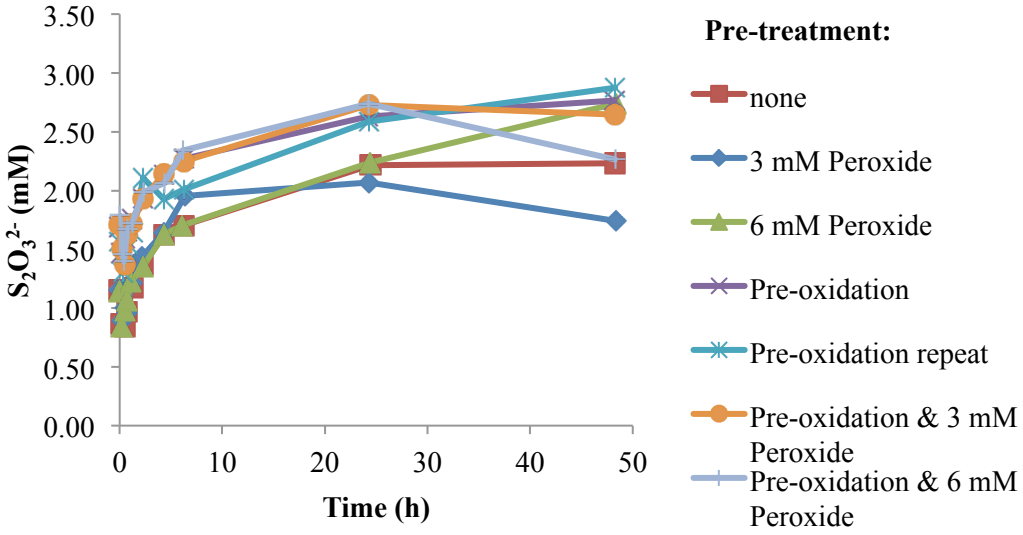

Figure 8-24: $S_2O_3^{2-}$ ions measured in solution during the leach tests on Ore B

The SO_4^{2-} ion concentration curves for all leach tests on Ore B are shown in Figure 8-25. The initial SO_4^{2-} ion solution concentrations, prior to NaCN addition (not shown) range between 40 and 48 mM, with no correlation between pre-treatment and concentration notable. This indicates, that the ore already contained significant amounts of oxidised sulphur species, prior to re-pulping for the tests. It can be seen, that apart from initial movements in the concentration (might be caused by detection issues), that all tests show near constant SO_4^{2-} concentration during the whole test time, or only minor increases from the initial value. This might be caused by the high amount of calcium present in the ore, causing the SO_4^{2-} to form gypsum and precipitate, hence being lost for detection in solution analysis. The pre-oxidation

repeat test is an outliner, showing higher SO_4^{2-} concentrations, most likely caused by the initial H_2SO_4 addition.

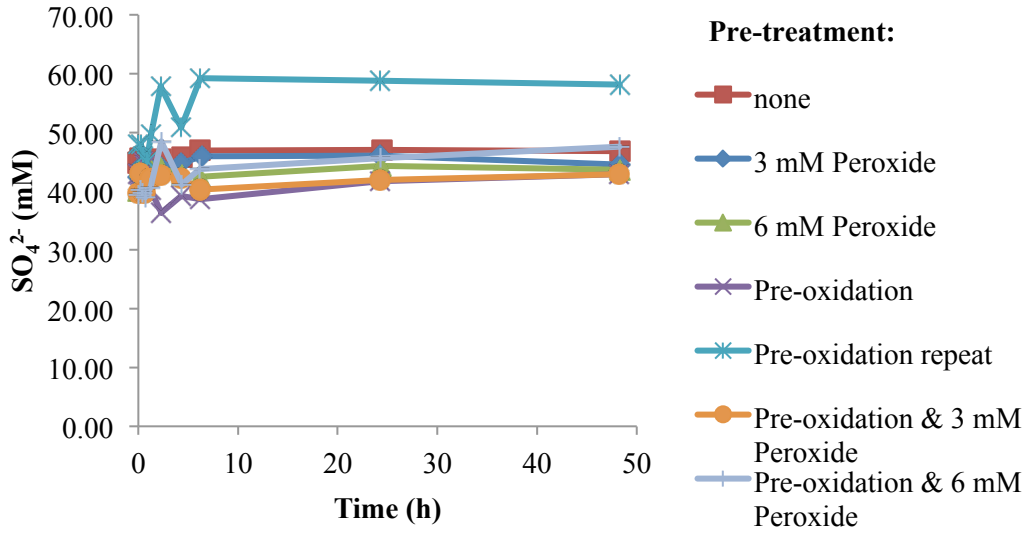

Figure 8-25: SO_4^{2-} ions measured in solution during the leach tests on Ore B

Summary

Ore B shows some signs (Au recovery, changes in sulphide species concentrations, initial DO values, and initial NaCN consumption) of susceptibility to pre-treatment by means of pre-oxidation, H_2O_2 addition, or combined pre-treatment. However, the data gathered cannot be interpreted to give a statistically sound outcome. Hence the standard methodology selected does not offer sufficient information on possible benefits or effects of H_2O_2 addition to the leach. It is further noted, that when comparing the results of this testwork to typical plant data obtained from site on the reactivity of the ore, indicated by typical recoveries, and solution chemistry (sample donor, 2015), it becomes evident that for leach test work investigating the impact of pre-treatment the sample taking, shipping and preparation are crucial factors, which can impact results significantly.

8.6.4 Ore C

8.6.4.1 Leach experiments

This section presents and interprets the data gathered during the comparative leach experiments on Ore C, where all factors were targeted to be exactly the same, apart from the four different pre-treatments.

Metals in solution

With the data gathered during the leach experiments on Ore C Au recovery curves were calculated. The calculations were made from Au concentration in solution, and the tails assay, creating 'calculated head grades'. These are shown in Table 8-8. It should be noted, that the calculated head grades determined were all between 1.62 and 1.82 g/t Au. The determined head grade by fire assay was 1.86±0.00 g/t (error based on variance in duplicate assay results). The comparison of calculated and measured head grade could indicate a high variability in gold content throughout the ore and a significant absolute analytical error (greatest absolute deviation equals 12.9%, which will mean the error in recovery calculation might be the same). Highly variable tail assay concentrations were obtained for the majority of the 25 g samples. Repeat analysis of 50 g samples resulted in more consistent duplicate results, however, it can still be assumed, that this material contains a large range of gold particle sizes and an uneven particle distribution.

Table 8-8: Measured and calculated head grades of Ore A

Test	Au in solution (mg/L)	Au in solids (g/t)	Head grade (g/t)
Fire assay	-	-	1.86±0.00
No pre-treatment	0.96	0.38	1.82
Pre-oxidation	0.86	0.33	1.62
3 mM H_2O_2	0.86	0.36	1.65
Pre-oxidation and 3 mM H_2O_2	0.86	0.35	1.64

The Au recovery curves calculated from the data gathered during the leach tests conducted on Ore C are plotted in Figure 8-26. During the initial two hours of the leach, a notable difference in Au leaching rates is visible. The slowest rates are displayed by the test with no pre-treatment, and the fastest for the test with pre-oxidation and H_2O_2 addition. However, the final recoveries are closely aligned: 79.1% (no pretreatment), 78.3% (3 mM H_2O_2), 79.6% (pre-oxidation) and 78.9% (pre-oxidation and 3 mM H_2O_2). These relatively close recovery levels cannot be used as an indication if a clear benefit of any pre-treatment, considering the deviation in total gold content in each experimental run.

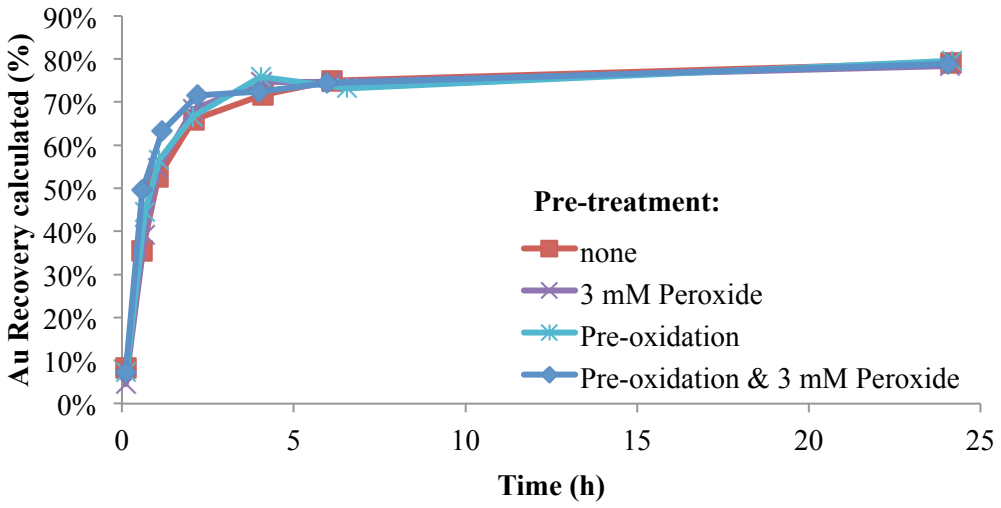

Figure 8-26: Au recovery curves during leach tests on Ore C

Figure 8-27 presents the Ag leached during the tests conducted on Ore C. All curves show a peak around 0.6 mg/L Ag in solution at the six hour mark, to then decrease again to only around 0.2-0.3 mg/L. When compared to the head assay of this ore, showing an Ag content of ~130 g/t, this is a very low recovery. This is most likely caused by non-gold associated silver mineralisation, not soluble by cyanide as well as Ag precipitation or adsorption in the ore material. The highest observed final Ag concentrations measured in solution are for the tests with only pre-oxidation, and no pre-treatment, similar to the Au recoveries observed.

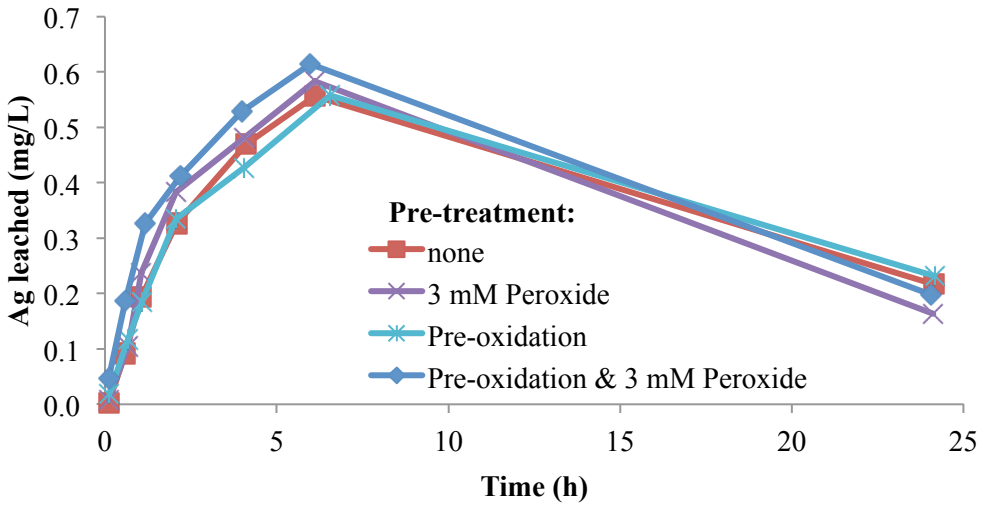

Figure 8-27: Ag leached during leach tests on Ore C

The amount of Cu leached during the tests on Ore C is plotted in Figure 8-28. A rapid initial leach (first few minutes between NaCN addition and the first sample being taken) can be observed for all tests. This is followed by a gradual slowing in the extraction speed. The final amounts of Cu leached are around 310 mg/L, with the pre-oxidation and H_2O_2 addition test achieving the highest value of 317 mg/L. This is followed by the H_2O_2 addition with 312 mg/L Cu leached, then the pre-oxidation test with 311 mg/L, and no pre-treatment with 304 mg/L. This reflects Cu recoveries of around 33%, when compared to the head assay of ~1470 g/t Cu. In an industrial

cyanidation plant application reduced Cu recoveries are beneficial, due to reduced CN^- consumption.

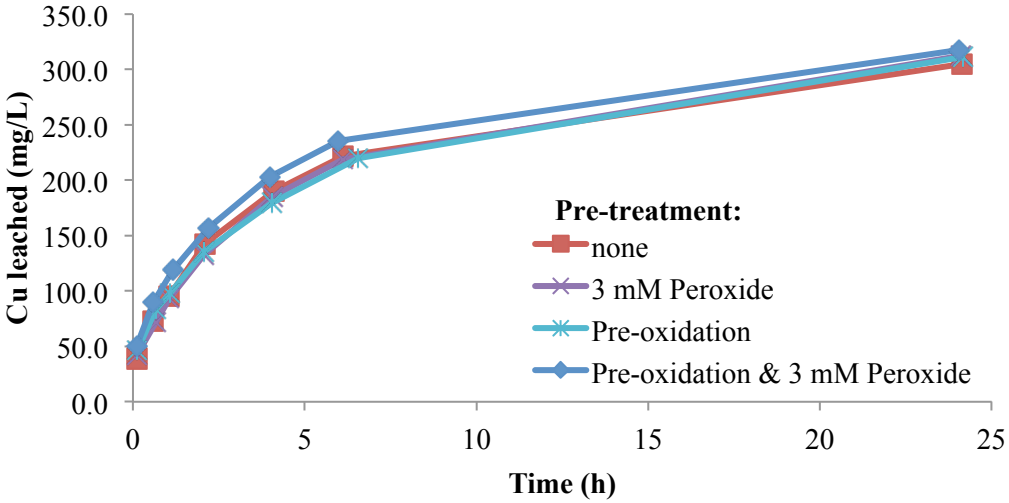

Figure 8-28: Cu leached during leach tests on Ore C

The amount of Ni leached during the tests on Ore C is shown in Figure 8-29. Two distinctive leach rate regions can be observed for all tests – one before and one after the six hour mark. The first region exhibits a near linear, faster leach rate, the second one a slower leach rate, however, due to the lack of sampling points no statement on curvature can be made. The final amounts of Ni leached are 3.8 mg/L (pre-oxidation and H_2O_2), 3.9 mg/L (pre-oxidation), 4.0 mg/L (no pre-treatment) and 4.0 mg/L (3 mM H_2O_2). These amounts only represent a fraction of the Ni (~160 g/t) present in Ore C, as determined in the elemental assay. Due to the small amount of ore used for each test no firm statement on the benefit of any pre-treatment can be made. However, it is notable, that the pre-oxidation treatments appear to reduce the formation of Ni-cyanide complexes, which is considered beneficial in a gold leaching plant.

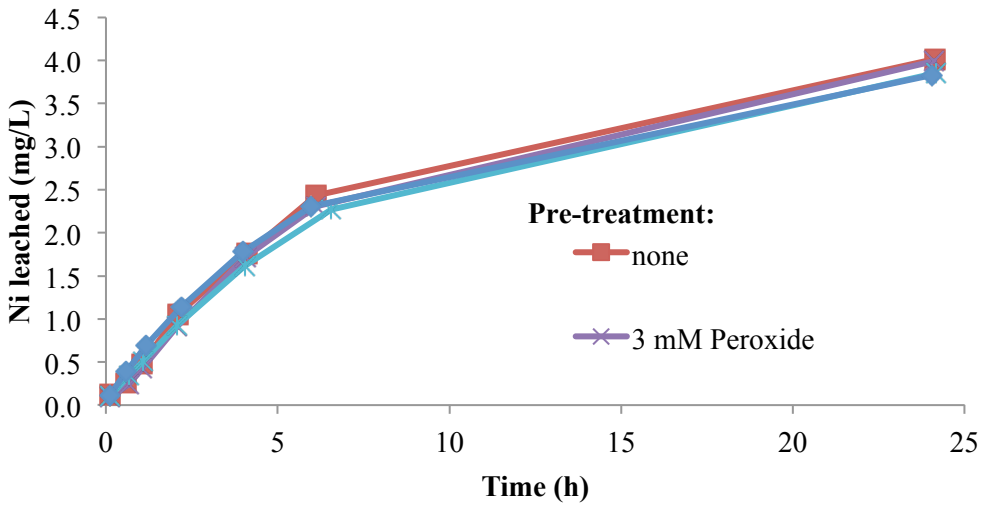

Figure 8-29: Ni leached during leach tests on Ore C

NaCN

The developments of the free cyanide concentration, shown as NaCN equivalent, in the solutions after the addition to 20 mM concentration in each test are shown in Figure 8-30. It is notable that the majority of NaCN in each test is consumed by the six hour mark. Of further interest is, that by the six hour mark varying NaCN concentrations in solution can be observed. In ascending order from the lowest to the highest residual concentration at the six hour mark are the tests with pre-oxidation and 3 mM H_2O_2, 3 mM H_2O_2, pre-oxidation, and no pre-treatment. This order and spread in concentrations is not reflected in the final NaCN concentrations measured in solution at the 24 hour mark, where all tests show a NaCN concentration in solution of 2.5±0.3 mM. This indicates, that throughout the whole run time sufficient NaCN was available in all tests. It can be concluded, that the tests with more oxygen available exhibit a faster initial reaction, which could lead to reduced leach times in an industrial plant.

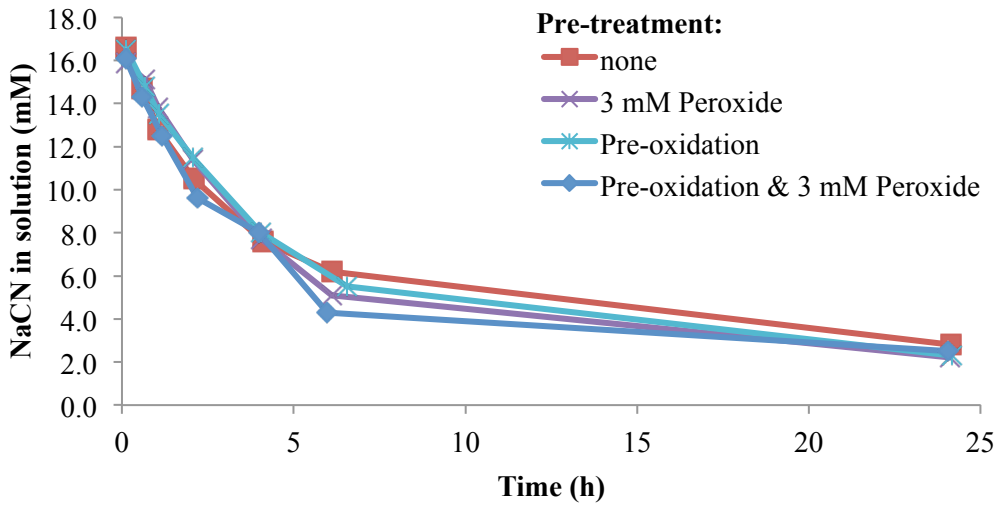

Figure 8-30: NaCN in solution during leach tests on Ore C

DO

The DO levels in the slurry immediately prior to the NaCN addition on the tests conducted on Ore C are as follows: 6.6 ppm (no pre-treatment), 19.0 ppm (3 mM H_2O_2), 18.8 ppm (pre-oxidation) and above detection limit (pre-oxidation and 3 mM H_2O_2). The development of the DO after the NaCN addition for all tests is shown in Figure 8-31. A lot of data points are not shown in the graph due to readings over the detection limit of the apparatus used, which in turn results in broken lines in the figure. The lower DO levels in the final samples with pre-oxidation, and pre-oxidation and 3 mM H_2O_2 might be caused by delays in measuring the DO in the slurry when sampling and degassing of these during the delays. Also, some issues occurred with an oxygen pressure loss during the later stages of the pre-oxidation leaches. However, the DO concentrations measured were still considered high enough and no evidence of hindered leaching was observed when analysing the metals in solution. The major notable difference between all tests shown is the DO immediately after the NaCN addition and its development during the first two hours of the tests. The test with no pre-treatment shows an initial DO of 3.5 ppm, which then rises beyond detection limit. The 3 mM H_2O_2 addition yields an initial DO of 6.6 ppm and again rises beyond the detection limit after the two hour mark. The pre-oxidation test has an initial DO of 15.6 ppm, and the test with pre-oxidation and 3

mM H_2O_2 is beyond detection limit. It can be assumed, that sufficient DO was available for leaching during all tests conducted on Ore C. Further, pre-oxidation appears to have a significant positive impact on the DO available during the first hour of leaching.

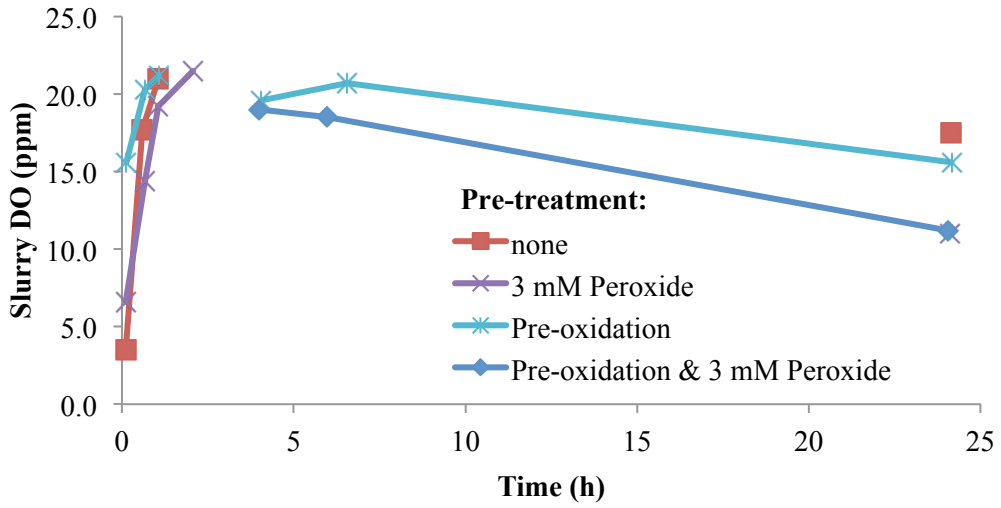

Figure 8-31: Slurry DO during leach tests on Ore C

pH

Figure 8-32 presents the pH measured in all leach test slurries of Ore C. From the initial pH values around pH 11.7, immediately after the NaCN addition, the majority of the pH value decrease observable takes places during the first hour of leaching. In all tests the final pH of 11.2 is reached by the 24 hour mark. This indicates little reactivity and alkalinity consumption of Ore C during the leach tests.

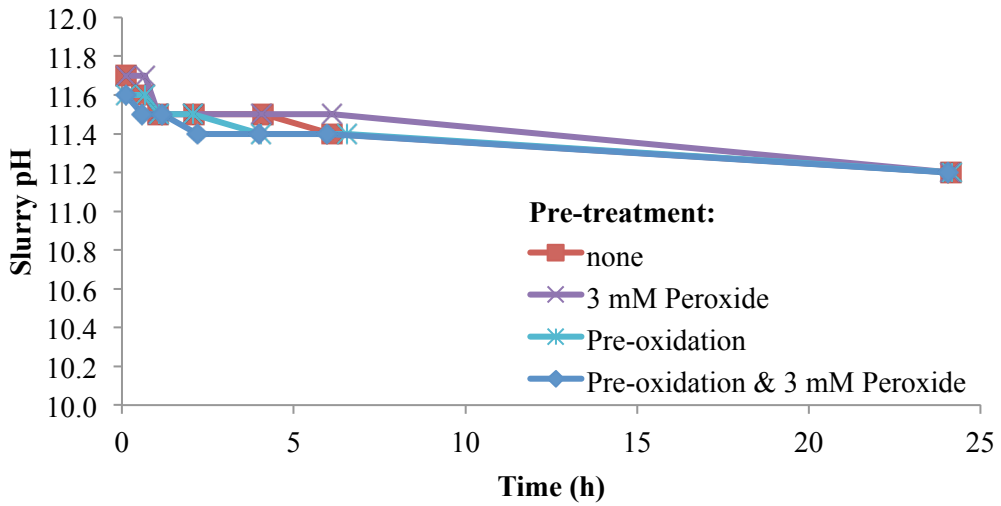

Figure 8-32: Slurry pH during leach tests on Ore C

Sulphur Species

During the leach tests conducted on Ore C no S^{2-} ions could be detected in the solutions.

Prior to the NaCN addition, the SCN^- ion concentration for all tests on Ore C was approximately 0.5 mM. The increase in SCN^- ions in the solutions for all tests is presented Figure 8-33. The initial SCN^- ion concentration shown in the graph after NaCN addition matches the ones prior (not shown in graph) to NaCN addition for all tests. Then a sharp rise in the SCN^- ion concentration can be observed over the first two hours, identical on all tests. The increase in concentration then slows and continues at a slower rate up to the final value, again, identical for all tests, of 3.7 mM. The reduced NaCN levels, as shown in Figure 8-30, cause the decrease in SCN^- ion formation. It can be concluded, that the pre-treatments investigated on Ore C do not impact the formation SCN^- ions.

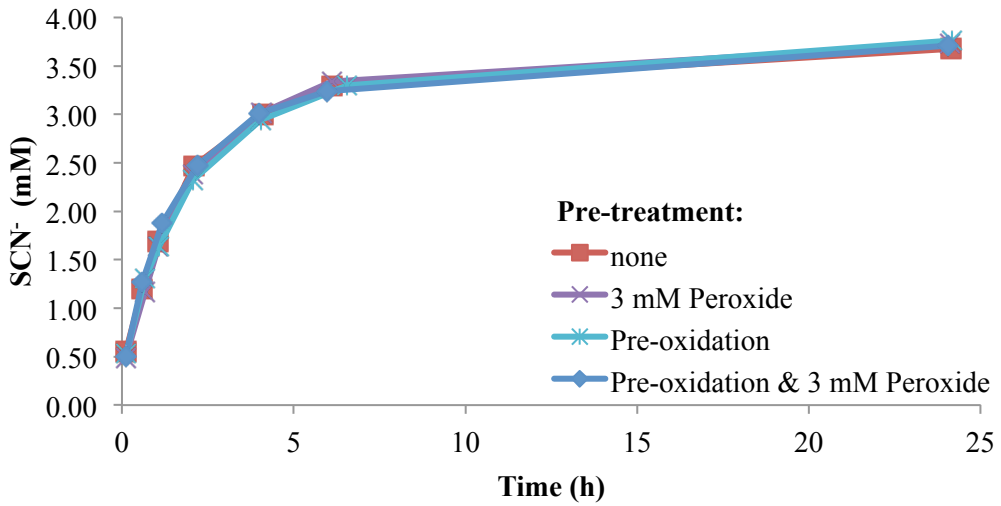

Figure 8-33: SCN^- ion concentration in solution during leach tests on Ore C

The $S_2O_3^{2-}$ ion concentrations measured in solution on all leach tests conducted on Ore C immediately prior the NaCN addition are 0.3 mM for both tests without pre-oxidation and 0.5 mM for both tests with pre-oxidation. This suggests, that some mineral is oxidised by the gaseous oxygen in solution, but that the H_2O_2 additions do not have an impact on it, when no NaCN is present. Figure 8-34 shows the $S_2O_3^{2-}$ ion concentration development for all tests once NaCN was present in solution. The two different $S_2O_3^{2-}$ concentration groups already observed prior to the NaCN addition can be noted at the zero hour mark. After a faster initial increase in the $S_2O_3^{2-}$ ion concentration up to the six hour mark, the further increase during the remainder of the test is slower. It can also be noted, that the further increase in concentration between the six and 24 hour mark occurs in near parallel for all tests. The final $S_2O_3^{2-}$ ion concentrations measured in solution suggest, that the pre-oxidation of this ore will cause an increase in $S_2O_3^{2-}$ ion concentration. It can also be concluded, when a 3 mM H_2O_2 pre-treatment was made, that the initial increase (first six hours) of $S_2O_3^{2-}$ ions in solution after the NaCN addition is marginally slower than without. This can be seen for both scenarios, with and without pre-oxidation, just at different levels. However, overall, the impact of pre-treatment on the appearance of $S_2O_3^{2-}$ ions can only be considered marginal, as the difference in final solution concentration is only 0.5 mM.

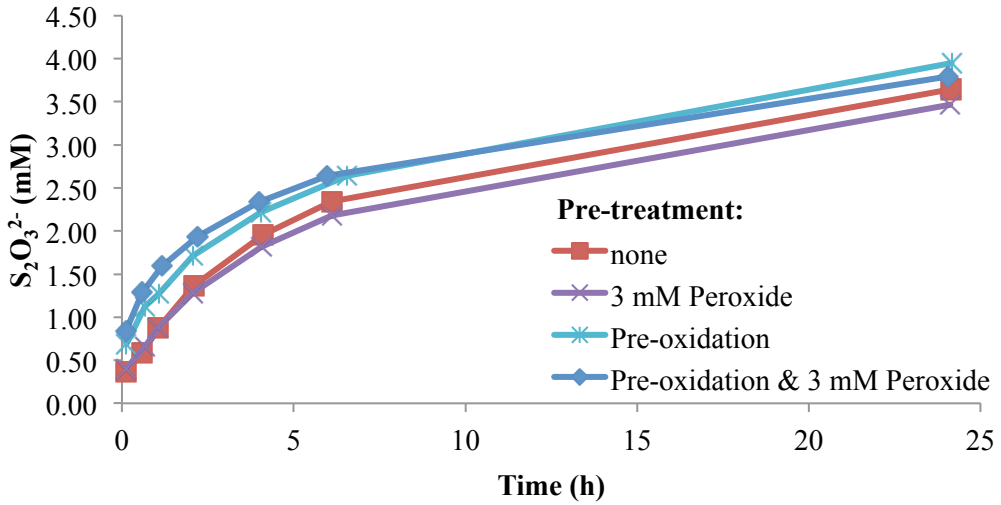

Figure 8-34: $S_2O_3^{2-}$ ion concentration in solution during leach tests on Ore C

The SO_4^{2-} ion concentrations of the leach tests on Ore C, immediately prior to NaCN addition are 1.8 mM (no pre-treatment), 1.6 mM (3 mM H_2O_2), 2.7 mM (pre-oxidation) and 2.3 mM (pre-oxidation and 3 mM H_2O_2). No explanation for the lower SO_4^{2-} ion concentration with only H_2O_2 addition can be made, as it was found, that H_2O_2 usually oxidises other sulphur species to SO_4^{2-} (see Section 2.4.2). Figure 8-35 presents the SO_4^{2-} ion concentration in solution during the leach tests on Ore C, once the NaCN was added. Due to an unknown species reporting close to the SO_4^{2-} ions, when analysing with the HPLC, some error might be present in the data. Also, the formation of gypsum due to calcium in the ore and gypsum (low solubility) already present may result in these readings. The main observation, which can be made in the graph, is that the SO_4^{2-} ion concentrations increase over all tests at a near parallel rate, which is expected due to only the oxygen gas offering a source of oxidant after the initial H_2O_2 additions are used up. It can further be seen, that the test with no pre-treatment shows the lowest final SO_4^{2-} ion concentration. The tests with the 3 mM H_2O_2 addition and pre-oxidation show similar final SO_4^{2-} ion concentrations and the highest concentration was measured for the test with pre-oxidation and 3 mM H_2O_2 addition. This can be explained by the sulphur species

release and oxidation during the pre-oxidation time. The more oxidant that is added, the more SO_4^{2-} that will be produced.

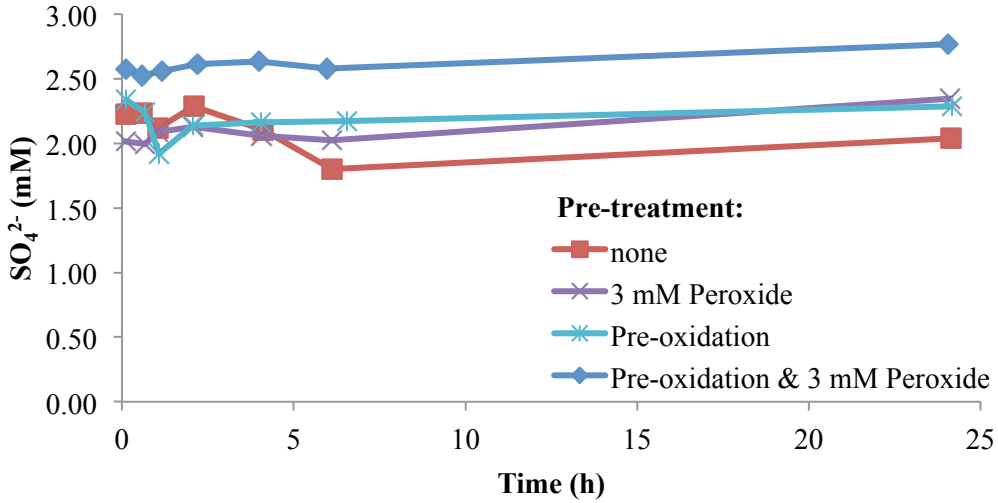

Figure 8-35: SO_4^{2-} ion concentration in solution during leach tests on Ore C

Summary

No significant differences in metal recoveries and amounts leached presented during the tests conducted on Ore C, especially in the light of the variability in tails grade being greater than the changes in recovery.

8.6.5 Conclusions

The ability to determine the impact of pre-treatments with H_2O_2, pre-oxidation, and combinations of the two in a simple, standard single test were evaluated on three industrial ores. As indicated in Section 8.6.1, Ore B was suspected to be most susceptible to the selected pre-treatments due to the presence of larger concentrations of pyrite and the possible benefits of galvanic coupling and the removal of sulphide ion passivation of the gold, as presented in sections 7.4.2. and 6.4.3 in pure solutions. The data gathered in this chapter does show the greatest variability in gold recovery with pre-treatments on Ore B, whereas the other ores showed lesser effects. The variability of natural substances found in ores makes determining interactions seen in

pure solutions difficult because of variation in samples, interferences of other elements and minerals and confounding of results. Hence, it could not be definitely shown that the pre-treatment on any of the ores lead to any of the suspected benefits. The normal method to overcome such variability of natural substances is to undertake large scale tests such as pilot plant or plant trials, unfortunately both beyond the resources of this project.

It is also evident, that transportation and preparation of the samples might have a significant impact on test outcomes and therefore will require careful consideration, when trying to establish the benefit of H_2O_2 in leach applications. It is also noteworthy, that the DO measured in the slurries during all tests was significantly higher, than typical DO values, which might be observed in industrial plants (see Section 2.4.1). This might mask a beneficial effect provided by the hydrogen peroxide.

Further, if the effectiveness of a pre-treatment for a site prior to site trials needs to be established, duplicate or triplicate testing of various pre-treatments with larger sample quantities is highly recommendable, so the error spread can be understood more accurately than in single tests. This was not done in this test work, due to the lack of sufficient sample quantity available for testing.

Chapter 9 Conclusions

The results presented throughout this thesis offer an extended and more detailed understanding on the impact that hydrogen peroxide has on cyanide leaching of gold. The influence of hydrogen peroxide on cyanide leaching of gold and silver surfaces in clean solutions as well as in the presence of sulphide ion contamination has been demonstrated. Further, the possible impact of selected sulphide minerals in galvanic interaction in the presence of hydrogen peroxide during cyanide leaching has been shown. An attempt at developing a simple test methodology to determine the susceptibility of an ore to hydrogen peroxide treatment was made.

The behaviour of electroplated gold/silver alloy during cyanide leaching in the presence of hydrogen peroxide was investigated and a model, for the conditions investigated, has been developed. Leach rate increases in the presence of hydrogen peroxide between ~120-185% in aerated solutions and up to ~200% in oxygenated solutions over solutions without hydrogen peroxide present were observed. If sufficient hydrogen peroxide and oxygen from either air or oxygen were available to reach cyanide limiting conditions a significant step change in OCP was observed.

This OCP jump was further investigated and lead to the discovery, that hydrogen peroxide reduces differently on a silver surface than on a gold surface. During cyanide limiting conditions gold will leach preferentially from a gold/silver alloy resulting in the exposure of a near 100% silver surface. However, this is only reproducible behaviour on freshly electro-plated gold. Leach rates obtained on electro-plated surface therefore cannot be translated onto non electroplated solid material. Further, solid gold/silver surfaces were discovered to develop a passive surface, mainly consisting of carbonates, when oxygen and cyanide limiting rates for the solution presented are of similar magnitude.

Hydrogen peroxide is a strong oxidant, which can fully oxidise sulphide ions at stoichiometric ratios of as low as 4:1 H_2O_2 : S^{2-}. Further, hydrogen peroxide has the ability to re-activate sulphide-poisoned gold surfaces to recover a leach rate equivalent to that of non-poisoned gold. During oxidation, the preferred oxidation

product of S^{2-} and $S_2O_3^{2-}$ ions in the presence of CN^- appears to be SCN^-. Depending on the addition time of the hydrogen peroxide this can be shifted, resulting in lower NaCN consumption for SCN^- generation, but instead generating more $S_2O_3^{2-}$ and SO_4^{2-}, when the hydrogen peroxide is added prior to the cyanide for cyanidation. The oxidation of $S_2O_3^{2-}$ to SO_4^{2-} by hydrogen peroxide or oxygen appears to be chemically limited and appears at the same rate in the presence or absence of CN^-. For industrial applications it might be preferred to target complete destruction of the unwanted sulphur species in solution prior to CN^- addition in order to reduce the CN^- consumption.

Many minerals are capable of partaking in the electrochemical reaction of cyanide leaching, as they are capable to act as an additional cathodic (oxygen reducing) surface. Depending on the kind of minerals, this ability can translate into increased leach rates, when the minerals are galvanically coupled with the gold. Hydrogen peroxide at low concentrations can further enhance the galvanic effect and increase leach rates, when there is sufficient free cyanide available to utilise the increased cathodic current for the anodic reaction. This benefit of the increased leach rate in galvanic coupling may not be seen in real ores, as the galvanic systems are significantly more complex and may only be intermittent during contact between separate particles.

The attempt to develop a time and cost efficient standardised test to establish an ore's susceptibility to hydrogen peroxide and pre-oxidation pre-treatment did not result in satisfying results. A standardised bottle roll test methodology, only using single tests, lacks analytical repeatability due to the inconsistent nature of ores. A further issue lies around the oversupply of oxygen in a laboratory test due to the significantly higher surface area to volume ratio. This possibly masks the negative effects of sulphidic ores to a level, that no clear benefit can be established. Additionally the sample taking, transport and preparation plays a major part in the results obtained in laboratory test work.

Scope of Future Works

Obviously this thesis has resulted in some recommendations for further work, particularly in the area of ore leaching and testing itself. As the results obtained during laboratory ore leach tests did not match the data seen on plants, it would be recommended to investigate the impact of sample taking, preparation for transport, laboratory preparation, and laboratory leach tests in greater detail to establish a more accurate representation of industrial site data, particularly for sulphide containing ores. The main detrimental factors are assumed to be representativeness of the sample and oxidation of the sample caused by the methods utilised. Factors, such as dry grinding and wet grinding, bottle geometry, bottle agitation and gas injection should be of particularly focus.

Chapter 10 References

Adam, B. (1989). *Einfluss des Oxidationsmittels auf den NaCN-Verbrauch bei der Goldlaugung sulfidischer Erze*. Degussa AG, Frankfurt/Germany. Internal Laboratory Report.

Aghamirian, M. M. (1997). *Reactivity of sulfide minerals and its effect on gold dissolution and its electrochemical behaviour in cyanide solution.* Queen's University at Kingston

Aghamirian, M. M., & Yen, W. T. (2005). Mechanisms of galvanic interactions between gold and sulfide minerals in cyanide solution. *Minerals Engineering, 18*(4), 393-407.

Anderson, M. J., & Whitcomb, P. J. (2005). *Response Surface Methods Simplified*: Productivity Press.

Awe, S. A., & Sandström, Å. (2010). Selective leaching of arsenic and antimony from a tetrahedrite rich complex sulphide concentrate using alkaline sulphide solution. *Minerals Engineering, 23*(15), 1227-1236.

Azizi, A., Petre, C. F., Olsen, C., & Larachi, F. (2010). Electrochemical behavior of gold cyanidation in the presence of a sulfide-rich industrial ore versus its major constitutive sulfide minerals. *Hydrometallurgy, 101*(3–4), 108-119.

Azizi, A., Petre, C. F., Olsen, C., & Larachi, F. (2011). Untangling galvanic and passivation phenomena induced by sulfide minerals on precious metal leaching using a new packed-bed electrochemical cyanidation reactor. *Hydrometallurgy, 107*(3–4), 101-111.

Bard, A. J. (1975). *Encyclopedia of Electrochemistry of the Elements*: Dekker.

Bard, A. J., & Faulkner, L. R. (1980). *Electrochemical Methods; Fundamentals and Applications*. New York: John Wiley & Sons.

Bayat, O., Vapur, H., Akyol, F., & Poole, C. (2003). Effects of oxidising agents on dissolution of Gumuskoy silver ore in cyanide solution. *Minerals Engineering, 16*(4), 395-398.

Biegler, T., Rand, D. A. J., & Woods, R. (1975). Oxygen reduction on sulphide minerals: Part I. Kinetics and mechanism at rotated pyrite electrodes. *Journal of Electroanalytical Chemistry and Interfacial Electrochemistry, 60*(2), 151-162.

Biesinger, M. C. (2013a). X-ray Photoelectron Spectroscopy (XPS) Reference Pages: carbon. Retrieved 11.08.2014, from http://www.xpsfitting.com/search/label/carbon

Biesinger, M. C. (2013b). X-ray Photoelectron Spectroscopy (XPS) Reference Pages: Oxygen. Retrieved 11.08.2014, from http://www.xpsfitting.com/search/label/Oxygen

Biesinger, M. C. (2013c). X-ray Photoelectron Spectroscopy (XPS) Reference Pages: Silver. Retrieved 11.08.2014, from http://www.xpsfitting.com/2013/04/silver.html

Blodau, C. (2006). A review of acidity generation and consumption in acidic coal mine lakes and their watersheds. *Science of The Total Environment, 369*(1–3), 307-332.

Bodlaender, G. (1896). Die Chemie des Cyanidverfahrens. *Angewandte Chemie, 9*(19), 583-587.

Breuer, P., Personal communication, 2016.

Breuer, P., Hewitt, D., & Meakin, R. (2008). *Does pre-oxidation or lead (II) addition reduce the impact of iron sulfides in cyanidation?* Paper presented at the Hydrometallurgy 2008: Proceedings of the Sixth International Symposium.

Breuer, P. L., Jeffrey, M. I., & Hewitt, D. M. (2008). Mechanisms of sulfide ion oxidation during cyanidation. Part I: The effect of lead (II) ions. *Minerals Engineering, 21*(8), 579-586.

Caldeira, C. L., Ciminelli, V. S. T., Dias, A., & Osseo-Asare, K. (2003). Pyrite oxidation in alkaline solutions: nature of the product layer. *International Journal of Mineral Processing, 72*(1–4), 373-386.

Cathro, K. J., & Koch, D. F. A. (1964). The Anodic Dissolution of Gold in Cyanide Solutions. *Journal of The Electrochemical Society, 111*(12), 1416-1420.

Cerovic, K., Hutchison, H., & Sandenbergh, R. F. (2005). Kinetics of gold and a gold-10% silver alloy dissolution in aqueous cyanide in the presence of lead. *Minerals Engineering, 18*(6), 585-590.

Choi, Y., Baron, J. Y., Wang, Q., Langhans, J., & Kondos, P. (2013). Thiosulfate Processing - From Lab Curiosity to Commercial Application*World Gold 2013*, *held in Brisbane,* (pp. 45-51). AusIMM.

Dai, X., & Breuer, P. L. (2013). Leaching and electrochemistry of gold, silver and gold-silver alloys in cyanide solutions: Effect of oxidant and lead(II) ions. *Hydrometallurgy, 133*, 139-148.

de Andrade Lima, L. R. P., & Hodouin, D. (2006). Analysis of the gold recovery profile through a cyanidation plant. *International Journal of Mineral Processing, 80*(1), 15-26.

Department of Foreign Affairs and Trade. (2016). *Composition of Trade Australia 2015*. Australia: DFAT.

Deschênes, G., & Ghali, E. (1988). Leaching of gold from a chalcopyrite concentrate by thiourea. *Hydrometallurgy, 20*(2), 179-202.

Deschênes, G., & Prud'homme, P. J. H. (1997). Cyanidation of a copper-gold ore. *International Journal of Mineral Processing, 50*(3), 127-141.

Deschênes, G., Rousseau, M., Tardif, J., & Prud'homme, P. J. H. (1998). Effect of the composition of some sulphide minerals on cyanidation and use of lead nitrate and oxygen to alleviate their impact. *Hydrometallurgy, 50*(3), 205-221.

Deschênes, G., & Wallingford, G. (1995). Effect of oxygen and lead nitrate on the cyanidation of a sulphide bearing gold ore. *Minerals Engineering, 8*(8), 923-931.

Descostes, M., Beaucaire, C., Mercier, F., Savoye, S., Sow, J., & Zuddas, P. (2002). Effect of carbonate ions on pyrite (FeS2) dissolution. *Bulletin de la Societe Geologique de France, 173*(3), 265-270.

Dimitrijevic, M., Antonijevic, M. M., & Dimitrijevic, V. (1999). Investigation of the kinetics of pyrite oxidation by hydrogen peroxide in hydrochloric acid solutions. *Minerals Engineering, 12*(2), 165-174.

Douglas, B. E., Alexander, J. J., & McDaniel, D. H. (1997). *Concepts and Models of Inorganic Chemistry*: John Wiley & Sons Canada, Limited.

Eksteen, J. (2015). Novel and environmentally benign processing options for low grade polymetallic base-precious metals ores*World Gold 2015*, *held in Misty Hills, Gauteng, South Africa*: The Southern African Institute of Mining and Metallurgy.

Elsner, L. (1846). Beobachtungen über das Verhalten regulinischer Metalle in einer wässrigen Lösung von Cyankalium. *Journal für Praktische Chemie, 37*(1), 441-446.

Eremenko, A., Korduban, A., Gnatiuk, I., Vityuk, N., Smirnova, N., Linnik, O., & Mukha, Y. (2011). *Silver and Gold Nanoparticles on Sol-Gel TiO2, ZrO2, SiO2 Surfaces: Optical Spectra, Photocatalytic Activity, Bactericide Properties*: INTECH Open Access Publisher.

Finkelstein, N. P. (1972). The chemistry of the extraction of gold from its ores. In R. J. Adamson (Ed.), *Gold Metallurgy in South Africa* (pp. 308-312). Cape Town: Cape & Transvaal Printers Ltd.

Fleming, C. A. (1992). Hydrometallurgy of precious metals recovery. *Hydrometallurgy, 30*(1–3), 127-162.

Gabe, D., & Walsh, F. (1983). The rotating cylinder electrode: a review of development. *Journal of Applied Electrochemistry, 13*(1), 3-21.

Gerlache, M., Senturk, Z., Quarin, G., & Kauffmann, J. M. (1997). Electrochemical behavior of H2O2 on gold. *Electroanalysis, 9*(14), 1088-1092.

Gorain, B., Kondos, P. D., & Lakshmanan, V. (2016). Innovations in Gold and Silver Processing *Innovative Process Development in Metallurgical Industry* (pp. 393-428): Springer.

Green, D., & Perry, R. (2007). *Perry's Chemical Engineers' Handbook, Eighth Edition*: McGraw-Hill Education.

Gregory, D. P., & Riddiford, A. C. (1956). 731. Transport to the surface of a rotating disc. *J. chem. Soc.*, 3756-3764.

Guan, Y., & Han, K. N. (1994). An electrochemical study on the dissolution of gold and copper from gold/copper alloys. *Metallurgical and Materials Transactions B, 25*(6), 817-827.

Guo, H., Deschênes, G., Pratt, A., Fulton, M., & Lastra, R. (2005). Leaching kinetics and mechanisms of surface reactions during cyanidation of gold in the presence of pyrite or stibnite. *Minerals and Metallurgical Processing, 22*(2), 89-95.

Guzman, L., Segarra, M., Chimenos, J. M., Fernandez, M. A., & Espiell, F. (1999). Gold cyanidation using hydrogen peroxide. *Hydrometallurgy, 52*(1), 21-35.

Habashi, F. (1966). The theory of cyanidation. *Transactions of the Society of Mining Engineers of AIME, 235*, 236-239.

Habashi, F. (1967). *Kinetics and mechanism of gold and silver dissolution in cyanide solution* (Vol. Bulletin 59).

Habashi, F. (2009). Gold - An historical introduction. In F. Habashi (Ed.), *Gold: History, Metallurgy, Culture*. Québec City, Canada: Métallurgie Extractive Québec.

Hewitt, D. M., Breuer, P. L., Jeffrey, M. I., & Naim, F. (2009). Mechanisms of sulfide ion oxidation during cyanidation. Part II: Surface catalysis by pyrite. *Minerals Engineering, 22*(13), 1166-1172.

Hoare, J. P. (1968). Electrochemistry of oxygen.

IFA. (2015). GESTIS-Stoffdatenbank. Retrieved 02.02.2015, from http://gestis.itrust.de/nxt/gateway.dll/gestis_de/002430.xml?f=templates$fn=default.htm$3.0

Jeffrey, M. I. (1997). *A Kinetic and Electrochemical Study of the Dissolution of Gold in Aerated Cyanide Solutions: The Role of Solid and Solution Phase Purity.* Doctor of Philosophy Curtin University of Technology Western Australia

Jeffrey, M. I., & Breuer, P. L. (2000). The cyanide leaching of gold in solutions containing sulfide. *Minerals Engineering, 13*(10–11), 1097-1106.

Jeffrey, M. I., & Ritchie, I. M. (2000). The leaching of gold in cyanide solutions in the presence of impurities II. The effect of silver. *Journal of the Electrochemical Society, 147*(9), 3272-3276.

Jeffrey, M. I., Zheng, J., & Ritchie, I. M. (2000). The development of a rotating electrochemical quartz crystal microbalance for the study of leaching and deposition of metals. *Measurement Science and Technology, 11*(5), 560-567.

Jeffrey, M. I., Zheng, J., & Ritchie, I. M. (2000). The development of a rotating electrochemical quartz crystal microbalance for the study of leaching and deposition of metals. *Measurement Science and Technology, 11*(5), 560.

Jia, Y. F., Steele, C. J., Hayward, I. P., & Thomas, K. M. (1998). Mechanism of adsorption of gold and silver species on activated carbons. *Carbon, 36*(9), 1299-1308.

Johnston, W. D. (1984). *United States of America Patent No*. *US Pat. 522260*. U. S. P. O. .

Kameda, M. (1949). Fundamental Studies on Dissolution of Gold in Cyanide Solutions. II: On Equations of Reactions and Effects of Cyanide Strength and other Variables on Dissolution Rate.

Karimi, P., Abdollahi, H., Amini, A., Noaparast, M., Shafaei, S. Z., & Habashi, F. (2010). Cyanidation of gold ores containing copper, silver, lead, arsenic and antimony. *International Journal of Mineral Processing, 95*(1-4), 68-77.

Kim, K. S., & Winograd, N. (1975). X-ray photoelectron spectroscopic binding energy shifts due to matrix in alloys and small supported metal particles. *Chemical Physics Letters, 30*(1), 91-95.

Kitis, M., Akcil, A., Karakaya, E., & Yigit, N. O. (2005). Destruction of cyanide by hydrogen peroxide in tailings slurries from low bearing sulphidic gold ores. *Minerals Engineering, 18*(3), 353-362.

Knorre, H., Loroesch, J., Gos, S., Stoll, M., & Ziegler, A. (1993). *US Patent No. 5,250,272*.

Kudryk, V., & Kellogg, H. H. (1954). Mechanism and rate controlling factors in the dissolution of gold in cyanide solution. *JOM*, 541-548.

La Brooy, S. R., Linge, H. G., & Walker, G. S. (1994). Review of gold extraction from ores. *Minerals Engineering, 7*(10), 1213-1241.

La Brooy, S. R., Muir, D. M., & Komosa, T. (1991). *Oxygen Requirements and Monitoring for Gold Ore Processing.* Paper presented at the World Gold '91, Cairns.

Lee, H. H. B., Park, A.-H., & Oloman, C. (2000). Stability of hydrogen peroxide in sodium carbonate solutions. *TAPPI JOURNAL, 83*(8)

Li, Q., Jiang, T., Yang, Y.-b., Li, G.-h., Guo, Y.-f., & Qiu, G.-z. (2010). Co-intensification of cyanide leaching gold by mercury ions and oxidant. *Transactions of Nonferrous Metals Society of China, 20*(8), 1521-1526.

Liu, G. Q., & Yen, W. T. (1995). Effects of sulphide minerals and dissolved oxygen on the gold and silver dissolution in cyanide solution. *Minerals Engineering, 8*(1–2), 111-123.

Lorenzen, L., & van Deventer, J. S. J. (1991). Electrochemical interactions between gold and its associated minerals during cyanidation. *Hydrometallurgy, 30*, 177-194.

Lorösch, J. (1989). *PAL - CIPAL - Laboratory Testwork on Flotation Residue*. Degussa AG, Frankfurt/Germany. Internal Laboratory Report.

Lorösch, J. (1990). Peroxide Assisted Leach - Three Years of Increasing Success*Randol Gold Forum 1990*, *held in Squaw Valley,* (pp. pp. 215-219). Randol Int. Ltd., Golden, CO, USA.

Lorösch, J. (2001). *Process and Enviornmental Chemistry of Cyanidation*. Frankfurt am Main: Degussa AG.

Lorösch, J., & Kappes, D. W. (1991, April 19-19). *Cost Effective Plant Design - The PAL Approach.* Paper presented at the Randol Gold Forum '91.

Los Alamos National Laboratory. (2015). PERIODIC TABLE OF ELEMENTS: LANL. Retrieved 02.02.2015, from periodic.lanl.gov/index.shtml

Mahlangu, T., Sandenbergh, R. F., Skudder, J., & Maree, D. C. S. (2007). Effect of Preoxidation and Lead Nitrate Addition on Sodium Cyanide Consumption and Gold Recovery at the Morila Mine Gold Plant*World Gold Conference*, *held in Cairns, QLD,* 22-24.10.2007

Mar, W. D. (1995). *A Text Book Of Chemistry Practicals (2 Vols.)*: APH Publishing Corporation.

Marsden, J. O., & House, I. C. (2006). *The Chemistry of Gold Extraction 2nd Edition*. Littleton, Colorado, USA 80127: Society of Mining, Metallurgy, and Exploration, Inc. (SME).

McMahon, M., Lopez, R., Meyer, H., Feldman, L., & Haglund, R. (2005). Rapid tarnishing of silver nanoparticles in ambient laboratory air. *Lasers and Optics, 80*(7), 915-921.

Moulder, J. F., Stickle, W. F., Sobel, P. E., & Bomben, K. D. (1995). *Handbook of X-ray Photoelectron Spectroscopy*. Minnesota, United States of America: Physical Electronics USA Inc.

Nguyen, H. H., Tran, T., & Wong, P. L. M. (1997). Copper interaction during the dissolution of gold. *Minerals Engineering, 10*(5), 491-505.

Nicol, M. J., Fleming, C. A., & Paul, R. L. (1987). The Chemistry of the Extraction of Gold. In G. G. Stanley (Ed.), *The Extractive Metallury of Gold in South Africa* (Vol. Volume 2). Johannesburg: The South African Institute of Mining and Metallurgy.

O.I. Analytical. (2009). Operations Manual CNSolution Cyanide Analyzer.

Pak, D., & Chang, W. (1997). Oxidation of aqueous cyanide solution using hydrogen peroxide in the presence of heterogeneous catalyst. *Environmental technology, 18*(5), 557-561.

Power, G. P., & Ritchie, I. M. (1975). Metal displacement reactions. *Modern Aspects of Electrochemistry, 11*, 199-250.

Puddephatt, R. J. (1987). *The chemistry of Gold*. Amsterdam, Netherlands: Elsevier Scientific Publishing Company.

Rand, D. A. J. (1977). Oxygen reduction on sulphide minerals: Part III. Comparison of activities of various copper, iron, lead and nickel mineral electrodes. *Journal of Electroanalytical Chemistry and Interfacial Electrochemistry, 83*(1), 19-32.

Rieger, P. H. (1994). *Electrochemistry*. New York: Chapman & Hall, Inc.

sample donor, personal communication with sample donor, 2015.

Sarla, M., Pandit, M., Tyagi, D. K., & Kapoor, J. C. (2004). Oxidation of cyanide in aqueous solution by chemical and photochemical process. *Journal of hazardous materials, 116*(1), 49-56.

Schumb, W. C., Satterfield, C. N., & Wentworth, R. L. (1953). Hydrogen peroxide - Part Two.

Senanayake, G. (2005). Kinetics and reaction mechanism of gold cyanidation: Surface reaction model via Au(I)-OH-CN complexes. *Hydrometallurgy, 80*(1-2), 1-12.

Senanayake, G. (2008). A review of effects of silver, lead, sulfide and carbonaceous matter on gold cyanidation and mechanistic interpretation. *Hydrometallurgy, 90*(1), 46-73.

Shirley, D. A. (1972). High-resolution X-ray photoemission spectrum of the valence bands of gold. *Physical Review B, 5*(12), 4709.

Tan, H., Feng, D., Lukey, G. C., & van Deventer, J. S. J. (2005). The behaviour of carbonaceous matter in cyanide leaching of gold. *Hydrometallurgy, 78*(3–4), 226-235.

Tan, H., Feng, D., van Deventer, J. S. J., & Lukey, G. C. (2006). An electrochemical study of pyrite oxidation in the presence of carbon coatings in cyanide medium. *International Journal of Mineral Processing, 80*(2-4), 153-168.

Thermo Fisher Scientific Inc. (2013a). XPS Interpretation of Gold. Retrieved 29.07.2014, from http://xpssimplified.com/elements/gold.php

Thermo Fisher Scientific Inc. (2013b). XPS Interpretation of Sulfur. Retrieved 29.07.2014, from http://xpssimplified.com/elements/sulfur.php

TPS Pty Ltd. (1998). Model WP-82 Dissolved Oxygen-Temp. Meter - Handbook. Brisbane, Australia.

Tshilombo, A. F., & Sandenbergh, R. f. F. (2001). An electrochemical study of the effect of lead and sulphide ions on the dissolution rate of gold in alkaline cyanide solutions. *Hydrometallurgy, 60*(1), 55-67.

U.S. Geological Survey. (2016). *Mineral Commodity Summaries 2016*. Reston, Virginia: U.S. Geological Survey.

US Peroxide. (2014). Coefficient of Diffusion H2O2, Hydrogen peroxide. Retrieved 13.02.2014, from http://www.h2o2.com/technical-library/physical-chemical-properties/physical-properties/default.aspx?pid=21&name=Coefficient-of-Diffusion

US Peroxide. (2015). Hydrogen Peroxide |H2O2| Solution Properties (CAS 7722-84-1). Retrieved 02.02.2015, from http://www.h2o2.com/technical-library/physical-chemical-properties/default.aspx?pid=12

van Stroe-Biezen, S. A. M., Everaerts, F. M., Janssen, L. J. J., & Tacken, R. A. (1993). Diffusion coefficients of oxygen, hydrogen peroxide and glucose in a hydrogel. *Analytica Chimica Acta, 273*(1–2), 553-560.

Wardell-Johnson, G., Personal communication: Gold distribution in Ore A, 2014a.

Wardell-Johnson, G., Private conversation - wet versus dry grinding, 2014b.

Wasserman, A. (2010). *Two sides to the coin: A history of gold*. Sarasota, FL: Adam Wasserman.

Yang, Y.-b., Li, Q., Jiang, T., Guo, Y.-f., Li, G.-h., & Xu, B. (2010). Co-intensification of gold leaching with heavy metals and hydrogen peroxide. *Transactions of Nonferrous Metals Society of China, 20*(5), 903-909.

Zhang, H.-G. (1997). *Some aspects of the use of thiourea in gold processing.* PhD Murdoch University

Zheng, J., Khan, M., La Brooy, S. R., Ritchie, I. M., & Singh, P. (1996). The chronopotentiometric method for measuring the kinetics of metal dissolution and cementation reactions. *Journal of applied electrochemistry, 26*(5), 509-514.

Zurilla, R., Sen, R., & Yeager, E. (1978). The kinetics of the oxygen reduction reaction on gold in alkaline solution. *Journal of the Electrochemical Society, 125*(7), 1103-1109.

Zurilla, R. W., & Yeager, E. (1969). OXYGEN ELECTRODE KINETICS OF GOLD. In L. A. B. Case Western Reserve Univ Cleveland Ohio Electrochemistry Research (Ed.).

Every reasonable effort has been made to acknowledge the owners of copyright material. I would be pleased to hear from any copyright owner who has been omitted or incorrectly acknowledged.

Appendix A XPS-Data peak interpretation

All figures in this section are plotted as intensity against binding energy. First the overview graph is presented and then the detected peaks, fitting of background and fitting of peaks with the GL30-function are shown and explained.

A.1 Specimen immediately after leaching

The first XPS scan, without any additional pre-treatment after the leach, is presented in Figure A-1. Elemental peak identification revealed the presence of gold, silver, carbon, oxygen, and sulphur. The identifying peaks were investigated in more detail, to determine a concentration of each element and also to understand possible chemical binding. The atomic fractions determined are 18.5%, 6.7%, 34.2%, 38.8% and 1.8% for gold, silver, oxygen, carbon and sulphur respectively.

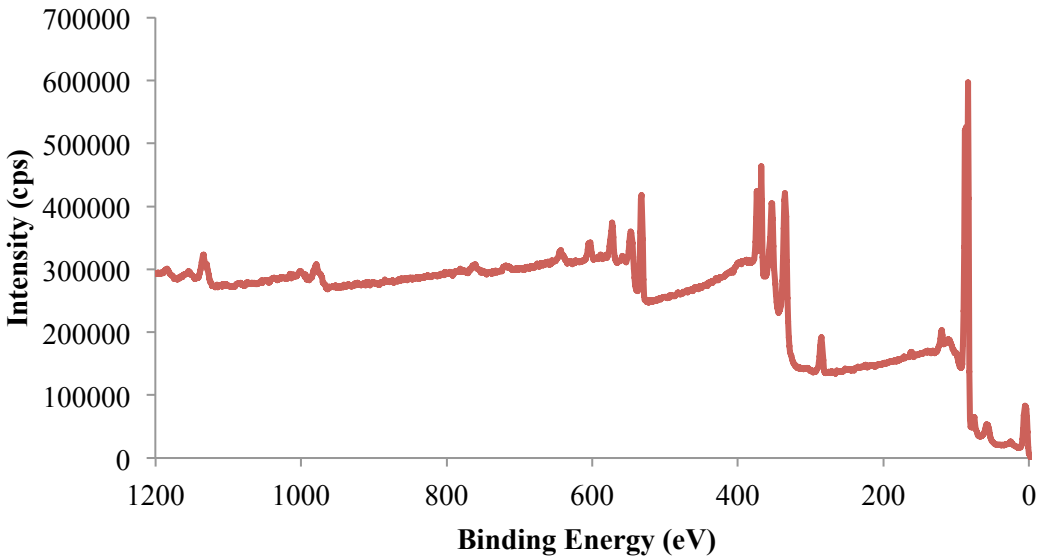

Figure A-1: XPS spectrum of the gold specimen, immediately after leaching

Gold

Figure A-2 shows the measured gold doublet peaks as the red line. The blue line represents the background fitted to the measured data.

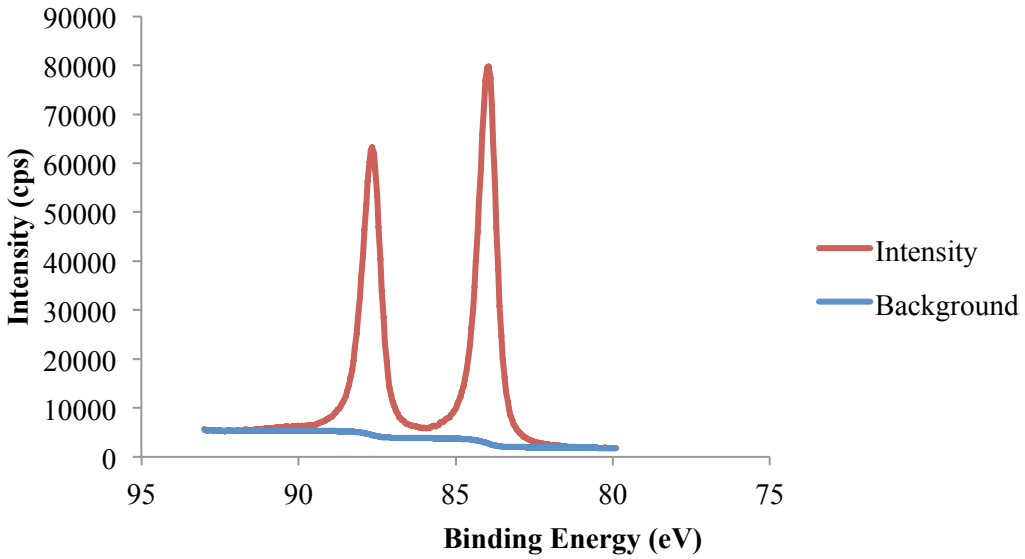

Figure A-2: Au 4f XPS peaks raw data and background fitting for freshly leached specimen

The peaks fitted to the background corrected raw data are presented in Figure A-3. It can be seen, that the standard gold orbital spin doublet with a binding energy of 84.0 eV (Thermo Fisher Scientific Inc., 2013a) for the first peak can be fitted and no additional peaks were required to match the data. This indicates, that only elemental gold in its natural charge state with no chemical bonding is present.

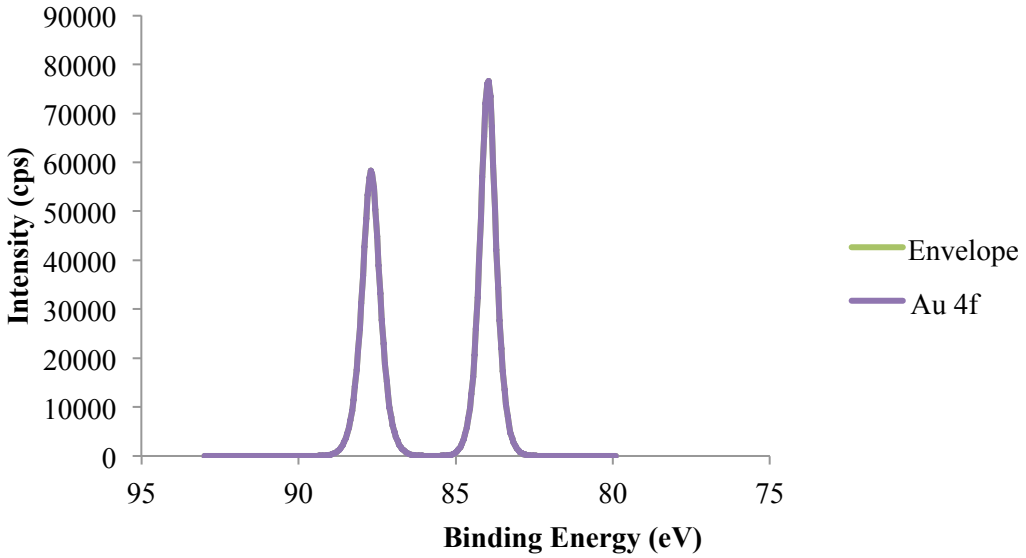

Figure A-3: Au 4f XPS peaks fitted and according envelope for freshly leached specimen

Silver

The silver orbital spin doublet observed during the XPS scanning of the untreated specimen is shown in Figure A-4. The red line represents the measured intensity, the blue line the background fitted to the data.

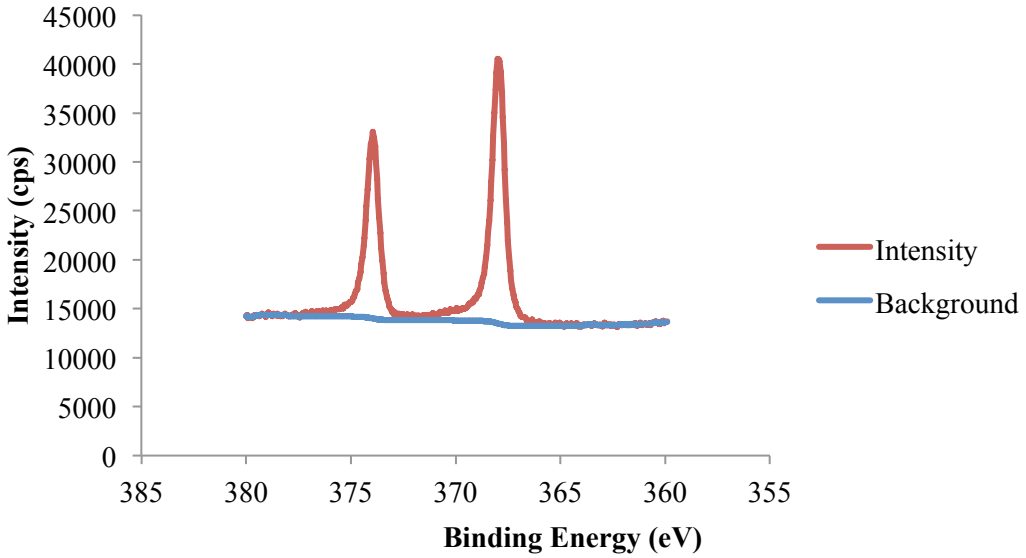

Figure A-4: Ag 3d XPS peaks raw data and background fitting for freshly leached specimen

In Figure A-5 the silver peaks fitted and the resulting envelope are plotted. It is notable, that four different silver peaks were required to fully match the measured

data. Each of those peaks indicates a different chemical state/bonding of the silver observed. The peaks were identified to have a binding energy of 368, 368.7, 366.8 and 370.6 eV for the 3d I, 3d II, 3d III, 3d IV peaks, respectively. Silver in its natural state has a binding energy of 368.2 eV (Biesinger, 2013c). It can be assumed, that the Ag 3d I peak represents elemental silver. This might be due to the co-existence with gold causing the detected binding energy to be lowered (Kim & Winograd, 1975). The other peaks fitted will be put into relation with the peaks of other elements observed on the specimen and explained there.

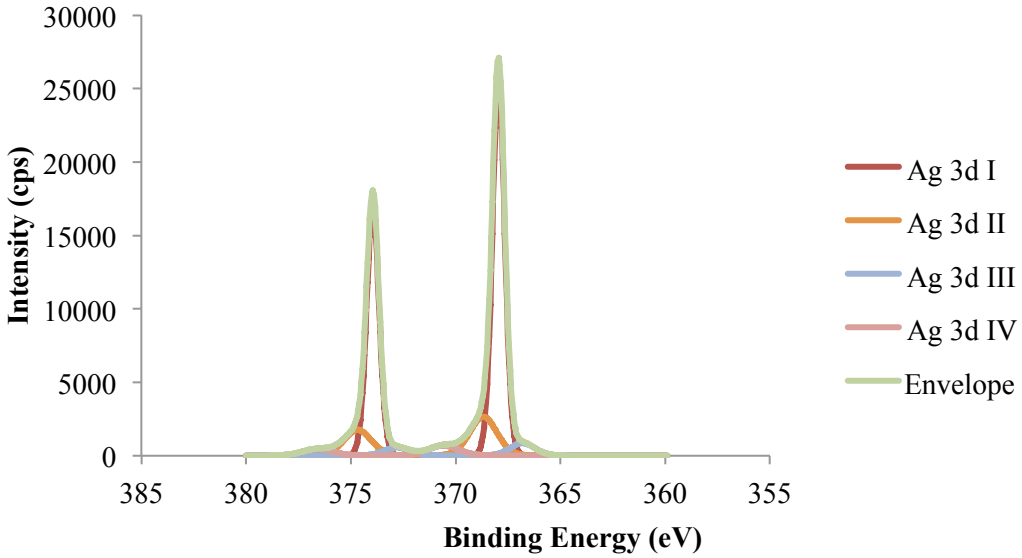

Figure A-5: Ag 3d XPS peaks fitted and according envelope for freshly leached specimen

Oxygen

Figure A-6 plots the measured oxygen peak with the red line. The blue line represents the fitted background correction data.

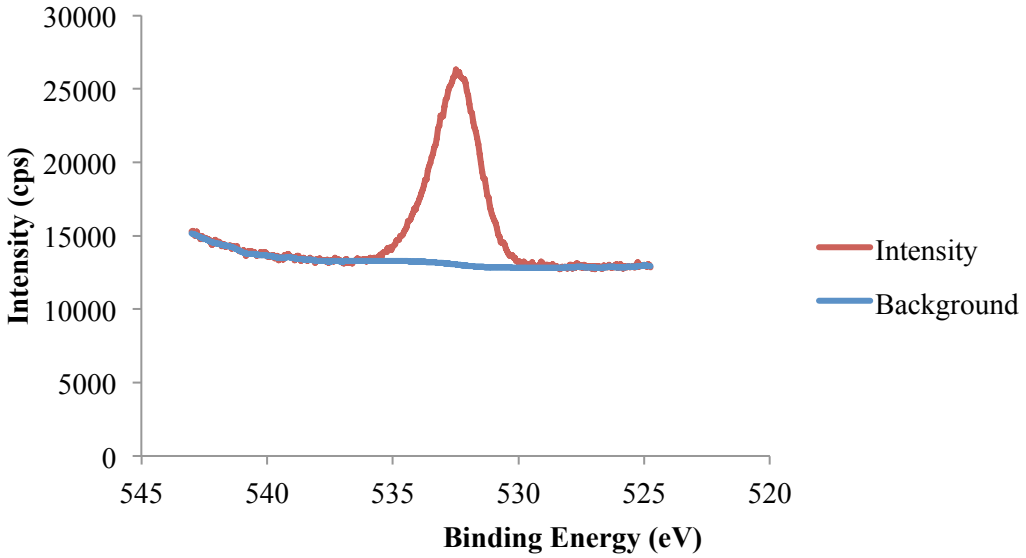

Figure A-6: O 1s XPS peak raw data and background fitting for freshly leached specimen

In Figure A-7 the resulting envelope and O 1s curves matched to the data are plotted. The binding energy of both oxygen peaks fitted could be a range of oxygen compounds, including metal carbonates and organic C=O bonds (Biesinger, 2013b).

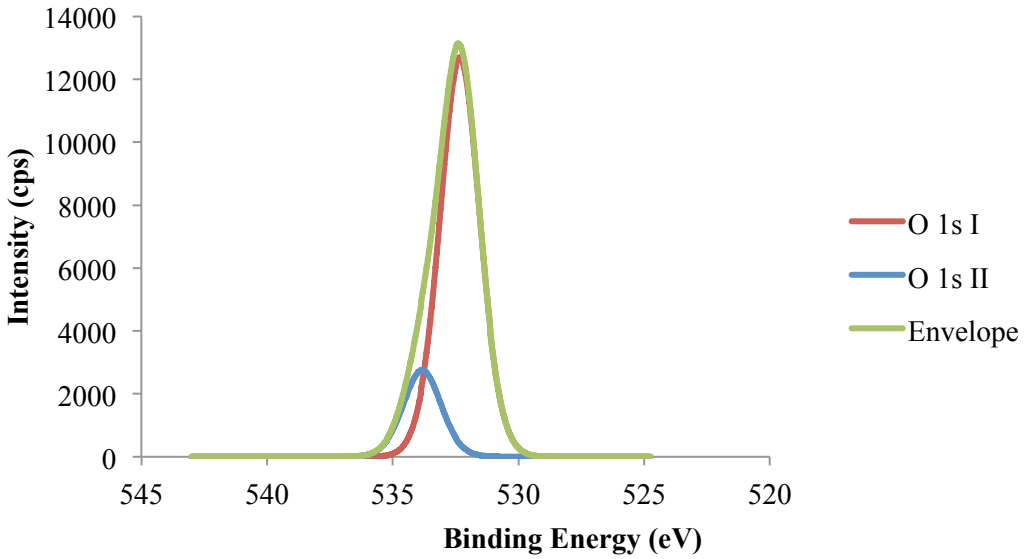

Figure A-7: O 1s XPS peak fitted and according envelope for freshly leached specimen

Carbon

The measured intensity for the C 1s peak is plotted as the red line in Figure A-8. The blue line represents the background fitted to this peak.

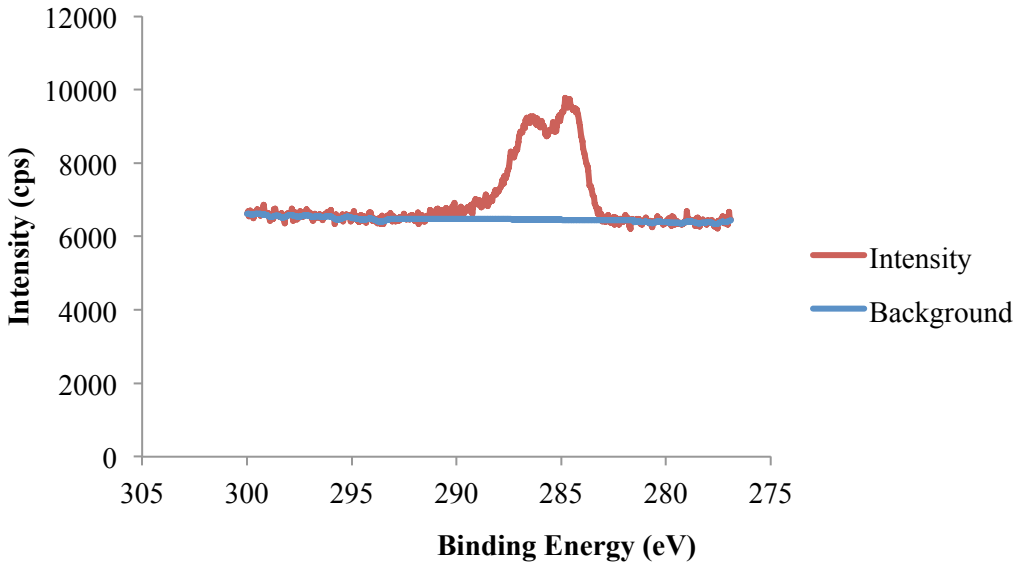

Figure A-8: C 1s XPS peak raw data and background fitting for freshly leached specimen

Figure A-9 shows the matched peaks for the C 1s peak measured. It can be noted, that four different peaks were required to create a match to the measured data. All peaks fitted, apart from the C 1s I peak at 284.5 eV indicate that the carbon is being chemically bound with other elements (Biesinger, 2013a). The C 1s III peak at 288.0 eV is very close to typical values for carbonate species, and might be reflective of silver carbonate. The other peaks observed will be matched to the other elements observed.

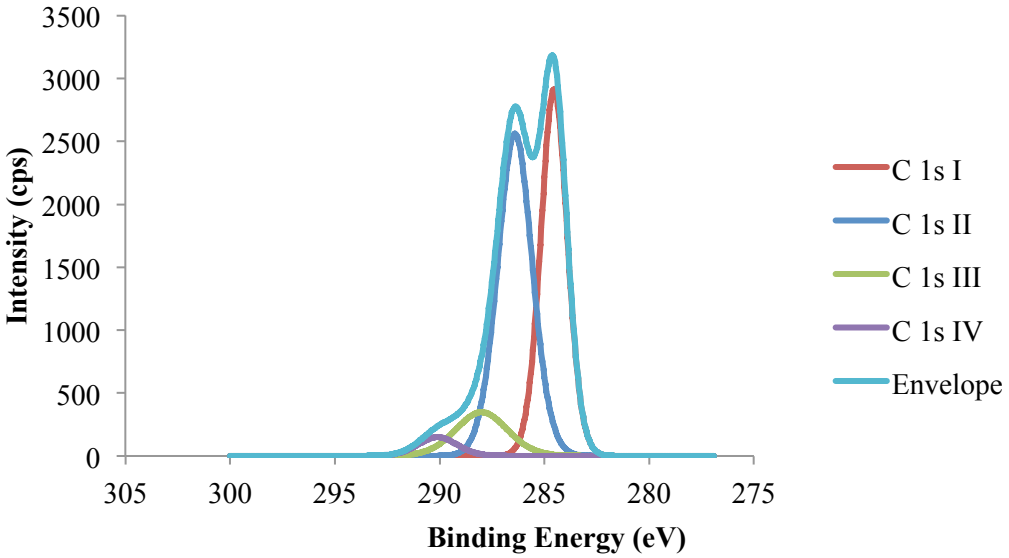

Figure A-9: C 1s XPS peaks fitted and according envelope for freshly leached specimen

Sulphur

A sulphur peak was noted in the overview plot. Its detailed peak intensity data and fitted background intensity are plotted in Figure A-10.

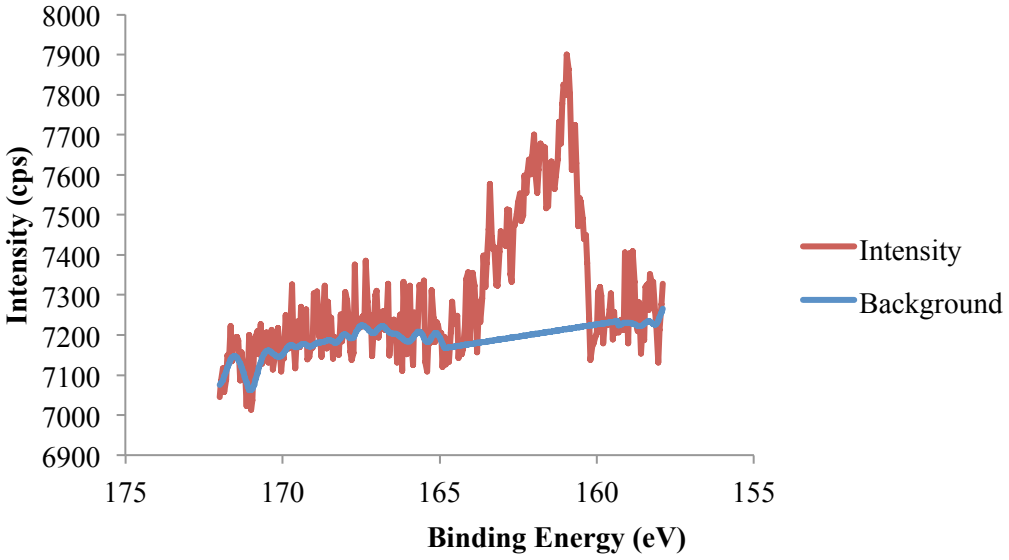

Figure A-10: S 2p XPS peak raw data and background fitting for freshly leached specimen

The peak fitting conducted on the raw data resulted in the observation of two S 2p peaks, as shown in Figure A-11. Both peaks observed are in the typical binding energy region for metal sulphides of ~161.5 eV (Thermo Fisher Scientific Inc., 2013b).

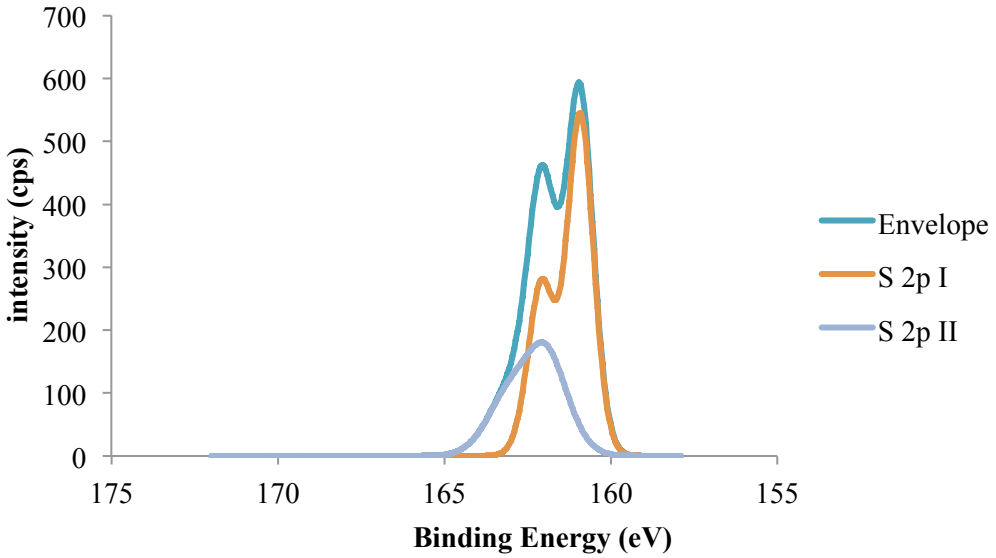

Figure A-11: S 2p XPS peaks fitted and according envelope for freshly leached specimen

Summary

All peaks identified for the freshly leached surface are listed in Table A-1. The identifying peak positions and calculated concentrations (atomic and mass) are shown for each peak identified. For orbital spin doublets, only the first (lower eV) peak position is mentioned, as it is usually agreed on in literature.

Table A-1: XPS identified peaks, their position and calculated concentrations for freshly leached specimen

Peak name	Peak Position (eV)	Atomic Concentration (%)	Mass Concentration (%)
Au 4f	84.00	18.5	66.8
Ag 3d I	367.95	4.9	9.8
Ag 3d II	368.70	1.1	2.2
Ag 3d III	366.80	0.3	0.7
Ag 3d IV	370.60	0.3	0.7
O 1s I	532.35	28.3	8.4
O 1s II	533.85	5.8	1.7
C 1s I	284.55	15.9	3.5
C 1s II	286.40	18.2	4.0
C 1s III	288.00	3.7	0.8
C 1s IV	290.10	1.2	0.3
S 2p I	160.90	1.2	0.7
S 2p II	162.05	0.6	0.3

A.2 Specimen after light etch

In Figure A-12 the measured intensity spectrum for the XPS scan after the light etch is plotted. Some of the peaks observed in the non-etched scan are reduced. The atomic fractions determined are 29.3%, 7.0%, 45.9%, 16.6% and 1.2% for gold, silver, oxygen, carbon and sulphur respectively.

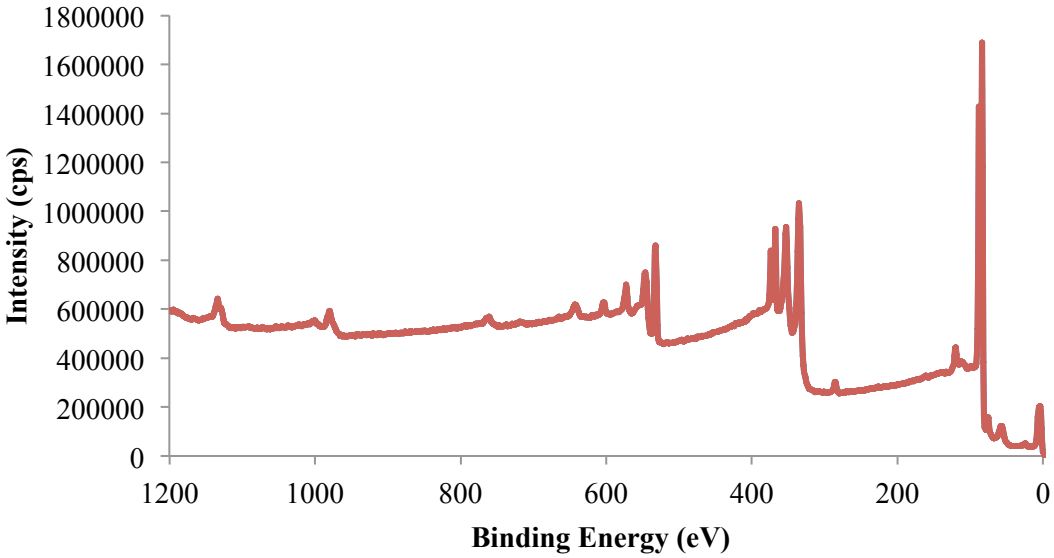

Figure A-12: XPS spectrum of the gold specimen, immediately after leaching and 1 min 5 kV light etching

Gold

The measured gold spectrum (red line) is plotted in Figure A-13. The fitted background is shown as the blue line.

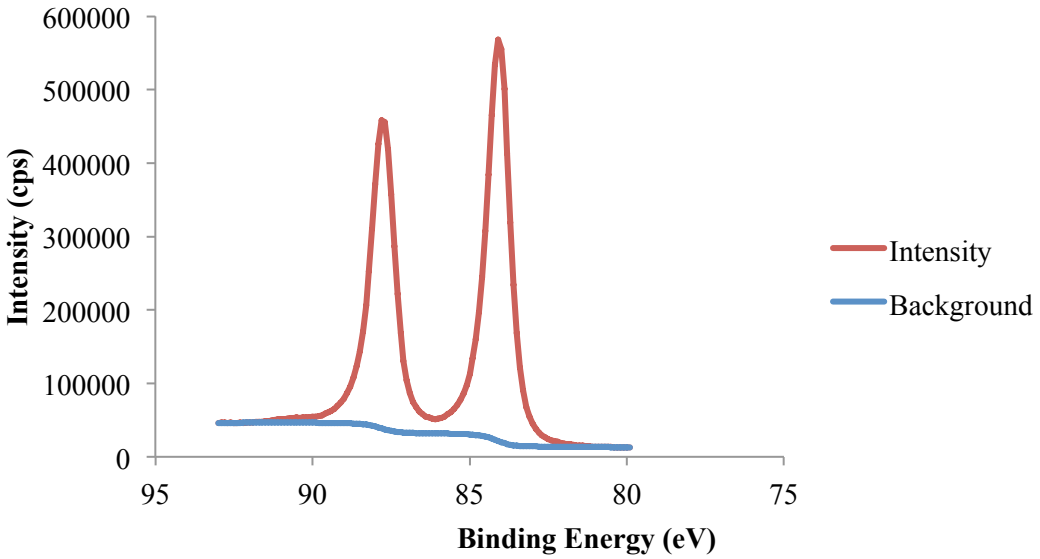

Figure A-13: Au 4f XPS peak raw data and background fitting for specimen after light etching

Figure A-14 displays the envelope and peak fitting generated on the data collected. Only one gold doublet can be seen, and the binding energy position coincides with a

typical gold peak in its natural state at 84.0 eV (Thermo Fisher Scientific Inc., 2013a).

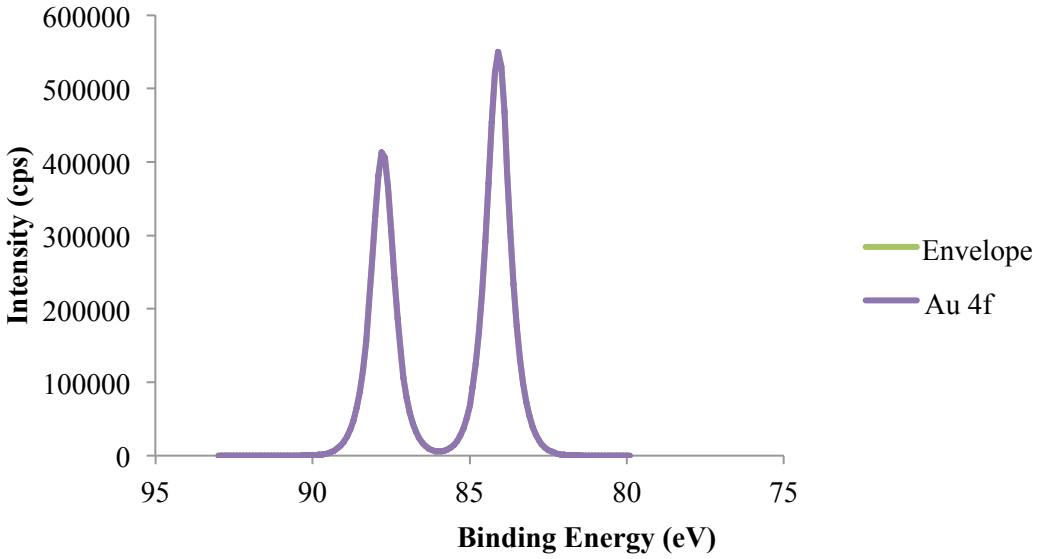

Figure A-14: Au 4f XPS peaks fitted and according envelope for specimen as after light etching

Silver

The measured intensity for the silver orbital spin doublet is shown with the red line in Figure A-15. The blue line represents the matched background correction.

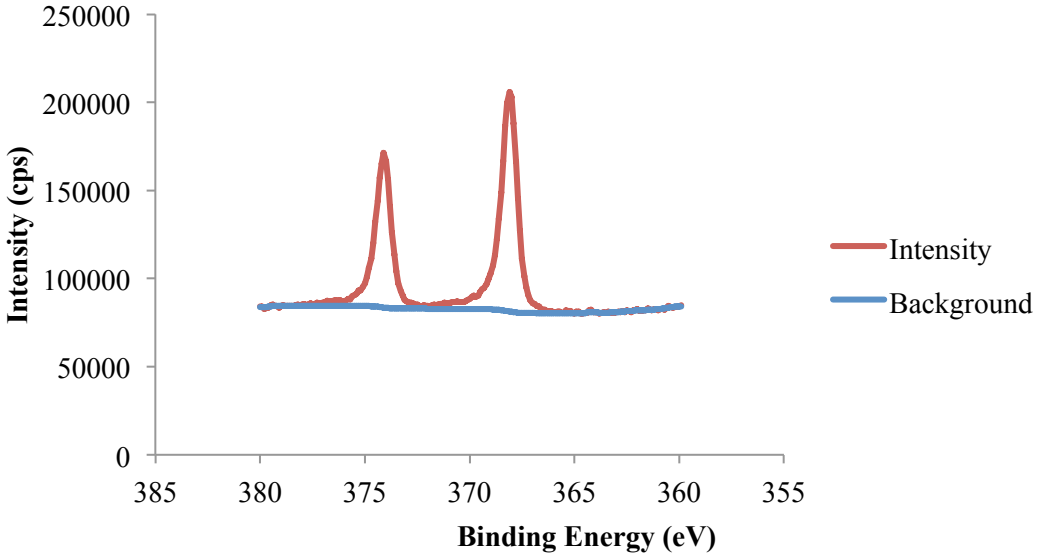

Figure A-15: Ag 3d XPS peak raw data and background fitting for specimen after light etching

The peaks fitted to the data collected including the resulting envelope are shown in Figure A-16. The Ag 3d I peaks binding energy is at 368.1 eV, which is close to the value for silver in its natural state (Biesinger, 2013c). The slight shift might be due to the gold present (Kim & Winograd, 1975). The Ag 3d II peak at 368.8 eV might represent silver in its charge transfer state (Eremenko et al., 2011).

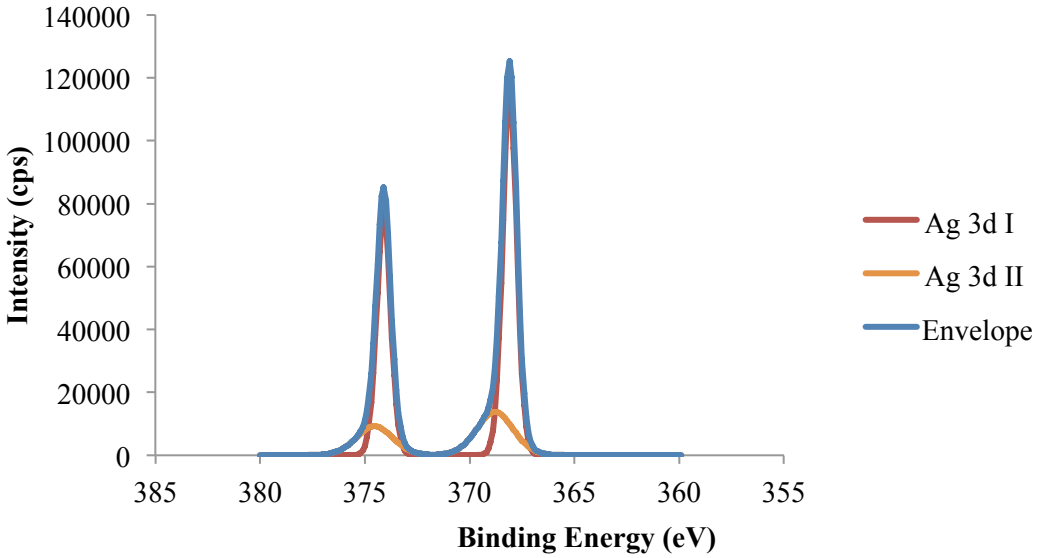

Figure A-16: Ag 3d XPS peaks fitted and according envelope for specimen as after light etching

Carbon

The measured C 1s intensity spectrum is drawn as the red line in Figure A-17. The blue line shows the background fitment added to this data.

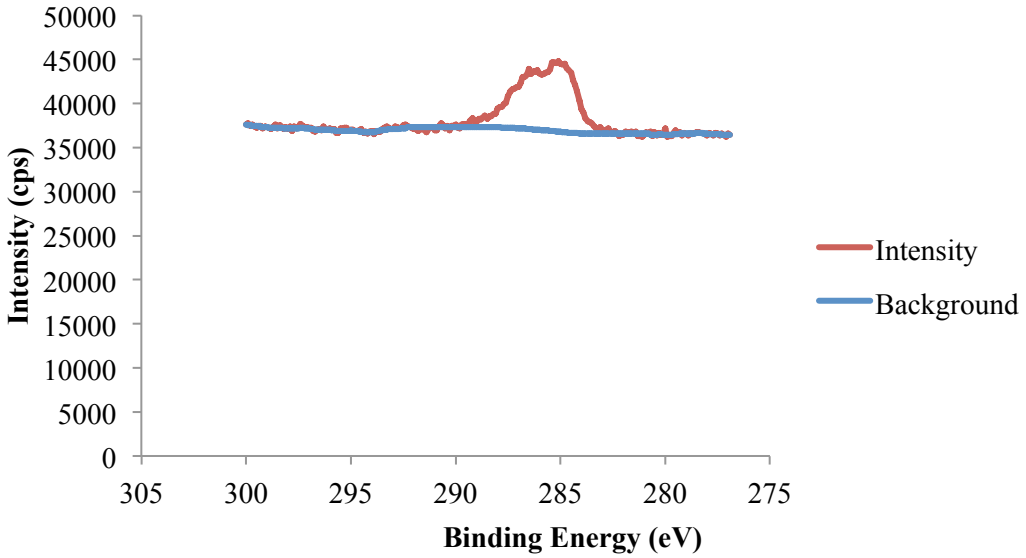

Figure A-17: C 1s XPS peak raw data and background fitting for specimen after light etching

Three peaks were required to acquire a good match to the data collected. The three peaks (C 1s I, C 1s II, and C 1s III) and the resulting envelope are shown in Figure A-18. The C 1s I binding energy of 284.8 eV is in range for carbon in its natural state. The C 1s III binding energy of 288.1 eV correlates with typical silver carbonate peaks (Biesinger, 2013a). For the C1s II peak various compounds are possible, and this has to be matched to the other data observed.

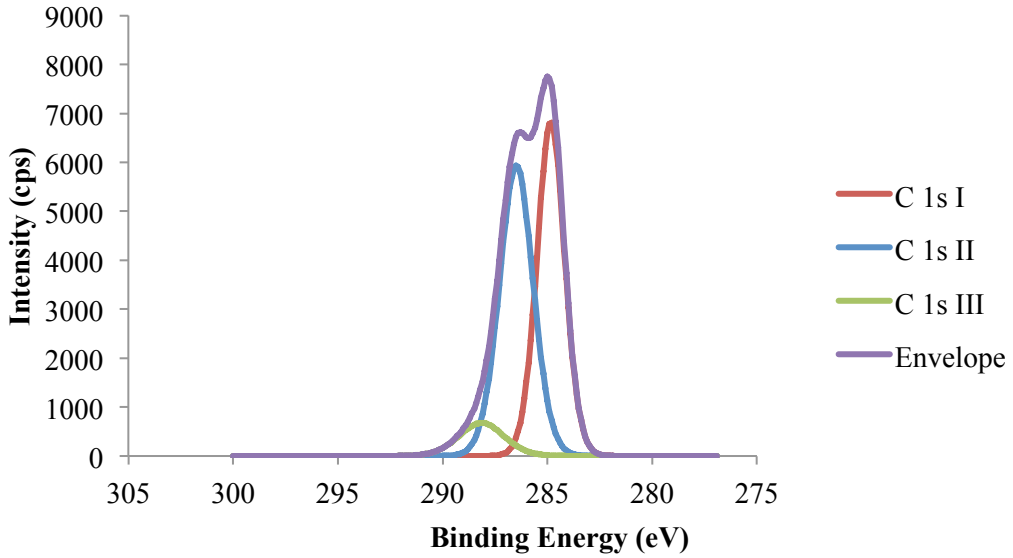

Figure A-18: C 1s XPS peaks fitted and according envelope for specimen as after light etching

Oxygen

In Figure A-19 the data acquired for the O 1s XPS spectrum is drawn as the red line. The fitted background is shown as a blue line.

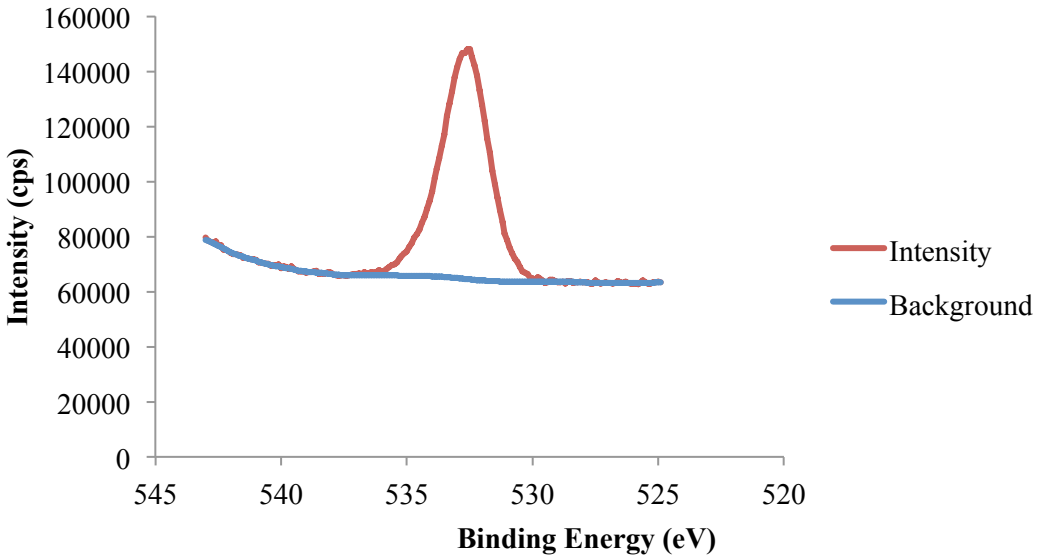

Figure A-19: O 1s XPS peak raw data and background fitting for specimen after light etching

The peak matching resulted in two peaks required to generate an envelope matching the measured data closely. These two O 1s peaks matched and the envelope are shown in Figure A-20. The binding energy of both oxygen peaks fitted could be a range of oxygen compounds, including metal carbonates and organic C=O bonds (Biesinger, 2013b).

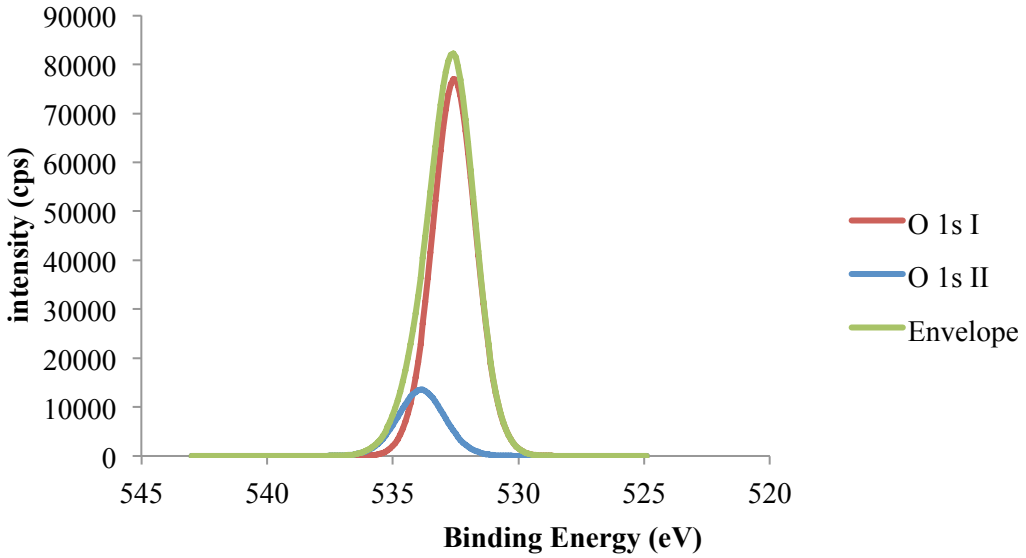

Figure A-20: O1s XPS peaks fitted and according envelope for specimen as after light etching

Sulphur

Figure A-21 shows the S 2p peak data measured (red line) and fitted baseline (blue line).

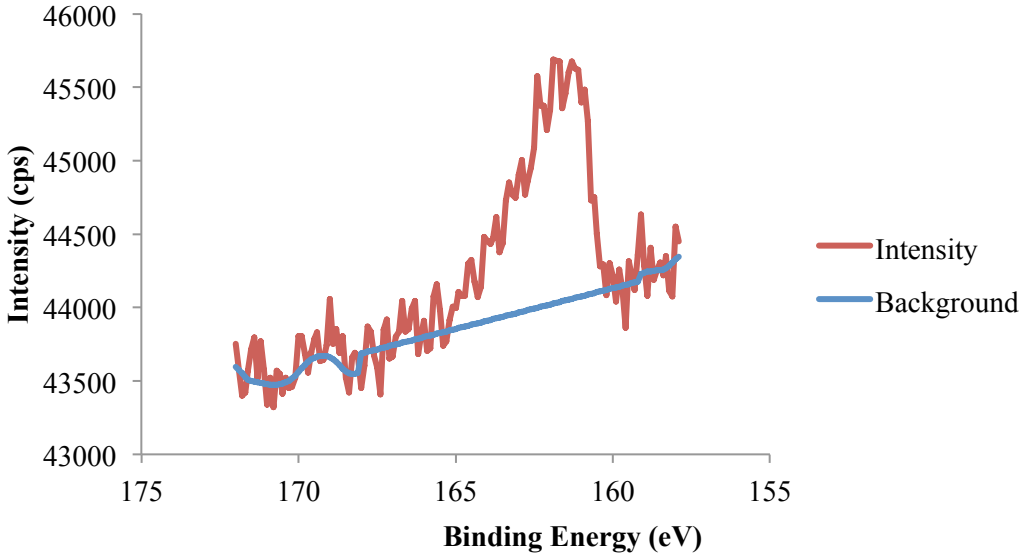

Figure A-21: S 2p XPS peak raw data and background fitting for specimen after light etching

The peaks matched to the data and the resulting envelope are shown in Figure A-22. Two peaks were required to generate an envelope matching the collected data. The S 2p I peak observed is in the typical binding energy region for metal sulphides of

~161.5 eV, and S 2p II could be some form of thoil-bound sulphur (Thermo Fisher Scientific Inc., 2013b).

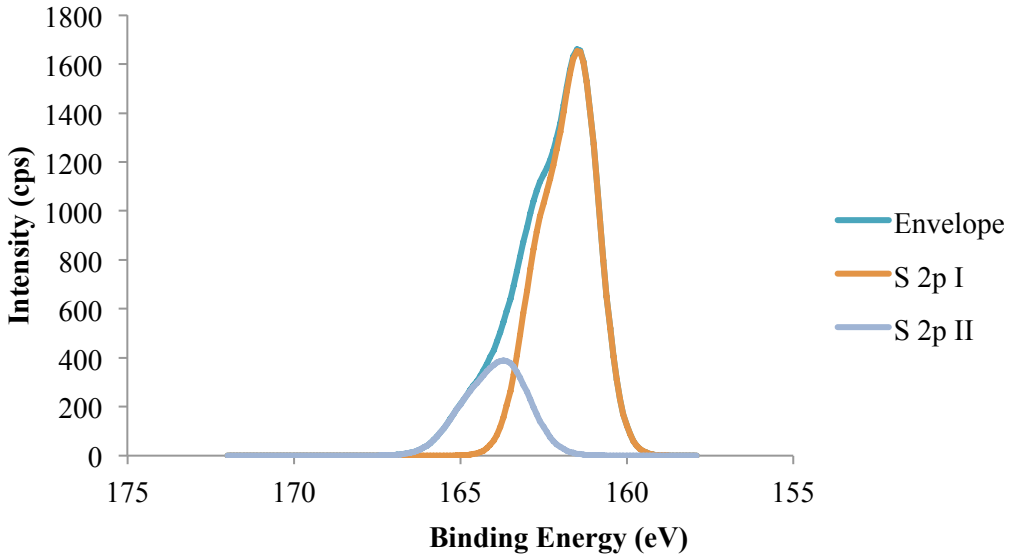

Figure A-22: S 2p XPS peaks fitted and according envelope for specimen as after light etching

Summary

The peaks identified on the specimen after the light etch are displayed in Table A-2. The identifying peak positions and calculated concentrations (atomic and mass) are shown for each peak identified. For orbital spin doublets, only the first (lower eV) peak position is mentioned, as it is usually agreed on in literature.

Table A-2: XPS identified peaks, their position and calculated concentrations for specimen after 1 min 5 kV light etching

Peak name	Peak Position (eV)	Atomic Concentration (%)	Mass Concentration (%)
Au 4f	84.10	28.5	76.6
Ag 3d I	368.10	5.1	7.5
Ag 3d II	368.80	1.6	2.3
O 1s I	532.60	39.4	8.6
O 1s II	533.90	7.4	1.6
C 1s I	284.80	7.6	1.2
C 1s II	286.50	8.0	1.3
C 1s III	288.10	1.2	0.2
S 2p I	161.50	1.0	0.4
S 2p II	163.70	0.3	0.1

A.3 Specimen after hard etching

In Figure A-23 the measured intensity for the XPS scan after the hard etch is drawn. It can be noted, that some of the peaks observed in the scans with no etching or a light etch are reduced. The atomic fractions determined are 31.1%, 6.3%, 46.1%, 15.3% and 1.2% for gold, silver, oxygen, carbon and sulphur respectively.

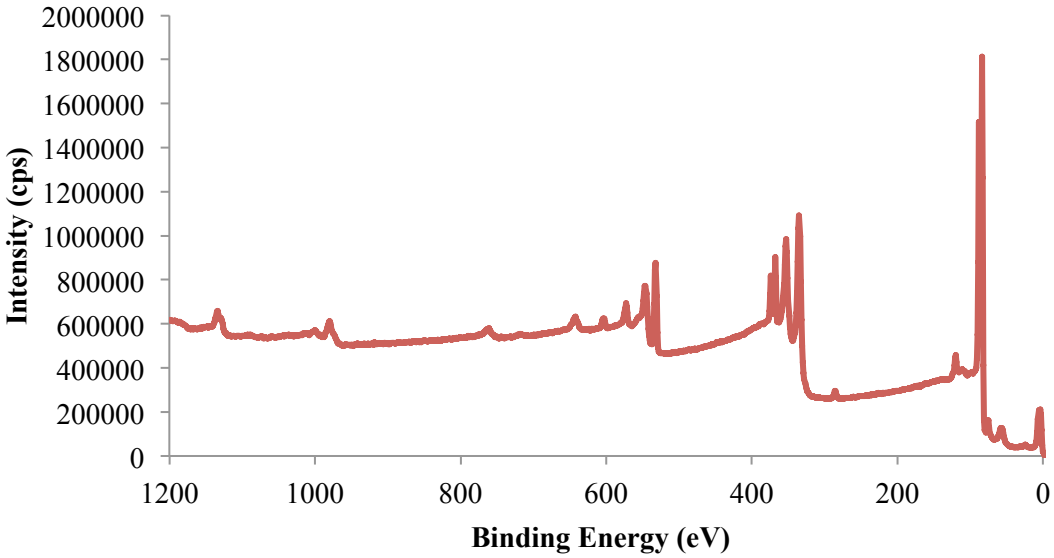

Figure A-23: XPS spectrum of the gold specimen, immediately after leaching and 5 min 20kV hard etching

Gold

The measured intensity (red line) and fitted background (blue line) for the specimen after the hard etch are presented in Figure A-24.

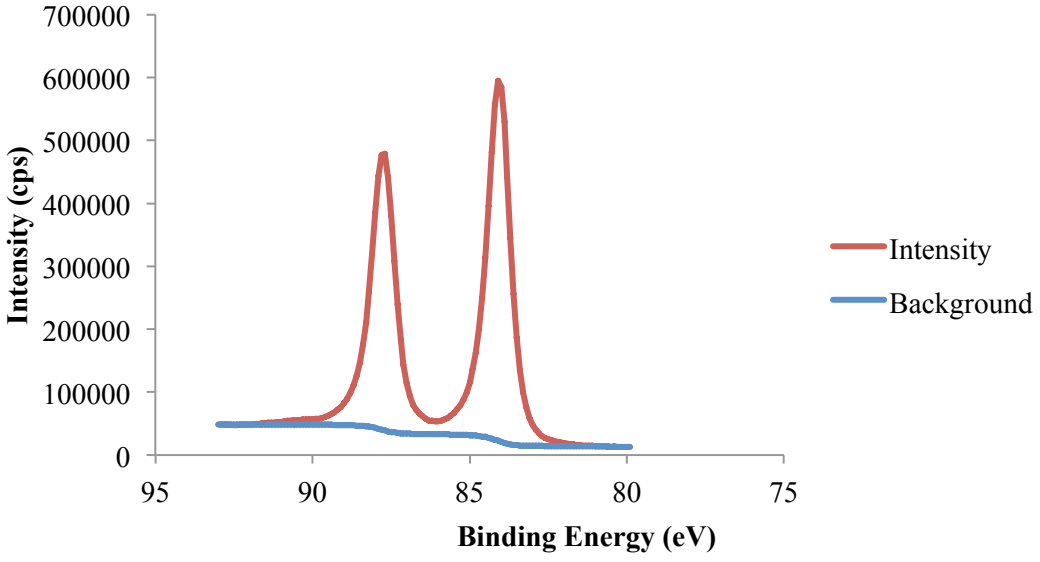

Figure A-24: Au 4f XPS peak raw data and background fitting for specimen after hard etch

Figure A-25 shows the Au 4f peak and envelope fitted to the acquired data. The peak has a binding energy of 84.1 eV, which is in close agreement with natural gold peak binding energy (Thermo Fisher Scientific Inc., 2013a).

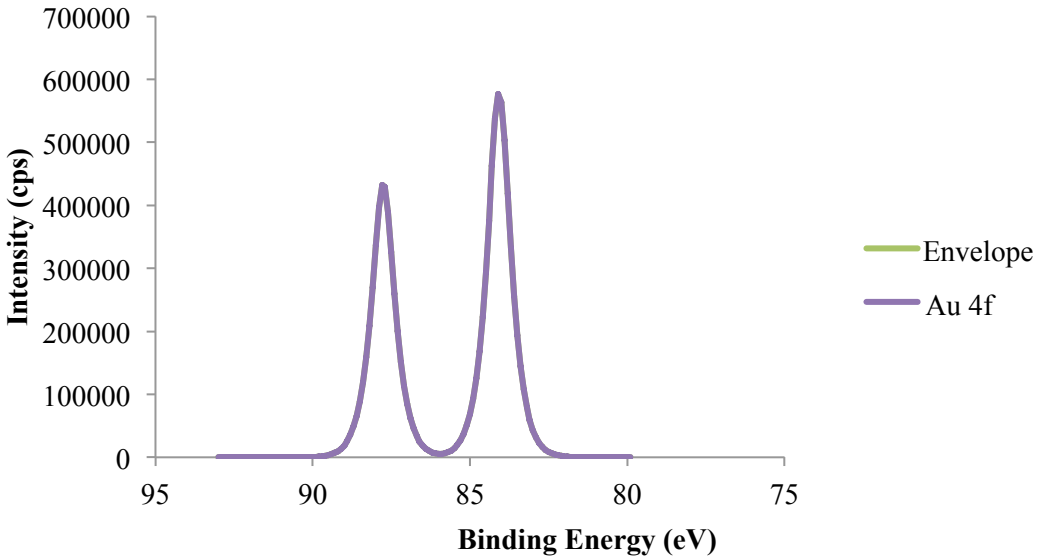

Figure A-25: Au 4f XPS peaks fitted and according envelope for specimen after hard etch

Silver

In Figure A-26 the Ag 3d peak observed is plotted as the red line. The blue line represents the fitted background correction.

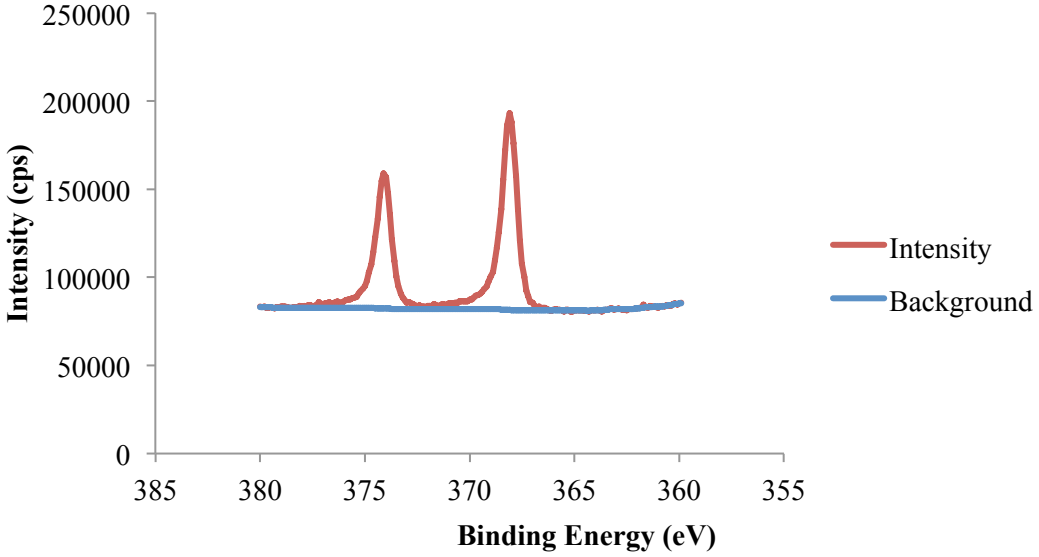

Figure A-26: Ag 3d XPS peak raw data and background fitting for specimen after hard etch

Figure A-27 displays the peaks fitted and the envelope fitted to the measured data. The Ag 3d I peaks binding energy is at 368.1 eV, which is close to the value for silver in its natural state (Biesinger, 2013c). The slight shift might be due to the gold present(Kim & Winograd, 1975). The Ag 3d II peak at 368.8 eV might represent silver in its charge transfer state (Eremenko et al., 2011).

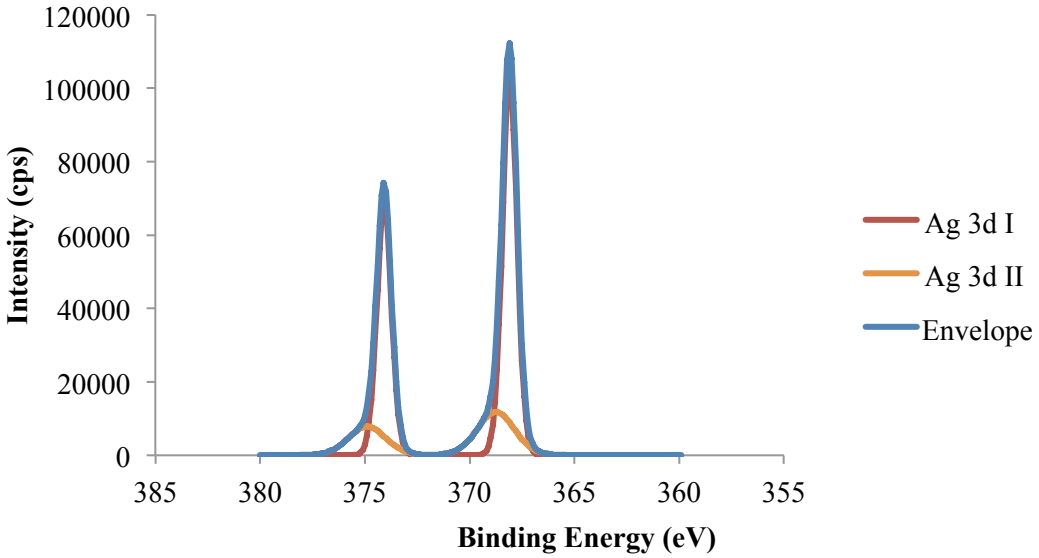

Figure A-27: Ag 3d XPS peaks fitted and according envelope for specimen after hard etch

Oxygen

The detailed peak intensity data for the O 1s peak is presented as a red line in Figure A-28. The blue line in the same graph represents the fitted background.

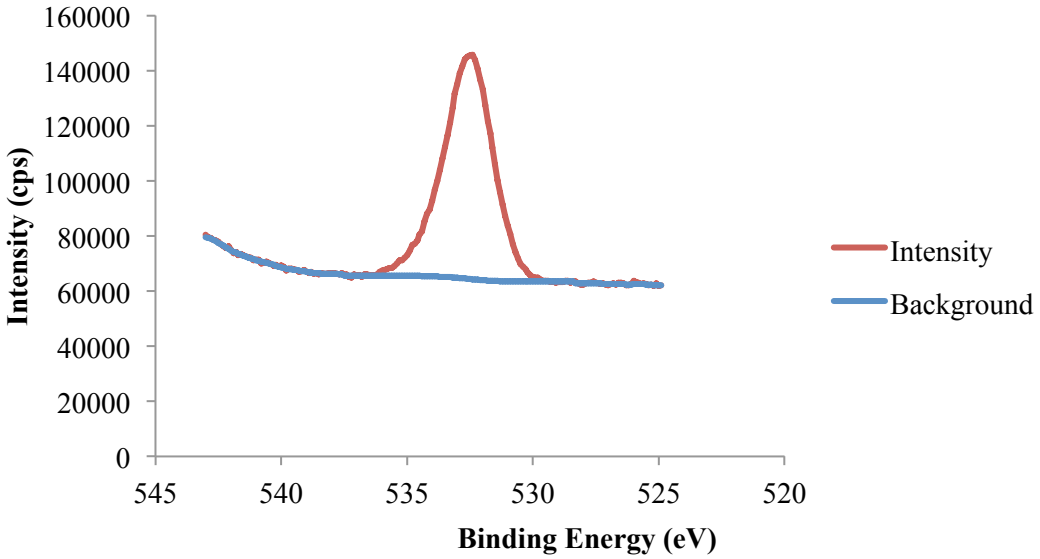

Figure A-28: O 1s XPS peak raw data and background fitting for specimen after hard etch

The envelope and O 1s peaks fitted to the raw data are shown in Figure A-29. The binding energy of both oxygen peaks fitted could be a range of oxygen compounds, including metal carbonates and organic C=O bonds (Biesinger, 2013b).

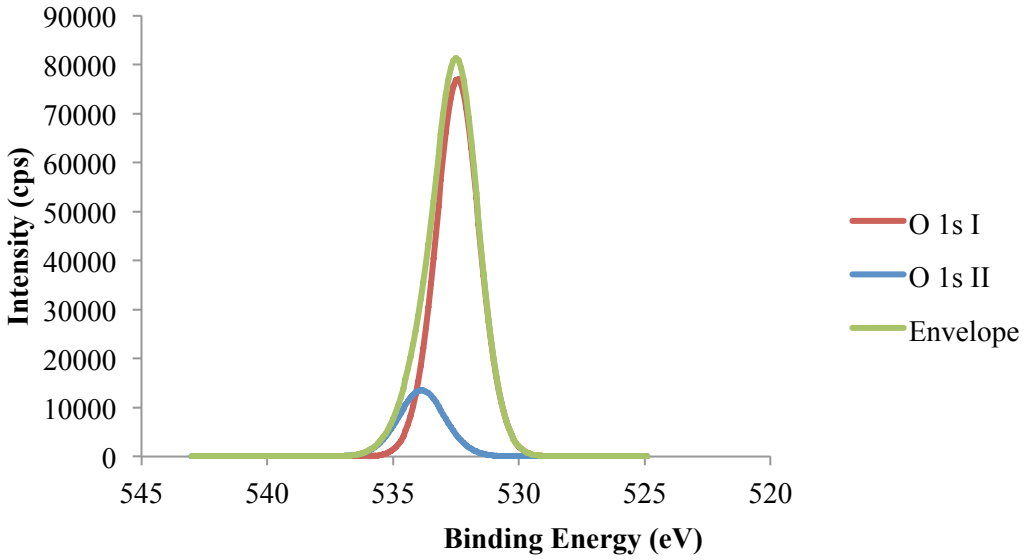

Figure A-29: O 1s XPS peaks fitted and according envelope for specimen after hard etch

Carbon

Figure A-30 shows the detailed intensity data acquired for the C 1s peak observed in the data as a red line. The blue line represents the background data matched to this peak.

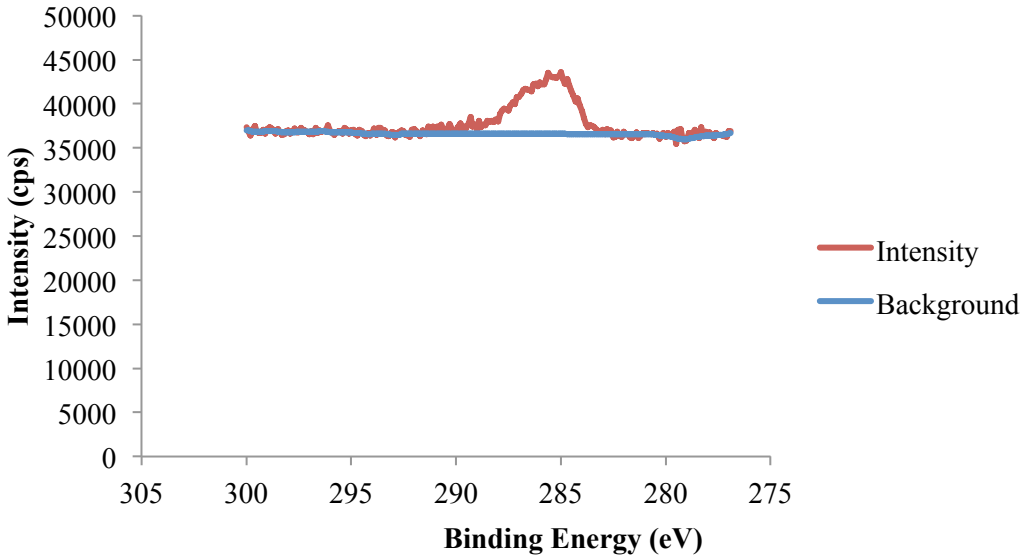

Figure A-30: C 1s XPS peak raw data and background fitting for specimen after hard etch

The envelope and required peaks to match the raw data are presented in Figure A-31. The binding energy of 284.9 eV detected for C 1s I is in range for carbon in its natural state. The C 1s III binding energy of 288.7 eV correlates with typical silver carbonate peaks (Biesinger, 2013a). For the C1s II peak various compounds are possible, and this has to be matched to the other data observed.

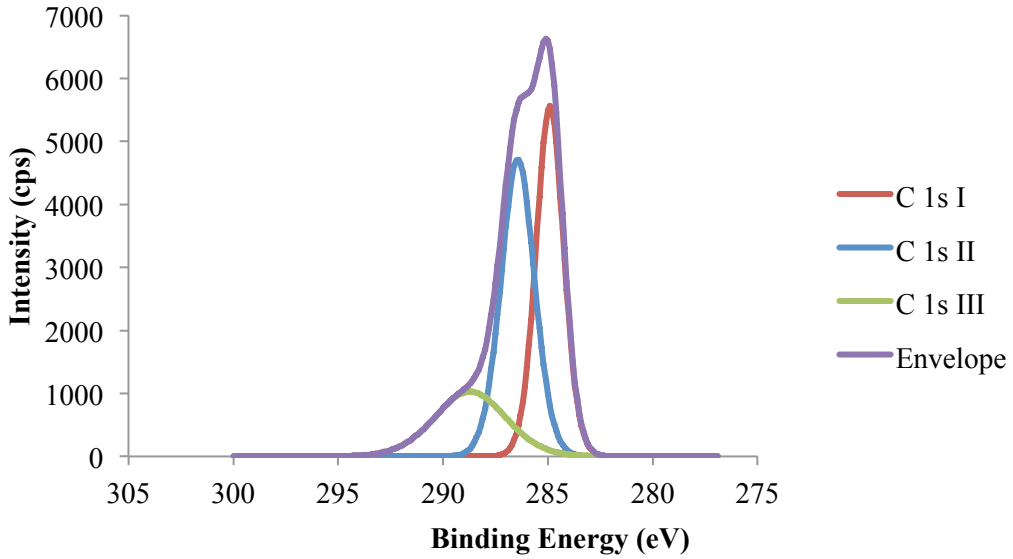

Figure A-31: C 1s XPS peaks fitted and according envelope for specimen after hard etch

Sulphur

An S 2p peak was observed in the raw data. This peak is plotted in detail in Figure A-32 as the red line. The blue line shows the background fitment to the raw data.

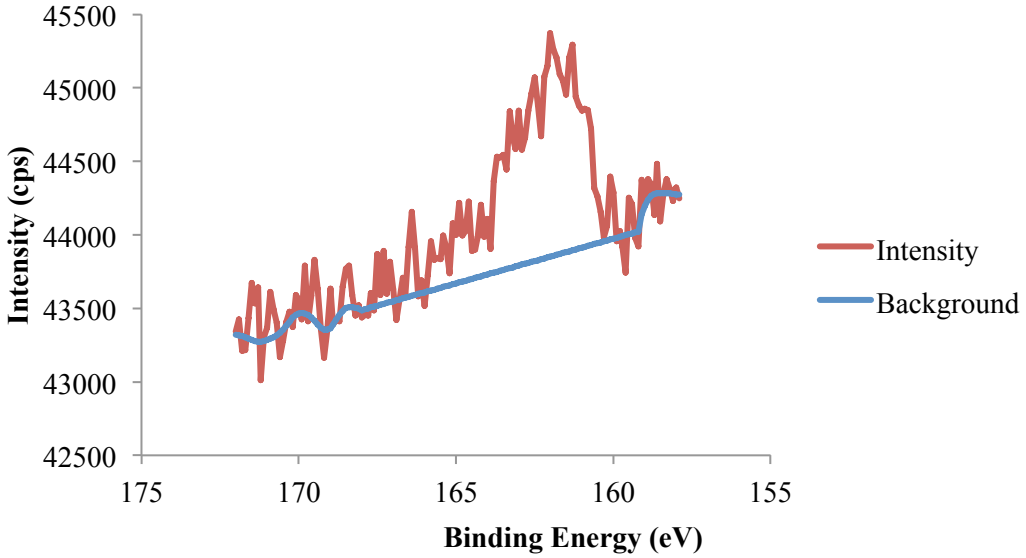

Figure A-32: S 2p XPS peak raw data and background fitting for specimen after hard etch

The envelope and peak fitted to the raw data for the S 2p data is plotted in Figure A-33. Only one S 2p peak, with a binding energy of 162.1 eV, could be fitted to the data. This is between the typical binding energy regions for metal sulphides or thio-

compounds of ~161.5 eV or 162.5 eV (Thermo Fisher Scientific Inc., 2013b). Due to the low intensity of the peak no better resolution could be gained, and this might represent two peaks, even though not visible.

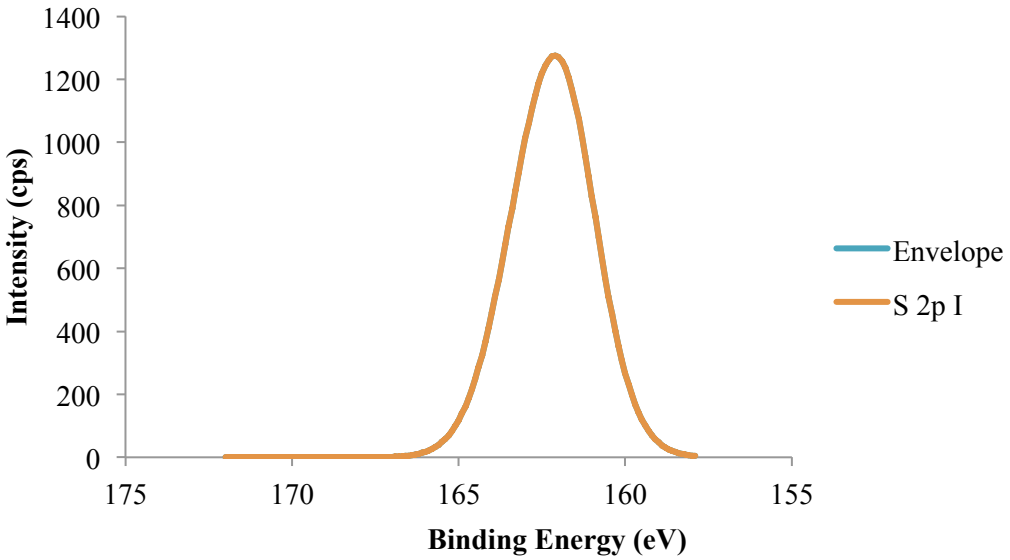

Figure A-33: S 2p XPS peaks fitted and according envelope for specimen after hard etch

Summary

The peaks identified on the specimen after the hard etch are displayed in Table A-3. The identifying peak positions and calculated concentrations (atomic and mass) are shown for each peak identified. For orbital spin doublets, only the first (lower eV) peak position is mentioned, as usually agreed on in literature.

Table A-3: XPS identified peaks, their position and calculated concentrations for specimen after 1 min 20 kV hard etching

Peak name	Peak Position (eV)	Atomic Concentration (%)	Mass Concentration (%)
Au 4f	84.10	30.1	78.3
Ag 3d I	368.10	4.8	6.8
Ag 3d II	368.80	1.4	2.0
O 1s I	532.40	39.7	8.4
O 1s II	533.90	7.5	1.6
C 1s I	284.90	6.2	1.0
C 1s II	286.40	6.4	1.0
C 1s III	288.70	3.0	0.5
S 2p I	162.10	1.1	0.5

A.4 Specimen after polish

Figure A-34 plots the measured intensity for the XPS scan, after polishing. The atomic fractions determined are 81.3%, 2.1%, 11.3% and 5.3% for gold, silver, oxygen, and carbon respectively.

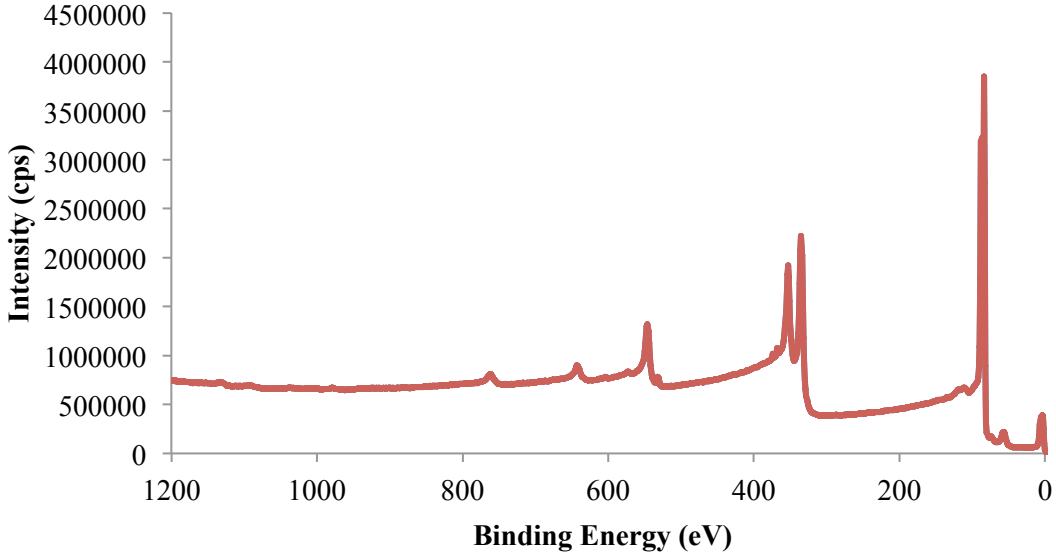

Figure A-34: XPS spectrum of the gold specimen with a polished surface

Gold

The measured intensity (red line) for the Au 4f peak and the fitted background (blue line) for the scan after polishing and a hard etch are presented in Figure A-35.

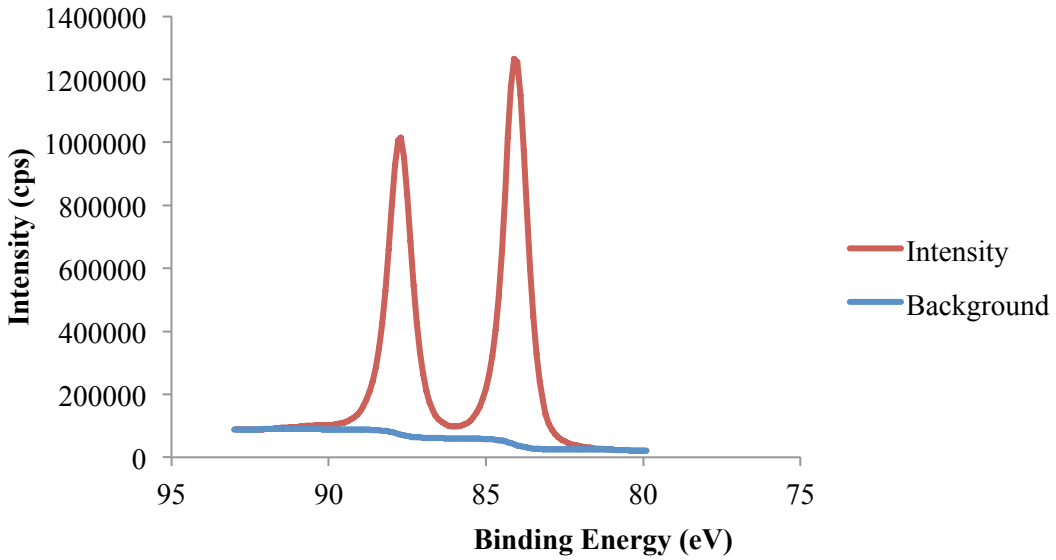

Figure A-35: Au 4f XPS peak raw data and background fitting for specimen with a polished surface

Figure A-36 shows the fitted Au 4f doublet peak and matching envelope as intensity over binding energy. It can be noted, that due to only peak required for fitting, the envelope is hidden behind the peak data. The Au 4f peak binding energy of 84.1 eV is in close agreement with the literature value for a native gold peak of 84.0 eV (Thermo Fisher Scientific Inc., 2013a).

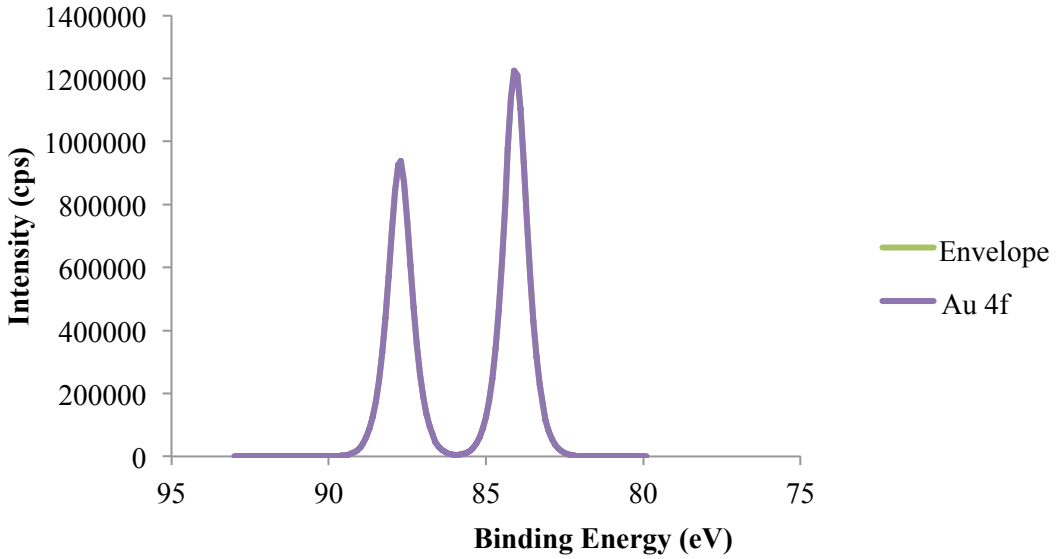

Figure A-36: Au 4f XPS peaks fitted and according envelope for specimen with a polished surface

Silver

The measured Ag 3d doublet peak data (red line) is plotted in Figure A-37. The blue line represents the background fitting conducted on the data.

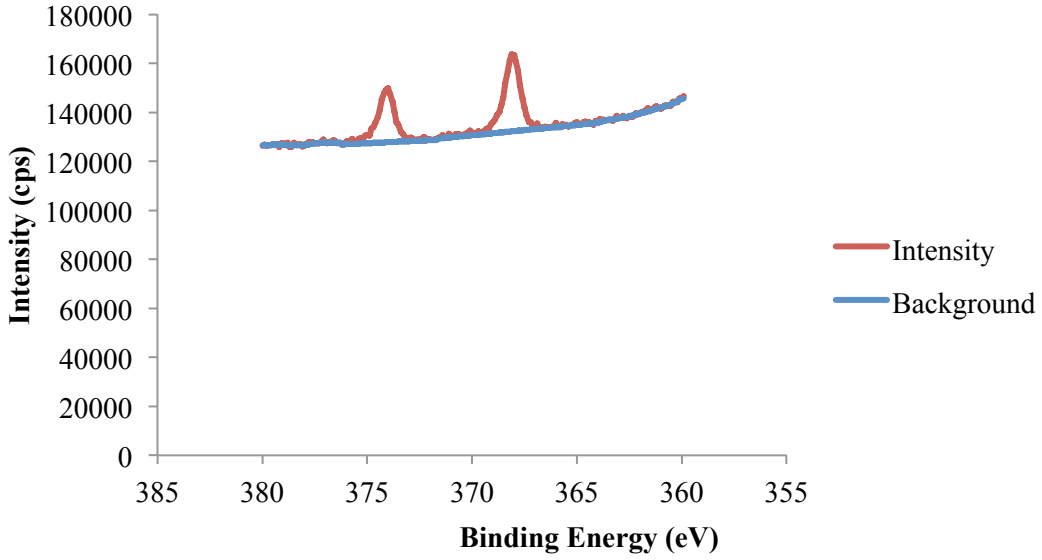

Figure A-37: Ag 3d XPS peak raw data and background fitting for specimen with a polished surface

The resulting envelope and the two doublets required to match the envelope are shown in Figure A-38. The Ag 3d I peak represents silver in its natural state with a slight offset in the peak binding energy notable, possibly due to the presence of the

gold/silver mixture (Kim & Winograd, 1975). The second peak represents silver in its charge transfer state (Eremenko et al., 2011).

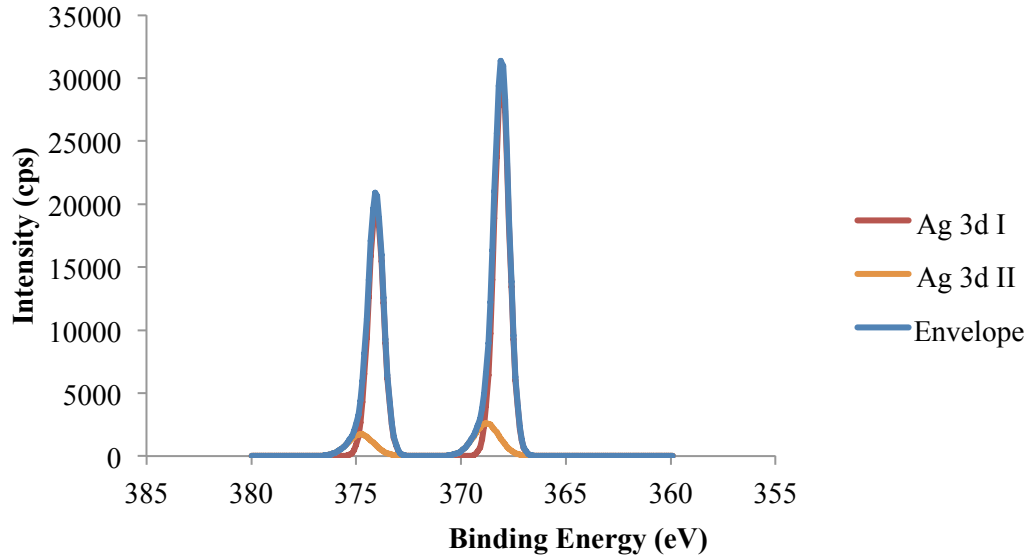

Figure A-38: Ag 3d XPS peaks fitted and according envelope for specimen with a polished surface

Oxygen

In Figure A-39 the peak data acquired for the O 1s peak is plotted as the red line. The background fit to the data is represented by the blue line.

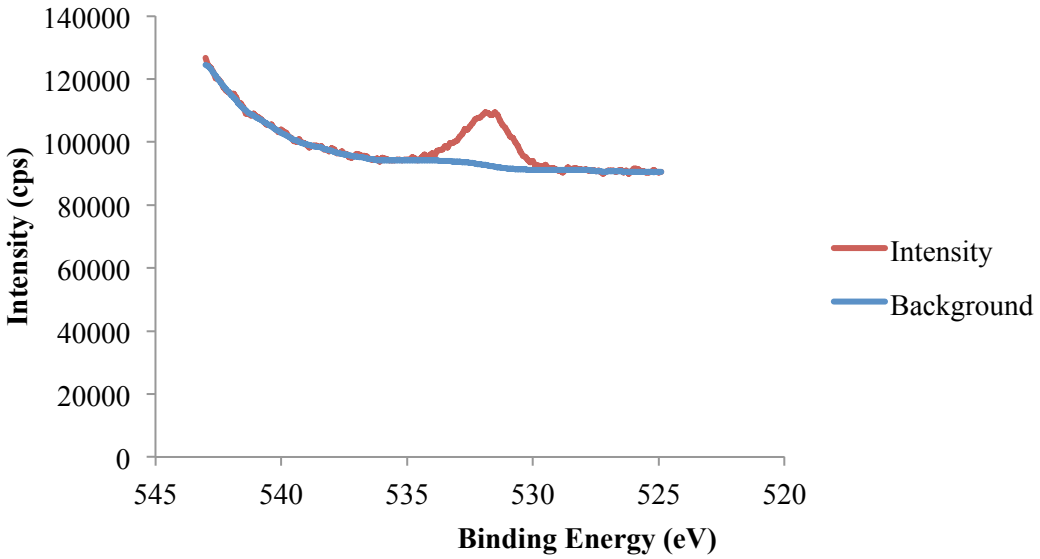

Figure A-39: O 1s XPS peak raw data and background fitting for specimen with a polished surface

The two resulting O 1s peaks fitted and the resulting envelope to match the measured data are presented in Figure A-40. The two peaks fitted indicate two different chemical bound oxygen forms on the surface, but cannot be clearly identified due to the possible options (Biesinger, 2013b).

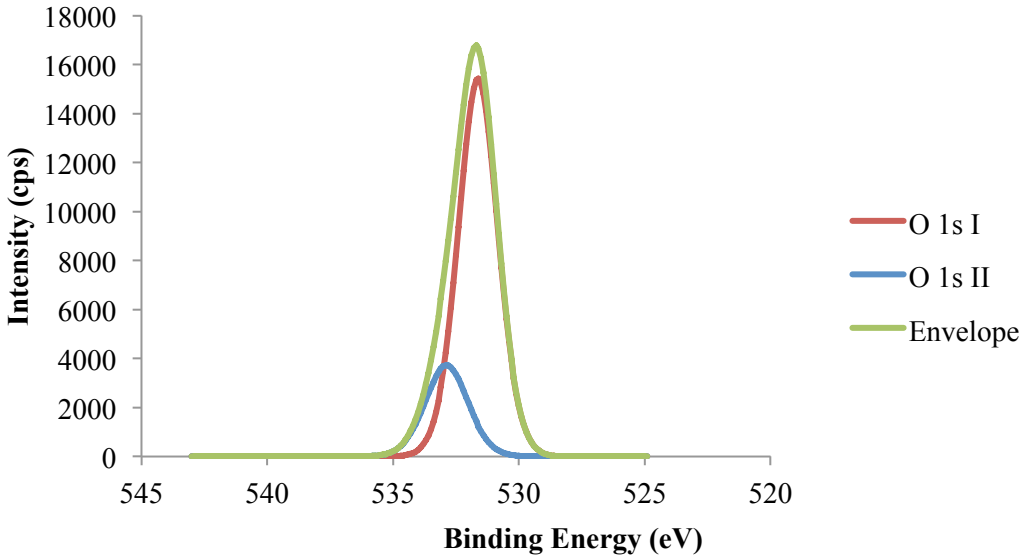

Figure A-40: O 1s XPS peaks fitted and according envelope for specimen with a polished surface

Carbon

The observed carbon peak data is presented in Figure A-41. The red line represents the observed intensity and the blue line the background data fitted. Due to the very small peak intensity no peak fitting was conducted on this data. The quantity of carbon present on the sample surface was estimated by calculating the area under the intensity curve.

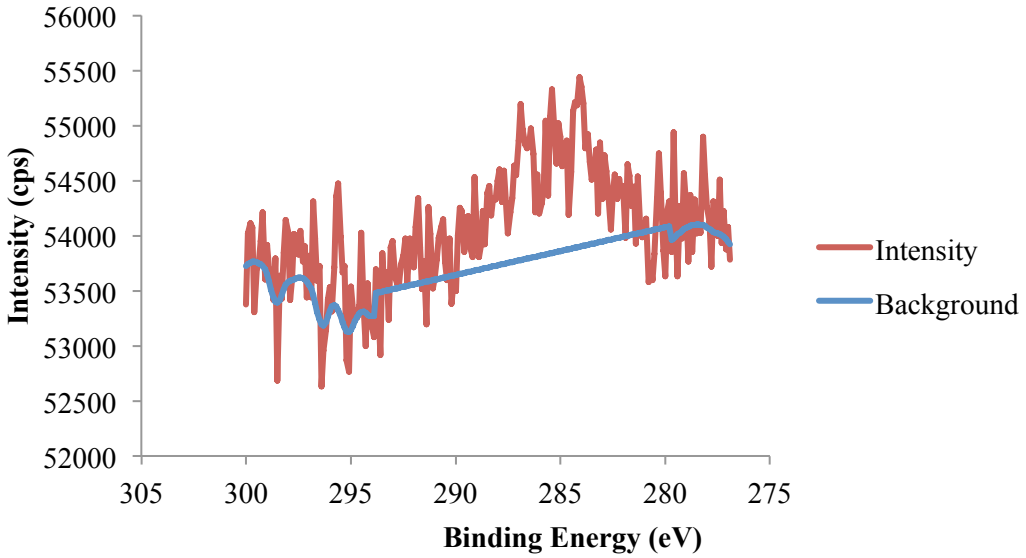

Figure A-41: C 1s XPS peak raw data and background fitting for specimen for a polished surface

Summary

The peaks identified on the specimen after the polish and hard etch are displayed in Table A-4. The identifying peak positions and calculated concentrations (atomic and mass) are shown for each peak identified. For orbital spin doublets, only the first (lower eV) peak position is mentioned, as usually agreed on in literature.

Table A-4: XPS identified peaks, their position and calculated concentrations for specimen with a polished surface

Peak name	Peak Position (eV)	Atomic Concentration (%)	Mass Concentration (%)
Au 4f	84.10	80.7	97.1
Ag 3d I	368.10	1.8	1.2
Ag 3d II	368.80	0.3	0.2
O 1s I	531.60	9.3	0.9
O 1s II	532.90	2.4	0.2
C 1s I	~280-290	5.6	0.4